**UNIVERSITY OF SOUTHAMPTON**
FACULTY OF PHYSICAL SCIENCES AND ENGINEERING
SCHOOL OF ELECTRONICS AND COMPUTER SCIENCE

# Spectrum/Energy Efficient Resource Allocation for Multi-User Multi-Relay OFDMA Cellular Networks: A Fractional Programming Approach

by

*Kent Tsz Kan Cheung*
BEng

*A thesis for the degree of*
*Doctor of Philosophy*
*at the University of Southampton*

June 2015

Supervisor: *Professor Lajos Hanzo*
FREng, FIEEE, FIET, FEURASIP
Chair in Telecommunications
and
Second Supervisor: *Dr. Shaoshi Yang*
BEng, PhD, MIEEE
Southampton Wireless Group
School of Electronics and Computer Science
University of Southampton
Southampton, SO17 1BJ
United Kingdom

*Dedicated to my family.*

UNIVERSITY OF SOUTHAMPTON

ABSTRACT

FACULTY OF PHYSICAL SCIENCES AND ENGINEERING
School of Electronics and Computer Science

Doctor of Philosophy

# SPECTRUM/ENERGY EFFICIENT RESOURCE ALLOCATION FOR MULTI-USER MULTI-RELAY OFDMA CELLULAR NETWORKS: A FRACTIONAL PROGRAMMING APPROACH

by Kent Tsz Kan Cheung

This thesis focuses on the energy efficiency (EE) of relay-aided cellular networks, which is motivated by the ever-increasing need to support higher and higher data rates, while reducing the energy costs. Relaying is a beneficial tool for either increasing the reliability or the coverage area of a wireless network as a result of the reduced communication distances, albeit this might increase the energy consumption in practice. Our approach in this thesis was to study and model progressively more complex and more realistic cellular networks. By utilizing novel transmission protocol designs, we were able to formulate their associated EE resource allocation optimization problems. Thus, efficient tools can be employed for solving these problems to maximize the EE.

We commenced by discussing the basic communication theory building blocks to be used in the later chapters. A state-of-the-art literature review was provided, which covers the energy-efficiency aspects (either based on EE or total power minimization) of orthogonal frequency division multiple access (OFDMA) networks, as well as their multiple-input–multiple-output (MIMO) and relay-assisted variants. We then provided a broad overview of the mathematical optimization tools that will be extensively used in this thesis. Our overview covered convex sets and functions, convex optimization forms and the important concept of duality. We then described a range of solution methods, which can be applied to various forms of optimization problems. Complex problems, such as mixed integer non-linear programming (MINLP) problems and fractional problems were also considered, as well as methods of reformulating them in a way, which facilitates their solution via standard convex optimization techniques. Furthermore, the important theoretic foundations of decomposition were highlighted, and examples of convex optimization applied in communication networks were provided.

Having laid the foundations, we embarked on studying a relay-aided OFDMA cellular network. In contrast to previous contributions in this area, our multi-relay multiuser network

supports simultaneous direct and relaying links. However, relay node (RN) selection is implicitly achieved, since the users rely on the specific RNs, which they are geographically nearest to. We formulated the (normalized) EE metric of the network as a function of the subcarrier and power allocation of the system. This metric was then employed in the formal definition of the EE maximization problem of the network, which is fractional and involves binary constraints. Therefore, solving it would typically require a computational complexity, which is exponentially proportional to the number of optimization variables. For the sake of developing a practical solution algorithm, we employed a convex relaxation of the binary-constrained optimization variables, thereby converting the problem into a quasi-concave form. Thus, the convex forms of the quasi-concave problem could be obtained from Dinkelbach's method, as well as from the Charnes-Cooper transformation and from the bi-section method. We developed algorithms based on dual decomposition for each method in order to evaluate their performance versus complexity trade-offs. In particular, we observed that the algorithm based on the Charnes-Cooper transformation is capable of attaining the optimal solution in much fewer iterations than the algorithms based on either Dinkelbach's method or on the bisection method, hence it was chosen as the preferred approach in our later studies. Furthermore, we characterized the trade-off associated with adjusting the various system parameters on the attainable EE and spectral-efficiency (SE) of the system. Most notably, we observed that increasing either the number of subcarriers or the number of relays suffers from diminishing returns as regards to the EE of the system, whilst increasing the number of active user equipment (UEs) improves both the EE and SE of the system owing to its increased multi-user diversity. Furthermore, we compared both EE maximization (EEM) and SE maximization (SEM) algorithms. In particular, we noted that increasing the available transmit power in certain scenarios, reduces the EE of the system, when using the SEM algorithm, even though it might result in an increased SE. By contrast, the EEM algorithm approaches an EE upper bound at a reduced SE.

We then proceeded to conceiving a novel transmission protocol for a general multi-relay multiuser MIMO- OFDMA cellular network based on joint transmit and receive beamforming. This transmission protocol is suitable for a network consisting of an arbitrary number of RNs and UEs, as well as any number of antennas on any of the communicating nodes. It operates based on designing the receive beamforming matrices for each subcarrier so that their associated MIMO channel matrices can be mathematically decomposed into several effective multiple-input–single-output (MISO) channels, which are referred to as spatial multiplexing components (SMCs) in this thesis. Transmitting on these SMCs without imposing interference amongst them can then be achieved by employing zero-forcing (ZF) transmit beamforming. For the sake of increasing the attainable spatial multiplexing gain, several SMCs may be grouped for transmission on each subcarrier. We proposed a pair of such grouping algorithms. The first one is based on an exhaustive search over all the possible grouping combinations, while the second is a low-complexity alternative, which iteratively

improves a fixed set of groups. Finding the optimal groups having the best EE or SE as well as their associated power allocation values were formulated as optimization problems. With the aid of the previously employed variable relaxation and transformations, the optimization problems were rewritten in their epigraph form. Thus, the resultant problems were convex and we developed algorithms based on dual decomposition for solving them. We characterized the performance of the grouping algorithms and observed that our lower-complexity alternative was also capable of finding near-optimal solutions, despite its much lower complexity. Furthermore, the effect of several system parameters imposed on both the SE and EE was observed. In particular, we concluded that the optimal EE is achieved by the system, when the maximum power constraint of both the base station (BS) and of each RN was set to 50dBm. Furthermore, the effect of the power constraint on the BS has a much more grave effect on the attainable SE and EE of the system, than the constraint of the RNs. Moreover, increasing the number of antennas at the BS increases both the SE and EE owing to their higher achievable multiplexing gains. However, increasing either the number of RNs or the number of subcarriers reduces the SE and EE, since these additional resources are not efficiently, utilized when maximizing the SE or EE.

Then our system model was further expanded to a multi-cell network. Thus, there were multiple BSs, RNs and UEs, all equipped with multiple antennas. For the sake of avoiding the potentially excessive co-channel interference (CCI), we employed the novel technique of interference alignment (IA), when designing a pair of transmission protocols. The first one was termed as the full-IA protocol, which aims for avoiding all CCI impinging from all possible transmitters, but requires that each BS has access to the channel state information (CSI) of all the channels associated with all other cells. On the other hand, the partial-IA protocol only requires the CSI of the limited set of channels associated with its own cell, and disregards the other-cell interference (OCI). Thus, its performance may be degraded, but benefits from a lower CSI feedback overhead. Both transmission protocols depend on carefully determining the number of signal dimensions available for each transmitter, when considering the IA technique. Since the number of available signal dimensions is inversely proportional to the number of channels, which IA algorithm operates on, we can conclude that the full-IA protocol also suffers from a reduced spatial multiplexing gain, when compared to the partial-IA protocol. Based on either the full-IA or the partial-IA protocols, we computed the relevant transmit and receive beamforming weight matrices. We then formulated the network-wide EE optimization problem and again, invoked the Charnes-Cooper transformation for obtaining the optimization problem in a convex form. Our proposed solution algorithm is based on dual decomposition and may be applied distributively in the network. The simulation results indicated that the partial-IA protocol outperforms the full-IA protocol in all cases, due to the full-IA protocol's action of overcompensating, when aiming for avoiding all possible interference, hence substantially reducing its attainable spatial multiplexing gain. Furthermore, increasing the spatial multiplexing

gain achievable by each RN beyond two actually reduces the network's EE, since the spatial multiplexing gain achieved by BSs would have to be reduced in order to accommodate IA. Additionally, deploying a single RN in each sector is sufficient for maximizing the attainable SE, although the EE is reduced, when increasing the number of RNs.

# Declaration of Authorship

I, **Kent Tsz Kan Cheung**, declare that the thesis entitled

**Spectrum/Energy Efficient Resource Allocation for Multi-User Multi-Relay OFDMA Cellular Networks: A Fractional Programming Approach**

and the work presented in it are my own and have been generated by me as the result of my own original research. I confirm that:

1. This work was done wholly or mainly while in candidature for a research degree at this University;
2. Where any part of this thesis has previously been submitted for a degree or any other qualification at this University or any other institution, this has been clearly stated;
3. Where I have consulted the published work of others, this is always clearly attributed;
4. Where I have quoted from the work of others, the source is always given. With the exception of such quotations, this thesis is entirely my own work;
5. I have acknowledged all main sources of help;
6. Where the thesis is based on work done by myself jointly with others, I have made clear exactly what was done by others and what I have contributed myself;
7. Parts of this work have been published, as seen in the list of publications.

**Signed**: Kent Tsz Kan Cheung

**Date**: 19 June 2015

# Acknowledgements

I wish to extend my heartfelt gratitude to my friend and mentor, Professor Lajos Hanzo. His excellent guidance and support has been with me since my time as an undergraduate student and I owe much of my success as a researcher to his enthusiasm, his encouragement and most of all, his patience.

I would also like to thank Dr. Shaoshi Yang, who assisted me tremendously throughout my research. His knowledge and attention to detail inspired me to always work harder to better myself as a researcher.

The support and kindness of the many friends and colleagues that I have made throughout these past few years has been invaluable to me. Their presence has helped me endure the ups and downs of being a researcher. Although there are too many names to mention, I would like to especially thank Halil Yetgin for our collaborations, and Chao Xu, Dr. Jing Zuo, and Dr. Chen Dong, who all generously provided their time and knowledge to me during my early years as a postgraduate student.

The financial support of the Industrial Companies who are Members of the Mobile VCE, and the additional financial support from the UK Government's Engineering & Physical Sciences Research Council (EPSRC) is also gratefully acknowledged.

# List of Publications

## Journal Papers:

1. **K.T.K. Cheung**, S. Yang, and L. Hanzo, "Distributed Energy Spectral Efficiency Optimization for Partial/Full Interference Alignment in Multi-User Multi-Relay Multi-Cell MIMO Systems" *submitted to IEEE Transactions on Signal Processing.*
2. H. Yetgin, **K.T.K. Cheung**, M. El-Hajjar and L. Hanzo, "Cross-Layer Network Lifetime Maximization in Interference-Limited WSNs," *accepted for publication in IEEE Transactions on Vehicular Technology.*
3. H. Yetgin, **K.T.K. Cheung**, M. El-Hajjar and L. Hanzo, "Cross-layer network lifetime optimisation considering transmit and signal processing power in wireless sensor networks," *IET Wireless Sensor Systems*, vol. 4, no. 4, pp. 176–182, Dec. 2014.
4. **K.T.K. Cheung**, S. Yang, and L. Hanzo, "Spectral and energy spectral efficiency optimization of joint transmit and receive beamforming based multi-relay MIMO-OFDMA cellular networks," *IEEE Transactions on Wireless Communications*, vol. 13, no. 11, pp. 6147–6165, Aug. 2014.
5. **K.T.K. Cheung**, S. Yang, and L. Hanzo, "Achieving maximum energy-efficiency in multi-relay OFDMA cellular networks: A fractional programming approach," *IEEE Transactions on Communications*, vol. 61, no. 7, pp. 2746–2757, Jul. 2013. United States, Sept. 2011.

## Conference Papers:

1. **K.T.K. Cheung**, S. Yang, and L. Hanzo, "Maximizing energy-efficiency in multi-relay OFDMA cellular networks," *IEEE Global Communications Conference*, Atlanta, United States, Dec. 2013.
2. H. Yetgin, **K.T.K. Cheung** and L. Hanzo, "Multi-objective routing optimization using evolutionary algorithms," *IEEE Wireless Communications and Networking Conference*, Paris, France, Apr. 2012.
3. **K.T.K. Cheung**, L. Li and L. Hanzo, "On-demand decode and forward cooperative MAC for VoIP in wireless mesh networks," *IEEE Vehicular Technology Conference Fall*, San Francisco, United States, Sept. 2011.

# General Notation

| | |
|---|---|
| $\mathbf{A}$ | boldface uppercase letters denote matrices. |
| $a_{ij}$ | the element of the matrix $\mathbf{A}$ at row $i$, column $j$. |
| $\mathbf{x}$ | boldface lowercase letters denote column vectors. |
| $x$ | standard lowercase letters denote scalars. |
| $x_i$ | the $i$th element of the vector $\mathbf{x}$. |
| Diag$\{\mathbf{x}\}$ | a diagonal matrix with $\mathbf{x}$ being its diagonal elements. |
| diag$\{\mathbf{A}\}$ | a vector comprised of the diagonal elements of the matrix $\mathbf{A}$. |
| Trace$(\mathbf{A})$ | trace of matrix $\mathbf{A}$. |
| $\mathbf{A}^T$ | transpose of the matrix $\mathbf{A}$. |
| $\mathbf{A}^H$ | Hermitian transpose of the matrix $\mathbf{A}$. |
| $\mathbf{A}^{-1}$ | inverse of the square matrix $\mathbf{A}$. |
| $\mathbf{A}^\dagger$ | Moore-Penrose inverse (pseudoinverse) of the matrix $\mathbf{A}$. |
| $\mathbf{rank}\,(\mathbf{A})$ | rank of matrix $\mathbf{A}$. |
| $\Re(\mathbf{A})$ | elementwise real part of the matrix $\mathbf{A}$. |
| $\Im(\mathbf{A})$ | elementwise imaginary part of the matrix $\mathbf{A}$. |
| $\mathbf{I}_N$ | the $(N \times N)$-element identity matrix. |
| $\mathbf{1}_N$ | the dimension-$N$ column vector of ones. |
| $\mathbb{R}$ | the field of real numbers. |
| $\mathbb{C}$ | the field of complex numbers |
| $\mathbb{Z}$ | the set of all integers. |
| $\mathbb{R}_+$ | the set of all nonnegative real numbers. |
| $\mathbb{R}_{++}$ | the set of all positive real numbers. |
| $\mathbb{R}_-$ | the set of all nonpositive real numbers. |
| $\mathbb{R}_{--}$ | the set of all negative real numbers. |
| $\mathbb{R}^n$ | the $n$-dimensional vector of real numbers. |
| $\mathbb{R}^{m\times n}$ | the $m \times n$-dimensional matrix of real numbers. |
| $\|\cdot\|_p$ | the p-norm of a vector. |
| $\|\cdot\|_F$ | the Frobenius norm of a matrix. |
| $\min(\cdot)$ | minimum operator. |
| $\max(\cdot)$ | maximum operator. |
| $\inf(\cdot)$ | infimum operator. |
| $\sup(\cdot)$ | supremum operator. |
| $\log(\cdot)$ | natural logarithm operator. |
| $\log_2(\cdot)$ | base 2 logarithm operator. |

| | |
|---|---|
| **aff** $\mathcal{S}$ | affine hull of set $\mathcal{S}$. |
| **dom** $f$ | domain of function $f$. |
| $[a, b]$ | closed set of real numbers between $a$ and $b$. |
| $(a, b)$ | open set of real numbers between $a$ and $b$. |
| $\nabla$ | first order vector differential operator. |
| $\nabla^2$ | second order vector differential operator. |
| $\mathbf{A} \succeq 0$ | $\mathbf{A}$ is a positive semidefinite matrix. |
| $\mathbf{x} \succeq a$ | vector $\mathbf{x}$ is elementwise greater than $a$. |
| **epi** $f$ | epigraph of function $f$. |
| **hypo** $f$ | hypograph of function $f$. |
| $h \circ g$ | the function composed of $h\,(g)$. |
| $f'$ | first order derivative of function $f$. |
| $f''$ | second order derivative of function $f$. |
| **relint** $\mathcal{D}$ | relative interior of set $\mathcal{D}$. |
| $Df\,(x)$ | first order derivative of function $f$ with respect to $x$. |
| $[\cdot]^+$ | projection onto the nonnegative field of real numbers. |
| $\lfloor\rfloor$ | floor operator. |

# Table of Contents

Chapter 1

# Introduction

Mobile data traffic has grown tremendously in recent years, which is a trend that is set to continue for the near future [1–3]. Consequently, the industry has been prompted into focusing their efforts on increasing the achievable area spectral efficiency (ASE) [4] of cellular systems using advanced technologies, which is expressed in $\left[\text{bits/sec/Hz/km}^2\right]$. In the interest of improving the ASE through spatial reuse of the available wireless resources, heterogeneous networks, small cells and MIMO antenna techniques may be employed [5–8]. However, these capacity-improvement methods conflict with the growing need to reduce the energy consumption of a wireless network [9–11], which was triggered by the perpetually increasing energy prices, as well as by societal and political pressures on mobile phone operators to reduce their 'carbon footprint' [12, 13]. To elaborate, more BSs are required in order to provide the same coverage using smaller cells, while employing more antenna components requires additional radio frequency (RF) chains. Both effects contribute to an increase of the network's operational energy costs. On the other hand, the EE of the network may be improved by employing intelligent resource allocation (RA) [8, 11, 14] for exploiting any available multi-user, time, spatial or frequency diversities. Nonetheless, the complexity of RA is further exacerbated by the impact of CCI in a network consisting of multiple cells [5].

Substantial joint academic and industrial research efforts have been dedicated to developing novel energy-saving techniques, as exemplified by the 'green radio' project [10], the GreenTouch alliance [15], and the energy aware radio and network technologies (EARTH) project [12, 16]. Substantial research efforts have also been dedicated to relay-aided OFDMA wireless networks, as exemplified by the third generation partnership project's (3GPP) long term evolution-advanced (LTE-A) and IEEE 802.16 worldwide interoperability for microwave access (WiMAX) [17] standards. The wireless resources of time and frequency have to be carefully assigned for increasing the system's SE or EE in an OFDMA system, which can be arranged by an intelligent RA scheduler. Furthermore, relaying between the BS and

the UE can improve the EE, since the quality of the communication link is maintained at reduced transmission power requirements owing to the reduced transmission distances. Thus, the need for expensive deployment and maintenance of additional BSs can be circumvented.

The complex interplay of the above issues motivates the investigations of this thesis, which focuses on the optimal RA for maximizing the SE or EE of multi-user multi-relay networks. In the following, the basics of the communication principles employed in this thesis are described.

## 1.1 Discrete Memoryless Time-Invariant Channel Capacity

For a discrete memoryless time-invariant channel, the symbol received at time instant $i$ can be modeled as

$$y[i] = \sqrt{g[i]}x[i] + n[i], \tag{1.1}$$

where $\sqrt{g[i]}$ is the channel gain, $x[i]$ is the transmitted symbol and $n[i]$ is the noise sample. The signal-to-noise ratio (SNR) at the receiver is then defined as

$$\gamma[i] = \frac{g[i]P[i]}{N_0 B}, \tag{1.2}$$

where $P[i] = |x[i]|^2$ is the transmission power, while $B$ is the received signal bandwidth. Furthermore, the power spectral density of the additive white Gaussian noise (AWGN) is given by $N_0/2$. The SNR determines the achievable Shannon capacity [4] of

$$C = \int_0^\infty B \log_2(1+\gamma)\, p(\gamma)\ \mathrm{d}\gamma, \tag{1.3}$$

which is the maximum mutual information (MI) that can be conveyed over the channel with a vanishingly low error probability. The Shannon capacity can be maximized if knowledge of the channel state information (CSI) $g[i]$ is available at both the transmitter and receiver. In that case, the Shannon capacity is simply given by

$$C = B \log_2\left(1 + \frac{g[i]P[i]}{N_0 B}\right), \tag{1.4}$$

and it is clear that a high channel capacity can be attained, when the channel gain is favorably high.

The wireless channel encountered in real-world scenarios is affected by fast-fading, shadowing and path-loss. In case of cellular systems, the fading encountered in both the downlink (DL) and uplink (UL) channels is typically frequency-selective, which is the result of having multiple signals paths of varying lengths between the transmitting BS and the user, as demonstrated in Fig. 1.1. A measure of the severity of the frequency-selective fading is

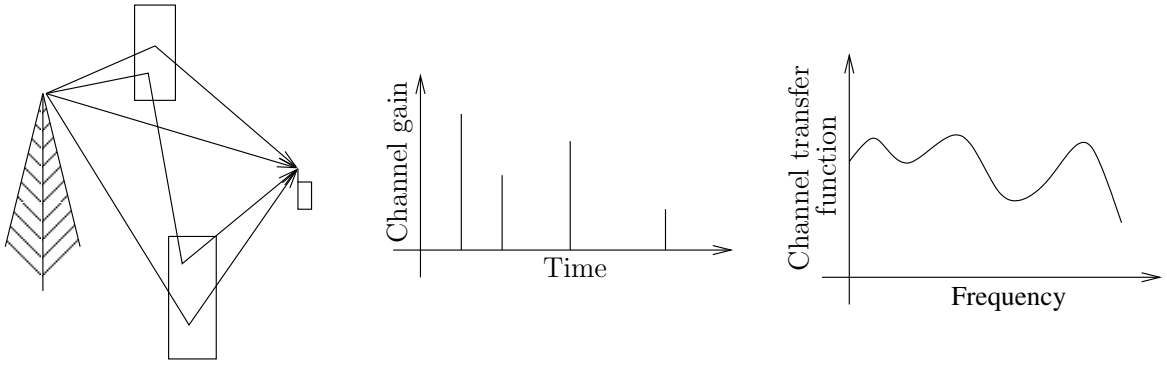


FIGURE 1.1: The multiple signal paths arriving at the user at different times causes frequency-selectivity in the channel transfer function.

given by the coherence bandwidth, which is the average bandwidth over which the complex valued fading envelope can be considered constant. If the signal bandwidth is similar to the coherence bandwidth, then the signal experiences frequency-flat fading. On the other hand, if the coherence bandwidth is lower than the signal bandwidth, the signal undergoes frequency-selective fading, which is detrimental to the quality of reception since it causes inter-symbol interference, hence increasing the error probability, unless intelligent counter-measures are invoked. In the LTE-A and the WiMAX standards, the OFDMA technique [18] is employed.

## 1.2 Orthogonal Frequency Division Multiple Access

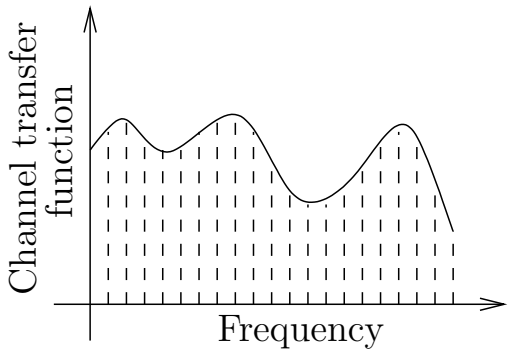


FIGURE 1.2: A demonstration of how OFDMA partitions the channel's bandwidth into multiple subchannels.

In OFDMA, the whole channel's bandwidth is divided into multiple subchannels, centered around the subcarriers, as depicted in Fig. 1.2, where each subcarrier is employed for transmitting different symbols. An immediate benefit of using OFDMA is that each subband signal's bandwidth is substantially reduced, thus making it more likely that each signal experiences frequency-flat fading.

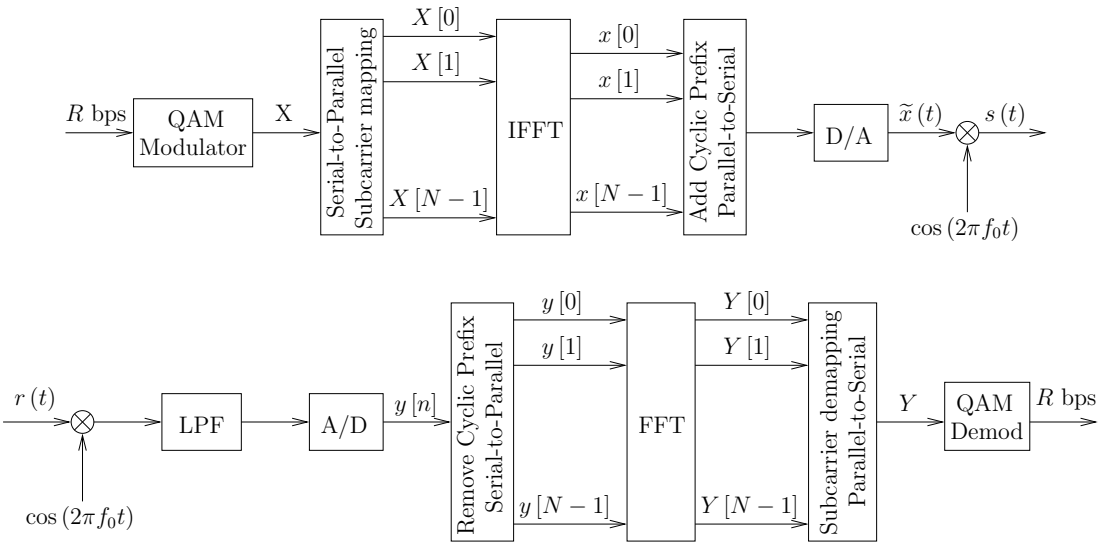


FIGURE 1.3: A block diagram of a point-to-point link employing OFDMA using the IFFT and the FFT. The operations performed by the transmitter are shown at the top, while the bottom details the receiver's operations. The blocks labelled D/A and A/D perform the digital-to-analogue and analogue-to-digital covnersion, respectively.

The OFDMA operation is performed as shown in Fig. 1.3. The data stream is initially modulated into $N$ complex-valued quadrature amplitude modulation (QAM) symbols

$$X[0], X[1], \cdots, X[N-1], \tag{1.5}$$

which are parallelized and mapped to specific OFDMA subcarriers. The inverse fast Fourier transform (IFFT) can be used for simultaneously modulating the phase and amplitude of a block of $N$ subcarriers instead of using a bank of $N$ parallel modems, which is formulated as

$$x[n] = \frac{1}{\sqrt{N}} \sum_{i=0}^{N-1} X[i] e^{j2\pi i/N}, \; n = 0, \cdots, N-1, \tag{1.6}$$

where $x[n]$ represents the OFDMA symbols. As seen in Fig. 1.3, a cyclic prefix is appended to each OFDMA symbol to ensure that consecutive OFDMA symbols are free from inter-symbol interference [4] and all OFDMA symbols are combined using the parallel-to-serial converter to yield the baseband OFDMA signal, which is upconverted to the carrier frequency of $f_0$ and transmitted. The inverse operations are performed at the receiver of Fig. 1.3, with the inclusion of a low pass filter (LPF) for removing the high frequency components. Since OFDMA modulation and demodulation is a linear process, it is convenient to manipulate the baseband QAM modulated symbol stream in simulations, instead of the RF signals.

In cellular systems, different subsets of these subcarriers may be allocated for transmission to different users in a cellular system [18], thus attaining two types of diversity, which may be jointly exploited for improving the attainable capacity of the system. Firstly, multi-user

diversity is attained with the aid of appropriate user mapping, since a channel spanning from the BS to a specific UE and undergoing severe fading may be freely reassigned for transmission to a different user with more friendly channel conditions. On the other hand, activating only those subcarriers that are suitable for high-quality transmission to a particular UE leads to frequency diversity. These philosophies are underpinned by several contributions in the literature [18,19], where the goal is to assign the available resources, for example power and subcarriers, so that a system-wide metric is maximized. These methods belong to the family of resource allocation policies and typically aim for solving one of two problems: either the SE [20–22] of the system is maximized while a maximum power constraint is enforced, or the power consumption is minimized under a minimum total system throughput or individual UE rate constraint [23–27], which may be viewed as ensuring fairness among the users, since each user achieves at least a minimum rate. Furthermore, for a given system bandwidth, the sum rate maximization and SEM solutions are identical. To avoid any additional abbreviations, they are both henceforth referred to as SEM.

## 1.3 Resource Allocation Fundamentals

Effective RA can be achieved by spectrum allocation and power allocation [28]. The goal of spectrum allocation is to assign the scarce time-, frequency- and code-domain radio resources to the transmissions associated with the set of active users. The majority of the CCI may be avoided be careful power allocation, if these resources are orthogonally assigned, so that there are no overlapping transmissions.

In the case of the LTE-A and the WiMAX standards [8, 29, 30], the time-domain (TD) resource is partitioned into frames in a time-division multiple access (TDMA) manner, while the frequency-domain (FD) resource is partitioned into subchannels using OFDMA. The benefit of using OFDMA, as described above, is that the frequency-selective wireless channel can be transformed into several low-rate, non-dispersive subchannels, which exhibit frequency-flat fading. This assists in intelligent scheduling by facilitating channel adaptation. The time-frequency partitions are then referred to as resource blocks (RBs), which are depicted in Fig. 1.4. As seen in Fig. 1.3, the role of the scheduler is to perform subcarrier mapping, so that the RBs are assigned to users in an intelligent manner, which maximizes some network-wide metric. The most common scheduling algorithms include round-robin (RR) and proportional fair (PF) scheduling [31]. The RR scheduler aims for maximizing the resource usage fairness by assigning a roughly equal number of resources to each user, while the PF scheduler takes into account the past history of the attained transmission rates of each user and assigns the future resources to balance equitably the longterm rate achieved by all users.

During the past decade, a large body of literature has been accumulated on the subject of

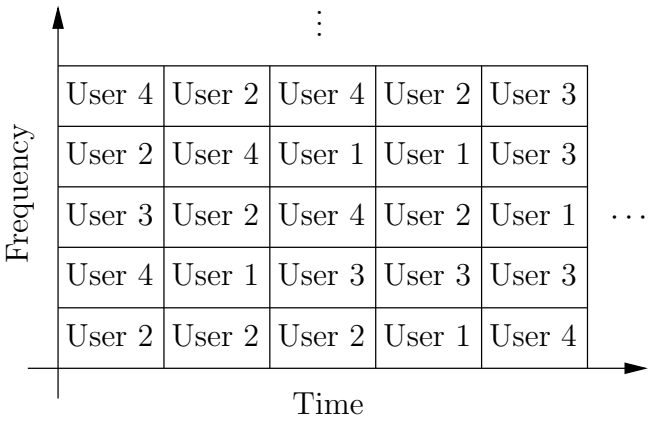


FIGURE 1.4: The wireless resources of time and frequency may be partitioned into RBs and assigned to particular users.

RA [23, 24, 26, 32]. While the basic RR and PF scheduling algorithms are still advocated in the wireless standards, the research community has developed more sophisticated algorithms based on exploiting the available CSI to perform opportunistic RA [33]. As shown in Fig. 1.5, wireless channels suffer from time- and frequency-selective fading, therefore it is inevitable that certain users will experience more favorable wireless links to the BS. The system's

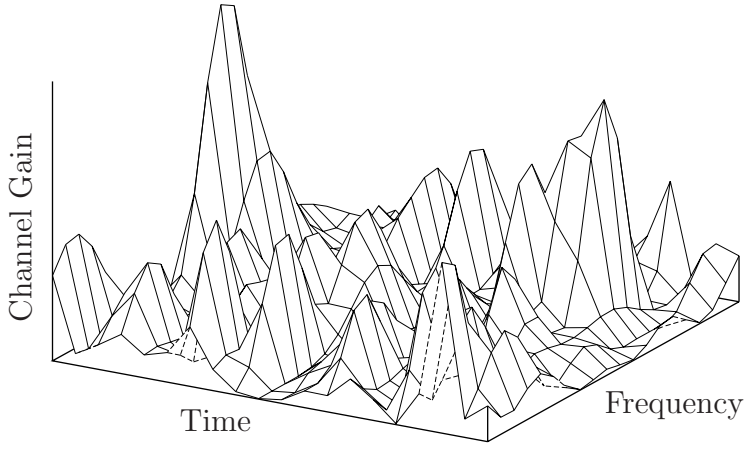


FIGURE 1.5: A conceptual illustration of the time- and frequency-varying nature of a wireless channel.

performance can be improved by assigning RBs to the wireless links corresponding to the preferable channel conditions, thus exploiting the so-called multi-user diversity [4].

The RA problem is further complicated in relay-aided multi-cell networks. Cellular networks employ a unity frequency reuse factor to improve the attainable ASE, while relaying is capable of improving either the quality of the end-to-end link or of reducing the transmission power requirement. However, the multiple simultaneous transmissions result in stronger CCI. Intelligent schedulers are required for allocating resources, while ensuring that the CCI is carefully managed and that the communication overhead required between BSs is not excessive. Beneficial methods of avoiding excessive CCI include geometric program-

ming (GP) [34–36] or iterative water-filling (IWF) [37]. Both approaches are derived from convex optimization. The latter one will be detailed in Section 2.8.2.

## 1.4 Relay-Aided Transmissions

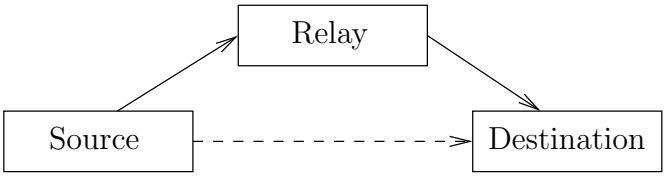


FIGURE 1.6: An example of a relay network. The direct link between the source and destination is indicated with a dashed line, while the relayed link using the RN is shown using the solid line.

The relay channel, as shown in Fig. 1.6, has been extensively studied in the research community [38–41]. In the context of cellular networks, the relay channel is created by employing RNs, thus extending the wireless coverage, reducing the required transmission power, or improving the reliability of the wireless link [17, 42]. The pair of relaying protocols advocated in the seminal work of [43] are the AF and the DF protocols [43]. The AF protocol is less complex than DF, since the RN needs only has to receive and linearly amplify the transmissions, before forwarding it to the destination. On the other hand, DF requires that the RN decodes and then re-encodes the symbol stream, thus requiring a more intelligent RN and imposing an additional delay on the end-to-end transmission. The effects of scheduling and frequency reuse in the context of the above-mentioned networks was studied in [44].

In the AF protocol, the complex-valued symbol sequence transmitted from the source node (SN), $\mathbf{x}_s$, is received at the RN and may be written as

$$\mathbf{y}_r = h_{s,r}\mathbf{x}_s + \mathbf{n}_r, \tag{1.7}$$

where $h_{s,r}$ is the complex-valued channel fading coefficient of the link between the SN and RN, which is assumed to be constant for the duration of the transmitted symbol sequence, while $\mathbf{n}_r$ is the complex-valued, zero-mean, circularly symmetric Gaussian random noise sequence with a variance of $N_0$. The RN applies an amplification factor to the received sequence given by

$$\beta = \sqrt{\frac{P_r}{|a_{s,r}|^2 P_s + N_0}}, \tag{1.8}$$

where $P_s$ and $P_r$ are the maximum instantaneous power constraints of the SN and RN, respectively. Then the RN transmits the sequence $\beta\mathbf{y}_r$, which now has an average power of $P_r$. After receiving the transmissions from both the SN and RN, the MI conveyed to the

destination node (DN) is given by [43]

$$I_{AF} \leq \frac{1}{2}\log_2\left(1+|h_{s,d}|^2\frac{P_s}{N_0}+f\left(|h_{s,r}|^2\frac{P_s}{N_0},|h_{r,d}|^2\frac{P_r}{N_0}\right)\right), \tag{1.9}$$

where $h_{s,d}$ and $h_{r,d}$ is the complex-valued channel coefficient of the SN-to-DN link and the RN-to-DN link, respectively, while the relaying-function is given by:

$$f(x,y) := \frac{xy}{x+y+1}. \tag{1.10}$$

If the channel between the SN and DN is undergoing severe fading, the SN-DN link may be ignored. Then the MI conveyed to the DN is given by

$$I_{AF} = \frac{1}{2}\log_2\left(1+f\left(|a_{s,r}|^2\frac{P_s}{N_0},|a_{r,d}|^2\frac{P_r}{N_0}\right)\right). \tag{1.11}$$

When employing the DF protocol, the RN first has to decode the symbol sequence received from the SN, before re-encoding and transmitting it to the DN. The MI conveyed to the DN is given by

$$I_{DF} \leq \min\left\{\frac{1}{2}\log_2\left(1+|a_{s,r}|^2\frac{P_s}{N_0}\right),\frac{1}{2}\log_2\left(1+|a_{s,d}|^2\frac{P_s}{N_0}+|a_{r,d}|^2\frac{P_r}{N_0}\right)\right\}. \tag{1.12}$$

Once again, if the SN-DN link is undergoing severe fading, it may be ignored, hence the MI is given by

$$I_{DF} \leq \min\left\{\frac{1}{2}\log_2\left(1+|a_{s,r}|^2\frac{P_s}{N_0}\right),\frac{1}{2}\log_2\left(1+|a_{r,d}|^2\frac{P_r}{N_0}\right)\right\}. \tag{1.13}$$

In other words, using the DF protocol while ignoring the SN-DN link, the MI is intuitively limited by the MI conveyed on either the SN-RN or the RN-DN links.

## 1.5 State-of-the-Art Literature Review of Energy-Efficient OFDMA Systems

As mentioned above, due to the scarcity of radio resources and the ever-higher capacity requirements, intelligent radio resource management (RRM) has become an important concern in current and future wireless networks [45, 46]. A stylized overview of the interplay amongst RRM techniques is provided in Fig. 1.7, which will be further discussed in the following. Furthermore, several studies, surveys and magazine articles investigating the general energy-efficiency issue and energy efficient RRM methods are available as exemplified by [11, 13, 14, 47–64].

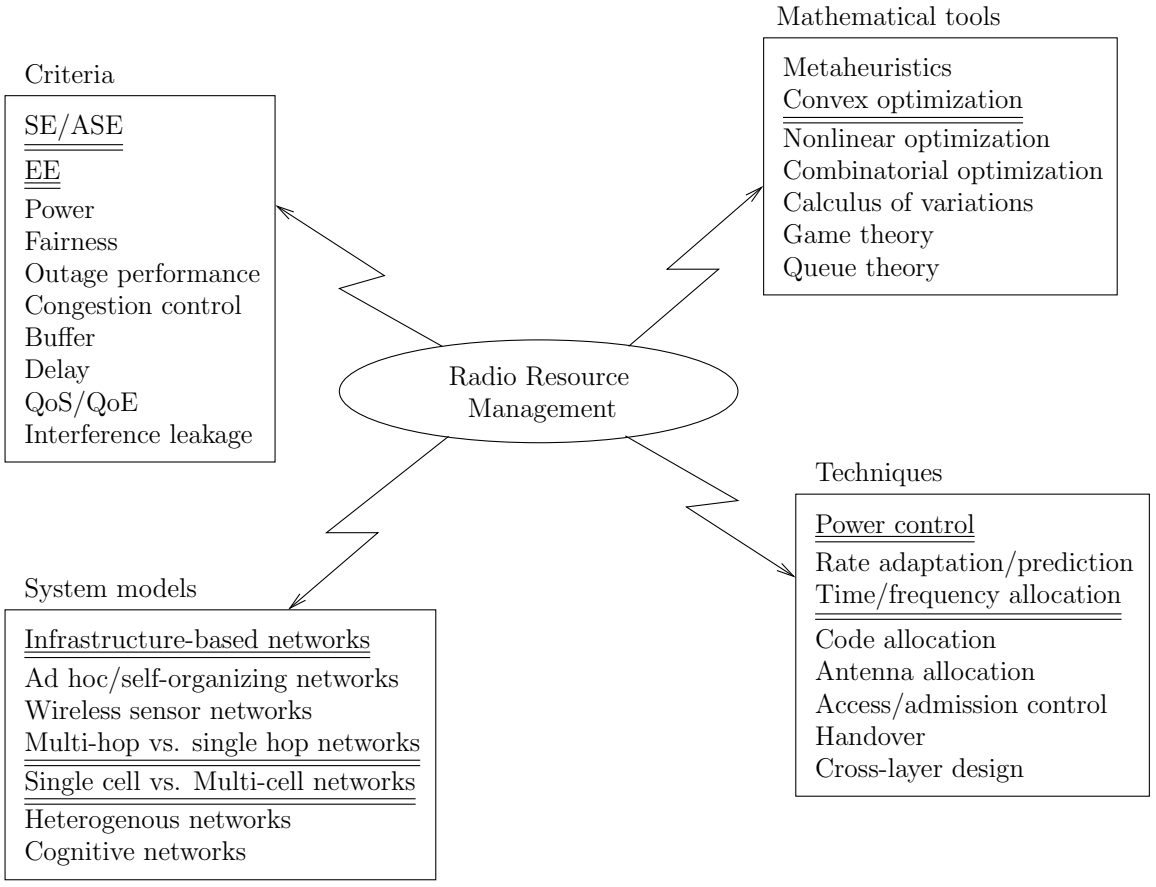


FIGURE 1.7: An overview of the major topics related to radio resource management.

### 1.5.1 Resource-Allocation Criteria

The optimization objectives of RRM shifted from high spectral-efficiency, which is measured in [bits/sec/Hz], or throughput [65–67], which is measured in [bits/sec], to high area-spectral efficiency [4, 68] measured in $\left[\text{bits/sec/Hz/m}^2\right]$. Concurrently, energy efficiency ([bits/Joule/Hz]) has become a grave concern [10, 11, 14, 55, 69–71], which is sometimes addressed by minimizing the power required for supporting the target performance criterion [72–80]. However, minimizing the power consumption is typically not equivalent to maximizing the EE [55].

On the other hand, due to the need for simultaneously satisfying several users, the issues of user-fairness [81–86] and outage performance [78,87,88] arose, with the objective of ensuring that the users are not 'rate-starved'. Furthermore, congestion control [83,86,89–92] aims for carefully managing the resources so that none of the wireless links are over-utilized, while buffer overflow also is avoided [86, 93]. Additionally, current devices are often required to support real-time interactive applications, such as voice and video, which come with their own service criteria. Often, this manifests itself as a restriction imposed on the maximum tolerable end-to-end delay [94, 95], or requirements in terms of quality-of-service (QoS) [33,

81, 82, 96–106], or even quality-of-experience (QoE) [107–109]. Naturally, wireless networks have to share the wireless spectrum, and it is beneficial to control the amount of interference that each transmitter inflicts [110–112].

### 1.5.2 System Model

Classic RRM is more naturally implemented in infrastructure-based networks, such as cellular systems [32, 46, 84, 85, 99, 100, 102, 113–123], wireless local area networks (WLANs) [98, 106, 114, 124–126] and paging systems [4], which all benefit from the assistance of access points (or BSs), when implementing centralized RRM algorithms. On the other hand, ad-hoc networks [81, 90, 96, 127–129], self-organizing networks [130–135] and wireless sensor networks [20, 136–139] have to distributively coordinate their own transmissions, which are typically of multi-hop nature. Although the traditional infrastructure-based networks are of single-hop nature, current networks may invoke relaying [20, 21, 65, 76, 88, 104, 140–155] for extending the wireless coverage or for improving the link reliability. RRM is further complicated, when there are multiple simultaneous transmitters, as in multi-cell networks [66, 94, 115, 156–160], and multi-tier (heterogeneous) networks [70, 133, 161–166]. This problem is further exacerbated, where there is no coordination amongst the transmitters, as exemplified by a cognitive network [67, 70, 78, 111, 126, 167–172], where the primary and secondary users belong to separate networks.

### 1.5.3 Resource-Allocation Techniques

Traditional RRM techniques include power control [32, 88, 91, 118, 135, 140, 149, 153, 159, 173–176], rate control or prediction [33, 132, 175, 177, 178], as well as the allocation of time and frequency resources [32, 75, 77, 109, 111, 149, 156, 159, 175, 179]. In the case of code-division multiple-access (CDMA) systems, code allocation is an important consideration [85, 124, 157, 167]. Furthermore, MIMO systems may employ antenna allocation [71, 80, 126, 180, 181]. In the case of infrastructure-based networks, the access points can perform access/admission control [69, 101, 163, 182–185] for ensuring that the network does not become oversubscribed. Additionally, handovers in cellular systems ensure that a smooth service is provided for the users [97, 101, 186]. All of these techniques can be applied simultaneously and harmoniously by utilizing cross-layer design for jointly fulfilling the objectives of RRM [33, 104–106, 137, 139, 187–190].

### 1.5.4 Mathematical Tools for Resource Allocation

The tools available for RRM include meta-heuristic based techniques [103, 115, 119, 127, 150, 191], such as genetic algorithms [192, 193], ant-colony optimization [79, 155, 176, 194]

and particle swarm optimization (PSO) [195, 196]. Typically, these algorithms are of low-complexity and are capable of finding acceptable solutions, but without any guarantees of optimality. On the other hand, convex optimization [121, 154, 170, 172, 197] can be implemented in form of both distributed and centralized algorithms, which are capable of finding optimal solutions at the cost of additional complexity. In the case of non-linear non-convex, and combinatorial optimization problems, the optimal or near-optimal solutions can still be found through reformulations, relaxations or by exploiting the specific system model [21, 22, 71, 120, 181, 198–202]. Additionally, these mathematical optimization techniques can be generalized under the umbrella of calculus of variations [203] for solving a wider range of problems. Efficient RRM may also be performed based on game-theoretical principles [14, 69, 70, 112, 128, 129, 147, 175, 204], which can model the RRM function as a non-cooperative [69, 72, 74, 148, 151, 152, 162, 164, 171, 173, 174, 205–208] or cooperative (coalition) game [14, 161, 169, 183, 209–211], resulting in Nash equilibria or Pareto optimal solutions, respectively. In the case of congestion controlled delay-constrained services, queuing theory [69, 83, 86, 92, 182, 185, 187, 212, 213] is often useful in making RRM decisions.

In this thesis, we focus our attention on convex optimization techniques invoked for maximizing either the spectral-efficiency or energy-efficiency through power and subcarrier allocation in multi-user, multi-cell, relay-aided, OFDMA cellular networks, which are related to the topics seen in Fig. 1.7. Due to the nature of the topic at hand, it is beneficial to limit our focus to topics closely related to homogeneous OFDMA cellular networks in order to offer a concise literature review.

### 1.5.5 Energy-Efficient Resource Management in Conventional OFDMA Cellular Networks

Some of the earliest studies of energy-awareness in communication channels were performed by Kwon *et al.* [232], Gallager [233] and Verdu [234]. Kwon *et al.* [232] introduced the energy-efficiency (EE) metric of

$$\frac{C}{S} \ [\text{bits/Joule}], \tag{1.14}$$

where $C$ is the well-known channel capacity, while $S$ is the signal power. Gallager [233] studied cost-limited channels, while Verdu [234] introduced the capacity per unit cost given by $C(\beta)/\beta$, which was subsequently employed in various network scenarios.

Later on, energy-awareness shifted away from the information-theoretic perspective to the protocol and algorithm design perspectives, as demonstrated by Wu *et al.* [235], Rulnick *et al.* [236, 237], and Zorzi *et al.* [238]. In [235], the authors presented an energy-efficient caching protocol for both reducing the bandwidth required by the wireless network and for reducing its battery power requirements. A single point-to-point link was studied in [236, 237], where the aim was to maintain a certain QoS in the face of arbitrary interference. Thus, an

| Reference | Year(s) | Summary of contribution |
|---|---|---|
| Wong *et al.* [23, 214] | 1999 | Formulated the total power minimization problem based on subcarrier allocation and bit-loading. A suboptimal method is employed for allocating subcarriers, then optimal bit-loading is performed. |
| Kivanc *et al.* [215, 216] | 2000-2003 | Built upon [23, 214] by developing low-complexity algorithms for the optimization problem. The resources required by each user are computed, which aided the subcarrier allocation. |
| Kim *et al.* [217, 218] | 2001-2006 | Reformulated [23, 214] as an ILP. Suboptimal subcarrier allocation is performed based on the relaxed ILP. |
| Seong *et al.* [219] | 2006 | Demonstrated that solving the power minimization problem with relaxed subcarrier constraints is asymptotically-optimal as the number of subcarriers increases. Their results showed that just 8 subcarriers is sufficient for this to be true. |
| Miao *et al.* [220–225] | 2008-2012 | Considered uplink EE with subcarrier allocation and rate adaptation. Optimal algorithms are presented. Problems featuring objective functions based on arithmetic and geometric averages of the EE are also solved. Interference-limited scenario is later considered using a game theory approach. |
| Isheden *et al.* [226, 227] | 2010-2012 | Provided a unifying framework for EE maximization. Solutions based on both Dinkelbach's method and the Charnes-Cooper transformation are studied. |
| Xiong *et al.* [228–231] | 2011-2012 | Presented methods to characterize the SE-EE tradeoff curve in both the DL and the UL. |
| Ng *et al.* [201] | 2012 | BS cooperation is employed for transmitting to multiple users without interference. The EE maximization problem is solved using suboptimal user selection and ZF combined with Dinkelbach's method. |

TABLE 1.1: A selection of the prominent contributions in the field of resource allocation for energy-efficiency in OFDMA cellular networks.

algorithm was developed for dynamically minimizing the transmit power. The authors of [238] studied the performance of various error control protocols conceived for different transmit power profiles. Although the metric of (1.14) was defined as early as 1986 [232], in terms of energy-awareness, the widely adopted mentality was to minimize the total transmit power, while the per bit power metric did not enjoy widespread use until much later. A selected list of notable contributions on this topic is provided in Table 1.1.

The seminal work of Wong *et al.* [23, 214] first investigated minimizing the total transmit power subject to subcarrier allocation constraints. The problem was reminiscent of the classic resource assignment problem. Rate constraints were introduced [23], and the binary constraints imposed on the assignment variables were relaxed for the sake of obtaining the optimal solution. Suboptimal heuristic algorithms were presented in [23] as low-complexity alternatives. The authors of [215,216] extended the previous work in [23] by presenting some lower-complexity alternatives based on determining the resources necessary for each user, and then assigning the available subcarriers based on these requirements. An alternative approach was adopted by Lee *et al.* [239], who grouped the subcarriers according to their channel gains, and allocated the bits to each group instead of each individual subcarrier. Kim *et al.* [217,218] reformulated the nonlinear problem of [23] as an integer linear programming (ILP) problem, and employed suboptimal subcarrier allocation based on the relaxation of the ILP. Single-user orthogonal frequency division multiplexing (OFDM) bit loading was then performed. The authors of [240] built upon the contribution of [214] to include the QoS constraints expressed in terms of rate and bit error rate (BER) requirements. The so-called Hungarian algorithm [241] was employed for obtaining the optimal subcarrier allocation matrix. Suboptimal heuristic methods were also presented in [240]. Liang *et al.* [242] adopted the approach of linearizing the objective function without sacrificing the optimality of the final solution. The ILP was thus transformed into a binary linear programming (BLP) problem and solved at a reduced complexity.

Li *et al.* [243] presented an alternative approach based on sectorizing the macrocell, before employing a heuristic method for subcarrier and bit allocation to minimize the total transmission power subject to specific minimum rate and maximum symbol error rate (SER) constraints. On the other hand, [244] incrementally assigned blocks of subcarriers according to particular rate and BER requirements in order to minimize the total transmission power.

Zhang *et al.* [245–247] adopted a cross-layer approach by employing a packet error rate (PER) constraint for ensuring error-free packet transmission at the medium access control (MAC) layer. Thus, fair queuing was emulated at the MAC layer and various packet scheduling schemes were employed. Both optimal, as well as relaxed and linear programming (LP)-based algorithms were proposed for obtaining the solution. A single-cell system was considered in [248], where the authors implemented a low-complexity algorithm for jointly optimizing the power allocation, bit-loading, automatic repeat-request (ARQ) transmissions, and adaptive modulation and coding (AMC) scheme. Similarly, Han *et al.* [249] employed a heuristic algorithm for selecting the modulation and coding scheme (MCS) for each user and for assigning subchannels to users. In another vein, Zarakovitis *et al.* [250] modeled the packet arrival process and imposed a maximum delay constraint. Furthermore, a robust bit-loading algorithm was employed for guarding against channel variations. The resultant optimization problem was shown to be convex after the binary constraints were relaxed.

The authors of [219] showed that the subcarrier and power allocation problem is non-convex, but solving its dual problem with the aid of relaxation is asymptotically optimal as the number of subcarriers increases. As a further advance in the field, Mao *et al.* [251] presented an efficient branch and bound method for allocating subcarriers. Two suboptimal algorithms were also presented. By contrast, the authors of [252] developed suboptimal algorithms based on a branch and bound technique combined with dynamic programming. Akbari *et al.* [253] performed sequential subcarrier allocation, followed by power allocation for maximizing the EE in a DL scenario. They presented solutions based on both time-sharing as well as without time-sharing of the subcarriers. However, they observed that employing time-sharing reduces the complexity involved, while resulting in an improved performance. The authors of [254] studied the UL, and presented a pair of suboptimal algorithms. On the other hand, Xu *et al.* [255] additionally took into account the DL energy consumption of the receiver in their problem formulation, where a quantum PSO algorithm was employed for obtaining the solution. Lim *et al.* [256] studied a network employing multiple radio access technologies (RATs).

Several authors studied the EE in multi-cell scenarios. For example, the authors of [257] assumed interference averaging and presented several algorithms for finding the solution to the power minimization problem. On the other hand, the authors of [74] adopted a game theoretical approach to the power-, rate- and subcarrier-allocation problem by modeling the network as a non-cooperative game with a referee. This referee regulates both the subcarrier usage as well as the rate requirements of every user in order to maximize the system-wide performance metric. Abrardo *et al.* [117,258] modeled the resource allocation problem cast in the context of a total power minimization as a network flow problem using graph theory. The resultant ILP is complex, hence suboptimal algorithms were presented for obtaining solutions at an affordable complexity. The authors of [259] studied the UL counterpart of [117, 258], but relaxed the integer constraints in order to formulate the problem as a LP. A heuristic and distributed algorithm was proposed for its practical implementation. By contrast, the authors of [260] employed a simple algorithm, which minimized the total transmission power and then performed subcarrier allocation for minimizing the maximum outage probability, while Bang *et al.* [261] investigated fractional frequency reuse and BS coordination for developing a suboptimal algorithm for minimizing the total power consumption. The authors of [262] modeled the uplink of a multi-cell system as a non-cooperative so-called potential game, where selfish users unconsciously benefit the overall network EE by adapting their transmit powers and subcarrier allocations. Venturino *et al.* [263] considered the sum EE of a multi-cell system, and proposed a suboptimal heuristic algorithm for solving the user scheduling and power allocation problem. Furthermore, an optimal algorithm was presented for a noise-limited scenario, where the interference terms were ignored. The same authors later considered clustering the BSs for the sake of coordinating their resource allocation objectives in [264]. Suboptimal algorithms were presented for optimizing diverse objective

functions based on the global EE as well as on the sum, or product of each BS's EE. Optimal algorithms were again presented for the noise-limited scenario. On the other hand, Liu *et al.* [265] presented a two-step algorithm, which obtains the Pareto-optimal power allocation values by modeling the problem as a non-cooperative super-modular game. Based on the optimal power allocation, the optimal subcarriers were chosen by examining the resultant signal-to-interference-plus-noise ratio (SINRs).

The normalized per bit EE metric of (1.14) was employed in [220], where Miao *et al.* studied the uplink of an OFDMA system in a flat fading channel. The Lagrange multiplier method was employed for obtaining the optimal subcarrier allocations, while the EE-optimal system rate was obtained based on the relationship between the transmission power and rate. This work was extended in [221,224] to frequency-selective fading channels, although only a single user was considered. Two algorithms were conceived for obtaining the optimal solution. Subsequently, lower-complexity algorithms were presented in [223, 225], which employed the exponentially time-averaged rate and the energy consumed in the objective function of each user. The scheduling metric was based on the arithmetic or geometric mean of each user's objective function. An interference-limited scenario was studied in [222], which proposed algorithms for solving the cooperative two-user and non-cooperative multi-user EE problems. Andreev *et al.* [266] later invoked the solution presented in [223,225] in a WiMAX network. An interference-aware power control algorithm was proposed for improving the cell-edge users' performance. By contrast, the reciprocal of the EE metric was minimized in [267], where the authors ordered the users according to their respective channel gains, and exploited the convexity of the objective function for developing a low-complexity algorithm for finding the EE-optimal system's rates and power variables. This work was then extended to multi-cell scenarios in [268].

The DL SE-EE tradeoff of power and subcarrier allocation was studied in [228, 229], where both the upper and lower bounds of the optimal SE-EE curve was obtained via dual decomposition and relaxation, respectively. A suboptimal algorithm was also presented for approaching this curve. This work was extended in [230, 231] to include the uplink scenario and to obtain the optimal solution by evaluating every possible subcarrier allocation. On the other hand, the same authors studied the EE-delay trade-off in [269, 270] using the concept of *effective capacity* in their problem formulation. The relaxed problem was solved to obtain a tight upper bound to the original solution. Furthermore, the EE-delay trade-off curve was also characterized. The authors later studied the optimal EE trade-off in the UL versus DL in a single cell system [271], where the users can harvest energy from the received DL signal for use in the UL. Then the multi-objective problem was transformed into a single-objective problem, where the subcarrier allocation constraints were subsequently relaxed. A branch and bound type algorithm was proposed for finding feasible weights for the formulating the single-objective function.

On the other hand, the authors of [272] also studied the SE-EE trade-off both in a single cell system and a multi-cell system. They observed that small cells and beamforming are preferred for EE. Furthermore, Zheng *et al.* [273,274] studied the SE-EE trade-off subject to rate constraints in both the UL and DL of a single-cell system. The optimal water level was determined for each user and suboptimal subcarrier allocation was employed for obtaining an appealing trade-off. Tang *et al.* [275] considered the SE-EE trade-off in the single cell DL scenario, while employing a resource efficiency metric, which was based on a combination of the SE and EE. Linear scalarization was employed again, and both optimal as well as suboptimal methods were proposed for solving the resultant single-objective problem. By contrast, a PSO based approach was pursued in [276] for optimizing the combined SE and EE objective function.

Ng *et al.* [201] employed Dinkelbach's method for maximizing the EE in a multi-cell system, subject to both user-rate and backhaul-capacity constraints. BS cooperation was assumed and the BSs formed a multiple antenna aided system employing ZF transmit beamforming, which eliminated the interference. Similarly, Haider *et al.* [277] employed Dinkelbach's method, but in a single cell system operating under rate constraints, where the branch and bound technique was used for finding the optimal subcarrier allocations. Loodaricheh *et al.* [278] also employed Dinkelbach's method in a single cell system, but utilized user cooperation for increasing the attainable EE performance. On the other hand, the authors of [279] relaxed the subcarrier allocation constraints to solve a similar problem at a reduced complexity. Shi *et al.* [280] demonstrated that OFDMA is the optimal multiple access method, when aiming for maximizing the EE in the single cell DL system, and presented algorithms based on Dinkelbach's method, for obtaining the optimal solution. Ng *et al.* [281] later studied the EE of a single-cell network, where the BS was equipped with an energy harvester. Offline EE maximization was performed with the aid of relaxation and Dinkelbach's method. However, the online optimization based on a dynamic stochastic method is excessively complex, hence a suboptimal algorithm was proposed. Dinkelbach's method was compared to other methods in [226, 227], which provided a unified framework of EE maximization.

| Reference | Year(s) | Summary of contribution |
|---|---|---|
| Klein *et al.* [282] | 2007 | Total power minimization is considered for a single cell scenario with simultaneous direct and relaying links. The subframe duration of the first hop is determined, followed by subcarrier allocation. The optimal bit and power allocations are then obtained by formulating and solving a LP problem. |
| Ma *et al.* [283] | 2008 | Total power minimization is considered for a three node network. Either the AF or DF protocol is invoked. Bit and power loading algorithms are proposed for either fixed or variable power ratios of the source and relay. |
| Girici *et al.* [284, 285] | 2008-2009 | Focused on DF relaying without direct links. The weighted total power minimization problem requires a complex solution algorithm. Therefore, a suboptimal method is proposed, which chooses the number of subcarriers and subframe duration, then applies subcarrier allocation and water-filling based power allocation. |
| Ho *et al.* [286] | 2011 | By contrast to the above, an UL scenario is considered, where relays employ the DF protocol, and an exponentially time-averaged EE metric is maximized. A low-complexity scheme is developed for power, subcarrier and relay allocation. |
| Joung *et al.* [27, 287] | 2011-2012 | Total power minimization subject to minimum SINR constraints is studied. Direct, and AF or DF relay-aided transmissions modes are available. A sequential heuristic algorithm is proposed for choosing the communication mode and performing the subcarrier allocation. |
| Zhang *et al.* [288] | 2013 | Joint subcarrier assignment, bit and power allocation is performed for the UL of a multiuser system. A suboptimal greedy algorithm is developed based on subcarrier permutations, while a more efficient algorithm using bisection method is later proposed. |
| Chen *et al.* [289] | 2014 | Total total power minimization in the DL of a multi-relay network using discrete modulation levels. A suboptimal algorithm is proposed, which consisting of a simple relay selection method, then a resource allocation method using virtual direct transmissions. |

TABLE 1.2: A selection of the prominent contributions in the field of RA for EE in relay-aided OFDMA cellular networks.

### 1.5.6 Energy-Efficient Resource Management in Relay-Aided OFDMA Cellular Networks

Although EE has been extensively studied in conventional cellular networks, the EE of relay-aided cellular networks has only recently become a subject of interest. Most of the existing literature considers fairness or sum-rate maximization [20–22, 199]. Here we exclude articles from this review regarding user cooperation, since user cooperation requires that both the relay and the user benefit from relaying, which is not the case in the classical relay-aided networks. Nonetheless, three-node networks and two-way relaying can be readily conceived with cellular networks, which are hence included in this literature review. A summary of some selected contributions on this topic is listed in Table 1.2.

In [282], Klein *et al.* studied the total power minimization problem in a single cell DF relay-aided network, which supports simultaneous direct and relaying links. The time duration of the first hop subframe was determined, before subcarrier, bit and power allocation was performed using the LP solver of [218]. Similarly, Wang *et al.* [290] considered both direct and relayed transmission in the context of total power minimization problem. However, the mode selection variable was relaxed and the problem was suboptimally solved using a duality approach and the Hungarian method. By contrast, Girici *et al.* [284, 285] assumed that the direct link was weak and hence only considered the relaying links and proposed a suboptimal procedure to compute the subframe durations and the number of subcarriers required by each link, before subcarrier allocation and power allocation was carried out based on water-filling. Chen *et al.* [289] formulated the power minimization problem in conjunction with discrete modulation levels and proposed a suboptimal algorithm relying on a simple relay selection method.

Some authors studied the effects of partial or outdated CSI. For example, Song *et al.* [291] assumed only the availability of statistical knowledge of the users' channels and proposed a suboptimal algorithm based on the dual problem formulated for relay selection, as well as for power and subcarrier allocation in order to minimize the total transmit power, while supporting a certain rate requirement. On the other hand, the authors of [292] assumed having outdated CSI, but also employed the dual problem for developing an algorithm for performing the resource allocation.

Xiao *et al.* [25, 293] adapted the transmission power of the first and second hops for ensuring that both links are capable of supporting the same rate. The same authors later studied the power minimization problem in a multi-cell scenario and employed non-cooperative game theory for developing a distributed algorithm to balance the rate achieved on both the first and second hop links for preventing the assignment of excessive power, while reducing the interference imposed. Joung *et al.* [27, 287] also studied the multi-cell scenario and incorporated both the direct as well as the AF or DF relaying links. A sequential heuris-

tic algorithm was developed for selecting the most appropriate communication mode and the subcarrier allocations. The multi-cell network can also be viewed as a multiple-source multiple-destination network. In [294], Wang *et al.* employed an objection function, which strikes a balance between the total power minimization and maintaining fairness for the users of a multiple-source multiple-destination network in terms of their guaranteed rate. The optimal power and subcarrier allocations were obtained using a dual approach. Although, the subcarrier selection variables were relaxed, it was shown that the optimal configurations were still found. Banizaman *et al.* [295] aimed for minimizing the total energy consumption, but observed that obtaining the optimal solution is too complex and may lead to unfairness. Thus, they developed a suboptimal algorithm for performing sequentially user selection, followed by relay and subcarrier selection, then finally by power and bit allocation. Huang *et al.* [296] also attempted to promote fairness and assigned weights to each packet according to their importance. The problem of carefully allocating the time domain, subcarrier, bit and power resources for minimizing the total energy consumption was formulated as an integer problem, which is excessively complex. Consequently, a suboptimal three-step algorithm was proposed.

The relay-assisted UL was studied in [286], where Ho *et al.* employed DF relays and maximized the exponentially time-averaged EE metric using a low-complexity algorithm for power, subcarrier and relay allocation. By contrast, Jiang *et al.* [297] proposed a suboptimal algorithm based on decomposition. Initially, subcarrier allocations were obtained for each user assuming equal power and bit allocation, then bit and power allocation was performed using a bisection search. Fairness was later considered to develop another algorithm. On the other hand, Zhang *et al.* [288] performed joint subcarrier assignment, as well as bit and power allocation using a greedy algorithm, which considers every possible permutation of the legitimate subcarrier assignments. A suboptimal algorithm based on a bisection search was also proposed. Similarly, Hao *et al.* [298] employed joint optimization for the sake of maximizing the EE. Dinkelbach's method was used for solving the problem optimally, while two lower-complexity algorithms were proposed for subcarrier pairing.

A three node network was considered in [283], where bit and power loading algorithms were proposed for either AF or DF relaying protocols in order to minimize the total energy consumption, while supporting fixed or variable power ratios of the source and relay. Yu *et al.* [299] also studied the EE maximization problem in the context of a three node network. However, they employed the AF protocol and devised a pair of algorithms for power allocation. One of their algorithms relies on an approximation assuming a high SNR and results in a low-complexity solution algorithm. The alternative is a higher-complexity solution, which does not rely on the aforementioned approximation. The authors of [300] formulated the subcarrier and power allocation as a mixed binary problem and proposed a suboptimal solution of separate subcarrier allocation and power allocation. Likewise, Chen *et al.* [301] studied the EE maximization problem in a three-node network featuring an AF relay. Their

low-complexity power allocation algorithm relies on subcarrier matching of the first and second hop links for forming a virtual direct link. On the other hand, Sun *et al.* [302] studied the EE maximization problem using bit allocation in a three node network subject to a requirement on the minimum number of bits transmitted. Their solution consisted of hybrid one-way and two-way relaying on separate subcarriers. Initially, the number of subcarriers required by each source was determined and then the optimal indices were found using a bisection search. Subsequently, optimal power and bit allocations were obtained based on classical water-filling. Chen *et al.* [303] also considered two-way relaying, but aimed for minimizing the total energy consumption in the network subject to specific queue stability constraints. They formulated and solved the associated convex optimization problem and subsequently designed a scheduling protocol based on their results. Similarly, Chang *et al.* [304] minimized the total energy consumption in a two-way relaying network using a low complexity phase, subcarrier and power allocation algorithm. The authors of [305] incorporated exclusive or (XOR)-based network coding into their two-way relaying network and proposed a suboptimal algorithm for power-aware relay selection and for opportunistic network coding. On the other hand, Liu *et al.* [306] did not consider network coding, but devised a three part suboptimal algorithm consisting of relay selection and subcarrier assignment, subcarrier pairing, as well as rate and power allocation for a two-way multi-relay network. By contrast, the authors of [307] invoked a full-duplex relay and modeled the subcarrier as well as power allocation as a three-stage Stackelberg game. The subgame-perfect equilibrium was analyzed for each stage using the backward induction method and an iterative algorithm was proposed to obtain this result.

| Reference | Year(s) | Summary of contribution |
|---|---|---|
| Hu *et al.* [308, 309] | 2004 | Employed eigendecomposition for obtaining the transmit and receive beamformers. Users corresponding to the maximal eigenvalues are chosen, and a greedy bit allocation algorithm minimized the total power. |
| Zhang *et al.* [82, 310, 311] | 2003-2005 | SVD-based MF is employed for the transmit and receive beamformers. A complex greedy algorithm and a lower-complexity alternative for bit and subcarrier allocation minimized the total power. These were extended to ZF and MMSE receiver types, where users were chosen according to their spatial correlations for reducing the resultant CCI. |
| Ho *et al.* [77, 312] | 2008-2009 | Similar to [82, 310, 311], but uses a Lagrangian method for resource allocation that approaches optimality as the number of subcarriers increases. |
| Kim *et al.* [313, 314] | 2008-2010 | Modeled the link adaptation problem as a GP problem of obtaining the optimal number of spatial streams, number of antennas, use of spatial multiplexing or STBC, constellation size, bandwidth, transmit power and choice of ML or ZF for MIMO decoding. The GP was solved with efficient convex optimization algorithms. |
| Prabhu *et al.* [315] | 2010 | Minimized the EPG of a SVD-based system using Dinkelbach's method, and evaluated multiple antenna configurations. |
| Ng *et al.* [71, 200] | 2012 | MRT beamforming is employed, which chooses users corresponding to the highest eigenvalue of the channel correlation matrix. The ratio of the weighted outage capacity over the total energy consumption formulated with multiple variables and was maximized with Dinkelbach's method. MRT is later employed in a cellular system with physical-layer security enhancements. |
| Xu *et al.* [316] | 2013 | Also employed SVD-based MF beamformers, but proposed a three-step searching algorithm to firstly find the continuous variable solution for the number of subcarriers occupied by each user based on the KKT conditions, then optimize the number of active RF chains, and finally discretize the number of subcarriers for each user with the optimal number of active RF chains. |

TABLE 1.3: A selection of the prominent contributions in the field of resource allocation for energy-efficiency in MIMO-aided OFDMA cellular networks.

### 1.5.7 Energy-Efficient Resource Management in MIMO-OFDMA Cellular Networks

The employment of multiple antennas in communication networks has grown in popularity as a benefit of their linear capacity improvement, whilst only logarithmic capacity increases are possible upon increasing the transmission power of a single-antenna system. In terms of sum rate maximization or EE optimization, the conventional approach is to design beamformers, which decouple the links between multiple transmit and receive antennas into several angularly selective links. Consequently, the traditional resource allocation techniques designed for single antenna aided systems can be readily applied. A summary of the notable contributions in this area is provided in Table 1.3.

A natural choice for the beamforming matrices designed for maximizing the sum rate are the matched filter (MF) matrices of the transmitter and receiver [317], which can be obtained by employing the singular value decomposition (SVD) of the MIMO channel matrix. Thus, the effective channel matrix is diagonalized and the remaining nonzero elements can be employed as the channel gains in the traditional water-filling algorithm.

In [82, 310, 311], Zhang *et al.* employed the aforementioned technique for a multiuser DL system. A complex greedy algorithm and a suboptimal lower-complexity alternative were proposed for obtaining the optimal bit and subcarrier allocation to minimize the total power. The authors later extended their work to both ZF and minimum mean-squared error (MMSE) receiver types, while taking into account the spatial correlations of the users in order to reduce the CCI. Similarly, Ho *et al.* [77, 312] employed SVD-based MF beamforming matrices, but used a Lagrangian approach for solving the resultant optimization problem. They proved that their solution is asymptotically optimal, as the number of subcarriers increases. Similarly, Prabhu *et al.* [315] considered SVD-based beamforming, but minimized the energy-per-goodbit (EPG) of the system using Dinkelbach's method. Xu *et al.* [316] instead adopted a three-step search algorithm to first find the continuous variable solution for the number of subcarriers occupied by each user based on the Karush-Kuhn-Tucker (KKT) conditions, before optimizing the number of active RF chains, and finally discretizing the number of subcarriers for each user in conjunction with the optimal number of active RF chains. SVD-based beamformers were also employed in [304, 318], where the authors formulated a joint resource allocation problem to determine the optimal antenna, subcarrier, transmission power configuration to minimize total energy consumption of the system. Zhao *et al.* [319] proposed optimal and suboptimal algorithms for obtaining the subcarrier, antenna, time slot, and power configurations for minimizing the total power in a high-speed railway network, where SVD-based beamformers were employed. Xiao *et al.* [320, 321] extended their previous work in [279] to MIMO-aided systems, and employed the SVD to find the interference nulling precoders for each user. Again, the SVD was employed to decompose the effective channel matrix for obtaining the MF beamformers, thus

diagonalizing the effective channel matrix. On the other hand, Liu *et al.* [322] considered full duplex MIMO-aided relaying in the DL and employed both Dinkelbach's method and discrete stochastic optimization methods for solving the associated energy-efficient resource allocation problem at a low-complexity.

Using the ZF beamformer facilitates serving multiple users on the same subcarrier without interference, although the effective channel gains will be lower than those obtained, when using MF based beamformers. For example, in [323], Shin *et al.* used ZF for eliminating the interference amongst the users selected by employing the user selection algorithm of [324]. She *et al.* [325] performed scheduling based on either dirty paper coding (DPC), ZF-DPC or ZF transmitters and employed waterfilling after determining the number of subcarriers assigned to each user. On the other hand, Kim *et al.* [313, 314] included maximum likelihood (ML) decoding, as well as ZF in their optimization problem. The reciprocal of the EE metric was minimized and the authors specifically formulated a GP problem for obtaining the optimal configuration in terms of the number of spatial streams, number of antennas, the choice of spatial multiplexing versus space-time block code (STBC), the constellation size, bandwidth, transmit power and decoding method. The GP problem was then efficiently solved using standard convex optimization techniques. Ersalan *et al.* [326–328] considered MMSE receivers in addition to ZF. Their EE metric consisted of a realistic modeling of the PER and it was maximized by choosing the optimal transmission mode, which encapsulates the transmission power, the number of spatial streams, number of antennas, modulation type and coding rate.

By contrast, Hu *et al.* [308, 309] employed the eigendecomposition to the MIMO channel matrix for designing the array weights of the transmit and receive beamformers. The users were selected based on the resultant eigenvalues, and a greedy algorithm was employed for bit allocation. Zappone *et al.* [329] considered maximum ratio combining (MRC) receivers in a multi-cell UL network and formulated a non-cooperative potential game for joint subcarrier allocation and transmit power control for the sake of maximizing the EE. On the other hand, Ng *et al.* [71, 200] employed maximum ratio transmission (MRT) beamformers at the BS, which had array weights obtained as the eigenvectors of the channel matrices corresponding to the highest eigenvalues. Dinkelbach's method was invoked for maximizing the ratio of the weighted outage capacity over the total energy consumption by finding the optimal power allocation, data rate adaptation, antenna allocation and subcarrier allocation. In [200], the same authors considered a similar system in the context of providing physical-layer security enhancements. They injected the transmitted signal with artificial noise, which was pre-nulled for the intended receivers.

## 1.6 Organization and Novel Contributions of this Thesis

We have previously discussed the motivation of this thesis and discussed some of the fundamental building blocks of wireless communication systems, which will be employed extensively in future chapters. Now that a state-of-the-art literature review has been performed, we present the organization of this thesis and highlight the novel contributions.

### 1.6.1 Organization of this Thesis

An overview of the structure of this thesis is provided in Fig. 1.8. As alluded to above, this thesis focuses on SEM/EEM of multi-user multi-relay OFDMA cellular networks. In particular, each chapter will explore progressively more complex system models, which require sophisticated transmission protocols and optimization models in order to develop their associated optimization algorithms. To elaborate, in

- **Chapter 2**, we explore convex analysis and optimization, which will form the basis of the work in later chapters. We commence by detailing the differences between convex and nonconvex sets and functions, as well as by providing some intuitive geometric examples to aid the reader. These building blocks can be manipulated by mathematical methods preserving convexity, so that a wide range of functions and sets become identifiable as convex. We then present the standard form of an optimization problem and the necessary conditions for classifying a problem as an instance of convex programming, MINLP, or fractional programming (FP). In particular, we explore solution methods designed for MINLP and FP problems, which typically involve reformulating the original nonconvex problem as a series of convex problems that can be efficiently solved. The concept of duality is presented along with the solution methods derived from satisfying the KKT optimality conditions. We then touch upon decomposition theory and conclude with some examples of convex optimization applied to the wireless communications field.
- **Chapter 3**, motivated by Chapter 1, we study maximizing the EE of a relay-aided OFDMA single-input–single-output (SISO) cellular network with the aid of both power and subcarrier allocation, where each network node is equipped with a single antenna. However, relay selection is not considered, since we assume that each user is associated with the specific relay, which is geographically nearest to itself. An optimization problem is formulated by considering both AF relays and simultaneous direct as well as relaying links on separate subcarriers, which results in a MINLP. However, with a relaxation of the binary constraints on the subcarrier selection variable, the problem is reformulated as a FP problem, and the solution methods detailed in Chapter 2 for this class of problems can be applied. We provided three solution algorithms based on these methods and compared their performance versus complexity trade-offs. Furthermore, we investigated

the SE versus EE trade-offs, when considering the effects of a wide range of system parameters.

- **Chapter 4**, we extend the work of Chapter 3 to MIMO-aided systems. For the sake of simultaneously serving multiple users while achieving a high SE, we develop a transmission protocol based on ZF beamforming, thus effectively removing any CCI amongst the users sharing the same subcarrier. As an additional benefit, the transmission protocol also takes into account simultaneous relaying and direct links using the same subcarrier, which allows for higher flexibility in scheduling decisions. Two user grouping algorithms are presented, which respectively employ an exhaustive search and a lower-complexity method. The problems of user group selection and power allocation for maximizing the SE or EE are formulated based on the optimization framework developed previously in Chapter 3. However, since now DF relays are considered, we adopt the epigraph form of the optimization problem, which leads to a convex formulation after several variable relaxations and transformations. Again, dual decomposition is employed for developing a solution algorithm and the SE versus EE performance of the system is evaluated for a range of parameters.
- **Chapter 5**, the contributions in Chapters 3 and 4 are further extended to multi-cell scenarios. Due to the potentially excessive CCI, we employ the IA technique for developing a pair of distributed transmission protocols, that either ensure that all interference is avoided, or all of the OCI is avoided. We refer to these two protocols as the full-IA and partial-IA protocols, respectively. We then employ the low-complexity grouping algorithm developed in Chapter 4 and formulate the EE maximization problem. We employ various relaxations and variable transformations for reformulating the problem in a convex form, which allowed us to develop a distributed solution algorithm based on dual decomposition. Subsequently, we compare the performance of the full-IA and partial-IA protocols for a range of system parameters.
- **Chapter 6**, we summarize the thesis and propose several future work ideas.

### 1.6.2 Contributions of this Thesis

The contributions of this thesis are centered around novel transmission protocols and algorithms designed for EE maximization in cooperative cellular networks. To elaborate:

- In [330, 331], we formulated the problem of EE maximization in a multiple AF relaying-assisted cellular network, where simultaneous direct and relayed transmissions are employed. The resultant MINLP problem is typically challenging to solve. Thus, we proposed several variable relaxations and transformations for the sake of reformulating the problem in a convex form. Three beneficial solutions algorithms were developed for finding the SE- or EE-optimal power and subcarrier allocations. The performance versus complexity of each algorithm was compared. Additionally, the SE and EE performances

obtained from these algorithms were compared across a wide range of system parameters.

- In [332], we built upon our previous work in [330,331] by incorporating MIMO transceivers into the previous network scenario. The MIMO transceivers are exploited for achieving a spatial multiplexing gain and for the sake of scheduling flexibility by employing a novel transmission protocol, which is based on ZF beamforming. This transmission protocols supports simultaneous direct and relaying links, as well as multiple users, sharing the same subcarrier. Furthermore, we proposed two novel grouping algorithms for obtaining sets of compatible simultaneous direct and relaying links. The first grouping algorithm is based on an exhaustive search of all possible combinations, while the second is a lower-complexity alternative. The problem of choosing the SE- or EE-optimal groups and their associated power allocations was formulated and along with multiple variable relaxations and transformations, the problem was proven to be convex. A solution algorithm based on dual decomposition was developed and the performance of our transmission protocol was evaluated in conjunction with diverse system parameters.
- In [333], we further develop the system model studied in [332] in order to include multiple cells, with multiple relays and multiple users in each cell. For the sake of avoiding the potentially excessive CCI arriving from multiple simultaneous transmitters, the IA technique is employed, and we developed two novel transmission protocols based on this IA technique. The first protocol is termed full-IA, which attempts to avoid any possible source of CCI at the expense of reducing the achievable spatial multiplexing gain. On the other hand, the second protocol is termed as partial-IA and only avoids the CCI generated that was generated within its own cell, thus supporting a higher spatial multiplexing gain than the full-IA protocol. Furthermore, these protocols were designed so that simultaneous direct and relaying links, as well as multiple users, can share the same subcarrier. This benefits the flexibility of the scheduling decisions. Groups of compatible links are found, and the problem of choosing the optimal groups and their power allocations is formulated as an optimization problem, which is then converted into a convex form with the aid of various variable relaxations and transformations. A distributed solution algorithm is then developed for this optimization problem, and the EE performance of the network is evaluated for a wide range of system parameters.

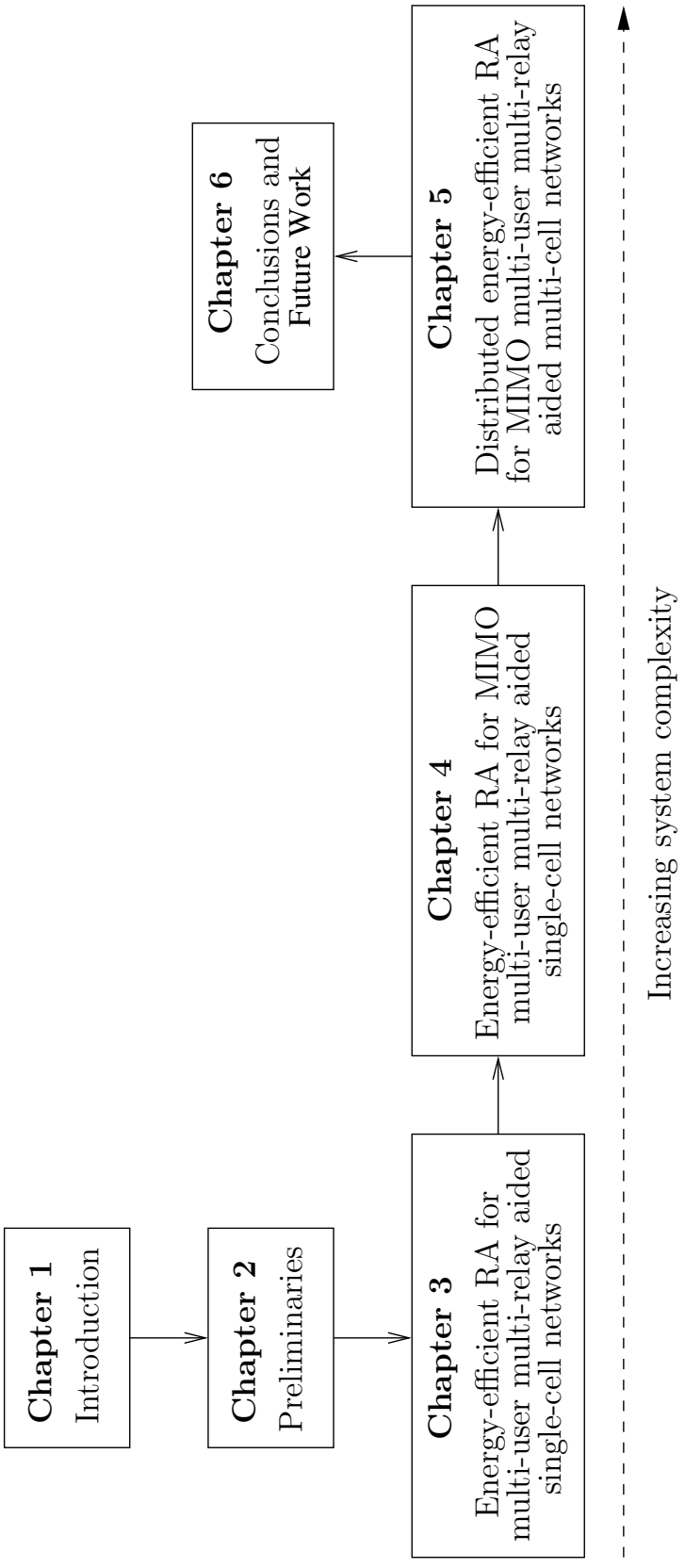


FIGURE 1.8: An illustration depicting the organization of this thesis.

Chapter 2

# Fundamentals of Convex Optimization and its Application Examples

## 2.1 Introduction

In Chapter 1, we examined the introduced the basics of wireless communications theory and provided a literature review for motivating the investigations of the later chapters of this thesis. An important tool, which is gaining progressively more attention in the field is convex optimization, which is introduced in this chapter. Explicitly, we will journey from the basics of convexity and convex functions, through convex optimization problems to their solution methods. We will conclude with some simple and intuitive examples of how convex optimization can be employed in the wireless communications field.

## 2.2 A Brief Historical Perspective of Mathematical Optimization

We commence by briefly reviewing the history of mathematical optimization. For a more complete discussion, we refer the reader to [334].

The earliest examples of mathematical optimization originated from 300 B.C., when Greek mathematicians studied geometry problems requiring optimal solutions. For example, Euclid considered the minimal distance between a point and a line, and the largest area contained within a rectangle with a fixed perimeter length. In 100 B.C., Heron proved that light travels between two points with the shortest path, when reflected off a mirror.

It was not until the 17th century that Fermat proved the gradient of a function vanishes at the extreme points of a function. Importantly, Newton and von Leibniz developed calculus, which paved the way for Johann and Jacob Bernoulli to develop the calculus of variations (CoV), which is a type of generalized optimization. Euler and Lagrange also worked on CoV in the 18th century. In the 19th century, Legendre made contributions towards CoV and developed the least-squares method, which Gauss also claims to have invented. In 1847, Cauchy presented the gradient method.

Research into mathematical optimization intensified in the early to mid 20th century. Jensen introduced convex functions in 1905, using ideas from Hadamard, Hölder, and Stolz. In 1939, Kantorovich presented the LP-model and a method for solving it, which won him and Koopmans a Nobel prize in 1975. During World War II, significant efforts were placed on operations research in conjunction with optimization. Most importantly, in 1947, Dantzig presented the classic Simplex method for solving LP problems, while during the same year von Neumann developed the theory of duality. In 1951, Kuhn and Tucker augmented the optimality conditions for nonlinear problems, which were previously presented in Karush's master thesis. On the other hand, Ford and Fulkerson studied network problems in 1954, which gave birth to the field of combinatorial optimization. An important contribution was made in 1984, when Karmarkar introduced his polynomial time algorithm for solving LP problems, which sparked intense research into interior point methods. Since the 1980s, computer technology has advanced to the point that they became capable of handling heuristic global optimization and large-scale problems, while mathematical optimization became popularized in acdemia and engineering.

## 2.3 An Introduction to Convex Sets and Functions

Convex optimization constitutes an important family of mathematical optimization techniques. More explicitly, it concerns the optimization of a convex objective function featuring decision variables restricted to convex sets. The definitions of affine/convex sets and affine/convex functions are given in the following, along with some examples.

### 2.3.1 Affine Sets and Functions

An affine set contains the line through any two points within the set, as depicted in Fig. 2.1. If $x_1, x_2 \in \mathcal{C}$, then we have $\alpha x_1 + (1-\alpha)\, x_2 \in \mathcal{C}$, $\forall \alpha \in \mathcal{C}$. Furthermore, this property can be extended to multiple points to form an *affine combination*

$$\alpha_1 x_1 + \alpha_2 x_2 + \cdots + \alpha_n x_n, \tag{2.1}$$

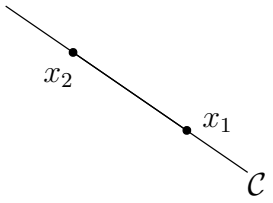


FIGURE 2.1: The line passing through the points $x_1$ and $x_2$ form the affine set denoted by $\mathcal{C}$.

which must also be part of the affine set if $x_1, x_2, \cdots, x_n \in \mathcal{C}$, $\alpha_1 + \alpha_2 + \cdots + \alpha_n = 1$, and $\alpha_1, \alpha_2, \cdots, \alpha_n \in \mathbb{R}$. For example, any subspace is an affine set.

The *affine hull* of any set $\mathcal{S}$ is defined as

$$\textbf{aff}\ \mathcal{S} = \{\alpha_1 x_1 + \alpha_2 x_2 + \cdots + \alpha_n x_n | x_1, x_2, \cdots, x_n \in \mathcal{S},\ \alpha_1 + \alpha_2 + \cdots + \alpha_n = 1\}. \quad (2.2)$$

In other words, it is the smallest affine set, which contains $\mathcal{S}$.

### 2.3.2 Convex Sets

A set, $C$, is convex if $\forall x_1, x_2 \in C$ and $\alpha \in [0, 1]$

$$\alpha x_1 + (1 - \alpha)\, x_2 \in C \quad (2.3)$$

is satisfied. Geometric examples of convex and nonconvex sets in $\mathbb{R}^2$ are given in Fig. 2.2. Some more examples of convex sets include the closed set $[a, b]$, where $a, b \in \mathbb{R}$, Euclidean

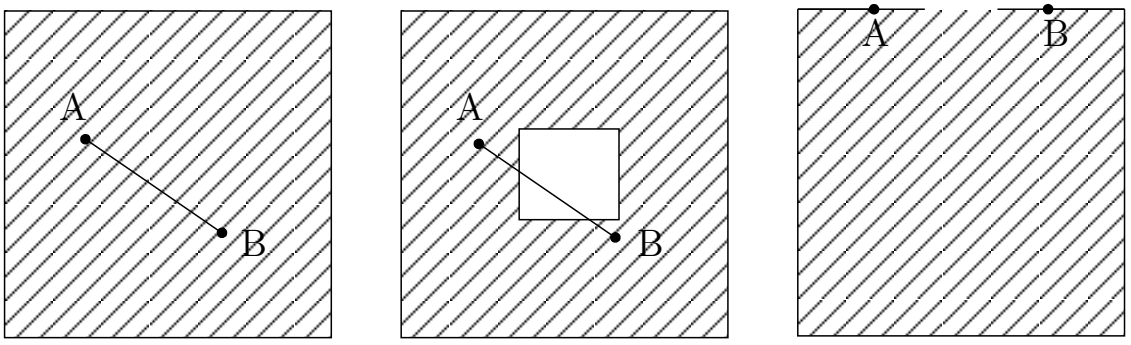


(a) This is a convex set. Any two points drawn from the set may be connected by a line, which remains in the set.

(b) This is not a convex set. The line formed between the points A and B passes outside the set.

(c) This is not a convex set. The direct line formed between points A and B exits the set.

FIGURE 2.2: Illustrations of convex and nonconvex sets, where the sets are shaded.

balls and ellipsoids, norm balls and cones and polyhedra. More importantly, $[0, \infty)$ is a ray (half-line) and hence convex. Loosely speaking, points in a convex set have an *unobstructed view* of every other point in the set.

### 2.3.3 Convex Functions

A function $f : \mathbb{R}^n \to \mathbb{R}$ is convex if its domain, indicated by **dom** $f$, is a convex set and $\forall x_1, x_2 \in$ **dom** $f$ and $\alpha \in [0, 1]$,

$$f(\alpha x_1 + (1-\alpha) x_2) \leq \alpha f(x_1) + (1-\alpha) f(x_2) \tag{2.4}$$

is satisfied [34]. This may be visualized geometrically in Fig. 2.3. In simple terms, the chord

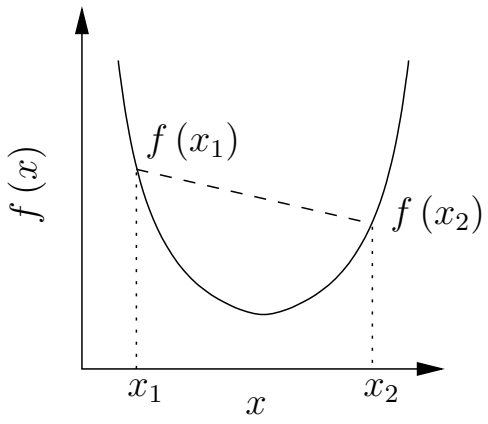


FIGURE 2.3: Geometric interpretation of the convex function definition.

formed between the points $(x_1, f(x_1))$ and $(x_2, f(x_2))$ lies *on* or *above* the curve formed by $f(x)$. In the case of Fig. 2.3, the chord *always* lies above the function curve. Therefore, $f(x)$ is in fact *strictly* convex. Assuming that the function is differentiable, the first-order necessary and sufficient condition for convexity may be stated as

$$f(y) \geq f(x) + \nabla f(x)^{\mathrm{T}} (y - x), \tag{2.5}$$

where the domain of $f$, denoted by **dom** $f$, is open and convex, while $x, y \in$ **dom** $f$. This is elucidated in Fig. 2.4, which demonstrates that the first order Taylor approximation of a convex function is a *global underestimator* [34]. A further result of this property is that if

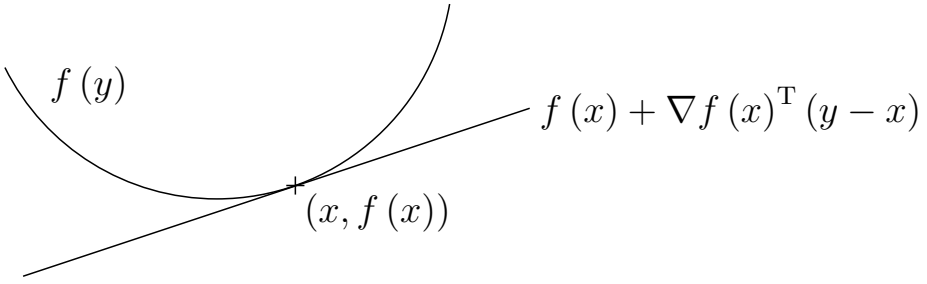


FIGURE 2.4: The first-order conditions for convexity of a function.

$\nabla f(x) = 0$, then (2.5) reduces to $f(y) \geq f(x)$, which implies that $x$ is the global minimizer

of $f$. Indeed, this simple result demonstrates why it is possible to effectively perform convex optimization.

If $f(x)$ is twice differentiable, the second-order necessary and sufficient condition for convexity is that its Hessian is *positive semidefinite*, which may be formally stated as

$$\nabla^2 f(x) \succeq 0, \forall x \in \mathbf{dom}\ f. \tag{2.6}$$

In other words, the function $f(x)$ has positive (upwards) curvature.

On the other hand, $f(x)$ is *concave* if $-f(x)$ is convex. In other words, if

$$f(\alpha x_1 + (1-\alpha) x_2) \geq \alpha f(x_1) + (1-\alpha) f(x_2), \forall x_1, x_2 \in \mathbf{dom}\ f \text{ and } \alpha \in [0,1], \tag{2.7}$$

then $f(x)$ is concave. Geometrically, the chord in the example of Fig. 2.3 is required to be below the function curve, which has a negative (downwards) curvature. It is important to observe that a function can be both convex *and* concave simultaneously, in other words, affine. More importantly, a function can be *neither* convex nor concave.

From the above descriptions, it is clear that all affine functions are convex (and concave). Some more examples, which may be readily proven [34], include the

- Exponential function (convex): $f(x) = e^{ax}$, for any $a \in \mathbb{R}$;
- Logarithm function (concave): $f(x) = \log(x)$, where $x \in \mathbb{R}_{++}$;
- Powers: $f(x) = x^a$ is convex for $a \leq 0$ and $a \geq 1$, but concave when $0 < a < 1$;
- Norm functions (convex): $f(\mathbf{x}) = \|\mathbf{x}\|_p$, $p > 1$;
- Max function (convex): $f(\mathbf{x}) = \max_i (x_i)$;
- Geometric mean (concave): $f(\mathbf{x}) = (\prod_{i=1}^n x_i)^{\frac{1}{n}}$, where $\mathbf{dom}\ f = \mathbb{R}^n_{++}$;
- Quadratic-over-linear function (convex): $f(x,y) = \frac{x^2}{y}$, where $x \in \mathbb{R}$ and $y > 0$.

#### 2.3.3.1 Sublevel Sets

A convex function $f(\mathbf{x}) : \mathbb{R}^n \to \mathbb{R}$ has *convex $\alpha$-sublevel sets*, which are defined as

$$C_\alpha = \{\mathbf{x} \in \mathbf{dom}\ f | f(\mathbf{x}) \leq \alpha\}. \tag{2.8}$$

An example is illustrated on the left of Fig. 2.5, where the dashed line indicates the *convex* set of $x$ values, which results in a function value of less than or equal to $\alpha$. However, a function having convex sublevel sets is *not* necessarily convex as well, which is demonstrated on the right of Fig. 2.5.

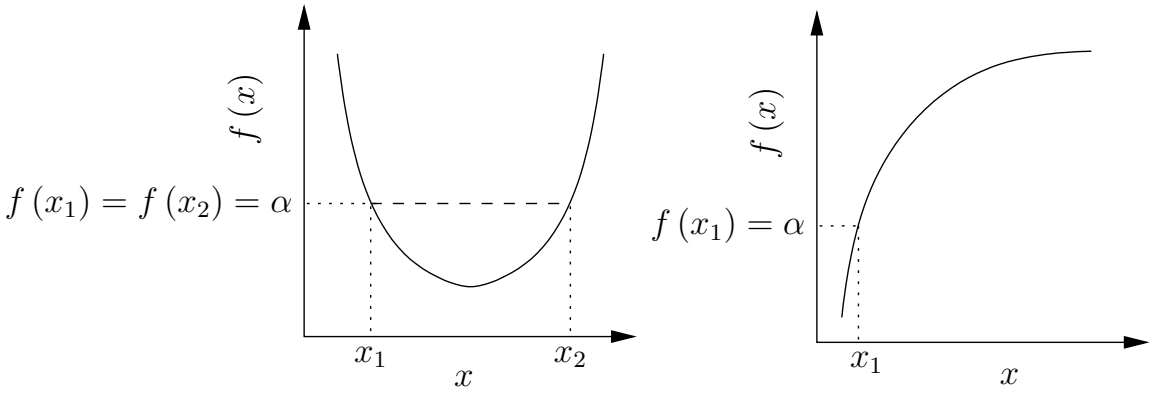


FIGURE 2.5: An illustration of two examples of sublevel sets. The left figure depicts a convex function, however, the figure on the right depicts a concave function.

Similarly, a concave function has *convex $\alpha$-superlevel sets*, defined as

$$C_\alpha = \{\mathbf{x} \in \mathbf{dom}\ f | f(\mathbf{x}) \geq \alpha\}. \tag{2.9}$$

In fact, this is demonstrated in the example on the right of Fig. 2.5 (since it depicts a concave function), which has *both* convex sublevel and superlevel sets.

#### 2.3.3.2 Epigraphs

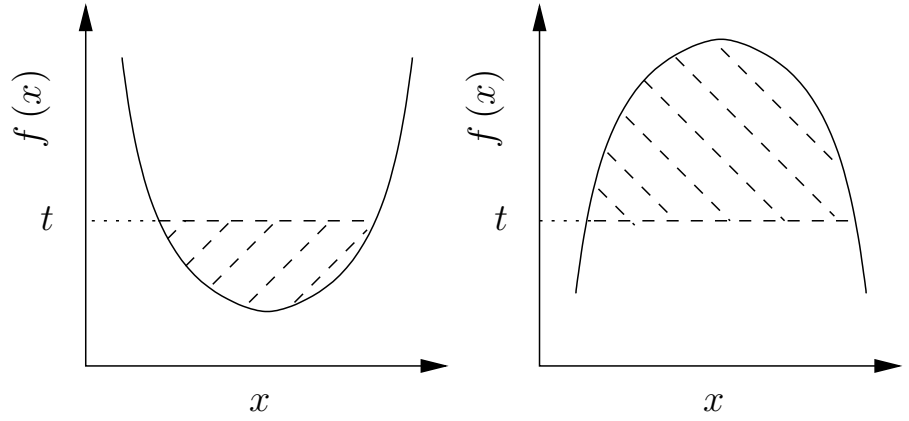


FIGURE 2.6: An illustration of the epigraph (left) and hypograph (right) of a convex function and a concave function, respectively.

An epigraph of the function $f(\mathbf{x}) : \mathbb{R}^n \to \mathbb{R}$ is simply defined as

$$\mathbf{epi}\ f = \{(\mathbf{x}, t) | \mathbf{x} \in \mathbf{dom}\ f,\ f(\mathbf{x}) \leq t\} \tag{2.10}$$

and it is a subset of $\mathbb{R}^{n+1}$. The epigraphs of a convex function are *convex* sets, which is demonstrated in Fig. 2.6. Similarly, concave functions have convex *hypographs*, which are

defined as

$$\mathbf{hypo}\ f = \{(\mathbf{x}, t)\,|\mathbf{x} \in \mathbf{dom}\ f,\ f(\mathbf{x}) \geq t\}\,. \tag{2.11}$$

### 2.3.4 Operations that Preserve Convexity

Apart from employing the above-mentioned fundamentals, the convexity of a function may also be verified by examining the operations that would lead to the specific form of the function itself. For example, the following operations preserve the convexity of a function, hence it is sufficient to verify the convexity of its constituent components:

- *Nonnegative weighted sum*: If $f$ is convex, the nonnegative weight $w > 0$ may be applied to it without affecting its convexity, resulting in $wf$. If $f_i$, $\forall i \in \{1, \cdots, m\}$, represents convex functions, while $w_i > 0$, $\forall i \in \{1, \cdots, m\}$, the nonnegative weighted sum given by

  $$f = w_1 f_1 + w_2 f_2 + \cdots + w_m f_m \tag{2.12}$$

  is also convex. Similarly, the nonnegative weighted sum of a series of concave functions results in a concave function. Furthermore, a nonnegative nonzero weighted sum of a series of strictly convex (concave) functions is strictly convex (concave).
- *Composition with an affine mapping*: An affine mapping, described as $\mathbf{Ax} + \mathbf{b}$, where $\mathbf{A} \in \mathbb{R}^{n\times m}$, $\mathbf{x} \in \mathbb{R}^m$ and $\mathbf{b} \in \mathbb{R}^n$ may form the input of a convex function given by $f : \mathbb{R}^n \to \mathbb{R}$. The resultant composition, given by

  $$g(\mathbf{x}) = f(\mathbf{Ax} + \mathbf{b})\,, \tag{2.13}$$

  where $\mathbf{dom}\ g = \{\mathbf{x}|\mathbf{Ax} + \mathbf{b} \in \mathbf{dom}\ f\}$, is convex as well. Similarly, if $f$ is concave, so is $g$.
- *Perspective transformation*: A perspective transformation of a convex function $f(\mathbf{x})$ defined as

  $$g(\mathbf{x}, t) = t \cdot f(\mathbf{x}/t)\,, \tag{2.14}$$

  where $\mathbf{dom}\ g = \{(\mathbf{x}, t)\,|\mathbf{x}/t \in \mathbf{dom}\ f, t > 0\}$, is also convex. Similarly, if $f$ is concave, so is $g$.
- *Pointwise maximum/supremum and pointwise minimum/infimum*: If $f_1(\mathbf{x})$ and $f_2(\mathbf{x})$ are convex functions, their pointwise maximum

  $$\max\{f_1(\mathbf{x}), f_2(\mathbf{x})\} \tag{2.15}$$

  is also convex. On the other hand, if $f_1(\mathbf{x})$ and $f_2(\mathbf{x})$ are concave functions, their pointwise minimum

  $$\min\{f_1(\mathbf{x}), f_2(\mathbf{x})\} \tag{2.16}$$

is concave.

- *Scalar composition*: A scalar function composition of $h : \mathbb{R} \to \mathbb{R}$ and $g : \mathbb{R}^n \to \mathbb{R}$, resulting in $f = h \circ g : \mathbb{R}^n \to \mathbb{R}$, may be written as

$$f(\mathbf{x}) = h(g(\mathbf{x})), \tag{2.17}$$

where $\mathbf{dom}\ f = \{\mathbf{x} \in \mathbf{dom}\ g | g(\mathbf{x}) \in \mathbf{dom}\ h\}$. Assuming that $g$ and $h$ are twice differentiable, the function $f$ is convex if

$$f''(\mathbf{x}) = h''(g(\mathbf{x}))\, g'(\mathbf{x})^2 + h'(g(\mathbf{x}))\, g''(\mathbf{x}) \geq 0. \tag{2.18}$$

Thus, the following rules may be derived

$$\begin{gathered} f \text{ is convex if } h \text{ is convex and nondecreasing, and } g \text{ is convex,} \\ f \text{ is convex if } h \text{ is convex and nonincreasing, and } g \text{ is concave,} \\ f \text{ is concave if } h \text{ is concave and nondecreasing, and } g \text{ is concave,} \\ f \text{ is concave if } h \text{ is concave and nonincreasing, and } g \text{ is convex,} \end{gathered} \tag{2.19}$$

where all function domains are $\mathbb{R}$. On the other hand, without the assumption that the function domains are all of $\mathbb{R}$, and without the assumption that the base functions are twice differentiable, the following rules may be derived

$$\begin{gathered} f \text{ is convex if } h \text{ is concave, } \tilde{h} \text{ is nondecreasing, and } g \text{ is convex,} \\ f \text{ is convex if } h \text{ is convex, } \tilde{h} \text{ is nonincreasing, and } g \text{ is concave,} \\ f \text{ is concave if } h \text{ is concave, } \tilde{h} \text{ is nondecreasing, and } g \text{ is concave,} \\ f \text{ is concave if } h \text{ is concave, } \tilde{h} \text{ is nonincreasing, and } g \text{ is convex.} \end{gathered} \tag{2.20}$$

Here, $\tilde{h}$ denotes the *extended-value extension* of the function $h$, which assigns the value $\infty$ ($-\infty$) to points not in $\mathbf{dom}\ h$ for convex (concave) functions [34], as depicted in Fig. 2.7.

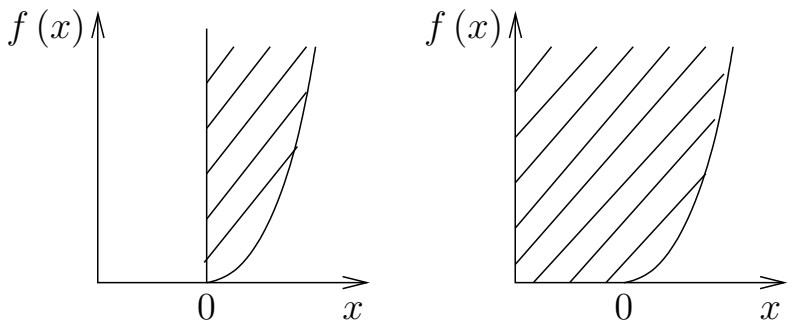


FIGURE 2.7: The function on the left is defined on the domain $\mathbb{R}_+$. Although convex, its extended-value extension is not nondecreasing. The function on the right is defined for all of $\mathbb{R}$, and is convex and nondecreasing.

- *Vector composition*: A vector function composition of $h : \mathbb{R} \to \mathbb{R}$ and $g_i : \mathbb{R}^n \to \mathbb{R}$, $\forall i \in \{1, \cdots, k\}$ is convex if

$$f''(\mathbf{x}) = g'(\mathbf{x})^{\mathrm{T}} \nabla^2 h(g(x)) g'(\mathbf{x}) + \nabla h(g(\mathbf{x}))^{\mathrm{T}} g''(\mathbf{x}) \geq 0, \tag{2.21}$$

  which is simply the vector equivalent of (2.18). Similarly, we may derive the following rules

  $f$ is convex if $h$ is convex, $h$ is nondecreasing in each argument, and $g_i$ are convex,
  $f$ is convex if $h$ is convex, $h$ is nonincreasing in each argument, $g_i$ are concave,
  $f$ is concave if $h$ is concave, $h$ is nondecreasing in each argument, $g_i$ are concave.

  The general rules are obtained, when enforcing monotonicity on the extended-value extensions of $h$.

## 2.4 Optimization Problems

An optimization problem in *standard form* is written as

$$\begin{aligned} \underset{\mathbf{x} \in \mathcal{D}}{\text{minimize}} \quad & f_0(\mathbf{x}) && (2.22) \\ \text{subject to} \quad & f_i(\mathbf{x}) \leq 0,\ i = 1, \cdots, m && (2.23) \\ & h_i(\mathbf{x}) = 0,\ i = 1, \cdots, p, && (2.24) \end{aligned}$$

where $\mathbf{x}$ is the vector of *optimization* or *decision variables*, $f_0(\mathbf{x}) : \mathbb{R}^n \to \mathbb{R}$ is the *objective function* or *cost function*, $f_i(\mathbf{x}) \leq 0$ are the *inequality constraints*, and $h_i(\mathbf{x}) = 0$ are the *equality constraints*. The functions $f_i : \mathbb{R}^n \to \mathbb{R}$ and $h_i : \mathbb{R}^n \to \mathbb{R}$ are referred to as the *inequality constraint functions* and the *equality constraint functions*, respectively. Furthermore, the domain, denoted by $\mathcal{D}$, of the optimization problem is defined as

$$\mathcal{D} = \left[\bigcap_{i=0}^{m} \mathbf{dom}\ f_i\right] \cap \left[\bigcap_{i=1}^{p} \mathbf{dom}\ h_i\right], \tag{2.25}$$

and any point $\mathbf{x} \in \mathcal{D}$ that satisfies the constraints (2.23)–(2.24) is said to be a *feasible point*, while any other point is said to be *infeasible*. In Fig. 2.8, the filled shape indicates the intersection of one hyperplane and two convex sets. A feasible point can be obtained from this intersection, it these sets depict the domains associated with the constraints of an optimization problem. On the other hand, an optimization problem without constraints is termed as being *unconstrained*.

The optimization problem is solved by finding a specific value of $\mathbf{x} \in \mathcal{D}$, which results in the

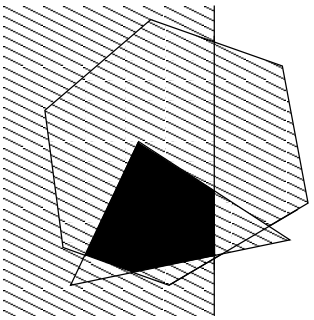

FIGURE 2.8: The filled section indicates the intersection of one hyperplane and two convex sets.

*optimal value* of the optimization problem defined as

$$p^* = \inf \{ f_0(\mathbf{x}) \, | f_i(\mathbf{x}) \leq 0, \, i = 1, \cdots, m, \, h_i(\mathbf{x}) = 0, \, i = 1, \cdots, p \} . \tag{2.26}$$

In order words, $\mathbf{x}$ minimizes $f_0$ among all the values of $\mathbf{x} \in \mathcal{D}$, which satisfy the constraints of (2.23)–(2.24). Any particular $\mathbf{x}$, which achieves this goal, is denoted by $\mathbf{x}^*$and it is termed as an *(globally) optimal point*, as is illustrated in Fig. 2.9. If there exists a feasible point resulting in $p^* = -\infty$, the optimization problem is *unbounded below*.

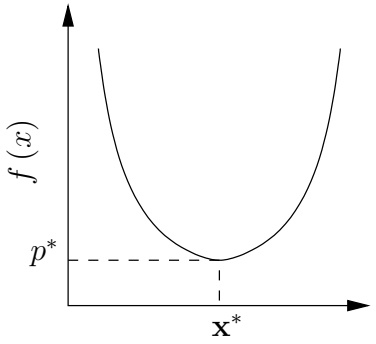


FIGURE 2.9: The infimum of $f_0$ is obtained at $\mathbf{x}^*$, when $f_0(\mathbf{x}^*) = p^*$.

As alluded to above, there may be many points, which achieve the optimal value of $p^*$. The corresponding *optimal set* is defined as

$$\mathcal{X} = \{ \mathbf{x} | f_i(\mathbf{x}) \leq 0, \, i = 1, \cdots, m, \, h_i(\mathbf{x}) = 0, \, i = 1, \cdots, p, \, f_0(\mathbf{x}) = p^* \} . \tag{2.27}$$

An empty optimal set implies that the optimal value is *not attained* or *not achieved*. An *$\epsilon$-suboptimal set* contains all feasible points $\mathbf{x}$, which satisfy $f_0(\mathbf{x}) \leq p^* + \epsilon$. Furthermore, given $R > 0$, a feasible point $\mathbf{x}$ is *locally optimal* if

$$f_0(\mathbf{x}) = \inf \{ f_0(\mathbf{z}) \, | f_i(\mathbf{z}) \leq 0, \, i = 1, \cdots, m, \, h_i(\mathbf{z}) = 0, \, i = 1, \cdots, p, \, ||\mathbf{z} - \mathbf{x}||_2 \leq R \} . \tag{2.28}$$

Clearly, if $f_0$ is convex, a locally optimal point is also globally optimal. These concepts are illustrated in Fig. 2.10.

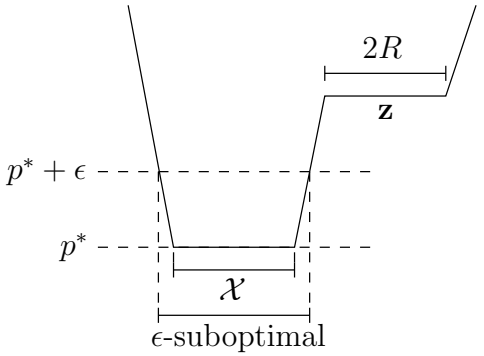


FIGURE 2.10: The set $\mathcal{X}$ indicates the optimal set of points, which obtain $p^*$ for the example function. The enveloping $\epsilon$-suboptimal set is also shown. On the other hand, the area indicated by $2R$ highlights the locally optimal set, which contains points that obtain objective function values identical to that obtained by the point $\mathbf{z}$.

### 2.4.1 Convex Optimization Problems

The optimization problem of (2.22)–(2.24) is a *convex optimization problem* if $f_i$, $i = 0, \cdots, m$ are convex, while $h_i$, $i = 1, \cdots, p$ are affine. Furthermore, the feasible set of the problem is convex, since it is the intersection of $m$ convex sets and $p$ hyperplanes.

The standard form of an optimization problem may be written in the *equivalent epigraph form* of

$$\begin{aligned} \underset{\mathbf{x}\in\mathcal{D},t\in\mathbb{R}}{\text{minimize}} \quad & t && (2.29)\\ \text{subject to} \quad & f_0(\mathbf{x}) - t \leq 0 && (2.30)\\ & f_i(\mathbf{x}) \leq 0,\ i = 1, \cdots, m && (2.31)\\ & h_i(\mathbf{x}) = 0,\ i = 1, \cdots, p, && (2.32) \end{aligned}$$

which is also convex.

### 2.4.2 Mixed Integer Nonlinear Programming

If the objective function involves both continuous and integer independent variables, while at least one of $f_i$, $i = 0, \cdots, m$ is nonlinear, the optimization problem constitutes an instance of MINLP problems, which are nonconvex. These problems may be solved using the classic branch-and-bound method [241, 335, 336], which pursues a *'divide-and-conquer'* approach. Although typically computationally complex, they are able to find the global optimum

of nonconvex MINLP problems and to guarantee that the solution found is at most $\epsilon$-suboptimal. The branch-and-bound method is described in the following and in Fig. 2.11.

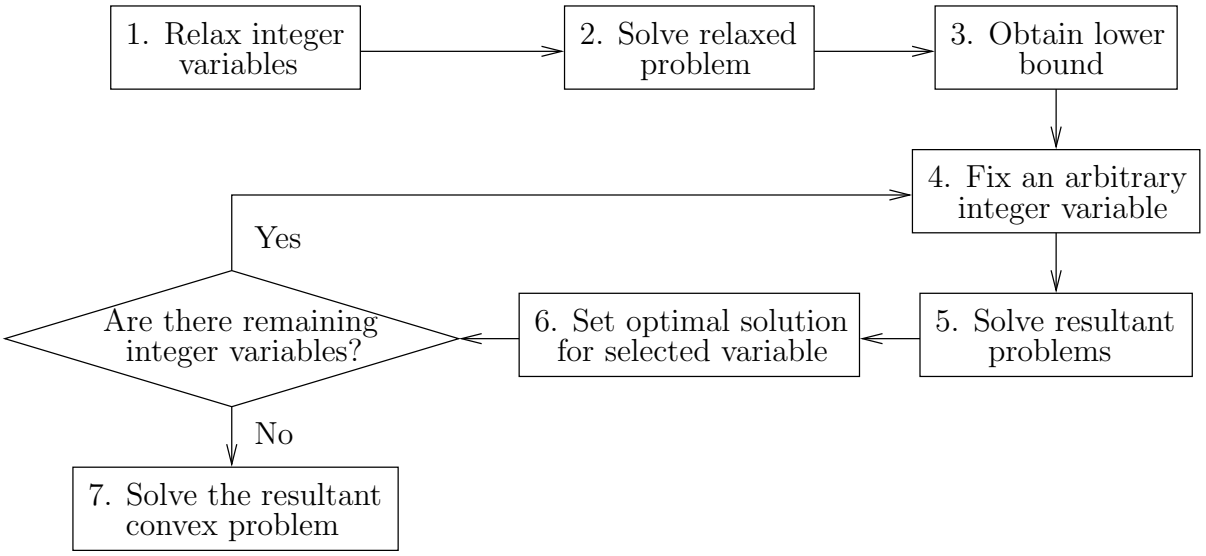


FIGURE 2.11: A flow diagram of the steps performed in the branch-and-bound method.

1. Relax all remaining integer variables so that their domains are continuous, hence convex.
2. Solve the relaxed problem using algorithms described later in Section 2.6 and obtain the optimal solution to this relaxed problem.
3. The optimal value of the relaxed problem is a lower bound of the original problem, since the integer constraints were loosened.
4. (*Branching*) Choose an arbitrary variable, which was subject to integer constraints, to fix at each of its feasible integer values. Then, formulate and solve each of the resultant optimization problems. Thus, an optimization problem is solved for every possible integer solution for the chosen variable.
5. The fixed value of the integer variable associated with the optimization problem that results in the lowest optimal value is then the optimal solution for that variable. Thus, the associated variable is fixed to this optimal value for future steps of this algorithm.
6. (*Bounding*) Furthermore, the optimal objective function value associated fixed integer variable is a *tighter* lower bound for the original optimization problem, since this new objective function value is obtained after having restricted that particular variable to an integer set. On the other hand, any solutions satisfying the original domain restrictions correspond to upper bounds for the optimal objective function value.
7. Repeat steps 4 to 6 until optimal values for all integer variables have been obtained.
8. Substitute the optimal integer values into the original optimization problem and solve the resultant convex problem.

#### 2.4.2.1 A Branch and Bound Example

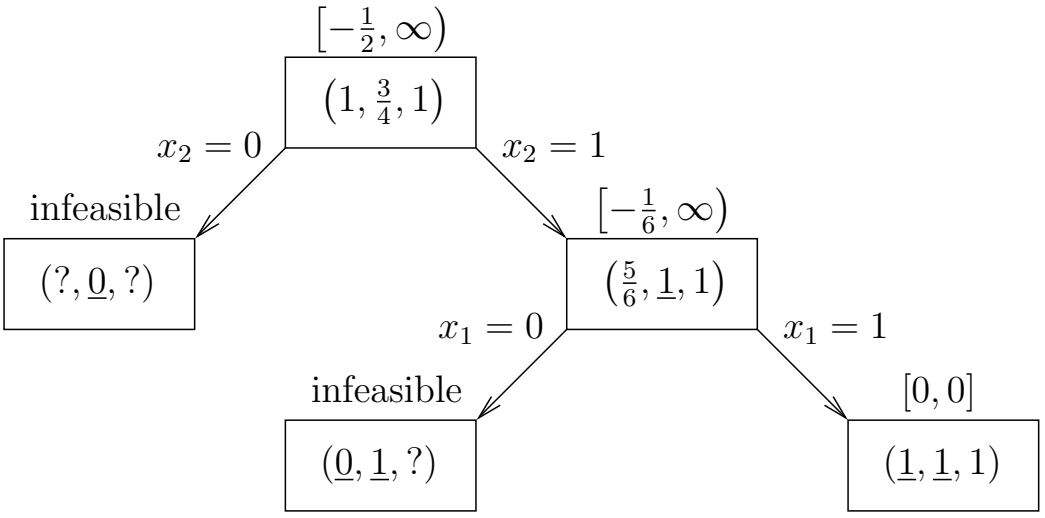


FIGURE 2.12: A Branch-and-Bound example. The upper and lower bounds of the optimal value are listed above the boxes, which contain the optimal solution at each stage of the algorithm. The underlined values indicate the fixed integer variable values.

An example is provided in Fig. 2.12, which solves the following naive Boolean minimization problem

$$\begin{aligned} \text{minimize} \quad & x_1 + 2x_2 - 3x_3 && (2.33) \\ \text{subject to} \quad & 3x_1 + 2x_2 + x_3 \geq 5.5 && (2.34) \\ & x_i \in \{0, 1\}\,,\ i = 1, 2, 3, && (2.35) \end{aligned}$$

which has the optimal solution of $(1, 1, 1)$. However, when employing the branch-and-bound method described above, Step 1 dictates that the integer variables are initially relaxed to the domain $[0, 1]^3$, which results in the optimal solution of $\left(1, \frac{3}{4}, 1\right)$ and a lower bound to the optimal value of $-\frac{1}{2}$, as was outlined in Steps 2 and 3. Since the optimal value of $x_2$ is non-integer, it may be chosen as the initial variable to fix to integer values as suggested in Step 4, resulting in two branches. However, $x_2 = 0$ is infeasible, since the inequality constraint can no longer be satisfied. As described in Steps 5 and 6, setting $x_2 = 1$ and solving the resultant problem results in an optimal solution of $\left(\frac{5}{6}, 1, 1\right)$ and a tighter lower bound of the optimal value of $-\frac{5}{6}$. Since there are remaining integer variables, branching is again performed, but with $x_1$. This reveals another infeasible solution, and an integer solution, which provides both a lower and an upper bound of 0 to the optimal value. The optimal solution for $x_3$ is also obtained as 1 and it is not necessary to branch with $x_3$. As optimal solutions for all integer variables have been obtained, Step 7 is not required and we conclude that the optimal solution is $(1, 1, 1)$ with an optimal value of 0.

### 2.4.3 Fractional Programming

A FP approach may be formulated as:

$$\underset{\mathbf{x}\in\mathcal{D}}{\text{minimize}} \quad f_0(\mathbf{x}) = \frac{g(\mathbf{x})}{h_0(\mathbf{x})} \tag{2.36}$$

$$\text{subject to} \quad f_i(\mathbf{x}) \leq 0,\ i = 1, \cdots, m \tag{2.37}$$

$$h_i(\mathbf{x}) = 0,\ i = 1, \cdots, p, \tag{2.38}$$

where $h_0(\mathbf{x}) > 0$, $\forall \mathbf{x} \in \mathcal{D}$. Furthermore, if both $g(\mathbf{x})$ and $h_0(\mathbf{x})$ are affine, the optimization problem constitutes an instance of *linear FP*. If $g(\mathbf{x})$ is convex (concave), while $h_0(\mathbf{x})$ is affine, the problem represents an instance of *quasiconvex (quasiconcave) programming*. A function is also quasiconvex (quasiconcave) if all of its sublevel (superlevel) sets are convex, as demonstrated in Fig. 2.13. A function that is both quasiconvex and quasiconcave is termed as being *quasilinear*. Clearly, all convex functions are quasiconvex, but not all quasiconvex functions are convex.

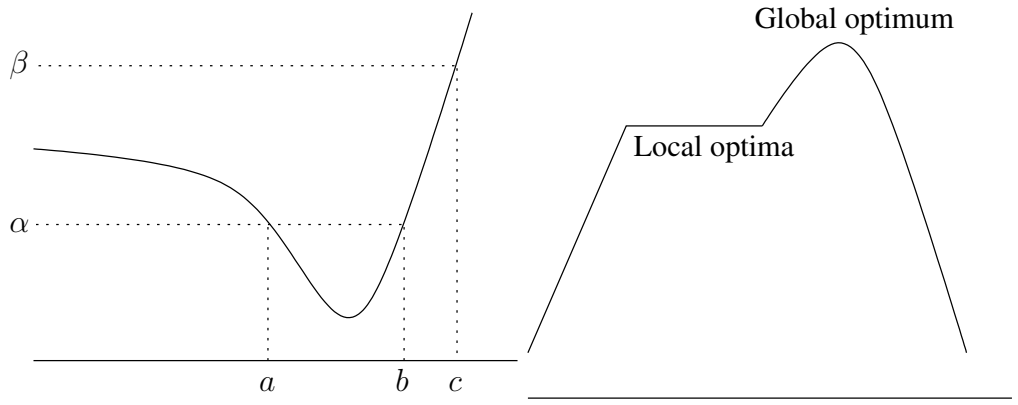


FIGURE 2.13: The sublevel sets for the left function are convex, so it is quasiconvex. However, it is not convex nor concave, since the function is concave for below $a$, but convex for values greater than $a$. The right function is quasiconcave, but not concave. Its local optima are not necessarily globally optimal.

As demonstrated in Fig. 2.13, the distinguishing difference between quasiconvex (quasiconcave) functions and convex (concave) functions is that quasiconvex (quasiconcave) functions may have locally optimal solutions, which are not globally optimal solutions. Furthermore, quasiconvex functions are not necessarily continuous. However, there are methods for converting a quasiconvex optimization problem into efficiently-solvable convex problem(s), which result in the optimal solution of the quasiconvex problem. It is important to observe that the methods detailed in the following may be readily applied to either quasiconvex minimization or quasiconcave maximization.

#### 2.4.3.1 Bisection Method

The bisection method [34] relies on the fact that quasiconvex functions have convex sublevel sets. Therefore, if a quasiconvex objective function value can attain the value of $\sigma$, there exists some $\mathbf{x} \in \mathcal{D}$ satisfying the *convex* inequality constraint

$$\frac{g(\mathbf{x})}{h_0(\mathbf{x})} \leq \sigma, \tag{2.39}$$

which may be verified by solving the following *feasibility* problem

$$\begin{aligned} \underset{\mathbf{x}\in\mathcal{D}}{\text{find}} \quad & \mathbf{x} && (2.40)\\ \text{subject to} \quad & \frac{g(\mathbf{x})}{h_0(\mathbf{x})} \leq \sigma && (2.41)\\ & f_i(\mathbf{x}) \leq 0,\ i = 1, \cdots, m && (2.42)\\ & h_i(\mathbf{x}) = 0,\ i = 1, \cdots, p. && (2.43) \end{aligned}$$

When written in the standard convex optimization form, the above problem may be expressed as

$$\begin{aligned} \underset{\mathbf{x}\in\mathcal{D}}{\text{minimize}} \quad & 0 && (2.44)\\ \text{subject to} \quad & \frac{g(\mathbf{x})}{h_0(\mathbf{x})} \leq \sigma && (2.45)\\ & f_i(\mathbf{x}) \leq 0,\ i = 1, \cdots, m && (2.46)\\ & h_i(\mathbf{x}) = 0,\ i = 1, \cdots, p, && (2.47) \end{aligned}$$

where the goal is to find a feasible value of $\mathbf{x}$, thus the objective function is unimportant. If (2.44)–(2.47) is feasible, the quasiconvex objective function can attain the value $\sigma$ and hence a lower value of $\sigma$ may be subsequently verified as being feasible, otherwise a higher value of $\sigma$ must be verified as being feasible. Thus, the bisection method may be employed for successively checking the feasibility of different values of $\sigma$, until the minimum value is attained. The bisection method is formally listed in Table 2.1. Given the initial parameters, the bisection method will converge within exactly $\lceil \log_2 \left( \frac{\sigma_U + \sigma_L}{\epsilon} \right) \rceil$ iterations. However, it is typically not possible to obtain tight upper and lower bounds of the optimal value beforehand. This coupled with the fact that a convex optimization problem must be solved at each iteration may result in an excessive complexity for the algorithm.

A method of obtaining an upper bound to the optimal value is to simply assume a naive, yet feasible $\mathbf{x}$ value, which clearly results in an objective function value that is higher than the optimal. Furthermore, if the objective function is strictly higher than zero, a naive lower bound is simply zero.

TABLE 2.1: The bisection method for quasiconvex minimization.

| | |
|---|---|
| Input: | $\sigma_U$ (initial upper bound to the optimal value) |
| | $\sigma_L$ (initial lower bound to the optimal value) |
| | $\epsilon > 0$ (convergence tolerance) |

1: $\sigma \leftarrow \frac{\sigma_U + \sigma_L}{2}$
2: **do while** $\sigma_U + \sigma_L > \epsilon$
3: Solve (2.44)–(2.47)
4: **if** $\sigma$ feasible
5: $\sigma_L \leftarrow \sigma$
6: **else**
7: $\sigma_U \leftarrow \sigma$
8: **end if**
9: **end do**

#### 2.4.3.2 Solving an Example Fractional Programing Problem with the Bisection Method

Let us elucidate the bisection method by working through a simple example. The problem of interest is given by

$$\underset{x \geq 0}{\text{minimize}} \quad \frac{x^2}{x+1}, \tag{2.48}$$

which clearly is solved by $x = 0$. However, when following the bisection method, we initially determine both upper and lower bounds of the optimal objective function value. By substituting $x = 0$, we obtain the lower bound of 0, while for the sake of this example, we assume an upper bound of 1. Following the Table 2.1, we formulate and solve the feasibility problem associated with the previously specified upper and lower bounds as follows

$$\underset{x \geq 0}{\text{minimize}} \quad 0 \tag{2.49}$$

$$\text{subject to} \quad 2x^2 - x - 1 \leq 0, \tag{2.50}$$

which can clearly be solved with $x = 0$. However, solving the above feasibility problem only determines that the objective value of $\sigma = \frac{\sigma_U + \sigma_L}{2} = \frac{1}{2}$ is obtainable. Thus, we are able to update the upper bound with $\sigma_L = \frac{1}{2}$ resulting in the following feasibility problem

$$\underset{x \geq 0}{\text{minimize}} \quad 0 \tag{2.51}$$

$$\text{subject to} \quad 2x^2 - 0.5x - 0.5 \leq 0, \tag{2.52}$$

which can again be solved by $x = 0$ and showing that the upper bound can be updated to $\sigma_L = \frac{1}{4}$. As is clearly seen, for this particular problem, the upper bound can be continually decreased and the associated feasibility problems solved with $x = 0$, until the stopping criterion is satisfied. In this case, we can see that the result will be $\sigma = 0$, which is obtained when $x = 0$.

#### 2.4.3.3 Dinkelbach's Method

TABLE 2.2: Dinkelbach's method for quasiconcave maximization.

| Input: | $\epsilon > 0$ (convergence tolerance) |
|---|---|
| 1: | $n \leftarrow 0$ |
| 2: | $q_n \leftarrow 0$ |
| 3: | **do** |
| 4: | Solve $F(q_n)$ to obtain $\mathbf{x}_n$ |
| 5: | $q_{n+1} \leftarrow \frac{g(\mathbf{x}_n^*)}{h_0(\mathbf{x}_n^*)}$ |
| 6: | $n \leftarrow n + 1$ |
| 7: | **while** $q_n - q_{n-1} > \epsilon$ |

Dinkelbach's method [337, 338] is constituted by an iterative algorithm employed for solving a quasiconcave problem in a parameterized concave form. The algorithm is formally summarized in Table 2.2. An objective function value of $q$ is assumed, which allows the objective function to be written in the concave subtractive form of $g(\mathbf{x}) - q \cdot h_0(\mathbf{x})$. At the optimal value of $q^*$, the following holds true

$$F(q^*) := \underset{\mathbf{x}}{\text{maximize}} \{g(\mathbf{x}) - q^* \cdot h_0(\mathbf{x})\} = 0. \tag{2.53}$$

Furthermore, it can be shown [200,337,338] that employing the optimal solution $\mathbf{x}_n$ of $F(q_n)$ generates

$$\frac{g(\mathbf{x}_n)}{h_0(\mathbf{x}_n)} = q_{n+1} > q_n, \tag{2.54}$$

implying that monotonically increasing objectives function values can be attained until the optimal value of the original quasiconcave problem is found, as depicted in Fig. 2.14. These facts lead to a simple algorithm for solving the quasiconcave problem solved by Dinkelbach's method of Table 2.2. For further details and a proof of convergence, please refer to [337]. Although the algorithm benefits from a superlinear convergence rate, this is achieved at the cost of having to solve a series of concave programming problems, which may lead to an excessive complexity.

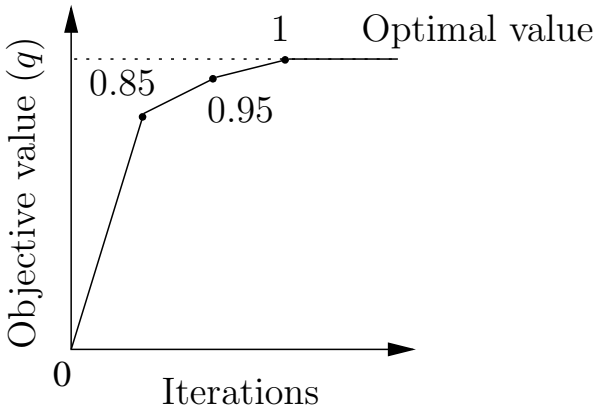


FIGURE 2.14: An example of the increasing objective function values of $q$ obtained by Dinkelbach's method of Table 2.2.

#### 2.4.3.4 Solving an Example Fractional Programing Problem with Dinkelbach's Method

Let us now employ Dinkelbach's method to solve the example of (2.48), which is listed again as follows

$$\underset{x\geq 0}{\text{minimize}} \qquad \frac{x^2}{x+1}. \tag{2.55}$$

We commence by rewriting the above problem as a maximization problem, which is a requirement of Dinkelbach's method. Thus, we now focus our attention on the following problem:

$$\underset{x\geq 0}{\text{maximize}} \qquad -\frac{x^2}{x+1} \tag{2.56}$$

and we choose the value of $q = -1$ to initialize Dinkelbach's method. Following Step 4 of Table 2.2, we formulate the problem in the subtractive form given by

$$\underset{x\geq 0}{\text{maximize}} \qquad -\left(x^2+x+1\right), \tag{2.57}$$

which is readily solved with $x = 0$, since any higher (feasible) value of $x$ only reduces the objective value. Thus, we obtain the updated value of $q = 0$ and formulate the associated subtractive problem of

$$\underset{x\geq 0}{\text{maximize}} \qquad -x^2, \tag{2.58}$$

which is again readily solved with $x = 0$. Since this obtains the same previously-obtained objective value, we can conclude that the original optimization has been solved.

#### 2.4.3.5 Charnes-Cooper Method

The distinguishing features of the Charnes-Cooper method [338] are that variable transformations are introduced and that the FP problem is reduced to a single optimization problem. The variables introduced are

$$\mathbf{y} = \frac{\mathbf{x}}{h_0(\mathbf{x})}, \tag{2.59}$$

where

$$t = \frac{1}{h_0(\mathbf{x})}. \tag{2.60}$$

Thus, the original quasiconcave problem may be equivalently rewritten as a concave programming problem [338]

$$\begin{aligned}
\underset{\mathbf{y}/t\in\mathcal{D},t>0}{\text{maximize}} \quad & t \cdot g\left(\frac{\mathbf{y}}{t}\right) && (2.61)\\
\text{subject to} \quad & t \cdot f_i\left(\frac{\mathbf{y}}{t}\right) \leq 0,\ i = 1, \cdots, m && (2.62)\\
& t \cdot h_i\left(\frac{\mathbf{y}}{t}\right) = 0,\ i = 1, \cdots, p, && (2.63)\\
& t \cdot h_0\left(\frac{\mathbf{y}}{t}\right) = 1, && (2.64)
\end{aligned}$$

and then optimally solved using any of the standard methods listed in Section 2.6.

#### 2.4.3.6 Solving an Example Fractional Programing Problem with the Charnes-Cooper Transformation

The Charnes-Cooper transformation may be applied for solving the above example of (2.48), which we again write as a maximization problem:

$$\underset{x\geq 0}{\text{maximize}} \quad \frac{-x^2}{x+1}. \tag{2.65}$$

We then introduce the auxiliary variables given by

$$t = \frac{1}{x+1} \tag{2.66}$$

and

$$y = \frac{x}{x+1} \tag{2.67}$$

to reformulate the optimization problem as

$$\begin{aligned}
\underset{y/t\geq 0,t>0}{\text{maximize}} \quad & -t \cdot \left(\frac{y}{t}\right)^2 && (2.68)\\
\text{subject to} \quad & t \cdot \left(\frac{y}{t} + 1\right) = 1, && (2.69)
\end{aligned}$$

which can be simplified to give

$$\underset{y\geq 0,t>0}{\text{maximize}} \quad -\frac{y^2}{t} \tag{2.70}$$

$$\text{subject to} \quad y+t=1. \tag{2.71}$$

The resulting objective is a negative quadratic-over-linear function, thus the problem is a concave maximization problem. Once again, the problem is readily solved with $y=0$, which maximizes the numerator of the objective function, meaning that $t=1$. If we substitute this value of $y$ back into 2.67, we obtain the solution $x=0$, which is the same as was obtained with the previous two methods of Sections 2.4.3.1 and 2.4.3.3.

## 2.5 Duality

This section explains the concept of duality and the methods that facilitate the approximate solution of convex optimization problems within a given tolerance. It is important to observe that although these methods are applied for convex minimization, they may be adapted for employment in concave maximization by simply negating the objective function to formulate the problem in its equivalent convex minimization form.

### 2.5.1 The Lagrangian Function and the Lagrange Dual Function

We commence by rewriting the standard form of an optimization problem as a single objective function summed with both its inequality and equality constraints in order to derive the *Lagrangian function* given by

$$\mathcal{L}\left(\mathbf{x},\boldsymbol{\lambda},\boldsymbol{\nu}\right)=f_0\left(\mathbf{x}\right)+\sum_{i=1}^{m}\lambda_i f_i\left(\mathbf{x}\right)+\sum_{i=1}^{p}\nu_i h_i\left(\mathbf{x}\right). \tag{2.72}$$

In (2.72), both the inequality and equality constraints are weighted by the variables $\lambda_i\in\mathbb{R}_+$, $i=1,\cdots,m$ and $\nu_i\in\mathbb{R}$, $i=1,\cdots,p$, respectively, which are termed as the *Lagrangian multipliers* associated with the inequality and equality constraints, respectively. To elaborate, the variable $\lambda_i$ is the Lagrangian multiplier associated with the inequality constraint $f_i\left(\mathbf{x}\right)$, while the variable $\nu_i$ is the Lagrangian multiplier associated with the equality constraint $h_i\left(\mathbf{x}\right)$. Furthermore, these variables are collected into the vectors $\boldsymbol{\lambda}$ and $\boldsymbol{\nu}$.

The *Lagrange dual function* is then defined as the minimum value of $\mathcal{L}\left(\mathbf{x},\boldsymbol{\lambda},\boldsymbol{\nu}\right)$ over all values of $\mathbf{x}$, which is written as

$$g\left(\boldsymbol{\lambda},\boldsymbol{\nu}\right)=\inf_{\mathbf{x}}\mathcal{L}\left(\mathbf{x},\boldsymbol{\lambda},\boldsymbol{\nu}\right)=\inf_{\mathbf{x}}\left(f_0\left(\mathbf{x}\right)+\sum_{i=1}^{m}\lambda_i f_i\left(\mathbf{x}\right)+\sum_{i=1}^{p}\nu_i h_i\left(\mathbf{x}\right)\right). \tag{2.73}$$

Since $g(\boldsymbol{\lambda}, \boldsymbol{\nu})$ is the infimum of a family of affine functions, it is always concave, regardless of the convexity of $f_i(\mathbf{x})$, $i = 0, \cdots, m$ or $h_i(\mathbf{x})$, $i = 1, \cdots, p$. If the optimal value of the original *(primal)* problem is denoted by $p^*$, any *dual feasible* point of $(\boldsymbol{\lambda}, \boldsymbol{\nu})$ results in the lower bound of

$$g(\boldsymbol{\lambda}, \boldsymbol{\nu}) \leq p^*. \tag{2.74}$$

This may be readily verified by noting that given a dual feasible point, each term in the first summation of (2.73) is nonpositive, while each term in the second summation is zero.

Let us now find the Lagrange dual function of the simple LP problem given by

$$\begin{aligned} \underset{\mathbf{x} \in \mathbb{R}^n}{\text{minimize}} \quad & \mathbf{c}^{\mathrm{T}} \mathbf{x} && (2.75) \\ \text{subject to} \quad & \mathbf{A}\mathbf{x} = \mathbf{b}, && (2.76) \\ & \mathbf{x} \succeq \mathbf{0}. && (2.77) \end{aligned}$$

The Lagrangian is given by

$$\mathcal{L}(\mathbf{x}, \boldsymbol{\lambda}, \boldsymbol{\nu}) = \mathbf{c}^{\mathrm{T}} \mathbf{x} - \sum_{i=1}^{n} \lambda_i x_i + \boldsymbol{\nu}^{\mathrm{T}} (\mathbf{A}\mathbf{x} - \mathbf{b}) = -\mathbf{b}^{\mathrm{T}} \boldsymbol{\nu} + \left(\mathbf{c} + \mathbf{A}^{\mathrm{T}} \boldsymbol{\nu} - \boldsymbol{\lambda}\right)^{\mathrm{T}} \mathbf{x}, \tag{2.78}$$

which results in the dual function

$$g(\boldsymbol{\lambda}, \boldsymbol{\nu}) = \inf_{\mathbf{x} \in \mathbb{R}^n} \mathcal{L}(\mathbf{x}, \boldsymbol{\lambda}, \boldsymbol{\nu}) = -\mathbf{b}^{\mathrm{T}} \boldsymbol{\nu} + \inf_{\mathbf{x} \in \mathbb{R}^n} \left\{ \left(\mathbf{c} + \mathbf{A}^{\mathrm{T}} \boldsymbol{\nu} - \boldsymbol{\lambda}\right)^{\mathrm{T}} \mathbf{x} \right\}. \tag{2.79}$$

It becomes plausible then that $g(\boldsymbol{\lambda}, \boldsymbol{\nu})$ is unbounded from below if we have $\mathbf{c} + \mathbf{A}^{\mathrm{T}} \boldsymbol{\nu} - \boldsymbol{\lambda} \neq \mathbf{0}$, while the nontrivial solution of $-\mathbf{b}^{\mathrm{T}} \boldsymbol{\nu}$ is obtained when we have $\mathbf{c} + \mathbf{A}^{\mathrm{T}} \boldsymbol{\nu} - \boldsymbol{\lambda} = \mathbf{0}$. Therefore, a lower bound to the above LP of $-\mathbf{b}^{\mathrm{T}} \boldsymbol{\nu}$ is obtained when we have $\boldsymbol{\nu} \in \mathbb{R}$, $\boldsymbol{\lambda} \in \mathbb{R}_+$ and $\mathbf{c} + \mathbf{A}^{\mathrm{T}} \boldsymbol{\nu} - \boldsymbol{\lambda} = \mathbf{0}$.

### 2.5.2 The Lagrange Dual Problem

The dual problem is defined as

$$\begin{aligned} \text{maximize} \quad & g(\boldsymbol{\lambda}, \boldsymbol{\nu}) && (2.80) \\ \text{subject to} \quad & \boldsymbol{\lambda} \succeq \mathbf{0}, && (2.81) \end{aligned}$$

which may be interpreted as the important problem of finding the *best lower bound* to the primal optimization problem. A feasible solution to the dual problem is given by the pair $(\boldsymbol{\lambda}, \boldsymbol{\nu})$ and is it termed as *dual feasible*. The optimal solution is denoted by $(\boldsymbol{\lambda}^*, \boldsymbol{\nu}^*)$ and it is termed as *dual optimal* or the *optimal Lagrangian multipliers.*

The nontrivial dual problem of the previous example LP is given by

$$\begin{aligned} \text{maximize} \quad & -\mathbf{b}^{\mathrm{T}}\boldsymbol{\nu} && (2.82)\\ \text{subject to} \quad & \mathbf{c}+\mathbf{A}^{\mathrm{T}}\boldsymbol{\nu}-\boldsymbol{\lambda}=\mathbf{0} && (2.83)\\ & \boldsymbol{\lambda}\succeq\mathbf{0}, && (2.84) \end{aligned}$$

which is equivalent to

$$\begin{aligned} \text{maximize} \quad & -\mathbf{b}^{\mathrm{T}}\boldsymbol{\nu} && (2.85)\\ \text{subject to} \quad & \mathbf{c}+\mathbf{A}^{\mathrm{T}}\boldsymbol{\nu}-\boldsymbol{\lambda}\succeq\mathbf{0}. && (2.86) \end{aligned}$$

### 2.5.3 Strong and Weak Duality

The optimal value of the dual problem, denoted by $d^*$, is the highest lower bound to the optimal value of the original minimization problem. In other words, *weak duality*, given by

$$d^* \leq p^*, \tag{2.87}$$

holds, which is true regardless of the convex or non-convex nature of the primal problem. The difference

$$p^* - d^* \geq 0 \tag{2.88}$$

is termed the *optimal duality gap*. Therefore, given a dual feasible point, it is possible to find a lower bound to the optimal value of an optimization problem, which is often useful when determining stopping criteria for solution algorithms.

Under certain conditions, strong duality holds, when we have:

$$d^* = p^*. \tag{2.89}$$

In other words, the optimal duality gap is zero, which means that solving the dual problem is equivalent to solving the primal problem. For example, strong duality usually holds for (but is not limited to) convex minimization problems. In all cases, *constraint qualifications* determine whether strong duality holds. For example, *Slater's theorem* [34] states that if the problem is convex and satisfies *Slater's condition*, then strong duality holds. Explicitly, Slater's condition is that there exists a point $\mathbf{x} \in \mathbf{relint}\ \mathcal{D}$ strictly satisfying the convex (but not affine) inequality constraints [34]. In many cases, this condition is trivially satisfied.

A geometric interpretation of strong and weak duality is presented in Figs. 2.15 and 2.16 for a simple optimization problem having only a single inequality constraint. Given a nonconvex problem, the set of tuples $(f_1(\mathbf{x}), f_0(\mathbf{x}))$, denoted by $\mathcal{G}$, is nonconvex. The dual function is a

supporting hyperplane to $\mathcal{G}$ and its intersection with the vertical axis indicates the obtained value of $f_0$. Solving the dual problem provides the highest lower bound, $d^*$, of the optimal primal value, $p^*$. In the case of a nonconvex problem, the difference obeys $p^* - d^* \neq 0$ and the duality gap is nonzero. On the other hand, in the case of a convex problem, $\mathcal{G}$ is a convex set and the supporting hyperplane reaches $p^*$. Thus, we have $d^* = p^*$ and hence the duality gap is zero.

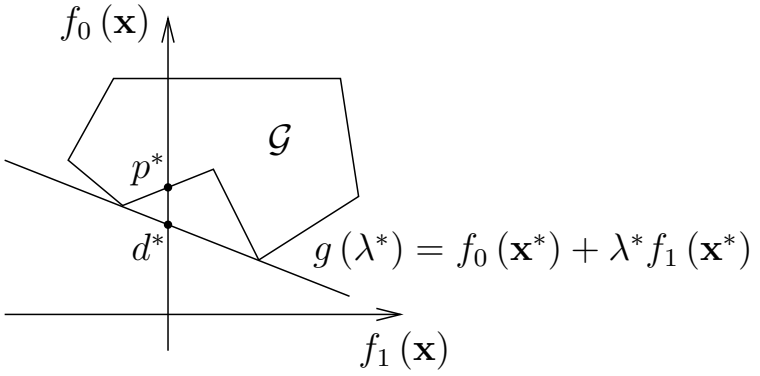


FIGURE 2.15: The set of tuples given by $\mathcal{G} = (f_1(\mathbf{x}), f_0(\mathbf{x}))$ is nonconvex. Hence, no supporting hyperplane to $\mathcal{G}$ can reach $p^*$, which implies weak duality and a nonzero duality gap.

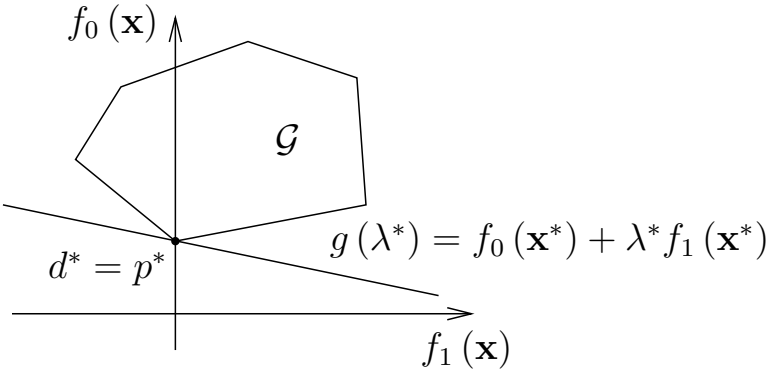


FIGURE 2.16: The set of tuples given by $\mathcal{G} = (f_1(\mathbf{x}), f_0(\mathbf{x}))$ is convex. There exists a supporting hyperplane to $\mathcal{G}$ at $(0, p^*)$, which implies strong duality and a zero duality gap.

### 2.5.4 The Karush-Kuhn-Tucker Conditions

For the special case of optimization problems exhibiting strong duality with differentiable objective, inequality and equality functions, the *KKT conditions* may be employed for verifying whether $\mathbf{x}$ and $(\boldsymbol{\lambda}, \boldsymbol{\nu})$ are primal and dual optimal, respectively.

Given a primal and dual feasible point, the optimal $\mathbf{x}^*$ that minimizes the Lagrangian

corresponds to the point, where its gradient vanishes. Therefore, we have:

$$\nabla f_0(\mathbf{x}^*) + \sum_{i=1}^{m} \lambda_i^* \nabla f_i(\mathbf{x}^*) + \sum_{i=1}^{p} \nu_i^* \nabla h_i(\mathbf{x}^*) = 0. \tag{2.90}$$

Additionally, given that strong duality holds, we have:

$$\sum_{i=1}^{m} \lambda_i^* f_i(\mathbf{x}^*) = 0. \tag{2.91}$$

However, each term in the above summation is nonpositive, so it follows that

$$\lambda_i^* f_i(\mathbf{x}^*) = 0, \ i = 1, \cdots, m, \tag{2.92}$$

which is termed *complementary slackness*. In other words, the optimal Lagrangian multiplier is zero unless its associated inequality constraint function is active at the optimal solution (when $f_i(\mathbf{x}^*) = 0$).

Combining the above two conditions with the conditions for primal and dual feasibility leads to the KKT conditions formulated as [34]:

$$\begin{aligned}
f_i(\mathbf{x}^*) &\leq 0, \ i = 1, \cdots, m && (2.93)\\
h_i(\mathbf{x}^*) &= 0, \ i = 1, \cdots, p && (2.94)\\
\lambda_i^* &\geq 0, \ i = 1, \cdots, m && (2.95)\\
\lambda_i^* f_i(\mathbf{x}^*) &= 0, \ i = 1, \cdots, m && (2.96)\\
\nabla f_0(\mathbf{x}^*) + \sum_{i=1}^{m} \lambda_i^* \nabla f_i(\mathbf{x}^*) + \sum_{i=1}^{p} \nu_i^* \nabla h_i(\mathbf{x}^*) &= 0. && (2.97)
\end{aligned}$$

Any primal and dual optimal point for an optimization problem with strong duality must satisfy the above conditions. In the case of convex optimization problems, the converse is true, implying that any point satisfying the KKT conditions must be primal and dual optimal.

## 2.6 Solution Algorithms

There exist numerous methods for solving different types of optimization problems [34]. For example, a popular method of solving linear problems is the simplex method [241], which often proves to be an efficient solution method. On the other hand, the ellipsoid, subgradient, and bundle methods are suitable for convex problems, while cutting-plane methods solve integer optimization problems [34,241,335]. In this section, we focus our attention on interior point (or barrier) methods by initially building our discussion upon fundamental solution

methods suitable for unconstrained optimization problems.

### 2.6.1 Unconstrained Minimization

In this section, we study unconstrained minimization problems of the form

$$\underset{\mathbf{x}\in\mathbb{R}^n}{\text{minimize}} \qquad f_0\left(\mathbf{x}\right), \tag{2.98}$$

where we assume that $f_0$ is convex and twice continuously differentiable. Therefore, $\mathbf{x}^*$ is optimal iff

$$\nabla f_0\left(\mathbf{x}^*\right) = 0, \tag{2.99}$$

which is equivalent to solving $n$ equations with $n$ unknowns. It is often not possible to solve (2.99) analytically, hence an iterative algorithm may be employed for obtaining a *minimizing sequence* of $\mathbf{x}^{(k)}$, where $f_0\left(\mathbf{x}^{(k)}\right) \to p^*$ as $k \to \infty$. These *descent methods* may be terminated, when we have $f_0\left(\mathbf{x}^{(k)}\right) - p^* \leq \epsilon$, where $\epsilon$ is the affordable *tolerance*. Furthermore, $\mathbf{x}^{(0)}$ is termed the *initial point*.

A minimizing sequence of $\mathbf{x}^{(k)}$ can be formulated as

$$\mathbf{x}^{(k+1)} = \mathbf{x}^{(k)} + t^{(k)}\Delta\mathbf{x}^{(k)}, \tag{2.100}$$

where $t^{(k)} > 0$ (except when $\mathbf{x}^{(k)}$ is optimal) is termed the *step size* or *step length*, while $\Delta\mathbf{x}^{(k)}$ is a vector denoting the *step* or *search direction*. Since the objective is minimization, the aim is to generate a minimizing sequence resulting in

$$f_0\left(\mathbf{x}^{(k+1)}\right) < f_0\left(\mathbf{x}^{(k)}\right), \tag{2.101}$$

(except when $\mathbf{x}^{(k)}$ is optimal) which requires that

$$\nabla f_0\left(\mathbf{x}^{(k)}\right)^{\mathrm{T}} \Delta\mathbf{x}^{(k)} < 0. \tag{2.102}$$

In other words, $\Delta\mathbf{x}^{(k)}$ must be a *descent direction*, which is illustrated in Fig. 2.17. Thus, the general structure of a descent method follows Table 2.3, where the particular choice of the stopping criterion depends on the specific method employed.

A *line search* is performed in Step 4 of Table 2.3 for determining a suitable value for the step size $t^{(k)}$. A naive method is the *exact line search* resulting in

$$t^{(k)} = \underset{s\geq 0}{\arg\min} f_0\left(\mathbf{x}^{(k)} + s\Delta\mathbf{x}^{(k)}\right), \tag{2.103}$$

which simply aims for minimizing the objective along the search direction. The exact line search is suitable when the cost of solving (2.103) is low. However, most practical solvers

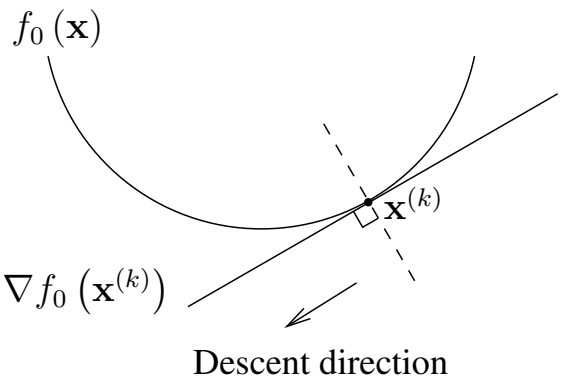


FIGURE 2.17: The line $\nabla f_0\left(\mathbf{x}^{(k)}\right)$ is the gradient of $f_0$ at $\mathbf{x}^{(k)}$. Therefore, any viable descent direction is to the left of the dashed line.

TABLE 2.3: A general descent method for minimization.

| | |
|---|---|
| Input: | $\mathbf{x}^{(0)} \in \mathbf{dom}\ f_0$ |
| | $\epsilon > 0$ |

1: $k \leftarrow 0$
2: **do**
3: Determine search direction $\Delta\mathbf{x}^{(k)}$
4: Choose step size $t^{(k)}$
5: $\mathbf{x}^{(k+1)} \leftarrow \mathbf{x}^{(k)} + t^{(k)}\Delta\mathbf{x}^{(k)}$
6: $k \leftarrow k + 1$
7: **while** stopping criterion not satisfied

employ *inexact* methods, which instead opt for reducing the objective by an acceptable amount along $\Delta\mathbf{x}^{(k)}$. Among the inexact methods, the *backtracking line search* benefits from both simplicity and efficiency. Given the two parameters of

$$0 < \alpha < 0.5 \tag{2.104}$$

and

$$0 < \beta < 1, \tag{2.105}$$

the backtracking line search may be performed, as detailed in Table 2.4. A geometric interpretation is provided in Fig. 2.18, which demonstrates that $\beta$ iteratively scales down the step size from unity, until the objective value becomes acceptably lower than that predicted using a modified linear interpolation at $f_0\left(\mathbf{x}^{(k)}\right)$.

Step 3 of Table 2.3 requires computing a search direction, $\Delta\mathbf{x}^{(k)}$. The *gradient descent method* adopts the natural choice of the negative gradient (or subgradient if the objective is nondifferentiable) at $\mathbf{x}^{(k)}$, denoted by $-\nabla f_0\left(\mathbf{x}^{(k)}\right)$, as the search direction. In this case, the stopping criterion is typically $\left|\left|\nabla f_0\left(\mathbf{x}^{(k)}\right)\right|\right|_2 \leq \eta$, which simply means that the method iterates until the gradient becomes sufficiently low. The gradient descent method exhibits

TABLE 2.4: The backtracking line search method [34].

| | |
|---|---|
| Input: | $0 < \alpha < 0.5$ |
| | $0 < \beta < 1$ |
| | $\Delta\mathbf{x}^{(k)}$ |

1: $t^{(k)} \leftarrow 1$
2: **do while** $f_0\left(\mathbf{x}^{(k)} + t^{(k)}\Delta\mathbf{x}^{(k)}\right) > f_0\left(\mathbf{x}^{(k)}\right) + \alpha t^{(k)}\nabla f_0\left(\mathbf{x}^{(k)}\right)^{\mathrm{T}}\Delta\mathbf{x}^{(k)}$
3: $\quad t^{(k)} \leftarrow \beta t^{(k)}$
4: **end do**

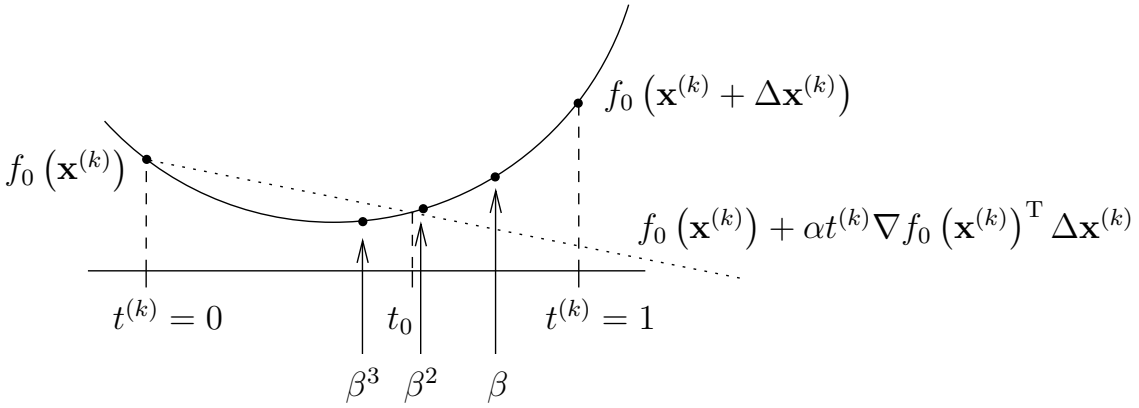


FIGURE 2.18: A geometric interpretation of the backtracking line search. The value of $t^{(k)}$ is iteratively scaled back from unity until $t^{(k)} < t_0$, which is the value needed to obtain the decease in the objective value predicted using the linear interpolation at $f_0\left(\mathbf{x}^{(k)}\right)$ using a gradient scaled by $\alpha$.

linear convergence and benefits from simplicity of implementation [34].

Alternatively, the *steepest descent method* employs the first-order Taylor approximation at $\mathbf{x}^{(k)}$ for determining a search direction that maximizes the approximated reduction of the objective value. If $v$ denotes the search direction, the approximated objective value is given by [34]

$$f_0\left(\mathbf{x}^{(k)} + v\right) \approx f_0\left(\mathbf{x}^{(k)}\right) + \nabla f_0\left(\mathbf{x}^{(k)}\right)^{\mathrm{T}} v, \tag{2.106}$$

where $\nabla f_0\left(\mathbf{x}^{(k)}\right)^{\mathrm{T}} v$ is the *directional derivative* of $f_0\left(\mathbf{x}^{(k)}\right)$ in the direction $v$, which should result in $\nabla f_0\left(\mathbf{x}^{(k)}\right)^{\mathrm{T}} v < 0$ and have a limited norm. Thus, a *normalized steepest descent* direction is given by [34]

$$\Delta\mathbf{x}_{nsd}^{(k)} = \underset{v\in\mathbb{R}^n}{\arg\min}\left\{\nabla f_0\left(\mathbf{x}^{(k)}\right)^{\mathrm{T}} v \,\middle|\, ||v|| = 1\right\}, \tag{2.107}$$

where $||\cdot||$ is any norm on $\mathbb{R}^n$. Geometrically, $\Delta\mathbf{x}_{nsd}^{(k)}$ is the vector directed to a point on the unit sphere of the norm, centered at $\mathbf{x}^{(k)}$, which minimizes $\nabla f_0\left(\mathbf{x}^{(k)}\right)^{\mathrm{T}} v$ resulting in the maximum reduction of the objective function value, as demonstrated in Fig. 2.19. In this case, a quadratic norm is employed, resulting in an ellipsoid for the unit sphere of the

norm. When the norm employed is the Euclidean norm, the unit sphere is circular and the steepest descent direction is simply a unit vector of the negative gradient. Furthermore, if the $\ell_1$-norm is employed, the steepest descent direction is simply the standard basis vector, corresponding to the minimum component of the gradient, in the direction of the negative gradient. The steepest descent method converges linearly, assuming that a suitable norm is employed [34].

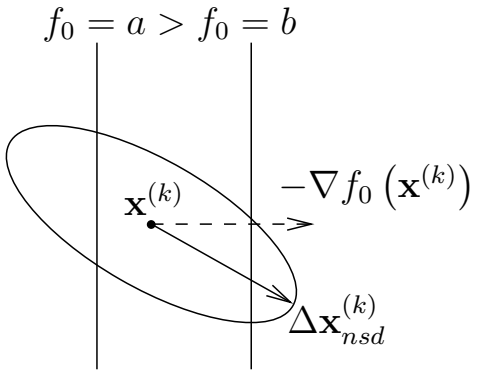


FIGURE 2.19: The steepest descent search direction is the unit length vector in some norm $||\cdot||$ in the direction of the negative gradient $\nabla f_0\left(\mathbf{x}^{(k)}\right)$ that maximizes the decrease in the objective value. the vertical lines represent level curves of the function $f_0$.

The final method presented in this section is *Newton's method* [34], which relies on employing the *Newton step* and the *Newton decrement*. The Newton step, given by [34]

$$\Delta \mathbf{x}_{nt}^{(k)} = -\nabla^2 f_0\left(\mathbf{x}^{(k)}\right)^{-1} \nabla f_0\left(\mathbf{x}^{(k)}\right), \tag{2.108}$$

may be interpreted in multiple ways. For example, it is the minimizer of the second-order Taylor approximation of $f_0$, given by [34]

$$f_0\left(\mathbf{x}^{(k)} + \mathbf{v}^{(k)}\right) \approx f_0\left(\mathbf{x}^{(k)}\right) + \nabla f_0\left(\mathbf{x}^{(k)}\right)^{\mathrm{T}} \mathbf{v} + \frac{1}{2}\mathbf{v}^{\mathrm{T}} \nabla^2 f_0\left(\mathbf{x}^{(k)}\right) \mathbf{v}, \tag{2.109}$$

while also being the solution of the linearized optimality condition, given by [34]

$$\nabla f_0\left(\mathbf{x}^{(k)} + \mathbf{v}\right) \approx \nabla f_0\left(\mathbf{x}^{(k)}\right) + \nabla^2 f_0\left(\mathbf{x}^{(k)}\right) \mathbf{v} = 0. \tag{2.110}$$

On the other hand, the Newton decrement is given by [34]

$$\lambda\left(\mathbf{x}^{(k)}\right) = \left[\nabla f_0\left(\mathbf{x}^{(k)}\right)^{\mathrm{T}} \nabla^2 f_0\left(\mathbf{x}^{(k)}\right)^{-1} \nabla f_0\left(\mathbf{x}^{(k)}\right)\right]^{\frac{1}{2}}. \tag{2.111}$$

Assuming that the second-order Taylor approximation using the Newton step obtains the optimal value of $p^*$, we may write (dropping the superscript $(k)$):

$$f_0(\mathbf{x}) - p^* = f_0(\mathbf{x}) - \left[f_0(\mathbf{x}) + \nabla f_0(\mathbf{x})^{\mathrm{T}} \Delta \mathbf{x}_{nt} + \frac{1}{2}\left(\Delta \mathbf{x}_{nt}\right)^{\mathrm{T}} \nabla^2 f_0(\mathbf{x}) \Delta \mathbf{x}_{nt}\right] \tag{2.112}$$

$$= \nabla f_0(\mathbf{x})^{\mathrm{T}} \nabla^2 f_0(\mathbf{x})^{-1} \nabla f_0(\mathbf{x}) - \frac{1}{2} \nabla f_0(\mathbf{x})^{\mathrm{T}} \nabla^2 f_0(\mathbf{x})^{-1} \nabla f_0(\mathbf{x}) \quad (2.113)$$

$$= \frac{1}{2} \nabla f_0(\mathbf{x})^{\mathrm{T}} \nabla^2 f_0(\mathbf{x})^{-1} \nabla f_0(\mathbf{x}) \quad (2.114)$$

$$= \frac{1}{2} \lambda(\mathbf{x})^2 . \quad (2.115)$$

Therefore, the Newton decrement is an estimate of the optimality gap and it is employed as the stopping criterion in Newton's method, as described in Table 2.5. In general, the convergence of Newton's method is rapid (quadratic near the optimal point), while being invariant to the problem size or the parameters employed [34], making it preferable over the previously discussed methods.

TABLE 2.5: Newton's method for optimization [34].

| | |
|---|---|
| Input: | $\mathbf{x}^{(0)} \in \mathbf{dom}\ f_0$ |
| | $\epsilon$ |

1: $k \leftarrow 0$
2: **do while true**
3: $\quad \Delta\mathbf{x}_{nt}^{(k)} \leftarrow -\nabla^2 f_0\left(\mathbf{x}^{(k)}\right)^{-1} \nabla f_0\left(\mathbf{x}^{(k)}\right)$
4: $\quad \lambda\left(\mathbf{x}^{(k)}\right)^2 \leftarrow \nabla f_0\left(\mathbf{x}^{(k)}\right)^{\mathrm{T}} \nabla^2 f_0\left(\mathbf{x}^{(k)}\right)^{-1} \nabla f_0\left(\mathbf{x}^{(k)}\right)$
5: $\quad$ **if** $\frac{1}{2}\lambda\left(\mathbf{x}^{(k)}\right)^2 \leq \epsilon$
6: $\quad\quad$ **break**
7: $\quad$ **end if**
8: $\quad$ Backtracking line search to obtain $t^{(k)}$
9: $\quad \mathbf{x}^{(k+1)} \leftarrow \mathbf{x}^{(k)} + t^{(k)} \Delta\mathbf{x}_{nt}^{(k)}$
10: $\quad k \leftarrow k + 1$
11: **end do**

### 2.6.2 Equality Constrained Minimization

Let us now turn our attention to equality-constrained minimization problems formulated as

$$\underset{\mathbf{x} \in \mathbb{R}^n}{\text{minimize}} \quad f_0(\mathbf{x}) \quad (2.116)$$

$$\text{subject to} \quad \mathbf{A}\mathbf{x} = \mathbf{b}, \quad (2.117)$$

where once again, $f_0$ is twice continuously differentiable and $\mathbf{A}^{p \times n} \in \mathbb{R}$ with $\mathbf{rank}(\mathbf{A}) = p < n$. Thus, there are $p$ independent equations with $n$ unknowns and the linear system is underdetermined. Upon employing the KKT conditions of (2.93)–(2.97), the optimal primal and dual variables, $\mathbf{x}^*$ and $\boldsymbol{\nu}^*$ respectively, obey

$$\mathbf{A}\mathbf{x}^* = \mathbf{b} \quad (2.118)$$

and

$$\nabla f_0\left(\mathbf{x}^*\right) + \mathbf{A}^{\mathrm{T}}\boldsymbol{\nu}^* = 0, \tag{2.119}$$

which in some rare cases can be solved analytically. For example, when applied to a problem associated with a quadratic objective function formulated as

$$\underset{\mathbf{x}\in\mathbb{R}^n}{\text{minimize}} \quad \frac{1}{2}\mathbf{x}^{\mathrm{T}}\mathbf{P}\mathbf{x} + \mathbf{q}^{\mathrm{T}}\mathbf{x} + r \tag{2.120}$$

$$\text{subject to} \quad \mathbf{A}\mathbf{x} = \mathbf{b}, \tag{2.121}$$

where we have $\mathbf{P} \in \mathbf{S}_+^n$ and $\mathbf{A}^{p\times n} \in \mathbb{R}$, the KKT conditions require that [34] $\mathbf{A}\mathbf{x}^* = \mathbf{b}$ and that

$$\mathbf{P}\mathbf{x}^* + \mathbf{q} + \mathbf{A}^{\mathrm{T}}\boldsymbol{\nu}^* = 0. \tag{2.122}$$

These two conditions may be written as the *KKT system* given by [34]

$$\begin{bmatrix} \mathbf{P} & \mathbf{A}^{\mathrm{T}} \\ \mathbf{A} & \mathbf{0} \end{bmatrix} \begin{bmatrix} \mathbf{x}^* \\ \boldsymbol{\nu}^* \end{bmatrix} = \begin{bmatrix} -\mathbf{q} \\ \mathbf{b} \end{bmatrix}, \tag{2.123}$$

where the matrix of coefficients is referred to as the *KKT matrix*. If the KKT matrix is nonsingular, there is a unique and optimal primal-dual pair, which solves (2.116)–(2.117). If it is singular but solvable, there are multiple solutions. If it is unsolvable, the problem is either infeasible or unbounded from below.

For general equality constrained minimization problems, typically a modified version of Newton's method is employed, which crucially requires that a feasible starting point is chosen and that each Newton step maintains this feasibility. More specifically, the starting point must satisfy [34]

$$\mathbf{A}\mathbf{x}^{(0)} = \mathbf{b}, \tag{2.124}$$

while the Newton step at iteration $k$ satisfies

$$\mathbf{A}\Delta\mathbf{x}_{nt}^{(k)} = \mathbf{0}. \tag{2.125}$$

The feasible Newton step at iteration $k$ is derived by replacing the objective function by its second-order Taylor approximation $\widehat{f}_0$ near $\mathbf{x}^{(k)}$ to yield [34]:

$$\underset{\mathbf{v}\in\mathbb{R}^n}{\text{minimize}} \quad \widehat{f}_0\left(\mathbf{x}^{(k)}+\mathbf{v}\right) = f_0\left(\mathbf{x}^{(k)}\right) + \nabla f_0\left(\mathbf{x}^{(k)}\right)^{\mathrm{T}}\mathbf{v} + \frac{1}{2}\mathbf{v}^{\mathrm{T}}\nabla^2 f_0\left(\mathbf{x}^{(k)}\right)\mathbf{v} \tag{2.126}$$

$$\text{subject to} \quad \mathbf{A}\left(\mathbf{x}^{(k)}+\mathbf{v}\right) = \mathbf{b}, \tag{2.127}$$

where the decision variable is now $\mathbf{v}$. Notice that the above problem is an equality-constrained quadratic problem, which may be analytically solved by finding the solution

to the KKT system given by [34]

$$\begin{bmatrix} \nabla^2 f_0\left(\mathbf{x}^{(k)}\right) & \mathbf{A}^{\mathrm{T}} \\ \mathbf{A} & \mathbf{0} \end{bmatrix} \begin{bmatrix} \mathbf{v} \\ \boldsymbol{\omega} \end{bmatrix} = \begin{bmatrix} -\nabla f_0\left(\mathbf{x}^{(k)}\right) \\ \mathbf{0} \end{bmatrix}, \tag{2.128}$$

where $\boldsymbol{\omega}$ is the dual variable associated with the quadratic problem. The optimal primal solution is $\mathbf{x}_{nt}^{(k)} = \mathbf{v}^*$, and since $\mathbf{A}\mathbf{v}^* = \mathbf{A}\Delta\mathbf{x}_{nt}^{(k)} = \mathbf{0}$, $\Delta\mathbf{x}_{nt}^{(k)}$ is a *feasible descent direction*, when Newton's method is initialized with a feasible starting point.

On the other hand, a generalized Newton method is effective in the case of possibly infeasible starting points and iterates. Recall that the KKT optimality conditions of (2.118)–(2.119) for an equality-constrained minimization problem are given by $\mathbf{A}\mathbf{x}^* = \mathbf{b}$ and $\nabla f_0\left(\mathbf{x}^*\right) + \mathbf{A}^{\mathrm{T}}\boldsymbol{\nu}^* = 0$. Given a current (possibly infeasible) iterate $\mathbf{x}^{(k)}$, the goal is to ensure that the next iterate of $\left(\mathbf{x}^{(k)} + \Delta\mathbf{x}^{(k)}\right)$ approximately satisfies the KKT conditions. Performing the first-order approximation for the gradient at the next iterate results in [34]

$$\nabla f_0\left(\mathbf{x}^{(k)} + \Delta\mathbf{x}^{(k)}\right) = \nabla f_0\left(\mathbf{x}^{(k)}\right) + \nabla^2 f_0\left(\mathbf{x}^{(k)}\right)\Delta\mathbf{x}^{(k)}, \tag{2.129}$$

which allows us to write the approximate KKT conditions as [34]

$$\mathbf{A}\left(\mathbf{x}^{(k)} + \Delta\mathbf{x}^{(k)}\right) = \mathbf{b} \tag{2.130}$$

and

$$\nabla f_0\left(\mathbf{x}^{(k)}\right) + \nabla^2 f_0\left(\mathbf{x}^{(k)}\right)\Delta\mathbf{x}^{(k)} + \mathbf{A}^{\mathrm{T}}\boldsymbol{\omega} = 0, \tag{2.131}$$

where $\boldsymbol{\nu}^*$ has been substituted by $\boldsymbol{\omega}$. This set of linear equations in $\Delta\mathbf{x}^{(k)}$ and $\boldsymbol{\omega}$ may be written as a KKT system given by

$$\begin{bmatrix} \nabla^2 f_0\left(\mathbf{x}^{(k)}\right) & \mathbf{A}^{\mathrm{T}} \\ \mathbf{A} & \mathbf{0} \end{bmatrix} \begin{bmatrix} \Delta\mathbf{x}^{(k)} \\ \boldsymbol{\omega} \end{bmatrix} = -\begin{bmatrix} \nabla f_0\left(\mathbf{x}^{(k)}\right) \\ \mathbf{A}\mathbf{x}^{(k)} - \mathbf{b} \end{bmatrix}. \tag{2.132}$$

Notice the similarities between (2.132) and (2.128). In fact, when the current iterate is feasible, the second block on the right-hand side vanishes and the method will proceed to descend with feasible steps, as in the case of the feasible-start Newton's method. Thus,

$$r_{pri}\left(\mathbf{x}^{(k)}, \boldsymbol{\omega}\right) = \mathbf{A}\mathbf{x}^{(k)} - \mathbf{b} \tag{2.133}$$

is the *primal residual* [34] at the current iterate. Furthermore, the *dual residual* is defined as the gradient of the Lagrangian, which is written as [34]

$$r_{dual}\left(\mathbf{x}^{(k)}, \boldsymbol{\omega}\right) = \nabla f_0\left(\mathbf{x}^*\right) + \mathbf{A}^{\mathrm{T}}\boldsymbol{\omega}. \tag{2.134}$$

We may interpret this Newton method as a *primal-dual method*, which updates both the

primal and dual variables to satisfy the KKT conditions. Let us define the *primal-dual* step applied to the primal-dual pair, given by $\mathbf{y}_{pd}^{(k)} = \left(\mathbf{x}^{(k)}, \boldsymbol{\omega}\right)$, as $\Delta\mathbf{y}_{pd}^{(k)} = \left(\Delta\mathbf{x}^{(k)}, \Delta\boldsymbol{\omega}\right)$. When minimizing the residual $r\left(\mathbf{y}_{pd}^{(k)}\right)$, the first-order Taylor approximate of the next iterate may be employed to give [34]

$$r\left(\mathbf{y}_{pd}^{(k)}\right) + Dr\left(\mathbf{y}_{pd}^{(k)}\right)\Delta\mathbf{y}_{pd}^{(k)} = 0, \tag{2.135}$$

which implies

$$Dr\left(\mathbf{y}_{pd}^{(k)}\right)\Delta\mathbf{y}_{pd}^{(k)} = -r\left(\mathbf{y}_{pd}^{(k)}\right), \tag{2.136}$$

where $Dr\left(\mathbf{y}_{pd}^{(k)}\right)$ is the derivative of $r\left(\mathbf{y}_{pd}^{(k)}\right)$ at $\mathbf{y}_{pd}^{(k)}$. Evaluating $Dr\left(\mathbf{y}_{pd}^{(k)}\right)$ results in [34]

$$\begin{bmatrix} \nabla^2 f_0\left(\mathbf{x}^{(k)}\right) & \mathbf{A}^{\mathrm{T}} \\ \mathbf{A} & \mathbf{0} \end{bmatrix} \begin{bmatrix} \Delta\mathbf{x}^{(k)} \\ \Delta\boldsymbol{\omega} \end{bmatrix} = -\begin{bmatrix} r_{pri} \\ r_{dual} \end{bmatrix} = -\begin{bmatrix} \nabla f_0\left(\mathbf{x}^{(k)}\right) + \mathbf{A}^{\mathrm{T}}\boldsymbol{\omega} \\ \mathbf{A}\mathbf{x}^{(k)} - \mathbf{b} \end{bmatrix}. \tag{2.137}$$

If the substitution of $\boldsymbol{\omega}^{+} = \boldsymbol{\omega} + \Delta\boldsymbol{\omega}$ is performed, the above system of equations simplifies to (2.132), where $\boldsymbol{\omega}^{+}$ is then the updated dual variable. Thus, we may conclude that the solution of (2.132) aims for minimizing both the primal and dual residuals. This motivates using the residual as the stopping criterion in the backtracking line search of the infeasible-start Newton method, as detailed in Table 2.6. It is possible to show that each iteration of this method reduces the norm of the residual by at least a fixed amount, while convergence is quadratic in the vicinity of the optimal solution [34].

TABLE 2.6: Infeasible-start Newton method [34].

| | |
|---|---|
| Input: | $0 < \alpha < 0.5$, $0 < \beta < 1$ |
| | $\mathbf{x}^{(0)} \in \mathbf{dom}\ f_0$, $\boldsymbol{\omega}$ |
| | $\epsilon > 0$ |

1: $k \leftarrow 0$
2: **do**
3: Compute $\Delta\mathbf{x}^{(k)}$ and $\Delta\boldsymbol{\omega}$ using (2.137)
4: $t \leftarrow 1$
5: **while** $\left|\left|r\left(\mathbf{x}^{(k)} + t\Delta\mathbf{x}^{(k)}, \boldsymbol{\omega} + t\Delta\boldsymbol{\omega}\right)\right|\right|_2 > (1 - \alpha t)\left|\left|r\left(\mathbf{x}^{(k)}, \boldsymbol{\omega}\right)\right|\right|_2$,
6: $t \leftarrow \beta t$
7: **end while**
8: Update $\mathbf{x}^{(k+1)} \leftarrow \mathbf{x}^{(k)} + t\Delta\mathbf{x}^{(k)}$, $\boldsymbol{\omega} \leftarrow \boldsymbol{\omega} + t\Delta\boldsymbol{\omega}$
9: $k \leftarrow k + 1$
10: **while** $\mathbf{A}\mathbf{x}^{(k)} \neq \mathbf{b}$ **or** $\left|\left|r\left(\mathbf{x}^{(k)}, \boldsymbol{\omega}\right)\right|\right|_2 > \epsilon$

### 2.6.3 Interior Point Methods

Let us now focus our attention on general convex minimization problems of the form

$$\underset{\mathbf{x}\in\mathcal{D}}{\text{minimize}} \quad f_0(\mathbf{x}) \tag{2.138}$$

$$\text{subject to} \quad f_i(\mathbf{x}) \leq 0,\ i = 1, \cdots, m \tag{2.139}$$

$$\mathbf{A}\mathbf{x} = \mathbf{b}, \tag{2.140}$$

where $f_i$, $i = 0, \cdots, m$ are twice continuously differentiable, while $\mathbf{A} \in \mathbb{R}^{p\times n}$ and $\mathbf{rank}(\mathbf{A}) = p < n$. Furthermore, the problem is strictly feasible and solvable. Thus, there exists primal and dual optimal points satisfying the KKT conditions of (2.93)–(2.97) [34].

#### 2.6.3.1 Barrier Method

The aim is to convert the above problem into a series of equality-constrained problems, which can be solved using Newton's method. This is accomplished by firstly introducing a *barrier function* [34] to formulate the general convex problem as an equivalent equality-constrained problem, given by

$$\underset{\mathbf{x}\in\mathcal{D}}{\text{minimize}} \quad f_0(\mathbf{x}) + \sum_{i=1}^{m} I_-(f_i(\mathbf{x})) \tag{2.141}$$

$$\text{subject to} \quad \mathbf{A}\mathbf{x} = \mathbf{b}, \tag{2.142}$$

where $I_-(u)$ is the nonpositive indicator function,

$$I_-(u) = \begin{cases} \infty & \text{if } u > 0, \\ 0 & \text{if } u \leq 0. \end{cases} \tag{2.143}$$

Clearly, the equality-constrained problem of (2.141)–(2.142) is infeasible if at least one of the original inequality constraints are not satisfied. However, $I_-(u)$ is not differentiable, hence Newton's method cannot be directly applied. To circumvent this setback, the approximation of [34]:

$$\widehat{I}_-(u) = -\frac{1}{t}\log(-u),\ \mathbf{dom}\ \widehat{I}_- = \mathbb{R}_{--} \tag{2.144}$$

is employed instead of $I_-(u)$, with the parameter $t > 0$ controlling the accuracy of the approximation, and, as depicted in Fig. 2.20, when $t \to \infty$, the approximation becomes progressively more accurate [34]. Thus, (2.141)–(2.142) may be approximated by [34]

$$\underset{\mathbf{x}\in\mathcal{D}}{\text{minimize}} \quad tf_0(\mathbf{x}) + \phi(\mathbf{x}) \tag{2.145}$$

$$\text{subject to} \quad \mathbf{A}\mathbf{x} = \mathbf{b}, \tag{2.146}$$

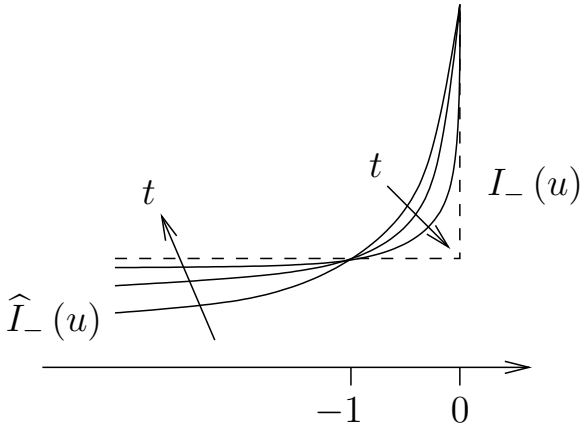


FIGURE 2.20: The approximation $\widehat{I}_-(u)$ models $I_-(u)$ more closely as $t \to \infty$.

where the *logarithmic barrier function* [34]

$$\phi(\mathbf{x}) = -\sum_{i=1}^{m} \log\left(-f_i(\mathbf{x})\right), \ \mathbf{dom}\ \phi = \{\mathbf{x} \in \mathcal{D} | f_i(\mathbf{x}) < 0,\ i = 1, \cdots, m\}, \tag{2.147}$$

is employed, and where the objective has been multiplied by the parameter $t$. The minimizers of (2.141)–(2.142) are identical to those of (2.145)–(2.146), which additionally benefits from having a differentiable objective function. Thus, the aforementioned Newton methods may be similarly applied for solving (2.145)–(2.146).

The minimizer of (2.145)–(2.146) given a parameter $t$ is termed a *central point*, which we denote as $\mathbf{x}^*(t)$. The sequence of $\mathbf{x}^*(t)$ as $t \to \infty$ is termed the *central path*. Central points must be strictly feasible, and each yield a dual feasible point $\widehat{\boldsymbol{\nu}}(t)$ satisfying [34]

$$0 = t\nabla f_0(\mathbf{x}^*(t)) + \nabla\phi(\mathbf{x}^*(t)) + \mathbf{A}^{\mathrm{T}}\widehat{\boldsymbol{\nu}}(t) \tag{2.148}$$

$$= t\nabla f_0(\mathbf{x}^*(t)) + \sum_{i=1}^{m} \frac{1}{-f_i(\mathbf{x}^*(t))} \nabla f_i(\mathbf{x}^*(t)) + \mathbf{A}^{\mathrm{T}}\widehat{\boldsymbol{\nu}}(t) \tag{2.149}$$

from which we can obtain a lower bound to the optimal value. We proceed by introducing:

$$\lambda_i^*(t) = \frac{1}{-t f_i(\mathbf{x}^*(t))} \tag{2.150}$$

and $\boldsymbol{\nu}^*(t) = \widehat{\boldsymbol{\nu}}(t)/t$, so that (2.149) may be rewritten as [34]

$$0 = \nabla f_0(\mathbf{x}^*(t)) + \sum_{i=1}^{m} \lambda_i^*(t) \nabla f_i(\mathbf{x}^*(t)) + \mathbf{A}^{\mathrm{T}}\boldsymbol{\nu}^*(t). \tag{2.151}$$

Therefore, $\mathbf{x}^*(t)$ is a minimizer of the Lagrangian

$$\mathcal{L}(\mathbf{x}, \boldsymbol{\lambda}, \boldsymbol{\nu}) = f_0(\mathbf{x}) + \sum_{i=1}^{m} \lambda_i f_i(\mathbf{x}) + \boldsymbol{\nu}^{\mathrm{T}}(\mathbf{A}\mathbf{x} - \mathbf{b}), \tag{2.152}$$

while $\boldsymbol{\lambda}^*(t) = (\lambda_1^*(t), \cdots, \lambda_m^*(t))$ and $\boldsymbol{\nu}^*(t)$ result in a dual function value of [34]

$$g(\boldsymbol{\lambda}^*(t), \boldsymbol{\nu}^*(t)) = f_0(\mathbf{x}^*(t)) + \sum_{i=1}^{m} \lambda_i^*(t) f_i(\mathbf{x}^*(t)) + \boldsymbol{\nu}^*(t)^{\mathrm{T}} (\mathbf{A}\mathbf{x}^*(t) - \mathbf{b}) \quad (2.153)$$

$$= f_0(\mathbf{x}^*(t)) - m/t, \quad (2.154)$$

when substituting in (2.150). In particular, observe that the resultant duality gap is simply $m/t$. Thus, we may conclude that

$$f_0(\mathbf{x}^*(t)) - p^* \leq m/t, \quad (2.155)$$

and $\mathbf{x}^*(t)$ is $m/t$-suboptimal. More importantly, it is clear that $\mathbf{x}^*(t) \to \mathbf{x}^*$ when $t \to \infty$. The barrier method is outlined in Table 2.7.

TABLE 2.7: The barrier method [34].

| | |
|---|---|
| Input: | Strictly feasible $\mathbf{x}^{(0)}$ |
| | Barrier parameters $t > 0$, $\mu > 1$ |
| | Tolerance $\epsilon > 0$ |

1: $k \leftarrow 0$
2: **do**
3: Compute $\mathbf{x}^*(t)$, which solves (2.145)–(2.146), with $\mathbf{x}^{(k)}$ as reference point
4: $\mathbf{x}^{(k+1)} \leftarrow \mathbf{x}^*(t)$
5: $t \leftarrow \mu t$, $k \leftarrow k + 1$
6: **while** $\mu m/t > \epsilon$

Step 3 of Table 2.7 is often referred to as a *centering step* or an *outer iteration* of the barrier method, which typically invokes Newton's method for solving the equality-constrained minimization problem. On the other hand, each iteration of Newton's method in Step 3 is termed an *inner iteration* of the barrier method.

Furthermore, the choice of $\mu > 1$ should be considered carefully. If $\mu$ is close to unity, $t$ increases only marginally with each outer iteration, but the previous value for $\mathbf{x}$ will be a good approximation of the solution for the minimization problem with the updated $t$. Thus, fewer inner iterations are expected to be required, albeit at the cost of a higher number of outer iterations since the iterate only progresses marginally. This approach is termed as the *path-following method* [34]. Alternatively, if $\mu$ is large, $t$ increases substantially and the previous iterate is likely to be far from the optimal solution for the updated minimization problem. Therefore, fewer outer iterations are required in exchange for more inner iterations.

A requirement of the barrier method is that of having a strictly feasible starting point. When such a point is not known, the barrier method is preceded by a *phase I* stage in which a strictly feasible point is found (or the constraints are found to be infeasible), which

is then employed as the starting point in the *phase II* (barrier method) stage. A possible method for computing an initial strictly feasible point is to solve

$$\begin{aligned} \underset{s\in\mathbb{R},\mathbf{x}\in\mathcal{D}}{\text{minimize}} \quad & s && (2.156)\\ \text{subject to} \quad & f_i(\mathbf{x}) \leq s,\ i=1,\cdots,m && (2.157)\\ & \mathbf{A}\mathbf{x}=\mathbf{b}. && (2.158) \end{aligned}$$

If $\mathbf{A}\mathbf{x}=\mathbf{b}$ has any solutions, (2.156)–(2.158) is strictly feasible, since we can compute its value for $\mathbf{A}\mathbf{x}^{(0)}=\mathbf{b}$ and set $s$ to be larger than $\max_{i=1,\cdots,m}\left(f_i\left(\mathbf{x}^{(0)}\right)\right)$. Thus, after obtaining a strictly feasible point for (2.156)–(2.158), the barrier method can be employed for finding the minimum $s$.

Clearly, if $s^*<0$, the corresponding $\mathbf{x}^*$ is a strictly feasible point for (2.138)–(2.140) and thus may be employed as the starting point for solving (2.138)–(2.140) using the barrier method. Furthermore, the barrier method for solving (2.156)–(2.158) may be terminated, when we have $s^{(k)}<0$, since any strictly feasible point will be adequate and it is not necessary to solve the problem with a high accuracy.

On the other hand, if we have $s^*>0$, (2.138)–(2.140) is infeasible. The barrier method for (2.156)–(2.158) may simply be terminated, when a dual feasible point resulting in a strictly positive dual objective value is found, which indicates that a lower bound for the primal objective value is strictly positive, proving that (2.138)–(2.140) is infeasible.

However, if we have $s^*=0$, the corresponding $\mathbf{x}^*$ is only a feasible point for (2.138)–(2.140). In practice, the barrier method is terminated when $|f_i(\mathbf{x}^*)|\leq\epsilon$, indicating that some $f_i(\mathbf{x}^*)\leq\epsilon$ and were infeasible, while some $f_i(\mathbf{x}^*)\leq-\epsilon$ and were feasible.

#### 2.6.3.2 Primal-Dual Interior Point Method

We will now briefly touch upon a basic *primal-dual* interior point method. Unlike for the barrier method, there is no distinction between the inner and outer iterations. Both the primal and dual search directions are computed simultaneously, and are not necessarily feasible at each iteration. For most problems of interest, the primal-dual interior point methods outperform the barrier methods, since they exhibit a better than linear convergence [34].

We commence by writing the modified KKT equations as [34]

$$\begin{aligned} f_i(\mathbf{x}^*) &\leq 0,\ i=1,\cdots,m && (2.159)\\ \mathbf{A}\mathbf{x}^* &= \mathbf{b},\ i=1,\cdots,p && (2.160)\\ \lambda_i^* &\geq 0,\ i=1,\cdots,m && (2.161)\\ -\lambda_i^* f_i(\mathbf{x}^*) &= \frac{1}{t},\ i=1,\cdots,m && (2.162) \end{aligned}$$

$$\nabla f_0(\mathbf{x}^*) + \sum_{i=1}^{m} \lambda_i^* \nabla f_i(\mathbf{x}^*) + \mathbf{A}^{\mathrm{T}} \boldsymbol{\nu}^* = 0. \tag{2.163}$$

The equality conditions of (2.159)–(2.163) may be written as

$$r_t(\mathbf{x}^*, \boldsymbol{\lambda}^*, \boldsymbol{\nu}^*) = \begin{bmatrix} r_{dual} \\ r_{cent} \\ r_{pri} \end{bmatrix} \tag{2.164}$$

$$= \begin{bmatrix} \nabla f_0(\mathbf{x}^*) + D\mathbf{f}(\mathbf{x}^*)^{\mathrm{T}} \boldsymbol{\lambda}^* + \mathbf{A}^{\mathrm{T}} \boldsymbol{\nu}^* \\ -\mathbf{diag}(\boldsymbol{\lambda}^*) \mathbf{f}(\mathbf{x}^*) - (1/t)\mathbf{1} \\ \mathbf{A}\mathbf{x} - \mathbf{b} \end{bmatrix} \tag{2.165}$$

$$= \mathbf{0}, \tag{2.166}$$

where $\mathbf{f} : \mathbb{R}^n \to \mathbb{R}^m$ is a function returning the values of the inequality-constraint functions of the optimization problem, while $D\mathbf{f}(\mathbf{x})$ is its *derivative matrix*. In other words, we have

$$\mathbf{f}(\mathbf{x}) = \begin{bmatrix} f_1(\mathbf{x}) \\ \vdots \\ f_m(\mathbf{x}) \end{bmatrix} \text{ and } D\mathbf{f}(\mathbf{x}) = \begin{bmatrix} \nabla f_1(\mathbf{x})^{\mathrm{T}} \\ \vdots \\ \nabla f_m(\mathbf{x})^{\mathrm{T}} \end{bmatrix}. \tag{2.167}$$

The first and last block of $r_t(\mathbf{x}, \boldsymbol{\lambda}, \boldsymbol{\nu})$ are dual and primal residuals, respectively. The middle block is termed as the *centrality residual*, which corresponds to the modified complementary condition of (2.162). Clearly, as $t \to \infty$, the solution to $r_t(\mathbf{x}, \boldsymbol{\lambda}, \boldsymbol{\nu}) = 0$ approaches the solution for the original KKT conditions.

Given the primal-dual point

$$y_{pd}^{(k)} = \left(\mathbf{x}^{(k)}, \boldsymbol{\lambda}^{(k)}, \boldsymbol{\nu}^{(k)}\right) \tag{2.168}$$

and a Newton step of

$$\Delta y_{pd}^{(k)} = \left(\Delta\mathbf{x}^{(k)}, \Delta\boldsymbol{\lambda}^{(k)}, \Delta\boldsymbol{\nu}^{(k)}\right), \tag{2.169}$$

the first-order Taylor approximation

$$r_t\left(y_{pd}^{(k)} + \Delta y_{pd}^{(k)}\right) \approx r_t\left(y_{pd}^{(k)}\right) + Dr_t\left(y_{pd}^{(k)}\right) \Delta y_{pd}^{(k)} = \mathbf{0} \tag{2.170}$$

$$Dr_t\left(y_{pd}^{(k)}\right) \Delta y_{pd}^{(k)} = -r_t\left(y_{pd}^{(k)}\right) \tag{2.171}$$

$$\begin{bmatrix} \nabla^2 f_0\left(\mathbf{x}^{(k)}\right) + \sum_{i=1}^{m} \lambda_i \nabla^2 f_i\left(\mathbf{x}^{(k)}\right) & D\mathbf{f}\left(\mathbf{x}^{(k)}\right)^{\mathrm{T}} & \mathbf{A}^{\mathrm{T}} \\ -\mathbf{diag}\left(\boldsymbol{\lambda}^{(k)}\right) D\mathbf{f}\left(\mathbf{x}^{(k)}\right) & -\mathbf{diag}\left(\mathbf{f}\left(\mathbf{x}^{(k)}\right)\right) & \mathbf{0} \\ \mathbf{A} & \mathbf{0} & \mathbf{0} \end{bmatrix} \begin{bmatrix} \Delta\mathbf{x}^{(k)} \\ \Delta\boldsymbol{\lambda}^{(k)} \\ \Delta\boldsymbol{\nu}^{(k)} \end{bmatrix} = - \begin{bmatrix} r_{dual} \\ r_{cent} \\ r_{pri} \end{bmatrix} \tag{2.172}$$

can be made. Thus, the Newton step at iteration $k$ may be computed by solving (2.172). Observe that the primal and dual update directions are coupled. Furthermore, when primal feasibility is satisfied we have $r_{pri} = \mathbf{0}$, which results in $\mathbf{A}\Delta\mathbf{x}^{(k)} = 0$ and primal feasibility is maintained in each step.

Since the primal and dual iterates of this primal-dual method may not be feasible, a *surrogate duality gap* is introduced [34], which is defined as

$$\widehat{\eta}\left(\mathbf{x}^{(k)}, \boldsymbol{\lambda}^{(k)}\right) = -\mathbf{f}\left(\mathbf{x}^{(k)}\right)^{\mathrm{T}} \boldsymbol{\lambda}^{(k)}. \tag{2.173}$$

The surrogate duality gap corresponds to the duality gap of the barrier method if $\mathbf{x}^{(k)}$ is strictly feasible, while $\boldsymbol{\lambda}^{(k)}$ and $\boldsymbol{\nu}^{(k)}$ are dual feasible. The value of $t$ corresponding to the surrogate duality gap is

$$t = \frac{\mu m}{\widehat{\eta}}, \tag{2.174}$$

which is the same as the value $t$ assuming that the aforementioned conditions are satisfied.

TABLE 2.8: The primal-dual interior point method [34].

| | |
|---|---|
| Input: | Strictly feasible $\mathbf{x}^{(0)}$, $\boldsymbol{\lambda}^{(0)} \succ \mathbf{0}$ |
| | Update parameter $\mu > 1$ |
| | Tolerances $\epsilon > 0$, $\epsilon_{feas} > 0$ |
| 1: | $k \leftarrow 0$ |
| 2: | **do** |
| 3: | Set $t \leftarrow \mu m/\widehat{\eta}$ |
| 4: | Compute primal-dual direction $\Delta y_{pd}^{(k)}$ using (2.172) |
| 5: | Line search to determine $s$ |
| 6: | Update $y_{pd}^{(k+1)} \leftarrow y_{pd}^{(k)} + s\Delta y_{pd}^{(k)}$ |
| 7: | $t \leftarrow \mu t$, $k \leftarrow k + 1$ |
| 8: | **while** $\|\|r_{pri}\|\|_2 > \epsilon_{feas}$ **or** $\|\|r_{pri}\|\|_2 > \epsilon_{feas}$ **or** $\widehat{\eta} > \epsilon$ |

The primal-dual interior point method is described in Table 2.8 and terminates, when primal and dual feasibility is satisfied within the tolerance of $\epsilon_{feas}$, and the surrogate duality gap is smaller than the tolerance $\epsilon$. Furthermore, a modified backtracking line search is performed in Step 5 of Table 2.8 for determining a value of $s$, which results in a sufficient reduction to the norm of the residual. The initial value of

$$s^{max} = \sup\left\{s \in [0,1] \,|\boldsymbol{\lambda}^{(k)} + s\Delta\boldsymbol{\lambda}^{(k)} \succeq \mathbf{0}\right\} \tag{2.175}$$

is computed to ensure that dual feasibility is established. Then, the value of $s = 0.99s^{max}$ is iteratively multiplied by $\beta \in (0,1)$, until strict primal feasibility is established. The value of $s$ is further multiplied by $\beta$, until a sufficient by rapid reduction of the residual is observed,

resulting in [34]

$$\left|\left|r_t\left(\mathbf{x}^{(k)}+s\Delta\mathbf{x}^{(k)},\boldsymbol{\lambda}^{(k)}+s\Delta\boldsymbol{\lambda}^{(k)},\boldsymbol{\nu}^{(k)}+s\Delta\boldsymbol{\nu}^{(k)}\right)\right|\right|_2 \leq (1-\alpha s)\left|\left|r_t\left(\mathbf{x}^{(k)},\boldsymbol{\lambda}^{(k)},\boldsymbol{\nu}^{(k)}\right)\right|\right|_2, \tag{2.176}$$

where $\alpha \in (0, 0.5)$.

## 2.7 Decomposition Theory

Let us now briefly describe a technique conceived for decomposing an optimization problem into several distributed *subproblems,* coordinated by a high-level *master problem* through *signaling*. Decomposing a problem often benefits its implementation in large-scale systems and can lead to more efficiently solvable formulations than the original problem [339]. Furthermore, they may offer physically-meaningful insights into the optimization problem and its optimal solution.

In this section, we consider both primal and dual decomposition techniques [339], which decompose the primal and Lagrange dual problems, respectively. In the case of primal decomposition, the signaling directed to the subproblems may be interpreted as explicit *resource allocation*, since each subproblem is informed of the amount of resources that it can access. On the other hand, the signaling in dual decomposition may be interpreted as *pricing*, since each subproblem is informed of the price of the available resources, allowing them to decide how much can be afforded. The basic schematic of decomposition is illustrated in Fig. 2.21.

### 2.7.1 Primal Decomposition

Primal decomposition [339] may be applied to a problem featuring *coupling variables*. For example, the variable $\mathbf{y}$ couples the variable $\mathbf{x}$ in the problem

$$\underset{\mathbf{y}\in\mathcal{Y},\mathbf{x}\in\mathcal{X}}{\text{maximize}} \quad \sum_{i=1}^{n} f_i\left(\mathbf{x}_i\right) \tag{2.177}$$

$$\text{subject to} \quad \mathbf{A}_i\mathbf{x}_i \preceq \mathbf{y},\ \forall i, \tag{2.178}$$

where we have $\mathbf{x} = \left[\mathbf{x}_1^{\mathrm{T}},\cdots,\mathbf{x}_n^{\mathrm{T}}\right]^{\mathrm{T}}$, while $\mathcal{X} = \mathcal{X}_1 \times \cdots \times \mathcal{X}_n$ is the Cartesian product of the closed convex sets of feasible values for each $\mathbf{x}_i$. When the value of $\mathbf{y}$ is fixed, the above problem can be decomposed into $n$ problems of the form

$$\underset{\mathbf{x}_i\in\mathcal{X}_i}{\text{maximize}} \quad f_i\left(\mathbf{x}_i\right), \tag{2.179}$$

$$\text{subject to} \quad \mathbf{A}_i\mathbf{x}_i \preceq \mathbf{y}, \tag{2.180}$$

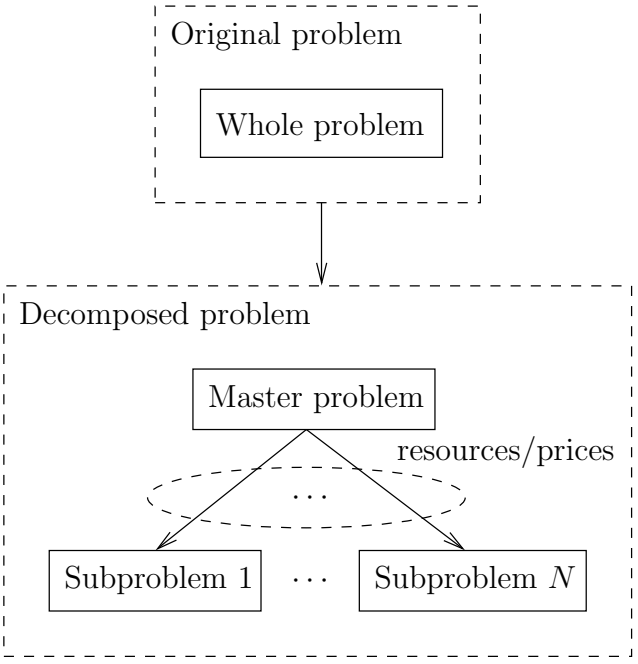


FIGURE 2.21: The general structure of a decomposed problem is shown at the bottom. In the case of primal decomposition, the signaling directed to the subproblems informs them of the amount of resources they can access. On the other hand, the signals are prices in the case of dual decomposition.

where only the *local* variable $\mathbf{x}_i$ is optimized. The optimal value of these subproblems is denoted by $\phi_i(\mathbf{y})$ and the master problem is given by

$$\underset{\mathbf{y}\in\mathcal{Y}}{\text{maximize}} \quad \sum_{i=1}^{n} \phi_i(\mathbf{y}), \tag{2.181}$$

which is typically solved with the aid of a gradient or subgradient based method. From sensitivity analysis [34,335], we know that a subgradient of $\sum_{i=1}^{n} \phi_i(\mathbf{y})$ is given by $\sum_{i=1}^{n} \boldsymbol{\lambda}_i^*(\mathbf{y})$, where $\boldsymbol{\lambda}_i^*(\mathbf{y})$ is the optimal Lagrange multiplier for the constraint (2.180) in each subproblem.

### 2.7.2 Dual Decomposition

On the other hand, dual decomposition [339] is suitable, when the problem features *coupling constraints*. For example, the problem

$$\underset{\mathbf{x}\in\mathcal{X}}{\text{maximize}} \quad \sum_{i=1}^{n} f_i(\mathbf{x}_i) \tag{2.182}$$

$$\text{subject to} \quad \sum_{i=1}^{n} \mathbf{A}_i\mathbf{x}_i \preceq \mathbf{c} \tag{2.183}$$

is coupled by its constraint. We can form the Lagrangian of the above problem to give

$$\mathcal{L}(\mathbf{x}, \boldsymbol{\lambda}) = \sum_{i=1}^{n} f_i(\mathbf{x}_i) - \boldsymbol{\lambda}^{\mathrm{T}} \left( \sum_{i=1}^{n} \mathbf{A}_i \mathbf{x}_i - \mathbf{c} \right) \tag{2.184}$$

$$= \sum_{i=1}^{n} \left( f_i(\mathbf{x}_i) - \boldsymbol{\lambda}^{\mathrm{T}} \mathbf{A}_i \mathbf{x}_i \right) - \boldsymbol{\lambda}^{\mathrm{T}} \mathbf{c}, \tag{2.185}$$

which naturally lends itself to decomposition. The subproblems are then given by

$$\underset{\mathbf{x} \in \mathcal{X}}{\text{maximize}} \quad f_i(\mathbf{x}_i) - \boldsymbol{\lambda}^{\mathrm{T}} \mathbf{A}_i \mathbf{x}_i, \tag{2.186}$$

while the master *dual* problem is formulated as:

$$\underset{\boldsymbol{\lambda} \succeq \mathbf{0}}{\text{minimize}} \quad \sum_{i=1}^{n} g_i(\boldsymbol{\lambda}) + \boldsymbol{\lambda}^{\mathrm{T}} \mathbf{c}, \tag{2.187}$$

where $g_i(\boldsymbol{\lambda})$ is the optimal value of the corresponding subproblem given $\boldsymbol{\lambda}$. Observe that the variable $\boldsymbol{\lambda}$ acts as a pricing parameter for the subproblems, since it penalizes increasing the value of $\mathbf{x}_i$. Furthermore, since this approach solves the dual problem, a sufficiently reliable result is only obtained, provided that strong duality exists.

### 2.7.3 Reformulations

We have seen that primal decomposition is applicable to a problem featuring coupling variables, while dual decomposition is applicable to a problem featuring coupling variables. However, it is possible to perform either primal or dual decomposition on the same problem with the aid of *auxiliary* variables.

Explicitly, for (2.177)–(2.178), we may introduce the auxiliary variables $\mathbf{y}_i$ and solve the equivalent problem of

$$\underset{\mathbf{y} \in \mathcal{Y}, \mathbf{y}_i, \mathbf{x} \in \mathcal{X}}{\text{maximize}} \quad \sum_{i=1}^{n} f_i(\mathbf{x}_i) \tag{2.188}$$

$$\text{subject to} \quad \mathbf{A}_i \mathbf{x}_i \preceq \mathbf{y}_i, \, \forall i \tag{2.189}$$

$$\mathbf{y}_i = \mathbf{y}, \, \forall i, \tag{2.190}$$

which is associated with the Lagrangian

$$\mathcal{L}(\mathbf{x}, \boldsymbol{\lambda}, \boldsymbol{\nu}) = \sum_{i=1}^{n} f_i(\mathbf{x}_i) - \left( \sum_{i=1}^{n} \boldsymbol{\lambda}_i^{\mathrm{T}} (\mathbf{A}_i \mathbf{x}_i - \mathbf{y}_i) \right) - \sum_{i=1}^{n} \boldsymbol{\nu}_i^{\mathrm{T}} (\mathbf{y} - \mathbf{y}_i). \tag{2.191}$$

Thus, the subproblems are given by

$$\underset{\mathbf{y}_i\in\mathcal{Y},\mathbf{x}_i\in\mathcal{X}_i}{\text{maximize}} \quad f_i\left(\mathbf{x}_i\right)-\boldsymbol{\lambda}_i^{\mathrm{T}}\left(\mathbf{A}_i\mathbf{x}_i-\mathbf{y}_i\right)-\boldsymbol{\nu}_i^{\mathrm{T}}\mathbf{y}_i, \tag{2.192}$$

while the master dual problem is given by

$$\underset{\boldsymbol{\lambda}\succeq\mathbf{0},\mathbf{y}\in\mathcal{Y}}{\text{minimize}} \quad g\left(\boldsymbol{\lambda},\boldsymbol{\nu}\right)-\sum_{i=1}^{n}\boldsymbol{\nu}_i^{\mathrm{T}}\mathbf{y}. \tag{2.193}$$

Similarly, for (2.182)–(2.183) the auxiliary variable $\mathbf{y}=\left[\mathbf{y}_1^{\mathrm{T}},\cdots,\mathbf{y}_n^{\mathrm{T}}\right]^{\mathrm{T}}$ may be introduced and the equivalent problem of

$$\begin{aligned}
\underset{\mathbf{x}\in\mathcal{X},\mathbf{y}}{\text{maximize}} \quad & \sum_{i=1}^{n} f_i\left(\mathbf{x}_i\right) && (2.194)\\
\text{subject to} \quad & \mathbf{A}_i\mathbf{x}_i\preceq\mathbf{y}_i,\ \forall i && (2.195)\\
& \sum_{i=1}^{n}\mathbf{y}_i\preceq\mathbf{c}, && (2.196)
\end{aligned}$$

may be solved using primal decomposition. The subproblems are given by

$$\begin{aligned}
\underset{\mathbf{x}\in\mathcal{X}}{\text{maximize}} \quad & f_i\left(\mathbf{x}_i\right) && (2.197)\\
\text{subject to} \quad & \mathbf{A}_i\mathbf{x}_i\preceq\mathbf{y}_i,\ \forall i, && (2.198)
\end{aligned}$$

while the master problem is formulated as

$$\begin{aligned}
\underset{\mathbf{y}}{\text{maximize}} \quad & \sum_{i=1}^{n}\phi_i\left(\mathbf{y}_i\right) && (2.199)\\
\text{subject to} \quad & \sum_{i=1}^{n}\mathbf{y}_i\preceq\mathbf{c},\ \forall i, && (2.200)
\end{aligned}$$

where $\phi_i\left(\mathbf{y}_i\right)$ is the optimal value for the corresponding subproblem, given $\mathbf{y}_i$.

## 2.8 Application Examples of Convex Optimization in Wireless Communication

We have explored the basics of convex optimization problems, along with various methods of finding their solutions. In this section, we study some representative examples of convex optimization applied to wireless communications problems, which are pertinent to this thesis. It is necessary to mention that the following is by no means an exhaustive review of optimization applied to wireless communications. For example, we refrain from considering semidefinite or second-order conic programming, which was discussed in [340], nor do we

explore geometric programing [35, 36] or robust optimization [341–345].

### 2.8.1 Classical Water-Filling and its Relation to Lagrangian Duality

We begin with the classical *water-filling* method of maximizing the capacity of $n$ discrete unit-bandwidth wireless channels. Given that the information theoretic limit of wireless channel $i$ having a channel gain $g_i$ is defined by $\log_2(1+g_i p_i)$, where $p_i$ is the transmitter power, the sum capacity of the system is

$$\sum_{i=1}^{n} \log_2(1+g_i p_i). \tag{2.201}$$

Moreover, the system is subject to a total power constraint of $P$. Thus, we may formulate the concave maximization problem of

$$\underset{\mathbf{p}\succeq\mathbf{0}}{\text{maximize}} \quad \sum_{i=1}^{n} \log_2(1+g_i p_i) \tag{2.202}$$

$$\text{subject to} \quad \sum_{i=1}^{n} p_i \leq P, \tag{2.203}$$

which has the well-known solution [4, 34] of

$$p_i^* = \left[c - \frac{1}{g_i}\right]^+, \tag{2.204}$$

where $c$ is some constant termed the *water-level*. The optimal solution is illustrated in Fig. 2.22 for a system associated with $n = 7$ discrete channels.

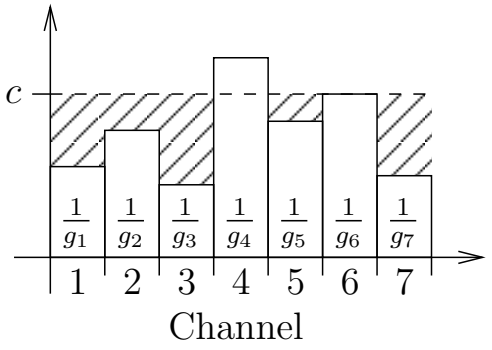


FIGURE 2.22: An illustration of the water-filling method. The shaded areas indicate the amount of power allocated to each discrete wireless channel, where $c$ is the maximum value that $\frac{1}{g_i} + p_i^*$ can reach. Hence, the optimal solution is analogous to pouring water into a container having a ragged bottom until the water-level of $c$ is reached.

We will now demonstrate how the optimal solution is derived from duality. We commence

by employing the KKT optimality conditions to derive

$$\begin{aligned} \sum_{i=1}^{n} p_i^* &\leq P && (2.205)\\ p_i^* &\geq 0, \forall i && (2.206)\\ \lambda^* &\geq 0 && (2.207)\\ \lambda^* \left( P - \sum_{i=1}^{n} p_i^* \right) &= 0 && (2.208)\\ \frac{g_i}{\ln 2\,(1+g_i p_i^*)} - \lambda^* &= 0, \forall i, && (2.209) \end{aligned}$$

where $\lambda^*$ is the optimal Lagrange multiplier associated with the maximum power constraint. Solving (2.209) for $p_i^*$ reveals that we have

$$p_i^* = \frac{1}{\lambda^* \ln(2)} - \frac{1}{g_i}, \tag{2.210}$$

which is

$$p_i^* = \left[ \frac{1}{\lambda^* \ln(2)} - \frac{1}{g_i} \right]^+, \tag{2.211}$$

when enforcing the nonnegativity constraint of (2.206). Thus, we arrive at

$$c = \frac{1}{\lambda^* \ln(2)} \tag{2.212}$$

and the water-level is determined by the optimal Lagrangian multiplier. Observe from the complementary slackness condition of (2.208), that the optimal Lagrangian multiplier is zero unless the inequality constraint function is active. Thus, the optimal Lagrangian multiplier is obtained when

$$\sum_{i=1}^{n} p_i^* = P. \tag{2.213}$$

In other words, the water-level $c$ is set to that specific value, which results in allocating all of the available power. Furthermore, observe that more power is allocated to channels featuring a higher channel gain (and a lower $1/g_i$) so that they may be exploited for increasing the overall system capacity.

### 2.8.2 Advanced Water-Filling Methods

In this section, we explore some advanced water-filling methods applied to the simple system described above. For example, if the system aims for maintaining fairness of resource allocation to channels, the optimization problem may be written as

$$\underset{\mathbf{p} \succeq \mathbf{0}}{\text{maximize}} \quad \sum_{i=1}^{n} \omega_i \log_2 (1 + g_i p_i) \tag{2.214}$$

$$\text{subject to} \quad \sum_{i=1}^{n} p_i \leq P, \tag{2.215}$$

where $\omega_i$ is a measure of allocation priority for channel $i$. The above problem has the optimal solution

$$p_i^* = \left[\frac{\omega_i}{\lambda^* \ln(2)} - \frac{1}{g_i}\right]^+. \tag{2.216}$$

Observe that the water-level for channel $i$ is now given by $\omega_i/\lambda^* \ln(2)$, implying that a channel associated with a greater value of $\omega_i$ is allocated more power, even if the channel gains are identical. This result is an example of *multi-level water-filling*.

In the case of maximizing the energy-efficiency of the system, the optimization problem can be written as

$$\underset{\mathbf{p}\succeq\mathbf{0}}{\text{maximize}} \quad \frac{\sum_{i=1}^{n} \log_2(1+g_i p_i)}{C + \sum_{i=1}^{n} p_i} \tag{2.217}$$

$$\text{subject to} \quad \sum_{i=1}^{n} p_i \leq P, \tag{2.218}$$

where the objective has units of [bits/sec/Hz/Jule] and $C$ is some constant. This is a case of FP and we may apply Dinkelbach's method for reformulating it as a series of convex programming problems of the form

$$\underset{\mathbf{p}\succeq\mathbf{0}}{\text{maximize}} \quad \sum_{i=1}^{n} \log_2(1+g_i p_i) - q_j \cdot \left(C + \sum_{i=1}^{n} p_i\right) \tag{2.219}$$

$$\text{subject to} \quad \sum_{i=1}^{n} p_i \leq P, \tag{2.220}$$

where $q_j$ is the value of the original objective function obtained in the previous iteration of Dinkelbach's method. The above problem has the optimal solution of

$$p_i^* = \left[\frac{1}{\ln(2)\,(\lambda^* + q_j)} - \frac{1}{g_i}\right]^+. \tag{2.221}$$

Observe that the water-level is now given by $1/\ln(2)\,(\lambda^* + q_j)$, which means that a higher value of $q_j$ results in a lower power allocation for every channel. In other words, as the resultant energy-efficiency increases, the optimal power allocation becomes progressively restrictive, until the equilibrium point of the maximum energy-efficiency is obtained.

Let us now explore the case, where the communication channels are mutually interfering. The associated optimization problem can be written as

$$\underset{\mathbf{p}\succeq\mathbf{0}}{\text{maximize}} \quad \sum_{i=1}^{n} \log_2\left(1 + \frac{g_i p_i}{\sum_{j\neq i} g_{j,i} p_j}\right) \tag{2.222}$$

$$\text{subject to} \qquad p_i \leq P_i, \, \forall i \tag{2.223}$$

where $g_{j,i}$ is the channel gain between the transmitter occupying channel $j$ and the receiver of channel $i$, while $\sum_{j \neq i} g_{j,i} p_j$ is the total interference power at the receiver of channel $i$. Furthermore, channel $i$ is subject to a maximum power constraint of $P_i$, which is associated with the Lagrangian multiplier $\lambda_i$.

Although the objective function is nonconvex, the authors of [37] showed that the optimal solution can be obtained using *iterative* water-filling, which requires that each channel is iteratively allocated the optimal power of

$$p_i^* = \left[ \frac{1}{\lambda_i^* \ln(2)} - \frac{\sum_{j \neq i} g_{j,i} p_j}{g_i} \right]^+, \tag{2.224}$$

assuming that every other channel has a fixed power allocation, until the objective value converges.

When the objective is to minimize the total transmission power subject to per channel capacity requirements of $R_i$ for channel $i$, the optimization problem can be formulated as

$$\underset{\mathbf{p} \succeq \mathbf{0}}{\text{minimize}} \qquad \sum_{i=1}^{n} p_i \tag{2.225}$$

$$\text{subject to} \qquad \log_2(1 + g_i p_i) \geq R_i, \, \forall i \tag{2.226}$$

$$\sum_{i=1}^{n} p_i \leq P, \tag{2.227}$$

which is a convex minimization problem. If we denote the Lagrangian multiplier for the $i$th channel's capacity constraint as $\nu_i$, the optimal solution is given by

$$p_i = \left[ \frac{\nu_i}{\ln(2)(1 + \lambda_i^*)} - \frac{1}{g_i} \right]^+. \tag{2.228}$$

Observe that if the capacity constraint is strictly satisfied for channel $i$, we have $\nu_i = 0$ and zero power is allocated for this channel. A nontrivial solution occurs when $\log_2(1 + g_i p_i) = R_i$, which requires that

$$p_i = \frac{\exp(R_i \ln(2)) - 1}{g_i}. \tag{2.229}$$

Thus, the optimal (and intuitive) solution is to allocate only the power necessary to fulfill the channel capacity requirements.

## 2.9 Chapter Summary and Conclusions

In this chapter, we have explored the basics of convexity and convex functions, as well as the various methods by which the convexity of a function may be determined. Given this knowledge, we were able to formally classify optimization problems as either convex or nonconvex. Moreover, we delved deeper into the topic of nonconvex optimization, and detailed several approaches for reformulating them so that they may be solved using convex optimization techniques.

In Section 2.5, we then examined duality, along with the Lagrangian function and the dual problem. The importance of both strong and weak dualities was illustrated, and the motivation for formulating problems as convex problems was provided. Most importantly, the KKT conditions of optimality were listed in Section 2.5.4, and the complementary slackness condition was explained.

Armed with the knowledge acquired in Section 2.5, we studied the various methods of solving convex optimization problems. In Section 2.6.1, we began with simple unconstrained problems, which can be solved using iterative descent methods, and in Section 2.6.2 we then proceeded to study equality-constrained problems, which required that the iterate progresses along a feasible descent direction. In Section 2.6.3, we explored interior points methods, which can be applied to problems featuring both equality and inequality constraints. We proceeded in Section 2.6.3.1 by studying the logarithmic barrier function and the method by which it can be employed for reformulating the problem as a series of equality-constrained problems. In Section 2.6.3.2, a simple primal-dual interior point method is additionally provided. Furthermore, we examined both primal and dual decompositions, along with reformulations that allow either method to be applied to decomposable optimization problems.

Finally, in Section 2.8 we explored some select examples of convex optimization applied to wireless communications. We began by studying the classical water-filling result and how it relates to the dual of the problem of channel capacity maximization. Furthermore, we progressed to more advanced optimization problems and studied their water-filling type optimal solutions.

Chapter 3

# Spectral/Energy Efficient Resource Allocation for SISO-Aided Single-Cell Networks

## 3.1 Introduction

As described in Chapter 1, the EE of wireless cellular networks is becoming an increasingly important design metric for mobile operators, when attempting to reduce their operating costs, whilst satisfying both societal and regulatory demands. Additionally, cellular networks employ multicarrier physical layer transmissions and heterogeneous network elements, thus increasing the complexity of the EE problem when accounting for all of these factors.

We now formally define the EE metric used in this thesis as a counterpart of the ASE metric [4], where the latter is normalized by area and has the units of $\left[\text{bits/sec/Hz/km}^2\right]$, while the unit of the EE metric is [bits/sec/Hz/W]. This results from forming the ratio of the SE obtained over the power dissipated. We simplify this by combining the units of time and power to give energy, thus the (normalized) EE may also be measured in [bits/Joule/Hz].

In this chapter, our focus is on the EEM problem cast in the context of a SISO multi-relay, multi-user cellular network, which employs the ubiquitous OFDMA scheme described in Section 1.3. Here, SISO means that the BS, the users and the RNs are each equipped with a single antenna. More specifically, the RNs may employ the AF protocol of Section 1.4 for relaying the information transmitted by the BS in the DL to the UE experiencing unfavorable channel conditions. Moreover, the BS and the RNs may transmit simultaneously, but on different OFDMA subcarriers, thus completely avoiding interference between the BS's and the RNs' DL transmissions. The specific selection of UEs to receive DL transmissions from

either the BS or the RNs as well as their associated power control variables is formulated as an optimization problem, where the optimization objective can be either the SEM or EEM.

An example of the SEM problem was considered in [22], where the authors formulated the optimization problem for the DL of an AF relaying-aided OFDMA cellular network and their goal was to optimize the power and subcarrier allocation so that the SE of the system was maximized, whilst satisfying a certain maximum outage probability and total power constraint. In the class of power minimization problems, an example is the often-cited work by Wong *et. al* [23], where a heuristic bit allocation algorithm was conceived for a multi-user OFDMA system with the goal of minimizing the power consumption under a minimum individual user rate constraint. With a similar goal, Piazzo [24] developed a sub-optimal bit allocation algorithm for an OFDM system as a lower-complexity alternative to the well-known Hughes-Hartogs algorithm [346]. This work was later extended to provide the optimal bit allocation in [26].

However, the SEM and the power minimization problems do not directly consider an EE objective function and in general they do not deliver the EEM solution. In recent years, research into resource allocation using an EE objective function has become increasingly popular. In reality, EEM may be viewed as an example of multi-objective optimization, since typically the goal is to maximize the SE achieved, whilst concurrently minimizing the power consumption required. From this perspective, [347] derives an aggregate objective function, which consists of a weighted sum of the sum rate achieved and the power dissipated. However, selecting appropriate weights for the two objective functions is not straightforward and different combinations of weights can lead to very different results. Another example is given in [348], where the EEM problem is considered in a multi-relay network employing the AF protocol. However, the authors of [347, 348] only optimize the user selection and power allocation without considering the subcarrier allocation in the network. Another formulation, demonstrated in [224, 225], considers power and subcarrier allocation in an OFDMA cellular network, but without a maximum total power constraint and without relaying. The contribution most similar to the work presented in this chapter is that of Ng *et. al* [200], where the authors formulated the EEM problem in the context of an OFDMA cellular network under a maximum total power constraint. The EEM problem is then solved using Dinkelbach's method [337]. However, in contrast to our work, relaying is not considered by Ng *et. al*. Furthermore, they did not employ and compare other methods of solving the fractional quasi-concave EEM problem.

In contrast to the above-mentioned contributions, we consider both the SE and EE optimization metrics. Furthermore, we solved their associated optimization problems with the aid of three separate methods, which we compare in terms of their performance attained versus the complexity imposed.

### 3.1.1 Novel Contributions

This chapter focuses on a solution method conceived for the EEM problem of a multi-relay, multi-user OFDMA cellular network, which jointly considers both power and subcarrier allocation under a certain maximum total power constraint. The contributions of this chapter are summarized as follows.

- The EEM problem of a multi-relay, multi-user OFDMA cellular network, in which both direct and relayed transmissions are employed, is formulated as a fractional programming problem, which jointly considers both the power and subcarrier allocation. In contrast to previous contributions such as [44], our goal is that of finding the optimal power and subcarrier allocations within a network context. Furthermore, in contrast to [20–26, 347, 348], our focus is on an EE objective function. It is demonstrated that in its original form the problem is a MINLP. As described in Section 2.4.2, MINLPs are typically challenging to solve. In order to make the problem more tractable, both a variable transformation and a relaxation of the integer variables is introduced.
- It is proven that the relaxed problem is a quasi-concave FP problem. Thus, we employ the methods described in Section 2.4.3 for converting the quasi-concave problem into one or several concave maximization problems. Each of these concave problems is solved using the dual decomposition approach of Section 2.7. The prevailing method employed in the existing literature for solving quasi-concave problems is Dinkelbach's method, as exemplified in [71, 200, 201]. However, the performance of the Charnes-Cooper transformation has rarely been explored [226, 227]. Furthermore, there are no comparisons between these algorithms and a baseline algorithm relying on the bisection method of Section 2.4.3. Thus, in this chapter, we demonstrate that the EEM algorithms based on either Dinkelbach's method of Section 3.4, or on the Charnes-Cooper transformation method of Section 3.5, or alternatively on the bisection method of Section 3.6 are capable of reaching the optimal solution obtained via an exhaustive search. Furthermore, the former two algorithms converge within a low number of iterations, which means that the original problem was solved at a low complexity.
- Comparisons are made between two multi-relay resource allocation problems, namely one that solves the EEM problem and another that considers SEM. It is shown in Section 3.7 that when the maximum affordable power is lower than a given threshold, the two problems have the same solutions. However, as the maximum affordable power is increased, the SEM algorithm attempts to achieve a higher SE at the cost of a lower EE, while given the total power, the EEM algorithm reaches the upper limit of the maximum achievable SE for the sake of maintaining the maximum EE.
- Since the system model is generalized, the EEM and SEM algorithms may be invoked for gaining insights into the specifics of network design, when we aim for maximizing either the EE or SE. To that end, a comprehensive range of results is presented, which

characterizes both the effect of increasing the number of available subcarriers and UEs in the system, whilst quantifying the impact of both the number as well as position of RNs. The algorithms may be used for characterizing the effects of many other system design choices on the maximum SE and EE.

### 3.1.2 Chapter Organization

The rest of this chapter is organized as follows. In Section 3.2, the multi-user, multi-relay OFDMA based cellular network model is described, which is followed by a formulation of our optimization problem in Section 3.3. Upon invoking a transformation of variables and a relaxation of the integer variables, it is proven that the objective function is quasi-concave. Three beneficial solution methods are contrasted. Specifically, Dinkelbach's method is used in Section 3.4, the Charnes-Cooper transformation method is employed in Section 3.5, while the bisection method is advocated in Section 3.6, all of which solve the quasi-concave problem by solving either one or several concave maximization problems. Furthermore, the algorithms required for solving these concave maximization problems are devised from dual decomposition. The performance of these EEM algorithms is demonstrated in Section 3.7, which includes results obtained when the EEM and SEM algorithms are employed for characterizing the effect of different system design choices on the achievable SE and EE. Lastly, a summary is given in Section 3.8.

## 3.2 System Model

Consider an OFDMA DL cellular system relying on a single BS, $M$ fixed RNs and $K$ uniformly-distributed UEs, as shown in Fig. 3.1. Although it is more realistic to consider a multi-cell system, which would lead to inter-cell interference, our system model assumes that intelligent interference coordination or mitigation techniques are employed such that the level of inter-cell interference is negligible [5]. However, a multi-cell scenario will be considered in Chapter 5.

The cell is divided into $M$ sectors, where each sector is served by one of the fixed RNs. Naturally, the path-loss is a major factor in determining the receiver's SNRs at the UEs, and thus has a substantial effect on the EE. Therefore, in order to minimize the RN-to-UE pathloss, we employ the so-called distance dependent relay-selection [349], where all the UEs in a specific sector are only supported by that sector's RN. Thus, relay selection is implicitly accomplished. Furthermore, since a single RN supports multiple UEs within its own sector, this protocol can be likened to the shared relay scheme described in [349, 350], which is elucidated in Fig. 3.2. On the other hand, this system model may be readily extended to

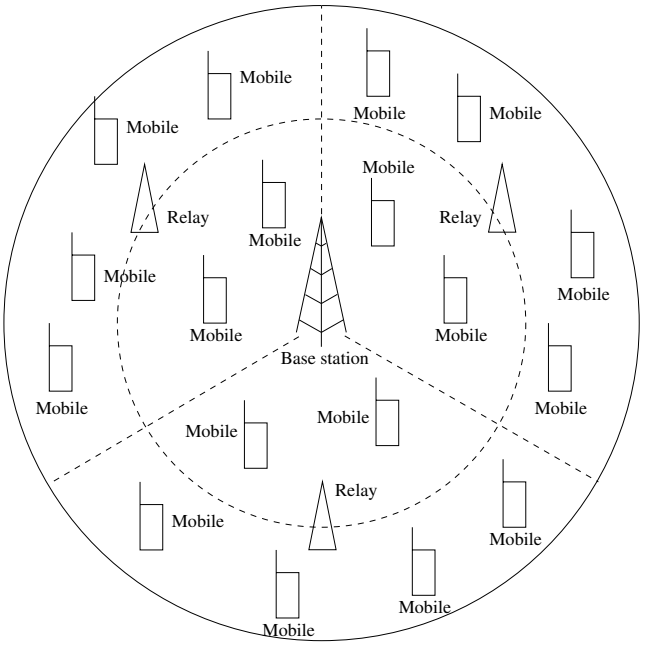


FIGURE 3.1: An example of a cellular network with $M = 3$ RNs and $K = 18$ UEs.

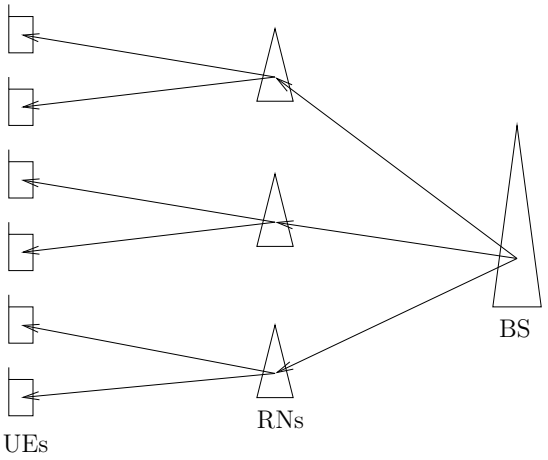


FIGURE 3.2: An illustration of the shared relay scheme employed in this chapter.

include sophisticated relay selection schemes, but for the sake of mathematical tractability, they are not included in this chapter.

This system model accounts for both the AF relayed link as well as for the direct link between the BS and UEs, while the variables related to these two communication protocols are distinguishable by the superscripts $A$ and $D$, respectively. When defining links, the subscript 0 is used for indicating the BS, whilst $\mathcal{M}(k) \in \{1, \cdots, M\}$ indicates the RN selected for assisting the DL-transmissions to user $k$. The proportion of the BS-to-RN distance to the cell radius is denoted by $D_r$, while the total available instantaneous transmission power of the network is $P_{max}$. Although it is more realistic to consider a system with separate power constraints for each transmitting entity, for simplicity, a certain total power constraint is

considered. The results obtained provide insights into holistic system design by granting a higher grade of freedom in terms of sharing the power among the transmitting entities, and thus attaining a higher performance.

Using the direct transmission protocol, the receiver's SNR at UE $k$ on subcarrier $n$ may be expressed as $\Gamma_k^{D,n}(\mathcal{P})$, whereas when using the AF relaying protocol described in Section 1.4, the receiver's SNR at UE $k$ on subcarrier $n$ may be expressed as

$$\Gamma_k^{A,n}(\mathcal{P}) = \frac{\gamma_{0,\mathcal{M}(k)}^{A,n}\gamma_{\mathcal{M}(k),k}^{A,n}}{\left(\gamma_{0,\mathcal{M}(k)}^{A,n} + \gamma_{\mathcal{M}(k),k}^{A,n} + 1\right)}, \tag{3.1}$$

where

$$\gamma_{a,b}^{X,n} = \frac{P_{a,b}^{X,n} G_{a,b}^{n}}{\Delta\gamma N_0 W} \tag{3.2}$$

is the SNR at receiver $b \in \{1, \cdots, M, 1, \cdots, K\}$ on subcarrier $n \in \{1, \cdots, N\}$, and $P_{a,b}^{X,n}$ is allocated to transmitter $a \in \{0, \cdots, M\}$ using protocol $X \in \{D, A\}$ for transmission to receiver $b$. Furthermore, $G_{a,b}^{n}$ represents the channel's attenuation between transmitter $a$ and receiver $b$ on subcarrier $n$, which is assumed to be known at the BS for all links. The channel's attenuation is modeled by the path-loss and the Rayleigh fading between the transmitter and receiver. Furthermore, $N_0$ is the AWGN variance and $W$ is the bandwidth of a single subcarrier. Still referring to (3.1), $\Delta\gamma$ is the SNR gap at the system's BER target between the SNR required at the discrete-input continuous-output memoryless channel (DCMC) capacity and the actual SNR required the modulation and coding schemes of the practical physical layer transceivers employed. For example, making the simplifying assumption that idealized transceivers operating exactly at the DCMC capacity are employed, then $\Delta\gamma = 0$dB. Although it is not possible to operate exactly at the DCMC channel capacity, several physical layer transceiver designs exist that operate arbitrarily close to it [351]. Additionally, the power allocation policy of the system is denoted by $\mathcal{P}$, which determines the values of $P_{a,b}^{X,n}$.

Assuming sufficiently high receiver's SNR values, the following approximation can be made

$$\Gamma_k^{A,n}(\mathcal{P}) \approx \frac{P_{0,\mathcal{M}(k)}^{A,n} G_{0,\mathcal{M}(k)}^{n} P_{\mathcal{M}(k),k}^{A,n} G_{\mathcal{M}(k),k}^{n}}{\Delta\gamma N_0 W \left(P_{0,\mathcal{M}(k)}^{A,n} G_{0,\mathcal{M}(k)}^{n} + P_{\mathcal{M}(k),k}^{A,n} G_{\mathcal{M}(k),k}^{n}\right)}, \tag{3.3}$$

which is valid for

$$P_{0,\mathcal{M}(k)}^{A,n} G_{0,\mathcal{M}(k)}^{n} + P_{\mathcal{M}(k),k}^{A,n} G_{\mathcal{M}(k),k}^{n} \gg \Delta\gamma N_0 W. \tag{3.4}$$

It is plausible that in next-generation systems, through the combination of multi-user and frequency diversity, this assumption holds true when an intelligent scheduler is employed [44].

The SE of an AF link to UE $k$ on subcarrier $n$ is then given by

$$R_k^{A,n}(\mathcal{P}) = \frac{1}{2}\log_2\left(1+\Gamma_k^{A,n}\right) \text{ [bits/s/Hz]}, \tag{3.5}$$

where the factor of $\frac{1}{2}$ accounts for the fact that two time slots are required for the two-hop AF transmission. The SE of a direct link to UE $k$ on subcarrier $n$ is similarly given by

$$R_k^{D,n}(\mathcal{P}) = \log_2\left(1+\Gamma_k^{D,n}\right) \text{ [bits/s/Hz]}. \tag{3.6}$$

The subcarrier indicator variable $s_k^{X,n} \in \{0,1\}$ is now introduced, which denotes the allocation of subcarrier $n$ for transmission to user $k$ using protocol $X$ for $s_k^{X,n}=1$, and $s_k^{X,n}=0$ otherwise. The weighted total SE of the system is calculated as

$$R_T(\mathcal{P},\mathcal{S}) = \sum_{k=1}^{K}\omega_k\sum_{n=1}^{N} s_k^{D,n}\log_2\left(1+\Gamma_k^{D,n}\right) + \frac{s_k^{A,n}}{2}\log_2\left(1+\Gamma_k^{A,n}\right) \text{ [bits/s/Hz]}, \tag{3.7}$$

where $\mathcal{S}$ denotes the subcarrier allocation policy of the system, which determines the values of the subcarrier indicator variable $s_k^{X,n}$. The weighting factor $\omega_k$ may be varied for ensuring fairness amongst users. However, since ensuring fairness is not the focus of this thesis, $\omega_k = 1$, $\forall k$ is assumed then the effect of $\omega_k$ may be ignored.

In order to compute the energy used in these transmissions, a model similar to [352] is adopted and the total power consumption of the system is assumed be governed by a constant term and a term that varies with the transmission powers, which may be written as (3.8).

$$P_T(\mathcal{P},\mathcal{S}) = \left(P_C^{(B)} + P_C^{(R)}M\right) + \sum_{k=1}^{K}\sum_{n=1}^{N} s_k^{D,n}\xi^{(B)}P_{0,k}^{D,n} + \frac{s_k^{A,n}\left(\xi^{(B)}P_{0,\mathcal{M}(k)}^{A,n} + \xi^{(R)}P_{\mathcal{M}(k),k}^{A,n}\right)}{2} \text{ [Watts]} \tag{3.8}$$

Here, $P_C^{(B)}$ and $P_C^{(R)}$ represent the fixed power consumption of each BS and each RN, respectively, while $\xi^{(B)} > 1$ and $\xi^{(R)} > 1$ denote the reciprocal of the drain efficiencies of the power amplifiers employed at the BS and the RNs, respectively. For example, an amplifier having a 25% drain efficiency would have $\xi = \frac{1}{0.25} = 4$.

Finally, the average EE metric of the system is expressed as

$$\eta_E(\mathcal{P},\mathcal{S}) = \frac{R_T(\mathcal{P},\mathcal{S})}{P_T(\mathcal{P},\mathcal{S})} \text{ [bits/Joule/Hz]}. \tag{3.9}$$

## 3.3 Problem Formulation

The aim of this chapter is to maximize the energy efficiency metric of (3.9) subject to a maximum total instantaneous transmit power constraint. In its current form, (3.9) is dependent on the set of $3KN$ continuous power variables $P_{0,k}^{D,n}$, $P_{0,\mathcal{M}(k)}^{A,n}$ and $P_{\mathcal{M}(k),k}^{A,n}$, $\forall k,n$ and on the $2KN$ binary subcarrier indicator variables $s_k^{D,n}$ and $s_k^{A,n}$, $\forall k,n$. Thus, it may be regarded as a MINLP problem, which hence can be solved using the classic branch-and-bound method described in Section 2.4.2. However, the computational effort required for branch-and-bound techniques typically increases exponentially with the problem size. Therefore, a simpler solution is derived by relaxing the binary constraint imposed on the subcarrier indicator variables, now denoted by $\widetilde{s}_k^{D,n}$ and $\widetilde{s}_k^{A,n}$, so that they may assume continuous values from the interval $[0,1]$, as demonstrated in [23, 353]. Furthermore, the auxiliary variables of $\widetilde{P}_{0,k}^{D,n} = P_{0,k}^{D,n}\widetilde{s}_k^{D,n}$, $\widetilde{P}_{0,\mathcal{M}(k)}^{A,n} = P_{0,\mathcal{M}(k)}^{A,n}\widetilde{s}_k^{A,n}$ and $\widetilde{P}_{0,\mathcal{M}(k)}^{A,n} = P_{0,\mathcal{M}(k)}^{A,n}\widetilde{s}_k^{A,n}$ are introduced. These new power variables form the set $\widetilde{\mathcal{P}}$, while the relaxed subcarrier indicator variables form the set $\widetilde{\mathcal{S}}$.

In [353], such a relaxation results in a time-sharing solution regarding each subcarrier. In this thesis, this relaxation may be viewed as time-sharing of each subcarrier, as multiple users can then occupy a fraction of each subcarrier in time. Naturally, the relaxation means that we do not accurately maximize the original objective function of (3.9). In fact, since we have expanded the space of feasible solutions, solving the relaxed problem results in an upper bound of the optimal objective value of the original problem. However, the algorithms devised in this thesis for obtaining the optimal solution to the relaxed problems will only retain integer values of the relaxed variables. Therefore, the algorithms essentially maximize a lower bound of the relaxed problem. Having said that, as shown in [200, 202, 330], the optimal solution to the original problem is still obtained with high probability when using the dual decomposition method on the relaxed problem (as in this thesis) as the number of subcarriers tends to infinity. It was shown that 8 subcarriers is sufficient for this to be true in the context of [219], while we will show that 2 subcarriers is sufficient in Section 3.7

The optimization problem is formulated as

$$\underset{\widetilde{\mathcal{P}},\widetilde{\mathcal{S}}}{\text{maximize}} \quad \frac{\widetilde{R}_T}{\widetilde{P}_T} \tag{3.10}$$

$$\text{subject to} \quad \sum_{k=1}^{K}\sum_{n=1}^{N} \widetilde{P}_{0,k}^{D,n} + \widetilde{P}_{0,\mathcal{M}(k)}^{A,n} + \widetilde{P}_{\mathcal{M}(k),k}^{A,n} \leq P_{max}, \tag{3.11}$$

$$\widetilde{s}_k^{D,n} + \widetilde{s}_k^{A,n} \leq 1,\ \forall k,n, \tag{3.12}$$

$$\sum_{k=1}^{K} \widetilde{s}_k^{D,n} + \widetilde{s}_k^{A,n} \leq 1,\ \forall n, \tag{3.13}$$

$$\widetilde{P}_{0,k}^{D,n},\ \widetilde{P}_{0,\mathcal{M}(k)}^{A,n},\ \widetilde{P}_{\mathcal{M}(k),k}^{A,n} \in \mathbb{R}_+,\ \forall k,n, \tag{3.14}$$

$$0 \leq \widetilde{s}_k^{D,n},\ \widetilde{s}_k^{A,n} \leq 1,\ \forall k, n, \tag{3.15}$$

where the objective function formulated by the ratio between

$$\begin{aligned}\widetilde{R}_T \quad = \quad & \sum_{k=1}^{K}\sum_{n=1}^{N} \widetilde{s}_k^{D,n} \log_2\left(1 + \frac{\widetilde{P}_{0,k}^{D,n} G_{0,k}^{n}}{\widetilde{s}_k^{D,n}\Delta\gamma N_0 W}\right) \\ & + \frac{\widetilde{s}_k^{A,n}}{2}\log_2\left(1 + \frac{\widetilde{P}_{0,\mathcal{M}(k)}^{A,n} G_{0,\mathcal{M}(k)}^{n} \widetilde{P}_{\mathcal{M}(k),k}^{A,n} G_{\mathcal{M}(k),k}^{n}}{\widetilde{s}_k^{A,n}\Delta\gamma N_0 W\left(\widetilde{P}_{0,\mathcal{M}(k)}^{A,n} G_{0,\mathcal{M}(k)}^{n} + \widetilde{P}_{\mathcal{M}(k),k}^{A,n} G_{\mathcal{M}(k),k}^{n}\right)}\right)\end{aligned} \tag{3.16}$$

and

$$\widetilde{P}_T = \left(P_C^{(B)} + P_C^{(R)} M\right) + \sum_{k=1}^{K}\sum_{n=1}^{N} \xi^{(B)} \widetilde{P}_{0,k}^{D,n} + \frac{\left(\xi^{(B)} \widetilde{P}_{0,\mathcal{M}(k)}^{A,n} + \xi^{(R)} \widetilde{P}_{\mathcal{M}(k),k}^{A,n}\right)}{2}. \tag{3.17}$$

In this formulation, the decision variables are contained in the sets $\widetilde{\mathcal{P}}$ and $\widetilde{\mathcal{S}}$. Physically, the constraint (3.11) ensures that the sum of the power allocated to variables $\widetilde{P}_{0,k}^{D,n}$, $\widetilde{P}_{0,\mathcal{M}(k)}^{A,n}$ and $\widetilde{P}_{\mathcal{M}(k),k}^{A,n}$ does not exceed the maximum power budget of the system. Constraint (3.12) ensures that a single transmission protocol, either direct or AF, is chosen for each user-subcarrier pair. The constraint (3.13) guarantees that each subcarrier is only allocated to at most one user, thus intra-cell interference is avoided. The constraints (3.14) and (3.15) describe the feasible region of the optimization variables.

### 3.3.1 Proving that the Objective Function of (3.10) is Quasi-Concave

We wish to determine whether the objective function is concave or quasiconcave so that the associated optimization problem can be efficiently solved. From Section 2.4.3, we know that in order to show that (3.10) is quasi-concave, it is sufficient to prove that the numerator is concave and the denominator is both affine as well as positive, while the domain is convex. It is plausible that the denominator is both affine and positive, since it is the linear combination of multiple nonnegative variables and a positive constant. The proof that the numerator is concave is as follows.

Firstly, the concavity of

$$f_1\left(\widetilde{P}_{0,\mathcal{M}(k)}^{A,n}, \widetilde{P}_{\mathcal{M}(k),k}^{A,n}\right) = \frac{\widetilde{P}_{0,\mathcal{M}(k)}^{A,n} G_{0,\mathcal{M}(k)}^{n} \widetilde{P}_{\mathcal{M}(k),k}^{A,n} G_{\mathcal{M}(k),k}^{n}}{\Delta\gamma N_0 W\left(\widetilde{P}_{0,\mathcal{M}(k)}^{A,n} G_{0,\mathcal{M}(k)}^{n} + \widetilde{P}_{\mathcal{M}(k),k}^{A,n} G_{\mathcal{M}(k),k}^{n}\right)} \tag{3.18}$$

is proven. This may be accomplished by examining the Hessian matrix of $f_1\left(\widetilde{P}_{0,\mathcal{M}(k)}^{A,n}, \widetilde{P}_{\mathcal{M}(k),k}^{A,n}\right)$ with respect to (w.r.t.) the variables $\widetilde{P}_{0,\mathcal{M}(k)}^{A,n}$ and $\widetilde{P}_{\mathcal{M}(k),k}^{A,n}$, which has the eigenvalues $e_1 = 0$

and

$$e_2 = -\frac{2\left(G^n_{0,\mathcal{M}(k)}G^n_{\mathcal{M}(k),k}\right)^2\left(\widetilde{P}^{A,n}_{0,\mathcal{M}(k)}+\widetilde{P}^{A,n}_{\mathcal{M}(k),k}\right)}{\Delta\gamma N_0 W\left(\widetilde{P}^{A,n}_{0,\mathcal{M}(k)}G^n_{0,\mathcal{M}(k)}+\widetilde{P}^{A,n}_{\mathcal{M}(k),k}G^n_{\mathcal{M}(k),k}\right)^3}, \tag{3.19}$$

which are non-positive, indicating that the Hessian is negative-semidefinite. From Section 2.3.3, we conclude that $f_1\left(\widetilde{P}^{A,n}_{0,\mathcal{M}(k)},\widetilde{P}^{A,n}_{\mathcal{M}(k),k}\right)$ is concave w.r.t. the variables $\widetilde{P}^{A,n}_{0,\mathcal{M}(k)}$ and $\widetilde{P}^{A,n}_{\mathcal{M}(k),k}$.

Employing the composition rules of (2.19)–(2.20) reveals that

$$f_2\left(\widetilde{P}^{A,n}_{0,\mathcal{M}(k)},\widetilde{P}^{A,n}_{\mathcal{M}(k),k}\right) = \log_2\left[1+f_1\left(\widetilde{P}^{A,n}_{0,\mathcal{M}(k)},\widetilde{P}^{A,n}_{\mathcal{M}(k),k}\right)\right] \tag{3.20}$$

is concave, since $\log_2(\cdot)$ is concave as well as non-decreasing and $1+f_1\left(\widetilde{P}^{A,n}_{0,\mathcal{M}(k)},\widetilde{P}^{A,n}_{\mathcal{M}(k),k}\right)$ is concave.

The second term in the summation of (3.16) may be written as

$$f_3\left(\widetilde{P}^{A,n}_{0,\mathcal{M}(k)},\widetilde{P}^{A,n}_{\mathcal{M}(k),k},\widetilde{s}^{A,n}_k\right) = \widetilde{s}^{A,n}_{k,n}\log_2\left(1+\frac{\widetilde{P}^{A,n}_{0,\mathcal{M}(k)}G^n_{0,\mathcal{M}(k)}\widetilde{P}^{A,n}_{\mathcal{M}(k),k}G^n_{\mathcal{M}(k),k}}{\widetilde{s}^{A,n}_k\Delta\gamma N_0 W\left(\widetilde{P}^{A,n}_{0,\mathcal{M}(k)}G^n_{0,\mathcal{M}(k)}+\widetilde{P}^{A,n}_{\mathcal{M}(k),k}G^n_{\mathcal{M}(k),k}\right)}\right), \tag{3.21}$$

which may be obtained using the perspective transformation of Section 2.3.4 yielding

$$f_3\left(\widetilde{P}^{A,n}_{0,\mathcal{M}(k)},\widetilde{P}^{A,n}_{\mathcal{M}(k),k},\widetilde{s}^{A,n}_k\right) = \widetilde{s}^{A,n}_k\cdot f_2\left(\frac{\widetilde{P}^{A,n}_{0,\mathcal{M}(k)}}{\widetilde{s}^{A,n}_k},\frac{\widetilde{P}^{A,n}_{\mathcal{M}(k),k}}{\widetilde{s}^{A,n}_k}\right), \tag{3.22}$$

thus preserving concavity. Strictly speaking, the perspective transformation also requires that $s>0$. However, convexity is also preserved for the situation when $s=0$ as proven in [22].

Using similar arguments, $\widetilde{s}^{D,n}_k\log_2\left(1+\frac{\widetilde{P}^{D,n}_{0,k}G^n_{0,k}}{\widetilde{s}^{D,n}_k\Delta\gamma N_0 W}\right)$ is proven to be concave w.r.t. the variables $\widetilde{s}^{D,n}_k$ and $\widetilde{P}^{D,n}_{0,k}$.

Finally, the numerator is shown to be concave w.r.t the variables $\widetilde{s}^{A,n}_k$, $\widetilde{s}^{D,n}_k$, $\widetilde{P}^{D,n}_{0,k}$, $\widetilde{P}^{A,n}_{0,k}$, $\widetilde{P}^{A,n}_{0,\mathcal{M}(k)}$ and $\widetilde{P}^{A,n}_{\mathcal{M}(k),k}$, $\forall k,n$, since it is the non-negative sum of multiple concave functions. Thus, the objective function (3.10) has a numerator that is concave, while its denominator is affine. Hence, (3.10) is quasi-concave.

### 3.3.2 Problem Solution Methods

As described in Section 2.4.3, quasi-concavity may be viewed as a type of generalized concavity, since it can describe discontinuous functions as well as functions that have multiple stationary points, which are clearly not concave. This means that a local maximum is not

guaranteed to be a global maximum and thus standard convex optimization techniques, such as interior-point or ellipsoid methods, cannot be readily applied for finding their optimal solution [34]. However, a quasi-concave function has convex superlevel sets, hence the bisection method of Section 2.4.3.1 may be used for iteratively closing the gap between an upper and lower bound solution, until the difference between the two becomes lower than a predefined tolerance. The drawback of this method is that there is no exact method of finding the initial upper as well as lower bounds. Additionally, a convex feasibility problem must be solved in each iteration, which may become computationally undesirable. Another approach is Dinkelbach's method described in Section 2.4.3.3, which solves the quasi-concave problem as a sequence of parameterized concave programming problems. A third method is based on the Charnes-Cooper variable transformation of Section 2.4.3.5, which transforms the quasi-concave problem into a concave problem with an additional linear constraint. Although this additional constraint makes the problem more complex, the original quasi-concave problem may then be solved as a single concave problem, which avoids the need for solving multiple problems as in the case of Dinkelbach's method.

In this chapter, we solve the relaxed problem using all three methods to compare their performance versus complexity in Section 3.7.

## 3.4 Dinkelbach's Method for Solving (3.10)–(3.15)

Dinkelbach's method, as described in Section 2.4.3.3, relies on solving the subtractive form of the FP problem in each iteration $j$. When applied to the problem of (3.10)–(3.15), the optimization problem may be written as

$$\begin{aligned}
\underset{\widetilde{\mathcal{P}},\widetilde{\mathcal{S}}}{\text{maximize}} \quad & \sum_{k=1}^{K}\sum_{n=1}^{N} \widetilde{s}_k^{D,n} \log_2\left(1+\frac{\widetilde{P}_{0,k}^{D,n} G_{0,k}^{n}}{\widetilde{s}_k^{D,n}\Delta\gamma N_0 W}\right) \\
& + \frac{\widetilde{s}_k^{A,n}}{2}\log_2\left(1+\frac{\widetilde{P}_{0,\mathcal{M}(k)}^{A,n} G_{0,\mathcal{M}(k)}^{n} \widetilde{P}_{\mathcal{M}(k),k}^{A,n} G_{\mathcal{M}(k),k}^{n}}{\widetilde{s}_k^{A,n}\Delta\gamma N_0 W\left(\widetilde{P}_{0,\mathcal{M}(k)}^{A,n} G_{0,\mathcal{M}(k)}^{n} + \widetilde{P}_{\mathcal{M}(k),k}^{A,n} G_{\mathcal{M}(k),k}^{n}\right)}\right) \\
& - q_j\left[\left(P_C^{(B)} + P_C^{(R)} M\right) + \sum_{k=1}^{K}\sum_{n=1}^{N} \xi^{(B)} \widetilde{P}_{0,k}^{D,n} + \frac{\left(\xi^{(B)}\widetilde{P}_{0,\mathcal{M}(k)}^{A,n} + \xi^{(R)}\widetilde{P}_{\mathcal{M}(k),k}^{A,n}\right)}{2}\right] \qquad (3.23)
\end{aligned}$$

$$\text{subject to} \quad \sum_{k=1}^{K}\sum_{n=1}^{N} \widetilde{P}_{0,k}^{D,n} + \widetilde{P}_{0,\mathcal{M}(k)}^{A,n} + \widetilde{P}_{\mathcal{M}(k),k}^{A,n} \leq P_{max}, \qquad (3.24)$$

$$\widetilde{s}_k^{D,n} + \widetilde{s}_k^{A,n} \leq 1,\ \forall k, n, \qquad (3.25)$$

$$\sum_{k=1}^{K} \widetilde{s}_k^{D,n} + \widetilde{s}_k^{A,n} \leq 1,\ \forall n, \qquad (3.26)$$

$$\widetilde{P}_{0,k}^{D,n},\ \widetilde{P}_{0,\mathcal{M}(k)}^{A,n},\ \widetilde{P}_{\mathcal{M}(k),k}^{A,n} \in \mathbb{R}_+,\ \forall k, n, \qquad (3.27)$$

$$0 \leq \widetilde{s}_k^{D,n},\ \widetilde{s}_k^{A,n} \leq 1,\ \forall k,n. \tag{3.28}$$

Since it has been shown that $R_T\left(\widetilde{\mathcal{P}},\widetilde{\mathcal{S}}\right)$ is concave whilst $P_T\left(\widetilde{\mathcal{P}},\widetilde{\mathcal{S}}\right)$ is affine, the objective function (3.23) is concave, and (3.23)– (3.28) is a concave maximization problem w.r.t. the variables $\widetilde{\mathcal{P}}$ and $\widetilde{\mathcal{S}}$. Assuming the existence of an interior point (Slater's condition as explained in Section 2.5.3), there is a zero duality gap between the dual problem of (3.23)–(3.28) and the primal problem of (3.10)– (3.15). Thus solving the dual problem is equivalent to solving the primal problem.

As described in Section 2.5, the Lagrangian of (3.23)– (3.28) is given by

$$\begin{aligned}\mathcal{L}\left(\widetilde{\mathcal{P}},\widetilde{\mathcal{S}},\lambda\right) \;=\; & \sum_{k=1}^{K}\sum_{n=1}^{N}\widetilde{s}_k^{D,n}\log_2\left(1+\frac{\widetilde{P}_{0,k}^{D,n}G_{0,k}^n}{\widetilde{s}_k^{D,n}\Delta\gamma N_0 W}\right)\\
&+\frac{\widetilde{s}_k^{A,n}}{2}\log_2\left(1+\frac{\widetilde{P}_{0,\mathcal{M}(k)}^{A,n}G_{0,\mathcal{M}(k)}^n\widetilde{P}_{\mathcal{M}(k),k}^{A,n}G_{\mathcal{M}(k),k}^n}{\widetilde{s}_k^{A,n}\Delta\gamma N_0 W\left(\widetilde{P}_{0,\mathcal{M}(k)}^{A,n}G_{0,\mathcal{M}(k)}^n+\widetilde{P}_{\mathcal{M}(k),k}^{A,n}G_{\mathcal{M}(k),k}^n\right)}\right)\\
&-q_j\left[\left(P_C^{(B)}+P_C^{(R)}M\right)+\sum_{k=1}^{K}\sum_{n=1}^{N}\xi^{(B)}\widetilde{P}_{0,k}^{D,n}+\frac{\left(\xi^{(B)}\widetilde{P}_{0,\mathcal{M}(k)}^{A,n}+\xi^{(R)}\widetilde{P}_{\mathcal{M}(k),k}^{A,n}\right)}{2}\right]\\
&+\lambda\left(P_{max}-\sum_{k=1}^{K}\sum_{n=1}^{N}\widetilde{P}_{0,k}^{D,n}+\widetilde{P}_{0,\mathcal{M}(k)}^{A,n}+\widetilde{P}_{\mathcal{M}(k),k}^{A,n}\right),\end{aligned} \tag{3.29}$$

where $\lambda \geq 0$ is the Lagrangian multiplier associated with the constraint (3.11). The feasible region constraints (3.14) and (3.15), and constraints (3.12) and (3.13) will be considered when deriving the optimal solution, which is detailed later.

The dual problem of (3.23)– (3.28) may be written as

$$\min_{\lambda\geq 0}.\ g(\lambda)=\min_{\lambda\geq 0}.\ \max_{\widetilde{\mathcal{P}},\widetilde{\mathcal{S}}}.\ \mathcal{L}\left(\widetilde{\mathcal{P}},\widetilde{\mathcal{S}},\lambda\right), \tag{3.30}$$

which is solved using the dual decomposition approach described in Section 2.7. Using dual decomposition, (3.30) may be readily solved via solving $NK$ similar subproblems to obtain both the power as well as subcarrier allocations, and by solving a master problem to update $\lambda(i)$ at iteration $i$. The dual decomposition approach of Section 2.7 adapted for solving (3.23)– (3.28) is outlined in the following.

### 3.4.1 Solving the Subproblem of Power and Subcarrier Allocation

For a value of $\lambda(i)$ at iteration $i$ of the dual decomposition method and a fixed value of $q_j$, $\max_{\widetilde{\mathcal{P}},\widetilde{\mathcal{S}}}.\ \mathcal{L}\left(\widetilde{\mathcal{P}},\widetilde{\mathcal{S}},\lambda(i)\right)$ is solved to obtain the corresponding optimal power and subcarrier allocations. Since the problem is now in a standard concave form, the KKT conditions given by (2.93)–(2.97), which are first-order necessary and sufficient conditions for optimality,

may be used in order to find the optimal solution. All optimal variables are denoted by a superscript asterisk. The total transmit power assigned for AF transmission to user $k$ over subcarrier $n$ is now denoted by $\widetilde{P}_k^{A,n} = \widetilde{P}_{0,\mathcal{M}(k)}^{A,n} + \widetilde{P}_{\mathcal{M}(k),k}^{A,n}$. Then, by substituting $\widetilde{P}_{\mathcal{M}(k),k}^{A,n} = \widetilde{P}_k^{A,n} - \widetilde{P}_{0,\mathcal{M}(k)}^{A,n}$ into (3.29), the following first-order derivatives may be obtained

$$\left.\frac{\partial \mathcal{L}\left(\widetilde{\mathcal{P}}, \widetilde{\mathcal{S}}, \lambda\left(i\right)\right)}{\partial \widetilde{P}_{0,k}^{D,n}}\right|_{\widetilde{P}_{0,k}^{D,n}=\widetilde{P}_{0,k}^{D,n*}} = 0, \tag{3.31}$$

$$\left.\frac{\partial \mathcal{L}\left(\widetilde{\mathcal{P}}, \widetilde{\mathcal{S}}, \lambda\left(i\right)\right)}{\partial \widetilde{P}_{k}^{A,n}}\right|_{\widetilde{P}_{k}^{A,n}=\widetilde{P}_{k}^{A,n*}} = 0 \tag{3.32}$$

and

$$\left.\frac{\partial \mathcal{L}\left(\widetilde{\mathcal{P}}, \widetilde{\mathcal{S}}, \lambda\left(i\right)\right)}{\partial \widetilde{P}_{0,\mathcal{M}(k)}^{A,n}}\right|_{\widetilde{P}_{0,\mathcal{M}(k)}^{A,n}=\widetilde{P}_{0,\mathcal{M}(k)}^{A,n*}} = 0. \tag{3.33}$$

The optimal values of $P_{0,k}^{D,n}$ may be readily obtained from (3.31) as

$$P_{0,k}^{D,n*} = \left[\frac{1}{\ln 2\left(q_j \xi^{(B)} + \lambda\left(i\right)\right)} - \frac{1}{\alpha_k^{D,n}}\right]^+, \tag{3.34}$$

where the effective channel gain of the direct transmission is given by

$$\alpha_k^{D,n} = \frac{G_{0,k}^n}{\Delta \gamma N_0 W} \tag{3.35}$$

and $[\cdot]^+$ denotes $\max(0, \cdot)$ since the powers allocated have to be nonnegative due to the constraint (3.14). Similarly the optimal values of $\widetilde{P}_{0,\mathcal{M}(k)}^{A,n}$ and $\widetilde{P}_{\mathcal{M}(k),k}^{A,n}$ may be obtained by equating (3.32) and (3.33) to give

$$P_{0,\mathcal{M}(k)}^{A,n*} = \beta_k^{A,n} P_k^{A,n*} \tag{3.36}$$

and

$$P_{\mathcal{M}(k),k}^{A,n*} = \left(1 - \beta_k^{A,n}\right) P_k^{A,n*}, \tag{3.37}$$

where the total transmit power assigned for the AF transmission to user $k$ over subcarrier $n$ is given by (3.38), (3.39) and (3.40).

$$P_k^{A,n*} = \left[\frac{1}{\ln 2\left(\beta_k^{A,n}\left(q_j \xi^{(B)} + 2\lambda\left(i\right)\right) + \left(1 - \beta_k^{A,n}\right)\left(q_j \xi^{(R)} + 2\lambda\left(i\right)\right)\right)} - \frac{1}{\alpha_k^{A,n}}\right]^+ \tag{3.38}$$

$$\alpha_k^{A,n} = \frac{\beta_k^{A,n}\left(1 - \beta_k^{A,n}\right) G_{0,\mathcal{M}(k)}^n G_{\mathcal{M}(k),k}^n}{\left(\beta_k^{A,n} G_{0,\mathcal{M}(k)}^n + \left(1 - \beta_k^{A,n}\right) G_{\mathcal{M}(k),k}^n\right) \Delta \gamma N_0 W} \tag{3.39}$$

$$\beta_k^{A,n} = \frac{-G^n_{\mathcal{M}(k),k}\left(q_j\xi^{(R)}+2\lambda\left(i\right)\right)+\sqrt{G^n_{0,\mathcal{M}(k)}G^n_{\mathcal{M}(k),k}\left(q_j\xi^{(B)}+2\lambda\left(i\right)\right)\left(q_j\xi^{(R)}+2\lambda\left(i\right)\right)}}{G^n_{0,\mathcal{M}(k)}\left(q_j\xi^{(B)}+2\lambda\left(i\right)\right)-G^n_{\mathcal{M}(k),k}\left(q_j\xi^{(R)}+2\lambda\left(i\right)\right)} \tag{3.40}$$

Observe that (3.40) is the fraction of the total AF transmit power that is allocated for the BS-to-RN link while obeying $0 \leq \beta_k^{A,n} \leq 1$.

Having calculated the optimal power allocations, the optimal subcarrier allocations may be derived using the first-order derivatives as follows:

$$\begin{aligned}\frac{\partial\mathcal{L}\left(\widetilde{\mathcal{P}},\widetilde{\mathcal{S}},\lambda\left(i\right)\right)}{\partial\widetilde{s}_k^{D,n}} &= \log_2\left(1+\alpha_k^{D,n}P_{0,k}^{D,n*}\right)-\frac{\alpha_k^{D,n}P_{0,k}^{D,n*}}{\ln 2\left(1+\alpha_k^{D,n}P_{0,k}^{D,n*}\right)}\\ &= D_k^n\begin{cases}<0 & \text{if } \widetilde{s}_k^{D,n*}=0,\\ =0 & \text{if } \widetilde{s}_k^{D,n*}\in(0,1),\\ >0 & \text{if } \widetilde{s}_k^{D,n*}=1\end{cases}\end{aligned} \tag{3.41}$$

and

$$\begin{aligned}\frac{\partial\mathcal{L}\left(\widetilde{\mathcal{P}},\widetilde{\mathcal{S}}\lambda\left(i\right)\right)}{\partial\widetilde{s}_k^{A,n}} &= \frac{1}{2}\log_2\left(1+\alpha_k^{A,n}P_k^{A,n*}\right)-\frac{\alpha_k^{A,n}P_k^{A,n*}}{2\ln 2\left(1+\alpha_k^{A,n}P_k^{A,n*}\right)}\\ &= A_k^n\begin{cases}<0 & \text{if } \widetilde{s}_k^{A,n*}=0,\\ =0 & \text{if } \widetilde{s}_k^{A,n*}\in(0,1),\\ >0 & \text{if } \widetilde{s}_k^{A,n*}=1.\end{cases}\end{aligned} \tag{3.42}$$

(3.41) and (3.42) stem from the fact that if the optimal value of $\widetilde{s}_k^{X,n}$ occurs at the boundary of the feasible region, then $\mathcal{L}\left(\widetilde{\mathcal{P}},\widetilde{\mathcal{S}},\lambda\left(i\right)\right)$ must be decreasing with the values of $\widetilde{s}_k^{X,n}$ that approach the interior of the feasible region. By contrast, for example, the derivative $D_k^n=0$ if the optimal $\widetilde{s}_k^{D,n}$ is obtained in the interior of the feasible region [23]. However, since each subcarrier may only be used for transmission to a single user, each subcarrier $n$ is allocated to the specific user $k$ having the highest value of $\max\left(A_k^n,D_k^n\right)$ in order to achieve the highest increase in $\mathcal{L}\left(\widetilde{\mathcal{P}},\widetilde{\mathcal{S}},\lambda\left(i\right)\right)$. The optimal allocation for subcarrier $n$ is as follows

$$\widetilde{s}_k^{D,n*}=\begin{cases}1, & \text{if } D_k^n=\max_j\left[\max\left(A_j^n,D_j^n\right)\right] \text{ and } D_k^n\geq 0,\\ 0, & \text{otherwise,}\end{cases} \tag{3.43}$$

and

$$\widetilde{s}_k^{A,n*} = \begin{cases} 1, & \text{if } A_k^n = \max_j \left[\max\left(A_j^n, D_j^n\right)\right] \text{ and } A_k^n \geq 0, \\ 0, & \text{otherwise.} \end{cases} \tag{3.44}$$

If there are multiple users that tie for the value of $\max\left(A_k^n, D_k^n\right)$, then a random user from the maximal set is chosen. Thus constraints (3.12)– (3.15) are satisfied and the optimal primal variables are obtained for a given $\lambda\left(i\right)$. Observe that the optimal power allocations given by (3.34) and (3.38) are indeed customized water-filling solutions described in Section 2.8, where the effective channel gains are given by $\alpha_k^{D,n}$ and $\alpha_k^{A,n}$, respectively, and where the water levels are determined both by the cost of allocating power, $\lambda\left(i\right)$, as well as the current cost of power to the EE given by $q_j$.

### 3.4.2 Updating the Dual Variable $\lambda$

Since (3.34), (3.36), (3.37), (3.43) and (3.44) give a unique solution for $\max\limits_{\widetilde{\mathcal{P}},\widetilde{\mathcal{S}}}$. $\mathcal{L}\left(\widetilde{\mathcal{P}},\widetilde{\mathcal{S}},\lambda\left(i\right)\right)$, it follows that $g\left(\lambda\right)$ is differentiable and hence the gradient method of Section 2.6 may be readily used for updating the dual variable $\lambda$. The gradient of $\mathcal{L}\left(\widetilde{\mathcal{P}},\widetilde{\mathcal{S}},\lambda\right)$ w.r.t. $\lambda$ is given by

$$\frac{\partial\mathcal{L}\left(\widetilde{\mathcal{P}},\widetilde{\mathcal{S}},\lambda\right)}{\partial\lambda} = P_{max} - \sum_{k=1}^{K}\sum_{n=1}^{N}\left(\widetilde{P}_{0,k}^{D,n} + \widetilde{P}_{0,\mathcal{M}(k)}^{A,n} + \widetilde{P}_{\mathcal{M}(k),k}^{A,n}\right). \tag{3.45}$$

Therefore, $\lambda\left(i\right)$ may be updated using the optimal variables to give (3.46),

$$\lambda\left(i+1\right) = \left[\lambda\left(i\right) - \alpha_\lambda\left(i\right)\left(P_{max} - \sum_{k=1}^{K}\sum_{n=1}^{N}\widetilde{P}_{0,k}^{D,n*} + \widetilde{P}_{0,\mathcal{M}(k)}^{A,n*} + \widetilde{P}_{\mathcal{M}(k),k}^{A,n*}\right)\right]^{+} \tag{3.46}$$

where $\alpha_\lambda(i)$ is the size of the step taken in the direction of the negative gradient for the dual variable $\lambda\left(i\right)$ at iteration $i$. For the performance investigations of Section 3.7, a constant step size is used, since it is comparatively easier to find a value that strikes a balance between optimality and convergence speed. The process of computing the optimal power as well as subcarrier allocations and subsequently updating $\lambda\left(i\right)$ is repeated until convergence is attained, indicating that the dual optimal point has been reached. Since the primal problem is concave, there is a zero duality gap between the dual and primal solutions as described in Section 2.5. Hence, solving the dual problem is equivalent to solving the primal problem. The inner loop solution method is summarized in Table 3.1.

### 3.4.3 Summary of Solution Algorithm Based on Dinkelbach's Method

Again, for additional clarity, the solution algorithm, based on Dinkelbach's method, is summarized in Fig. 3.3. Firstly, the relaxed problem (3.10)– (3.15) expressed in a fractional

TABLE 3.1: Inner loop solution method for obtaining the optimal power and subcarrier allocations for a given $q_j$.

**Algorithm 2** Inner loop solution method for obtaining the optimal power and subcarrier allocations for a given $q_j$.

Input: $I^D_{inner}$ (maximum number of iterations)
$\epsilon^D_{inner} > 0$ (convergence tolerance)
$i \leftarrow 0$
**do while** $|\lambda(i) - \lambda(i-1)| > \epsilon^D_{inner}$ **and** $i < I^D_{inner}$
  $i \leftarrow i + 1$
  **for** $n$ **from** 1 **to** $N$
    **for** $k$ **from** 1 **to** $K$
      Obtain the optimal power allocation using (3.34), (3.36) and (3.37)
    **end for**
    Obtain the optimal subcarrier allocation using (3.43) and (3.44)
  **end for**
  Update the dual variables $\lambda$ using (3.46)
**end do**
**return**

form is rewritten as a subtractive, parameterized concave form, where $q_j$ is the parameter. Solving this problem for a given $q_j$ is termed an outer iteration, and is illustrated in the upper block of Fig. 3.3. The lower block of Fig. 3.3 illustrates the dual decomposition approach that is employed for solving the subtractive, concave problem. Each iteration of the dual decomposition approach is termed an inner iteration. In each inner iteration, $2NK$ subproblems are solved to obtain the optimal power and subcarrier variables for a given $q_j$ and for the dual variable $\lambda(i)$. The dual variable $\lambda$ is then updated, depending on the power and subcarrier variables obtained. Multiple inner iterations are completed until convergence of the optimal dual and primal solutions is reached. The optimal $\mathcal{P}^*$ and $\mathcal{S}^*$ are then fed back into the upper block of Fig. 3.3 to evaluate the updated value of $q_j$, which is used in the next outer iteration. Several outer iterations are completed until convergence to the optimal $q_j$ is obtained. The corresponding optimal $\mathcal{P}^*$ and $\mathcal{S}^*$ values are the power and subcarrier allocation variables that solve the problem (3.10)– (3.15). The algorithmic complexity of this method is dominated by the comparison operations given by (3.43) and (3.44), which leads to a total complexity of $\mathcal{O}(I_{dual} \times 2NK)$ when $NK$ is large, where $I_{dual}$ is the total number of inner iterations required for reaching convergence in Dinkelbach's method.

## 3.5 Charnes-Cooper Transformation Method for Solving (3.10)– (3.15)

Another method of solving the problem (3.10)– (3.15) is the Charnes-Cooper transformation method described in Section 2.4.3.5, which transforms the FP problem into a parameter-free

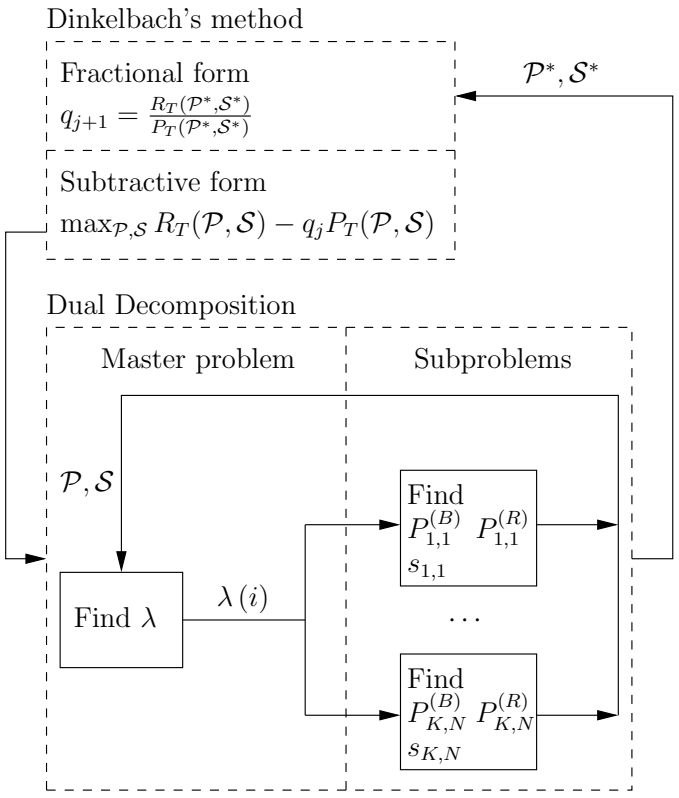


FIGURE 3.3: Summary of the solution algorithm based on Dinkelbach's method.

concave problem. This provides an advantage over the method described in Section 3.4 since it is not necessary to iteratively determine the optimal parameter $q^*$.

Let us introduce the variable transformations

$$t = \frac{1}{\left(P_C^{(B)} + P_C^{(R)} M\right) + \sum_{k=1}^{K}\sum_{n=1}^{N} \xi^{(B)} \widetilde{P}_{0,k}^{D,n} + \frac{1}{2}\left(\xi^{(B)} \widetilde{P}_{0,\mathcal{M}(k)}^{A,n} + \xi^{(R)} \widetilde{P}_{\mathcal{M}(k),k}^{A,n}\right)} \tag{3.47}$$

and $\widehat{P}_{0,k}^{D,n} = \widetilde{P}_{0,k}^{D,n} t$, $\widehat{P}_{0,\mathcal{M}(k)}^{A,n} = \widetilde{P}_{0,\mathcal{M}(k)}^{A,n} t$, $\widehat{P}_{\mathcal{M}(k),k}^{A,n} = \widetilde{P}_{\mathcal{M}(k),k}^{A,n} t$, $\widehat{s}_k^{D,n} = \widetilde{s}_k^{D,n} t$ and $\widehat{s}_k^{A,n} = \widetilde{s}_k^{A,n} t$. Let us furthermore collect the power variables into a set denoted by $\widehat{\mathcal{P}}$, while the subcarrier indicator variables are in a set denoted by $\widehat{\mathcal{S}}$. The problem (3.10)– (3.15) may then be written as

$$\begin{aligned} \underset{t>0,\widehat{\mathcal{P}},\widehat{\mathcal{S}}}{\text{maximize}} \quad & t \sum_{k=1}^{K}\sum_{n=1}^{N} \frac{\widehat{s}_k^{D,n}}{t} \log_2\left(1 + \frac{\frac{\widehat{P}_{0,k}^{D,n}}{t} G_{0,k}^n}{\frac{\widehat{s}_k^{D,n}}{t}\Delta\gamma N_0 W}\right) \\ & + \frac{\widehat{s}_k^{A,n}}{2t} \log_2\left(1 + \frac{\frac{\widehat{P}_{0,\mathcal{M}(k)}^{A,n}}{t} G_{0,\mathcal{M}(k)}^n \frac{\widehat{P}_{\mathcal{M}(k),k}^{A,n}}{t} G_{\mathcal{M}(k),k}^n}{\frac{\widehat{s}_k^{A,n}}{t}\Delta\gamma N_0 W\left(\frac{\widehat{P}_{0,\mathcal{M}(k)}^{A,n}}{t} G_{0,\mathcal{M}(k)}^n + \frac{\widehat{P}_{\mathcal{M}(k),k}^{A,n}}{t} G_{\mathcal{M}(k),k}^n\right)}\right) \end{aligned} \tag{3.48}$$

$$\text{subject to} \quad t\left(\sum_{k=1}^{K}\sum_{n=1}^{N}\frac{\widehat{P}_{0,k}^{D,n}}{t}+\frac{\widehat{P}_{0,\mathcal{M}(k)}^{A,n}}{t}+\frac{\widehat{P}_{\mathcal{M}(k),k}^{A,n}}{t}-P_{max}\right)\leq 0, \tag{3.49}$$

$$t\left(\frac{\widehat{s}_k^{D,n}}{t}+\frac{\widehat{s}_k^{A,n}}{t}-1\right)\leq 0,\ \forall k,n, \tag{3.50}$$

$$t\left(\sum_{k=1}^{K}\frac{\widehat{s}_k^{D,n}}{t}+\frac{\widehat{s}_k^{A,n}}{t}-1\right)\leq 0,\ \forall n, \tag{3.51}$$

$$t\left(\frac{\widehat{P}_{0,k}^{D,n}}{t}\right),\ t\left(\frac{\widehat{P}_{0,\mathcal{M}(k)}^{A,n}}{t}\right),\ t\left(\frac{\widehat{P}_{\mathcal{M}(k),k}^{A,n}}{t}\right)\in\mathbb{R}_+,\ \forall k,n, \tag{3.52}$$

$$t\left(\frac{\widehat{s}_k^{D,n}}{t}-1\right),\ t\left(\frac{\widehat{s}_k^{A,n}}{t}-1\right)\leq 0\leq t\left(\frac{\widehat{s}_k^{D,n}}{t}\right),\ t\left(\frac{\widehat{s}_k^{A,n}}{t}\right),\ \forall k,n, \tag{3.53}$$

$$t\left[\left(P_C^{(B)}+P_C^{(R)}M\right)+\sum_{k=1}^{K}\sum_{n=1}^{N}\xi^{(B)}\frac{\widehat{P}_{0,k}^{D,n}}{t}+\frac{1}{2}\left(\xi^{(B)}\frac{\widehat{P}_{0,\mathcal{M}(k)}^{A,n}}{t}+\xi^{(R)}\frac{\widehat{P}_{\mathcal{M}(k),k}^{A,n}}{t}\right)\right]=1, \tag{3.54}$$

which can be rewritten as

$$\underset{t>0,\widehat{\mathcal{P}},\widehat{\mathcal{S}}}{\text{maximize}} \quad \sum_{k=1}^{K}\sum_{n=1}^{N}\widehat{s}_k^{D,n}\log_2\left(1+\frac{\widehat{P}_{0,k}^{D,n}G_{0,k}^{n}}{\widehat{s}_k^{D,n}\Delta\gamma N_0 W}\right)$$
$$+\frac{\widehat{s}_k^{A,n}}{2}\log_2\left(1+\frac{\widehat{P}_{0,\mathcal{M}(k)}^{A,n}G_{0,\mathcal{M}(k)}^{n}\widehat{P}_{\mathcal{M}(k),k}^{A,n}G_{\mathcal{M}(k),k}^{n}}{\widehat{s}_k^{A,n}\Delta\gamma N_0 W\left(\widehat{P}_{0,\mathcal{M}(k)}^{A,n}G_{0,\mathcal{M}(k)}^{n}+\widehat{P}_{\mathcal{M}(k),k}^{A,n}G_{\mathcal{M}(k),k}^{n}\right)}\right) \tag{3.55}$$

$$\text{subject to} \quad \sum_{k=1}^{K}\sum_{n=1}^{N}\widehat{P}_{0,k}^{D,n}+\widehat{P}_{0,\mathcal{M}(k)}^{A,n}+\widehat{P}_{\mathcal{M}(k),k}^{A,n}\leq t\cdot P_{max}, \tag{3.56}$$

$$\widehat{s}_k^{D,n}+\widehat{s}_k^{A,n}\leq t,\ \forall k,n, \tag{3.57}$$

$$\sum_{k=1}^{K}\widehat{s}_k^{D,n}+\widehat{s}_k^{A,n}\leq t,\ \forall n, \tag{3.58}$$

$$\widehat{P}_{0,k}^{D,n},\ \widehat{P}_{0,\mathcal{M}(k)}^{A,n},\ \widehat{P}_{\mathcal{M}(k),k}^{A,n}\in\mathbb{R}_+,\ \forall k,n, \tag{3.59}$$

$$0\leq\widehat{s}_k^{D,n},\ \widehat{s}_k^{A,n}\leq t,\ \forall k,n, \tag{3.60}$$

$$1-\left[t\left(P_C^{(B)}+P_C^{(R)}M\right)+\sum_{k=1}^{K}\sum_{n=1}^{N}\xi^{(B)}\widehat{P}_{0,k}^{D,n}+\frac{1}{2}\left(\xi^{(B)}\widehat{P}_{0,\mathcal{M}(k)}^{A,n}+\xi^{(R)}\widehat{P}_{\mathcal{M}(k),k}^{A,n}\right)\right]=0. \tag{3.61}$$

Strictly speaking, the constraint $t>0$ is also needed, but this is guaranteed due to constraint (3.47). Observe that the objective function has a similar form to $f_3\left(\widetilde{P}_{k,n}^{(B)},\widetilde{P}_{k,n}^{(R)},\widetilde{s}_{k,n}\right)$ and it is thus concave, while all constraints are affine. Therefore, (3.55)–(3.61) is a concave maximization problem, which can be efficiently and optimally solved using the dual decom-

position method, as described in Section 3.4.

### 3.5.1 Solution Method for the Transformed Problem (3.55)–(3.61)

The method of solving (3.55)–(3.61) is similar to that of Section 3.4, where we first form the Lagrangian of (3.55)–(3.61) as

$$\begin{aligned}\mathcal{L}\left(\widehat{\mathcal{P}},\widehat{\mathcal{S}},t,\lambda,\mu\right) &= \sum_{k=1}^{K}\sum_{n=1}^{N}\widehat{s}_k^{D,n}\log_2\left(1+\frac{\widehat{P}_{0,k}^{D,n}G_{0,k}^{n}}{\widehat{s}_k^{D,n}\Delta\gamma N_0 W}\right)\\ &+\frac{\widehat{s}_k^{A,n}}{2}\log_2\left(1+\frac{\widehat{P}_{0,\mathcal{M}(k)}^{A,n}G_{0,\mathcal{M}(k)}^{n}\widehat{P}_{\mathcal{M}(k),k}^{A,n}G_{\mathcal{M}(k),k}^{n}}{\widehat{s}_k^{A,n}\Delta\gamma N_0 W\left(\widehat{P}_{0,\mathcal{M}(k)}^{A,n}G_{0,\mathcal{M}(k)}^{n}+\widehat{P}_{\mathcal{M}(k),k}^{A,n}G_{\mathcal{M}(k),k}^{n}\right)}\right)\\ &+\lambda\left(t\cdot P_{max}-\sum_{k=1}^{K}\sum_{n=1}^{N}\widehat{P}_{0,k}^{D,n}+\widehat{P}_{0,\mathcal{M}(k)}^{A,n}+\widehat{P}_{\mathcal{M}(k),k}^{A,n}\right)\\ &+\mu\left(1-\left[t\left(P_C^{(B)}+P_C^{(R)}M\right)\right.\right.\\ &\left.\left.+\sum_{k=1}^{K}\sum_{n=1}^{N}\xi^{(B)}\widehat{P}_{0,k}^{D,n}+\frac{1}{2}\left(\xi^{(B)}\widehat{P}_{0,\mathcal{M}(k)}^{A,n}+\xi^{(R)}\widehat{P}_{\mathcal{M}(k),k}^{A,n}\right)\right]\right),\end{aligned}\tag{3.62}$$

where $\lambda \geq 0$ and $\mu \in \mathbb{R}$ are the Lagrangian multipliers associated with the constraints of (3.56) and (3.61), respectively, while the other constraints and $t > 0$ will be satisfied during the optimization process, which is detailed below.

Using the KKT conditions of (2.93)–(2.97) and setting the derivative w.r.t. the optimal variables to zero, we may write

$$\left.\frac{\partial\mathcal{L}\left(\widehat{\mathcal{P}},\widehat{\mathcal{S}},t,\lambda,\mu\right)}{\partial\widehat{P}_{0,k}^{D,n}}\right|_{\widehat{P}_{0,k}^{D,n}=\widehat{P}_{0,k}^{D,n*}} = 0,\tag{3.63}$$

which imply that

$$\widehat{P}_{0,k}^{D,n*}=\widehat{s}_k^{D,n}\left[\frac{1}{\ln 2\left(\lambda\left(i\right)+\mu\left(i\right)\xi^{(B)}\right)}-\frac{1}{\alpha_k^{D,n}}\right]^{+},\tag{3.64}$$

where $\alpha_k^{D,n}$ is once again given by (3.35) and $i$ is the iteration index of the dual decomposition method.

Using a similar method as described in Section 3.4, the total power assigned to the relaying link assisting UE $k$ may be denoted as $\widehat{P}_k^{A,n}=\widehat{P}_{0,\mathcal{M}(k)}^{A,n}+\widehat{P}_{\mathcal{M}(k),k}^{A,n}$. Thus, the optimal total

relaying power variables are obtained by the KKT conditions given by

$$\left.\frac{\partial\mathcal{L}\left(\widehat{\mathcal{P}},\widehat{\mathcal{S}},t,\lambda,\mu\right)}{\partial\widehat{P}_k^{D,n}}\right|_{\widehat{P}_k^{D,n}=\widehat{P}_k^{D,n*}} = 0, \tag{3.65}$$

which imply that

$$\widehat{P}_k^{A,n*} = \widehat{s}_k^{A,n}\left[\frac{1}{\ln 2\left(\beta_k^{A,n}\left(\mu\left(i\right)\xi^{(B)}+2\lambda\left(i\right)\right)+\left(1-\beta_k^{A,n}\right)\left(\mu\left(i\right)\xi^{(R)}+2\lambda\left(i\right)\right)\right)}-\frac{1}{\alpha_k^{A,n}}\right]^+, \tag{3.66}$$

where $\alpha_k^{A,n}$ and $\beta_k^{A,n}$ are given by (3.39) and (3.40), with $\mu\left(i\right)$ replacing the parameter $q_j$. The optimal powers assigned for each BS-to-RN and RN-to-UE are then given by

$$\widehat{P}_{0,\mathcal{M}(k)}^{A,n*} = \beta_k^{A,n}\widehat{P}_k^{A,n*} \tag{3.67}$$

and

$$\widehat{P}_{\mathcal{M}(k),k}^{A,n*} = \left(1-\beta_k^{A,n}\right)\widehat{P}_k^{A,n*}, \tag{3.68}$$

respectively.

The first order derivatives of the Lagrangian (3.62) w.r.t. the subcarrier indicator variables are given by

$$\begin{aligned}\frac{\partial\mathcal{L}\left(\widehat{\mathcal{P}},\widehat{\mathcal{S}},t,\lambda,\mu\right)}{\partial\widehat{s}_k^{D,n}} &= \log_2\left(1+\alpha_k^{D,n}P_{0,k}^{D,n*}\right)-\frac{\alpha_k^{D,n}P_{0,k}^{D,n*}}{\ln 2\left(1+\alpha_k^{D,n}P_{0,k}^{D,n*}\right)}\\ &= D_k^n\begin{cases}<0 & \text{if } \widehat{s}_k^{D,n*}=0,\\ =0 & \text{if } \widehat{s}_k^{D,n*}\in(0,t),\\ >0 & \text{if } \widehat{s}_k^{D,n*}=t^*\end{cases}\end{aligned} \tag{3.69}$$

and

$$\begin{aligned}\frac{\partial\mathcal{L}\left(\widehat{\mathcal{P}},\widehat{\mathcal{S}},t,\lambda,\mu\right)}{\partial\widehat{s}_k^{A,n}} &= \frac{1}{2}\log_2\left(1+\alpha_k^{A,n}P_k^{A,n*}\right)-\frac{\alpha_k^{A,n}P_k^{A,n*}}{2\ln 2\left(1+\alpha_k^{A,n}P_k^{A,n*}\right)}\\ &= A_k^n\begin{cases}<0 & \text{if } \widehat{s}_k^{A,n*}=0,\\ =0 & \text{if } \widehat{s}_k^{A,n*}\in(0,t),\\ >0 & \text{if } \widehat{s}_k^{A,n*}=t^*.\end{cases}\end{aligned} \tag{3.70}$$

Following a similar logical argument to that given in Section 3.4, the optimal subcarrier

indicator variables are given by

$$\widehat{s}_k^{D,n*} = \begin{cases} t^*, & \text{if } D_k^n = \max_j \left[\max\left(A_j^n, D_j^n\right)\right] \text{ and } D_k^n \geq 0, \\ 0, & \text{otherwise,} \end{cases} \tag{3.71}$$

and

$$\widehat{s}_k^{A,n*} = \begin{cases} t^*, & \text{if } A_k^n = \max_j \left[\max\left(A_j^n, D_j^n\right)\right] \text{ and } A_k^n \geq 0, \\ 0, & \text{otherwise.} \end{cases} \tag{3.72}$$

Observe that the optimal value of $t$ is yet to be determined. However, having obtained the optimal subcarrier assignments, the optimal value of $t^*$ is given by

$$t^* = \frac{1}{\left(P_C^{(B)} + P_C^{(R)} M\right) + \sum_{k=1}^{K}\sum_{n=1}^{N} \frac{\xi^{(B)} \widehat{P}_{0,k}^{D,n*}}{\widehat{s}_k^{D,n*}} + \frac{1}{2\widehat{s}_k^{A,n*}} \left(\xi^{(B)} \widehat{P}_{0,\mathcal{M}(k)}^{A,n*} + \xi^{(R)} \widehat{P}_{\mathcal{M}(k),k}^{A,n*}\right)}, \tag{3.73}$$

which only depends on the dual variables.

Now that all optimal primal variables have been obtained, $\lambda$ may be updated as follows

$$\lambda\left(i+1\right) = \left[\lambda(i) - \alpha_\lambda\left(i\right)\left(t^* \cdot P_{max} - \sum_{k=1}^{K}\sum_{n=1}^{N} \widehat{P}_{0,k}^{D,n*} + \widehat{P}_{0,\mathcal{M}(k)}^{A,n*} + \widehat{P}_{\mathcal{M}(k),k}^{A,n*}\right)\right]^+, \tag{3.74}$$

where $i$ is the current iteration index and $\alpha_\lambda\left(i\right)$ is a sufficiently small step size.

However, observe that this method cannot be applied to update $\mu$ since the constraint (3.61), which ensures that $t$ is the reciprocal of the denominator in (3.10), is always satisfied because we calculate $t$ exactly using (3.73). In this case, any real value of $\mu$ satisfies the KKT conditions. Therefore, we propose an alternative method, where we substitute the optimal primal variables of $\widetilde{\mathcal{P}}$ and $\widetilde{\mathcal{S}}$ into $\mathcal{L}\left(\widehat{\mathcal{P}}, \widehat{\mathcal{S}}, t, \lambda, \mu\right)$ and find the derivative w.r.t. the optimal $t$ to give

$$\begin{aligned} \frac{\partial \mathcal{L}\left(\widehat{\mathcal{P}}, \widehat{\mathcal{S}}, t, \lambda, \mu\right)}{\partial t} = & \sum_{k=1}^{K}\sum_{n=1}^{N} \widetilde{s}_k^{D,n*} \log_2\left(1 + \frac{\widetilde{P}_{0,k}^{D,n*} G_{0,k}^n}{\widetilde{s}_k^{D,n*} \Delta\gamma N_0 W}\right) \\ & + \frac{\widetilde{s}_k^{A,n*}}{2} \log_2\left(1 + \frac{\widetilde{P}_{0,\mathcal{M}(k)}^{A,n*} G_{0,\mathcal{M}(k)}^n \widetilde{P}_{\mathcal{M}(k),k}^{A,n*} G_{\mathcal{M}(k),k}^n}{\widetilde{s}_k^{A,n*} \Delta\gamma N_0 W \left(\widetilde{P}_{0,\mathcal{M}(k)}^{A,n*} G_{0,\mathcal{M}(k)}^n + \widetilde{P}_{\mathcal{M}(k),k}^{A,n*} G_{\mathcal{M}(k),k}^n\right)}\right) \\ & + \lambda\left(P_{max} - \sum_{k=1}^{K}\sum_{n=1}^{N} \widetilde{P}_{0,k}^{D,n*} + \widetilde{P}_{0,\mathcal{M}(k)}^{A,n*} + \widetilde{P}_{\mathcal{M}(k),k}^{A,n*}\right) \\ & - \mu\left[\left(P_C^{(B)} + P_C^{(R)} M\right)\right. \end{aligned}$$

TABLE 3.2: Solution algorithm for transformation method.

**Algorithm 3** Solution algorithm for transformation method

Input: $I_{max}^{CC}$ (maximum number of iterations)
$\epsilon > 0$ (convergence tolerance)

$i \leftarrow 0$
**do while** $|\lambda(i) - \lambda(i-1)| > \epsilon$ **and** $|\mu(i) - \mu(i-1)| > \epsilon$ **and** $i < I_{max}^{CC}$
  $i \leftarrow i + 1$
  **for** $n$ **from** 1 **until** $N$ **do**
    **for** $k$ **from** 1 **until** $K$ **do**
      Obtain the optimal power allocation using (3.64)–(3.68)
    **end for**
    Obtain the optimal subcarrier assignments using (3.71) and (3.72)
  **end for**
  Obtain the optimal $t$ using (3.73)
  Update the dual variable $\lambda$ using (3.74)
  Update the dual variable $\mu$ using (3.76)
**end do**
**return**

$$+\sum_{k=1}^{K}\sum_{n=1}^{N}\xi^{(B)}\widetilde{P}_{0,k}^{D,n*}+\frac{1}{2}\left(\xi^{(B)}\widetilde{P}_{0,\mathcal{M}(k)}^{A,n*}+\xi^{(R)}\widetilde{P}_{\mathcal{M}(k),k}^{A,n*}\right)\Bigg]=0. \tag{3.75}$$

Thus, the updated value of $\mu$ is given by

$$\begin{aligned}\mu(i+1) \;=\; &\Bigg[\sum_{k=1}^{K}\sum_{n=1}^{N}\widetilde{s}_k^{D,n*}\log_2\left(1+\frac{\widetilde{P}_{0,k}^{D,n*}G_{0,k}^{n}}{\widetilde{s}_k^{D,n*}\Delta\gamma N_0 W}\right)\\
&+\frac{\widetilde{s}_k^{A,n*}}{2}\log_2\left(1+\frac{\widetilde{P}_{0,\mathcal{M}(k)}^{A,n*}G_{0,\mathcal{M}(k)}^{n}\widetilde{P}_{\mathcal{M}(k),k}^{A,n*}G_{\mathcal{M}(k),k}^{n}}{\widetilde{s}_k^{A,n*}\Delta\gamma N_0 W\left(\widetilde{P}_{0,\mathcal{M}(k)}^{A,n*}G_{0,\mathcal{M}(k)}^{n}+\widetilde{P}_{\mathcal{M}(k),k}^{A,n*}G_{\mathcal{M}(k),k}^{n}\right)}\right)\\
&+\lambda(i)\left(P_{max}-\sum_{k=1}^{K}\sum_{n=1}^{N}\widetilde{P}_{0,k}^{D,n*}+\widetilde{P}_{0,\mathcal{M}(k)}^{A,n*}+\widetilde{P}_{\mathcal{M}(k),k}^{A,n*}\right)\Bigg]\cdot\\
&\left[\left(P_C^{(B)}+P_C^{(R)}M\right)+\sum_{k=1}^{K}\sum_{n=1}^{N}\xi^{(B)}\widetilde{P}_{0,k}^{D,n*}+\frac{1}{2}\left(\xi^{(B)}\widetilde{P}_{0,\mathcal{M}(k)}^{A,n*}+\xi^{(R)}\widetilde{P}_{\mathcal{M}(k),k}^{A,n*}\right)\right]^{-1}.\end{aligned} \tag{3.76}$$

This process iterates until the dual variables reach a predefined convergence tolerance $\epsilon$. We summarize this solution method in Table 3.2.

## 3.6 Bisection Method for Solving (3.10)–(3.15)

As described in Section 3.3, the quasi-concave objective function (3.10) has convex super-level sets, and it follows that (3.10)– (3.15) can be solved using the bisection method of Section 2.4.3.1. We commence by writing (3.10) in a quasiconvex form with an upper bound as follows

$$\frac{-\widetilde{R}_T}{\widetilde{P}_T} \leq \sigma, \tag{3.77}$$

where

$$\sigma = \frac{\sigma_U + \sigma_L}{2}, \tag{3.78}$$

and $\sigma_U$ as well as $\sigma_L$ are the current upper and lower bounds on the objective value, respectively. Rewriting (3.77) as

$$-\widetilde{R}_T - \sigma \widetilde{P}_T \leq 0, \tag{3.79}$$

we see that if $-\widetilde{R}_T - \sigma \widetilde{P}_T \leq 0$ is not satisfied, then the objective function cannot obtain the value $\sigma$, which means that $\sigma_L$ may be set to $\sigma$, otherwise $\sigma_U$ may be set to $\sigma$. Observe that by writing the objective function in a quasiconvex form, the objective value will always be negative, and the goal is to increase it's magnitude in the negative direction. Thus, if a value of $\sigma$ cannot be achieved, the lower bound of $\sigma_L$ is updated rather than the upper bound of $\sigma_U$. For a given $\sigma$, (3.79) may be verified using the minimization problem given by

$$\underset{\widetilde{\mathcal{P}},\widetilde{\mathcal{S}}}{\text{minimize}} \quad -\widetilde{R}_T - \sigma \widetilde{P}_T \tag{3.80}$$

$$\text{subject to} \quad \sum_{k=1}^{K}\sum_{n=1}^{N} \widetilde{P}_{0,k}^{D,n} + \widetilde{P}_{0,\mathcal{M}(k)}^{A,n} + \widetilde{P}_{\mathcal{M}(k),k}^{A,n} \leq P_{max}, \tag{3.81}$$

$$\widetilde{s}_k^{D,n} + \widetilde{s}_k^{A,n} \leq 1, \, \forall k, n, \tag{3.82}$$

$$\sum_{k=1}^{K} \widetilde{s}_k^{D,n} + \widetilde{s}_k^{A,n} \leq 1, \, \forall n, \tag{3.83}$$

$$\widetilde{P}_{0,k}^{D,n}, \, \widetilde{P}_{0,\mathcal{M}(k)}^{A,n}, \, \widetilde{P}_{\mathcal{M}(k),k}^{A,n} \in \mathbb{R}_+, \, \forall k, n, \tag{3.84}$$

$$0 \leq \widetilde{s}_k^{D,n}, \, \widetilde{s}_k^{A,n} \leq 1, \, \forall k, n. \tag{3.85}$$

Clearly, the objective function (3.80) is now in a convex form, while the constraints (3.81)–(3.85) remain convex. Therefore, (3.80)–(3.85) is a convex minimization problem and can be optimally and efficiently solved using the dual decomposition method described in Section 3.4. If the optimal value of (3.80)–(3.85) is less than zero, the objective function (3.10) can attain the value of $\sigma$, and the upper bound $\sigma_U$ can be set to $\sigma$. Otherwise, the lower bound $\sigma_L$ is set to $\sigma$. A new value of $\sigma$ is computed from (3.78) and the process iterates until the difference between the upper and lower bounds becomes less than $\epsilon$.

### 3.6.1 Solution Algorithm for (3.80)–(3.85)

The Lagrangian for the problem (3.80)–(3.85) can be written as

$$\begin{aligned}\mathcal{L}\left(\widetilde{\mathcal{P}},\widetilde{\mathcal{S}},\lambda\right) &= -\Bigg[\sum_{k=1}^{K}\sum_{n=1}^{N}\widetilde{s}_k^{D,n}\log_2\left(1+\frac{\widetilde{P}_{0,k}^{D,n}G_{0,k}^{n}}{\widetilde{s}_k^{D,n}\Delta\gamma N_0 W}\right)\\ &\quad+\frac{\widetilde{s}_k^{A,n}}{2}\log_2\left(1+\frac{\widetilde{P}_{0,\mathcal{M}(k)}^{A,n}G_{0,\mathcal{M}(k)}^{n}\widetilde{P}_{\mathcal{M}(k),k}^{A,n}G_{\mathcal{M}(k),k}^{n}}{\widetilde{s}_k^{A,n}\Delta\gamma N_0 W\left(\widetilde{P}_{0,\mathcal{M}(k)}^{A,n}G_{0,\mathcal{M}(k)}^{n}+\widetilde{P}_{\mathcal{M}(k),k}^{A,n}G_{\mathcal{M}(k),k}^{n}\right)}\right)\Bigg]\\ &\quad-\sigma\left[\left(P_C^{(B)}+P_C^{(R)}M\right)+\sum_{k=1}^{K}\sum_{n=1}^{N}\xi^{(B)}\widetilde{P}_{0,k}^{D,n}+\frac{\left(\xi^{(B)}\widetilde{P}_{0,\mathcal{M}(k)}^{A,n}+\xi^{(R)}\widetilde{P}_{\mathcal{M}(k),k}^{A,n}\right)}{2}\right]\\ &\quad+\lambda\left(\left[\sum_{k=1}^{K}\sum_{n=1}^{N}\widetilde{P}_{0,k}^{D,n}+\widetilde{P}_{0,\mathcal{M}(k)}^{A,n}+\widetilde{P}_{\mathcal{M}(k),k}^{A,n}\right]-P_{max}\right).\end{aligned}\tag{3.86}$$

Once again, $\lambda$ is the dual variable associated with the constraint (3.81), while the constraints (3.82)–(3.85) are implicitly satisfied using the solution algorithm to be described below.

In the case of minimization, the dual problem can be written as

$$\max_{\lambda\geq 0}.\ g\left(\lambda\right)=\max_{\lambda\geq 0}.\ \min_{\widetilde{\mathcal{P}},\widetilde{\mathcal{S}}}.\ \mathcal{L}\left(\widetilde{\mathcal{P}},\widetilde{\mathcal{S}},\lambda\right).\tag{3.87}$$

Observe that the goal is to maximize the dual function rather than minimizing it, which was the case in Sections 3.4 and 3.5. However, in a similar fashion to Sections 3.4 and 3.5, the KKT optimality conditions may be employed to find the optimal direct link power variables as

$$P_{0,k}^{D,n*}=\left[\frac{1}{\ln 2\left(\lambda\left(i\right)-\sigma\xi^{(B)}\right)}-\frac{1}{\alpha_k^{D,n}}\right]^{+}\tag{3.88}$$

at iteration $i$ of the dual decomposition method, while the total power assigned to the RN-UE link $k$, denoted by $P_k^{A,n}=P_{0,\mathcal{M}(k)}^{A,n}+P_{\mathcal{M}(k),k}^{A,n}$, is optimal when we have

$$P_k^{A,n*}=\left[\frac{1}{\ln 2\left[2\lambda\left(i\right)-\sigma\left(\xi^{(B)}\beta+\xi^{(R)}\left(1-\beta\right)\right)\right]}-\frac{1}{\alpha_k^{D,n}}\right]^{+},\tag{3.89}$$

where $\beta$ is given by (3.40) with $-\sigma$ replacing $q_j$, and $\alpha_k^{D,n}$ is given by (3.35).

In a similar fashion to that presented in Sections 3.4 and 3.5, the derivatives of the La-

grangian (3.86) w.r.t. the subcarrier indicator variables are

$$\begin{aligned}\frac{\partial \mathcal{L}\left(\widetilde{\mathcal{P}},\widetilde{\mathcal{S}},\lambda\right)}{\partial \widetilde{s}_k^{D,n}} &= -\quad \log_2\left(1+\alpha_k^{D,n}P_{0,k}^{D,n*}\right)+\frac{\alpha_k^{D,n}P_{0,k}^{D,n*}}{\ln 2\left(1+\alpha_k^{D,n}P_{0,k}^{D,n*}\right)} \\ &= \quad D_k^n\begin{cases}<0 & \text{if } \widetilde{s}_k^{D,n*}=1,\\ =0 & \text{if } \widetilde{s}_k^{D,n*}\in(0,1),\\ >0 & \text{if } \widetilde{s}_k^{D,n*}=0\end{cases}\end{aligned} \tag{3.90}$$

and

$$\begin{aligned}\frac{\partial \mathcal{L}\left(\widetilde{\mathcal{P}},\widetilde{\mathcal{S}},\lambda\right)}{\partial \widetilde{s}_k^{A,n}} &= -\frac{1}{2}\log_2\left(1+\alpha_k^{A,n}P_k^{A,n*}\right)+\frac{\alpha_k^{A,n}P_k^{A,n*}}{2\ln 2\left(1+\alpha_k^{A,n}P_k^{A,n*}\right)} \\ &= \quad A_k^n\begin{cases}<0 & \text{if } \widetilde{s}_k^{A,n*}=1,\\ =0 & \text{if } \widetilde{s}_k^{A,n*}\in(0,1),\\ >0 & \text{if } \widetilde{s}_k^{A,n*}=0.\end{cases}\end{aligned} \tag{3.91}$$

Since the goal is to minimize the Lagrangian, the optimal subcarrier indicator variables are given by

$$\widetilde{s}_k^{D,n*}=\begin{cases}1, & \text{if } D_k^n=\min_j\left[\min\left(A_j^n,D_j^n\right)\right] \text{ and } D_k^n\le 0,\\ 0, & \text{otherwise,}\end{cases} \tag{3.92}$$

and

$$\widetilde{s}_k^{A,n*}=\begin{cases}1, & \text{if } A_k^n=\min_j\left[\min\left(A_j^n,D_j^n\right)\right] \text{ and } A_k^n\le 0,\\ 0, & \text{otherwise.}\end{cases} \tag{3.93}$$

Having obtained all the optimal primal variables, the dual variable $\lambda$ may be updated. Since the goal is to maximize the dual function, $\lambda$ should be incremented in the direction of its positive gradient as follows

$$\lambda\left(i+1\right)=\left[\lambda\left(i\right)+\alpha_\lambda\left(i\right)\left(\left[\sum_{k=1}^{K}\sum_{n=1}^{N}\widetilde{P}_{0,k}^{D,n*}+\widetilde{P}_{0,\mathcal{M}(k)}^{A,n*}+\widetilde{P}_{\mathcal{M}(k),k}^{A,n*}\right]-P_{max}\right)\right]^{+}. \tag{3.94}$$

The process of updating the primal and dual variables repeats until the objective value converges to the predefined tolerance of $\epsilon$. The value of $\sigma$ is then updated and the minimization problem is repeatedly solved until the value of $\sigma$ converges. The bisection method used for solving (3.10)– (3.15) is summarized in Table 3.3 and illustrated in Fig. 3.4.

TABLE 3.3: Solution algorithm for bisection method.

**Algorithm 3** Solution algorithm for bisection method

Input: $I^B_{max}$ (maximum number of iterations)
$\epsilon > 0$ (convergence tolerance)
$\sigma_U$ (upper bound)
$\sigma_L$ (lower bound)

**do while** $|\sigma_U - \sigma_L| > \epsilon$
  $\sigma \leftarrow \frac{\sigma_U + \sigma_L}{2}$
  $i \leftarrow 0$
  **do while** $|\lambda(i) - \lambda(i-1)| > \epsilon$ **and** $i < I^B_{max}$
    $i \leftarrow i + 1$
    **for** $n$ **from** 1 **until** $N$ **do**
      **for** $k$ **from** 1 **until** $K$ **do**
        Obtain the optimal power allocation using (3.88)–(3.89)
      **end for**
      Obtain the optimal subcarrier assignments using (3.92) and (3.93)
    **end for**
    Update the dual variable $\lambda$ using (3.94)
  **end do**
  **if** $-\widetilde{R}_T - \sigma\widetilde{P}_T > 0$
    $\sigma_L \leftarrow \sigma$
  **else**
    $\sigma_U \leftarrow \sigma$
  **end if**
**end do**
**return**

## 3.7 Results and Discussions

This section presents the results of applying the EEM algorithm described in Section 3.4 to the relay-aided cellular system shown in Fig. 3.1. Again, the channel is modeled by the path-loss [354] and uncorrelated Rayleigh fading obeying the complex normal distribution, $\mathcal{CN}(0,1)$. It is assumed that the BS-to-RN link has line-of-sight (LOS) propagation, implying that a RN was placed on a tall building. However, the BS-to-UE and RN-to-UE links typically have no LOS, since these links are likely to be blocked by buildings and other large obstructing objects. The RNs are evenly distributed at a fixed distance around the central BS and the UEs are uniformly distributed within the cell. An independently-random set of UE locations as well as fading channel realizations are generated for each channel sample. For fair comparisons, the metrics used are the average SE per subcarrier and the average EE per subcarrier. On the other hand, the sum rate may be calculated by multiplying the average SE by $NW$. Additionally, $\rho$ is introduced to denote the average fraction of the total number of subcarriers that are used for AF transmission. Thus, $\rho$ quantifies the benefit attained from introducing RNs into the system. The main simulation parameters are given in Table 3.4. In all cases, the step size and the initial value of $\lambda$ was empirically

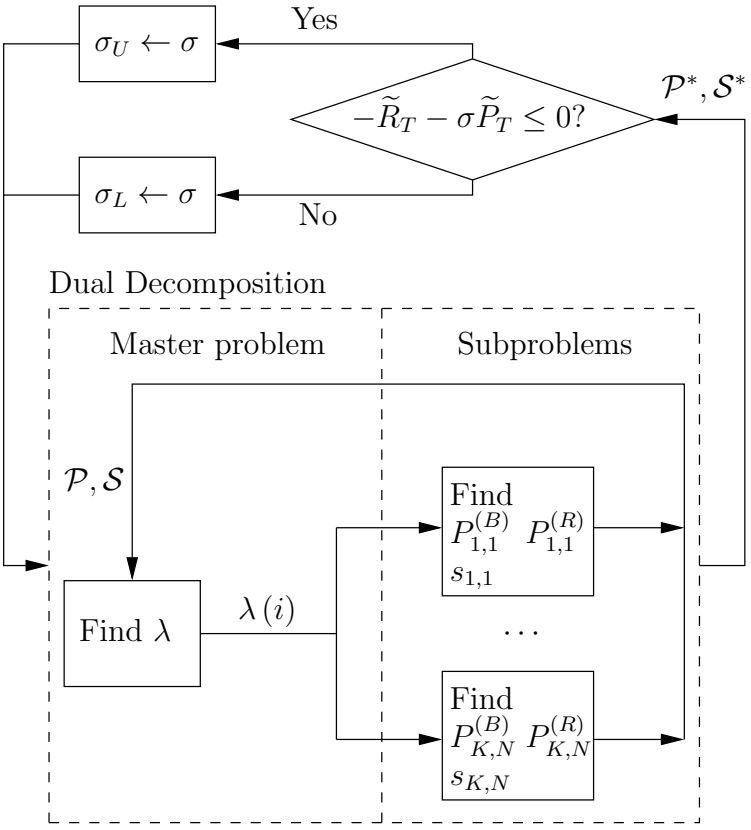


FIGURE 3.4: Summary of the solution algorithm based on the bisection method.

optimized to give the optimal objective value in as few iterations as possible, although the exact analytical method for achieving this still remains an open issue.

### 3.7.1 Convergence of Iterative Algorithms to Optimal Value

Fig. 3.5 illustrates the convergence behavior of all three methods applied to a selection of small-scale systems, averaged over $10^4$ different channel realizations. Since the problem size is small, it is possible to generate also the exhaustive-search based solution within a reasonable computation time. The number of iterations is measured by the total number of primal-dual updates required for the dual decomposition algorithms to converge. This metric is chosen as each method employs the dual decomposition method for solving their convex/concave problems, where each primal-dual update requires roughly similar complexities. Observe in Fig. 3.5 that the bisection method requires the most iterations for converging to the optimal value obtained by the exhaustive search. This matches our expectation, since the bisection method has to solve a convex optimization problem for each value of $\sigma$, which leads to a potentially excessive number of iterations. By contrast, the algorithms that rely on Dinkelbach's method and on the Charnes-Cooper transformation method converge within 30 iterations, as shown in Fig. 3.5(b). However, the algorithm relying on Dinkelbach's

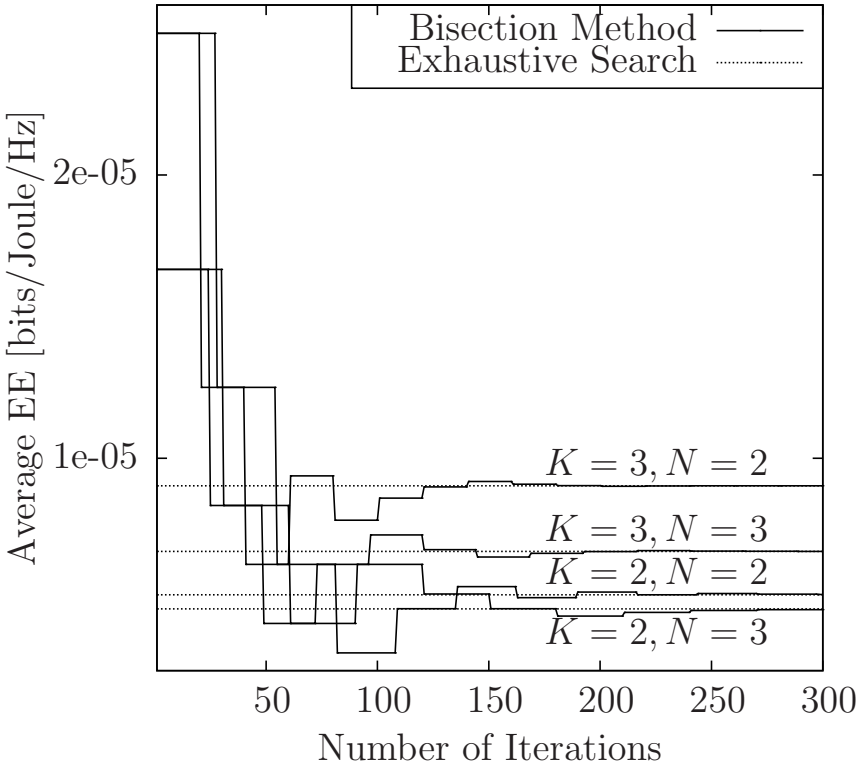


(a) Convergence plot for the bisection method.

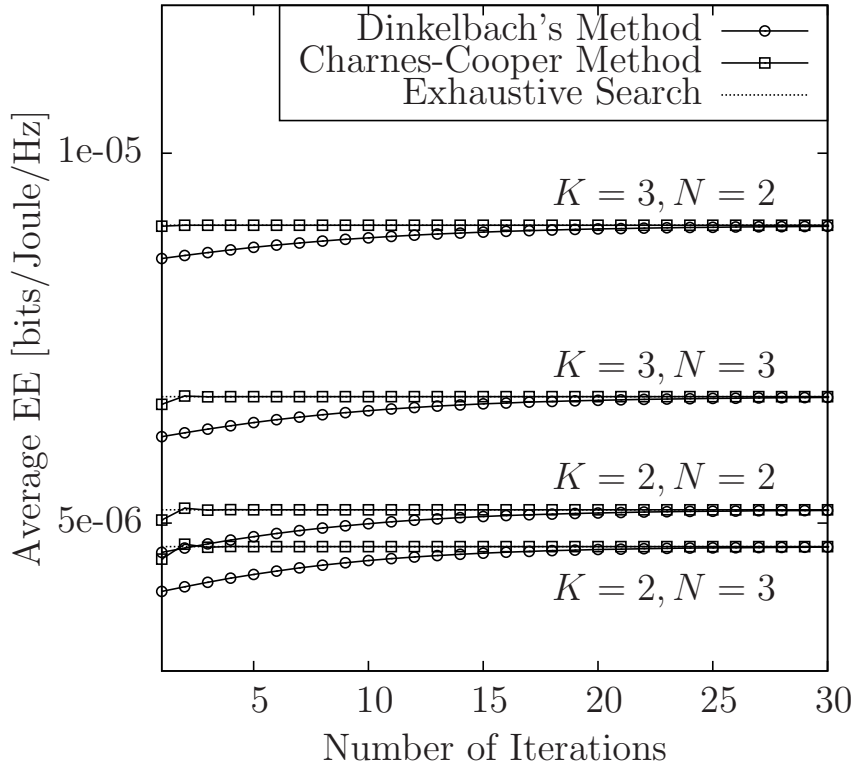


(b) Convergence plot for both the Dinkelbach's method and the Charnes-Cooper transformation method.

FIGURE 3.5: Average EE versus the total number of iterations needed by each of the solution methods when using the simulation parameters from Table 3.4 with $P_{max} = 0$dBm, $D_r = 0.5$, $M = 0$ and with a cell radius of 1km.

TABLE 3.4: Simulation parameters used to obtain all results in this section unless otherwise specified.

| Simulation parameter | Value |
|---|---|
| Subcarrier bandwidth, $W$ Hertz | 12k |
| Number of RNs, $M$ | $\{0, 1, 2, 3, 5, 6\}$ |
| Number of subcarriers, $N$ | $\{128, 512, 1024\}$ |
| Number of UEs, $K$ | $\{30, 60, 120\}$ |
| Cell radius, km | $\{0.75, 1, 1.25, 1.5, 1.75, 2\}$ |
| Ratio of BS-to-RN distance to the cell radius, $D_r$ | $\{0.1, 0.3, 0.5, 0.7, 0.9\}$ |
| SNR gap of wireless transceivers, $\Delta\gamma$ dB | 0 |
| Maximum total transmission power, $P_{max}$ dBm | $\{0, 5, 10, 15, 20, 25, 30, 35, 40, 45, 50, 55, 60\}$ |
| Fixed power consumption of the BS, $P_C^{(B)}$ Watts [352] | 60 |
| Fixed power consumption of RNs, $P_C^{(R)}$ Watts [352] | 20 |
| Reciprocal of the BS power amplifier's drain efficiency, $\xi^{(B)}$ [352] | 2.6 |
| Reciprocal of the RNs' power amplifier's drain efficiency, $\xi^{(R)}$ [352] | 5 |
| Noise power spectral density, $N_0$ dBm/Hz | $-174$ |
| Maximum number of outer iterations in Dinkelbach's algorithm, $I^D_{outer}$ | 10 |
| Maximum number of inner iterations in Dinkelbach's algorithm, $I^D_{inner}$ | 100 |
| Convergence tolerance of iterative algorithms, $\epsilon^D_{outer} = \epsilon^D_{inner}$ | $10^{-8}$ |
| Number of channel samples | $10^4$ |

method still requires solving multiple optimization problems and thus exhibits a slower convergence than the algorithm relying on the Charnes-Cooper transformation method, which only solves a single optimization problem.

Additionally, these results demonstrate that the EEM algorithms indeed result in the optimal power and subcarrier allocations obtained using an exhaustive search, even though the relaxed problem is solved and a high receiver's SNR was assumed.

### 3.7.2 Effect of the Number of UEs on the Attainable SE and EE

Additionally, the EEM algorithm may be employed for evaluating the effects of system-level design choices on the network's SE and EE. The maximum SE is obtained in the first outer iteration of Dinkelbach's method with $q_0 = 0$, since this equates to zero penalty for any

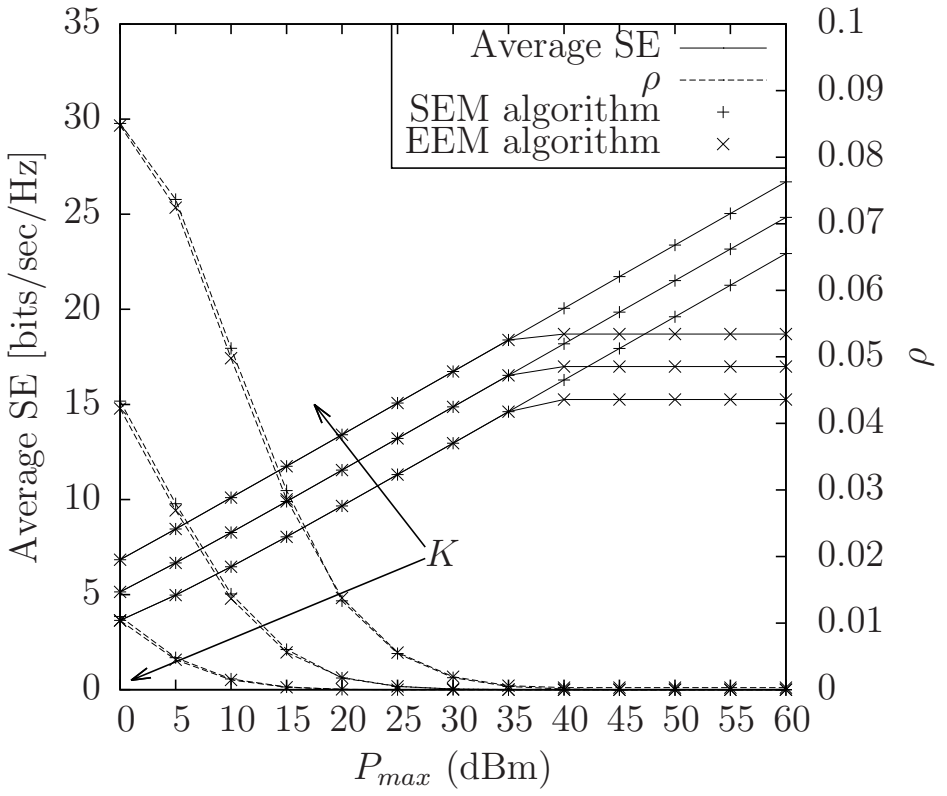


(a) Average SE and $\rho$ versus $P_{max}$ for $K = 30$, 60 and 120.

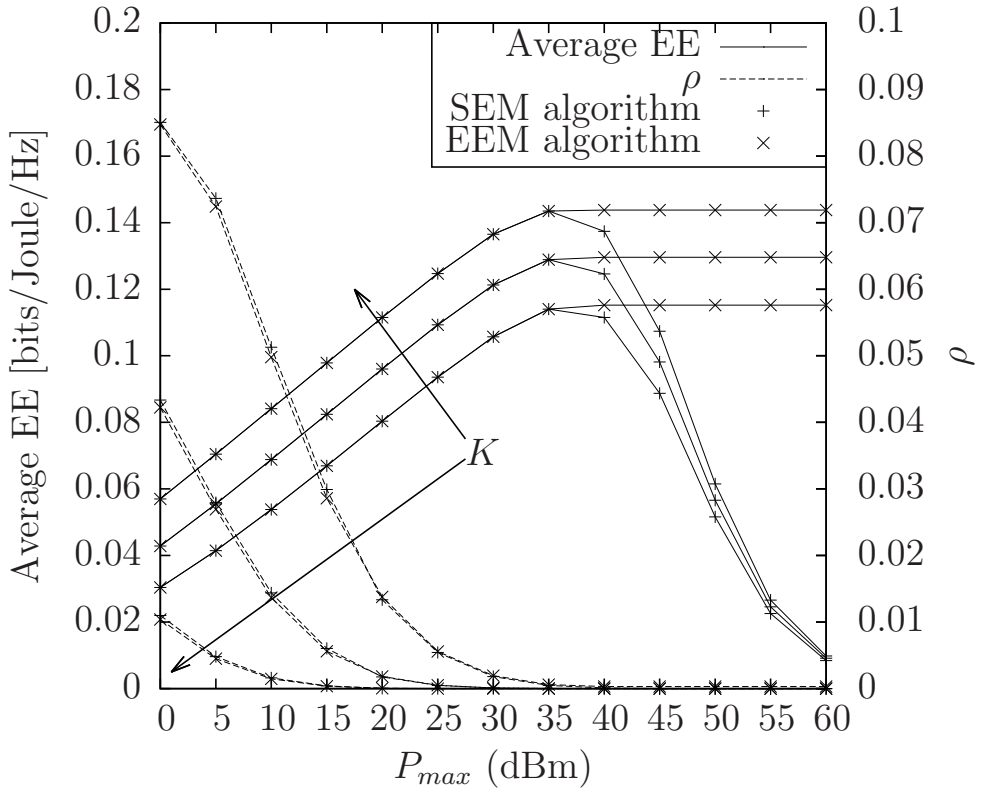


(b) Average EE and $\rho$ versus $P_{max}$ for $K = 30$, 60 and 120.

FIGURE 3.6: Average SE, EE and $\rho$, and the effect of an increasing number of users, $K$, for a system with simulation parameters from Table 3.4 with $N = 128$, $M = 3$, $D_r = 0.5$ and with a cell radius of 1.5km.

power consumption. In the case of the Charnes-Cooper transformation method, $t$ can be set to unity to obtain the SE solution.

The effect of $K$ on the average EE and SE is depicted in Fig. 3.6. As expected, upon increasing $K$, the multi-user diversity of the system is increased, since the scheduler is allowed to choose its subcarrier allocations from a larger pool of channel gains. More specifically, additional terms are included in both the numerator and denominator of the objective function given by (3.10), when $K$ is increased. Thus, the optimization algorithm will selectively allocate more power and subcarriers for transmissions to those UEs, which are associated with more favorable direct or relayed links, in order to achieve a higher SE or EE performance, as illustrated in Fig. 3.7. This results in an increase of both the maximum EE as well as of the SE attained.

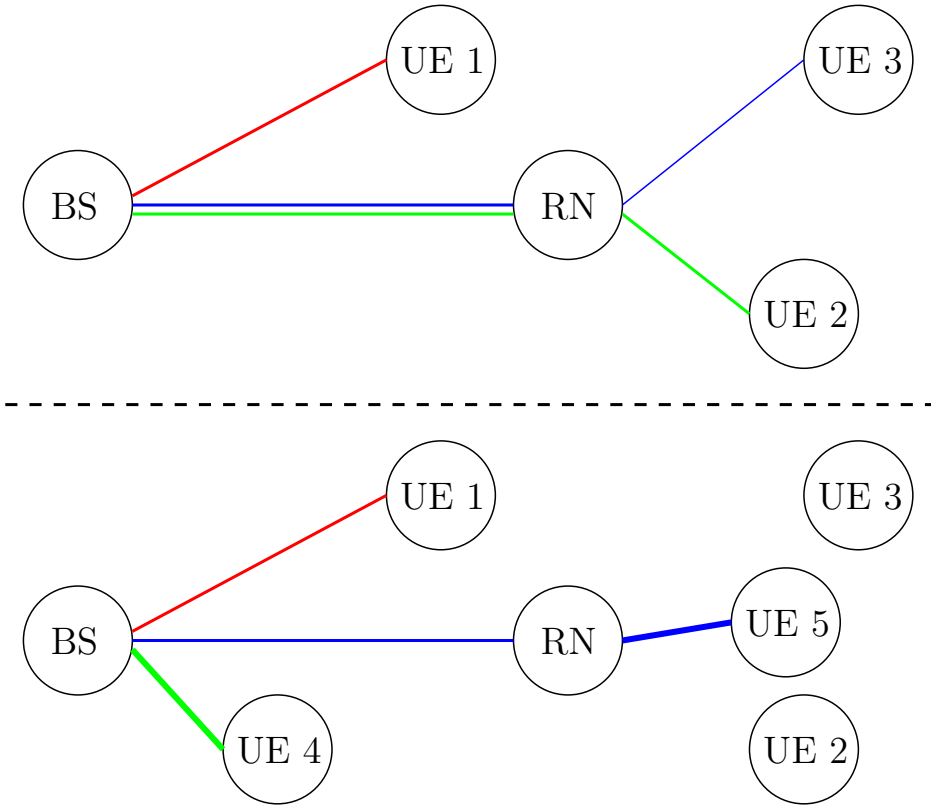


FIGURE 3.7: An illustration of the effect of increasing $K$. When more UEs are added to the system, the optimization algorithm selectively allocates more power and subcarriers to those UEs associated with more favorable channel conditions.

Furthermore, Fig. 3.6 shows that as $P_{max}$ is increased, the SEM algorithm continues to allocate more power in order to achieve a higher average SE at the cost of EE, while the EEM algorithm attains the maximum EE and does not continue to increase its attainable SE by sacrificing the achieved EE. This trend is demonstrated in terms of the objective function of (3.10), since the numerator increases only logarithmically upon increasing the transmission power, while the denominator grows linearly. Thus, the objective function value initially experiences a sharp increase, when increasing the transmission power. However, the

logarithmic increase of the numerator engendered by increasing the transmission power is rapidly outweighed by the linear increase of the denominator. Thus, the EE curve of Fig. 3.6 features a peak, but falls off as the transmission power is further increased.

On the other hand, $\rho$ is inversely proportional to $K$. This indicates that as the multi-user diversity increases, the subcarriers are less likely to be allocated for AF transmissions, simply because there are more favorable BS-to-UE channels owing to having more UEs nearer to the cell-center, as demonstrated in Fig. 3.7. Moreover, the value of $\rho$ decreases as $P_{max}$ increases, because there is more power to allocate to the BS-to-UE links for UEs near the cell-center, which benefit from a reduced pathloss as well as from a more efficient power amplifier at the BS.

### 3.7.3 Effect of the Number of Subcarriers on the Attainable SE and EE

Fig. 3.8 illustrates the effect of increasing $N$ on the attainable SE and EE. Fig. 3.8 shows much of the same trends as Fig. 3.6. For example, the SE continues to rise at the cost of EE, as $P_{max}$ increases when using the SEM algorithm, while the EEM algorithm attains the maximum EE and the corresponding SE. However, in Fig. 3.8 both the SE and EE, averaged over $N$, decreases upon increasing $N$, which implies that the subcarriers are used inefficiently, when more of them are available. Since the achievable SE and EE values are primarily limited by the total power constraint of the system, even if $N$ is increased, the numerator of the objective function given by (3.10) would increase only logarithmically via more beneficial subcarrier allocations, while the SE and EE values obtained suffer from a linear reduction, since they are normalized by the total available bandwidth.

In Fig. 3.8, it is noticeable that $\rho$ increases upon increasing $N$, which is in contrast to the trend observed in Fig. 3.6. This may be understood by considering the UEs within the network. Since the UEs positions are fixed, as $N$ increases the scheduler has access to a larger pool of channel gains for each individual UE, thus more cell-edge users may be supported for the sake of maximizing either the SE or EE. As shown in Fig. 3.9, the scheduler may opt for serving these cell-edge UEs, which were not previously selected, in order to take advantage of the initially sharp increase of the logarithmic numerator of (3.10), when the allocated power is low. However, it is observed that increasing $K$ does not exhibit this effect, since a larger $K$ value indicates that there are more UEs near the cell-center. Furthermore, since both the SEM and EEM algorithms are greedy, these cell-center UEs are served before the cell-edge UEs, hence $\rho$ decreases. The reduction of $\rho$ when $P_{max}$ is very small suggests that the total available power in the system is not high enough to take advantage of the AF transmissions.

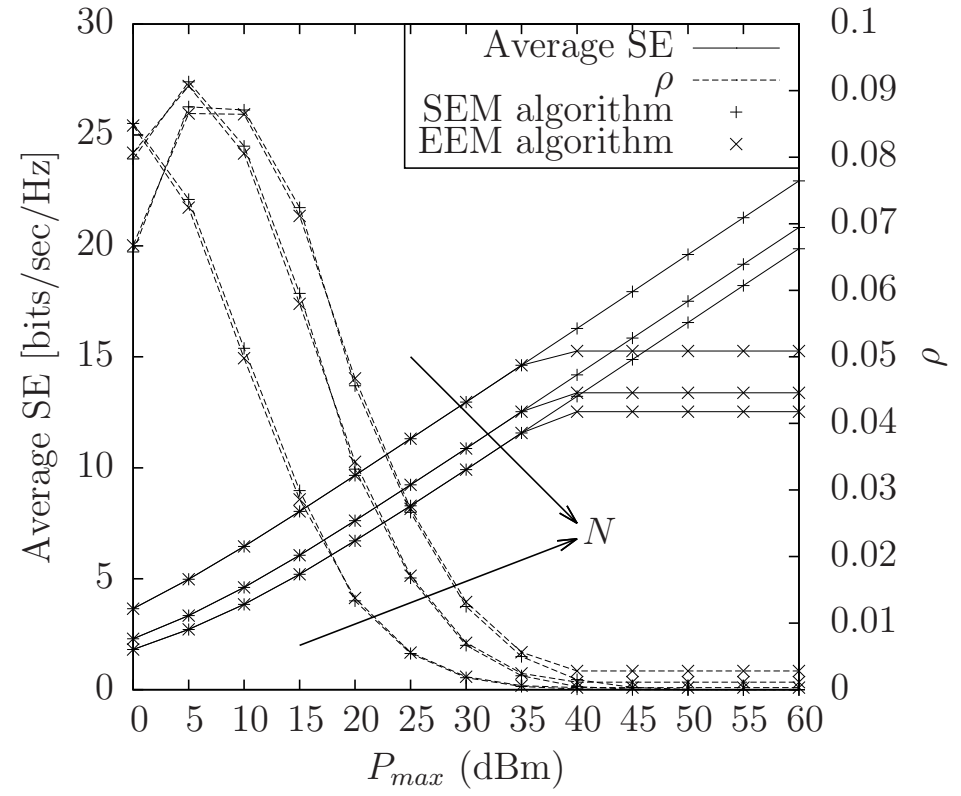


(a) Average SE and $\rho$ versus $P_{max}$ for $N = 128$, 512 and 1024.

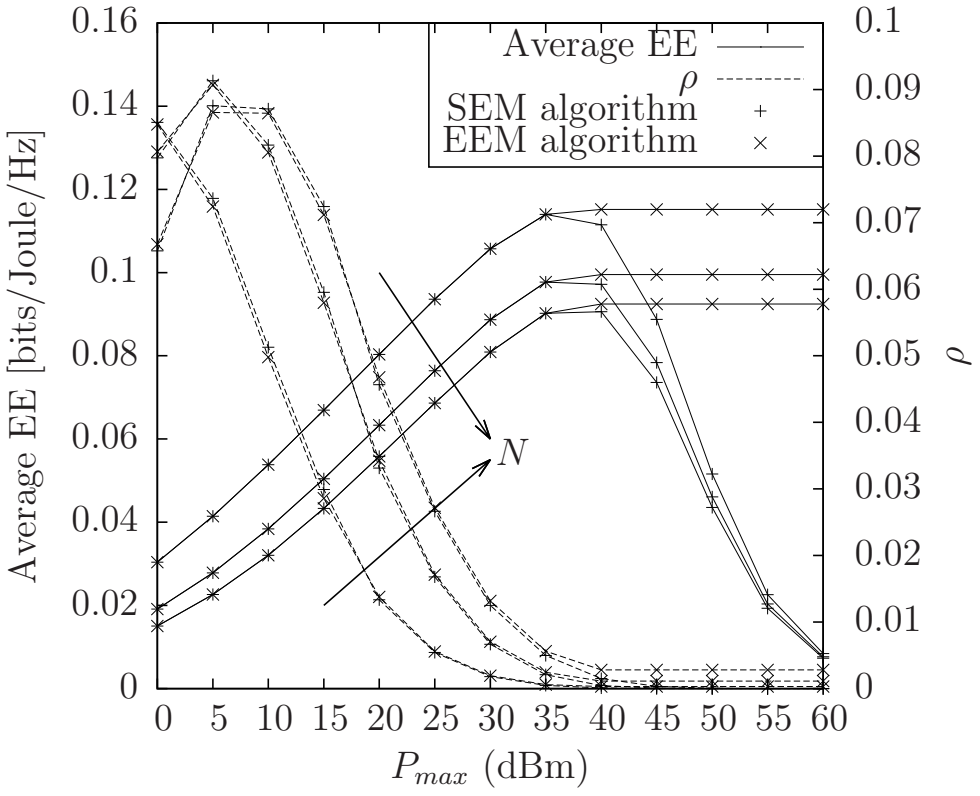


(b) Average EE and $\rho$ versus $P_{max}$ for $N = 128$, 512 and 1024.

FIGURE 3.8: Average SE, EE and $\rho$, and the effect of an increasing number of subcarriers, $N$, for a system with simulation parameters from Table 3.4 with $K = 30$, $M = 3$, $D_r = 0.5$ and with a cell radius of 1.5km.

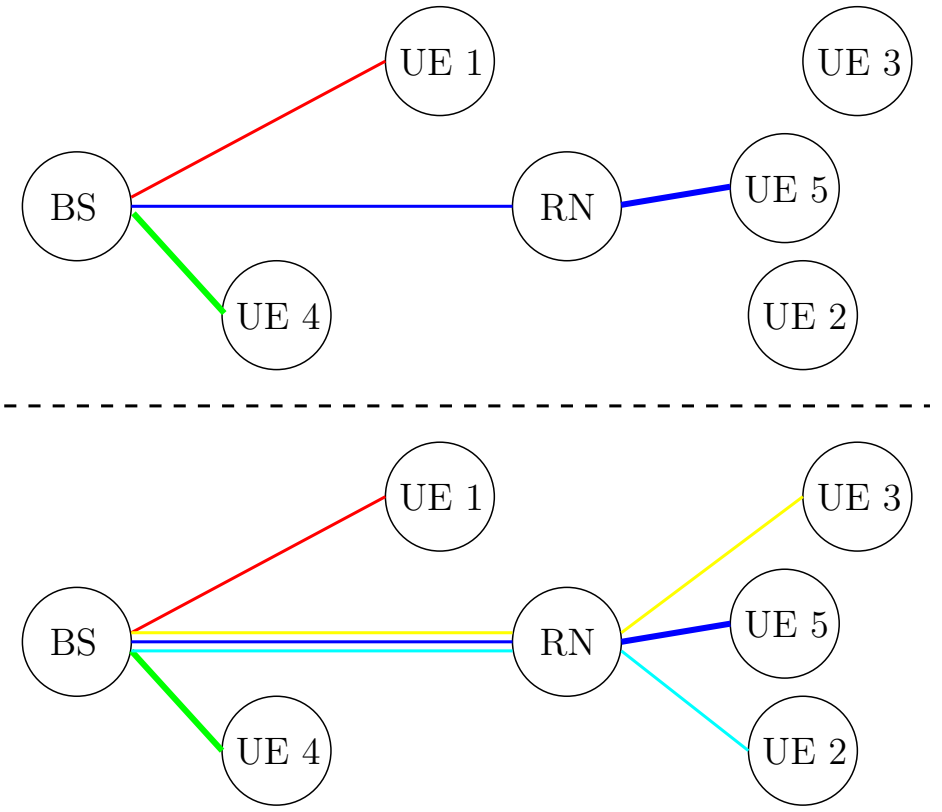


FIGURE 3.9: An illustration of the effect of increasing $N$. When more subcarriers are added to the system, the optimization algorithm may opt for serving extra UEs, which were not previously selected, in order to benefit from the initially sharp rise in the obtainable SE and EE values, owing to the logarithmic nature of the numerator of the objective function given by (3.10).

### 3.7.4 Effect of the Cell Radius on the Attainable SE and EE

The effect of increasing the cell radius on the attainable SE and EE is characterized in Fig. 3.10. As expected, increasing the cell radius has a detrimental effect on both the SE and EE of the system regardless of the number of RNs employed owing to the increased pathlosses experienced. Additionally, it is noteworthy that $\rho$ increases as the cell radius increases, indicating that in line with our expectation, relaying is more beneficial for larger cells. Since the UEs are uniformly-distributed, a larger proportion of the UEs are closer to the cell edge, when the cell radius is increased, as shown in Fig. 3.11. This is coupled with the fact that these UEs near the cell edge have a lower channel gain owing to their higher pathloss. Thus, relaying becomes more beneficial in terms of the attainable SE or EE in larger cells.

On the other hand, the increase in the SE obtained from employing RNs in a large cell is small. For example, the SE is improved by a factor of 1.03 when $M = 6$ RNs are used instead of $M = 0$ at a cell radius of 2km. This improvement is modest when compared to the reduction in EE of a factor of 0.34 due to having to support additional transmitting

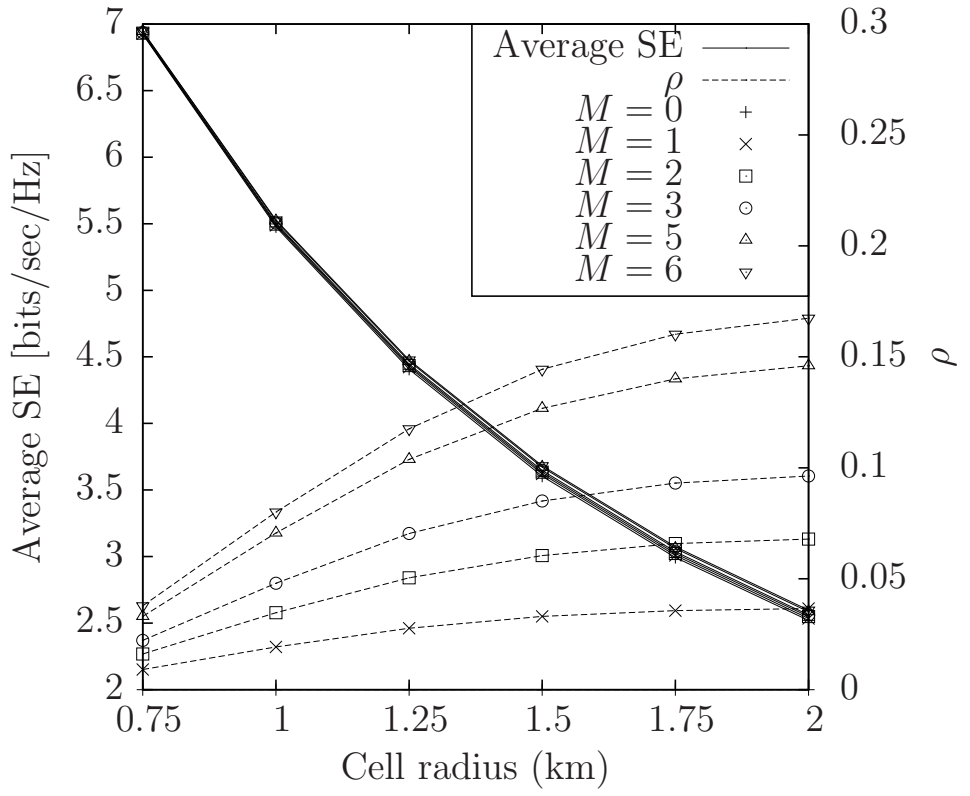


(a) Average SE and $\rho$ versus $P_{max}$ for $M = 0$, 1, 2, 3, 5 and 6.

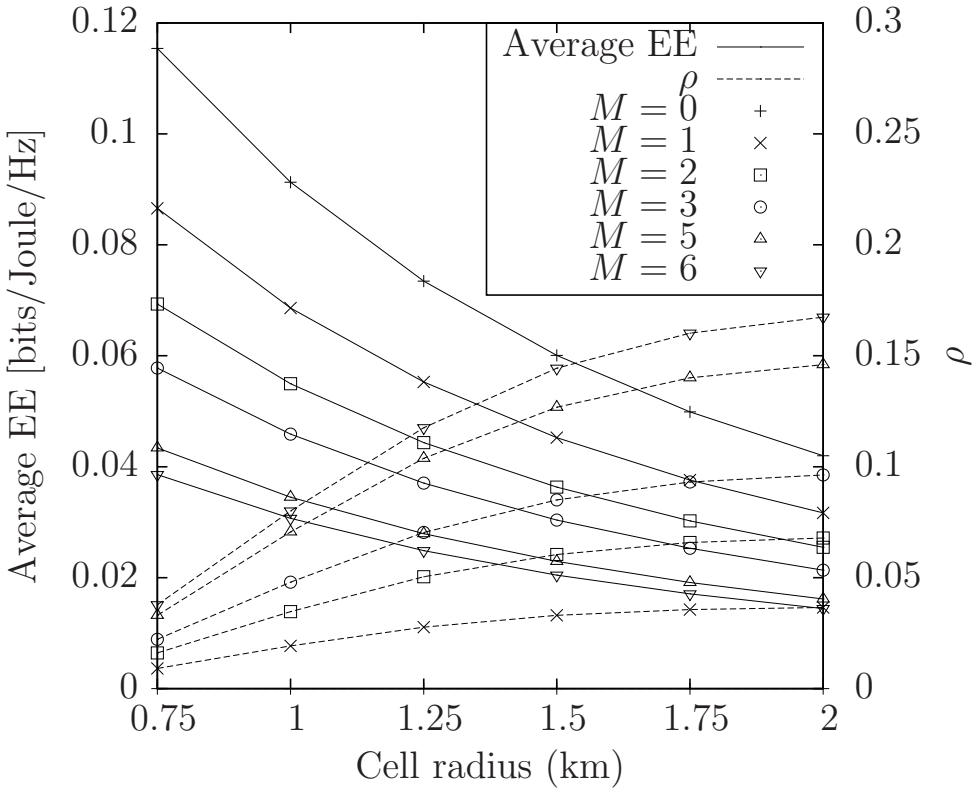


(b) Average EE and $\rho$ versus $P_{max}$ for $M = 0$, 1, 2, 3, 5 and 6.

FIGURE 3.10: Average SE, EE and $\rho$, and the effect of an increasing cell radius for a system with simulation parameters from Table 3.4 with $K = 30$, $N = 128$, $M \in \{0, 1, 2, 3, 5, 6\}$, $D_r = 0.5$ and with a $P_{max} = 0$dBm.

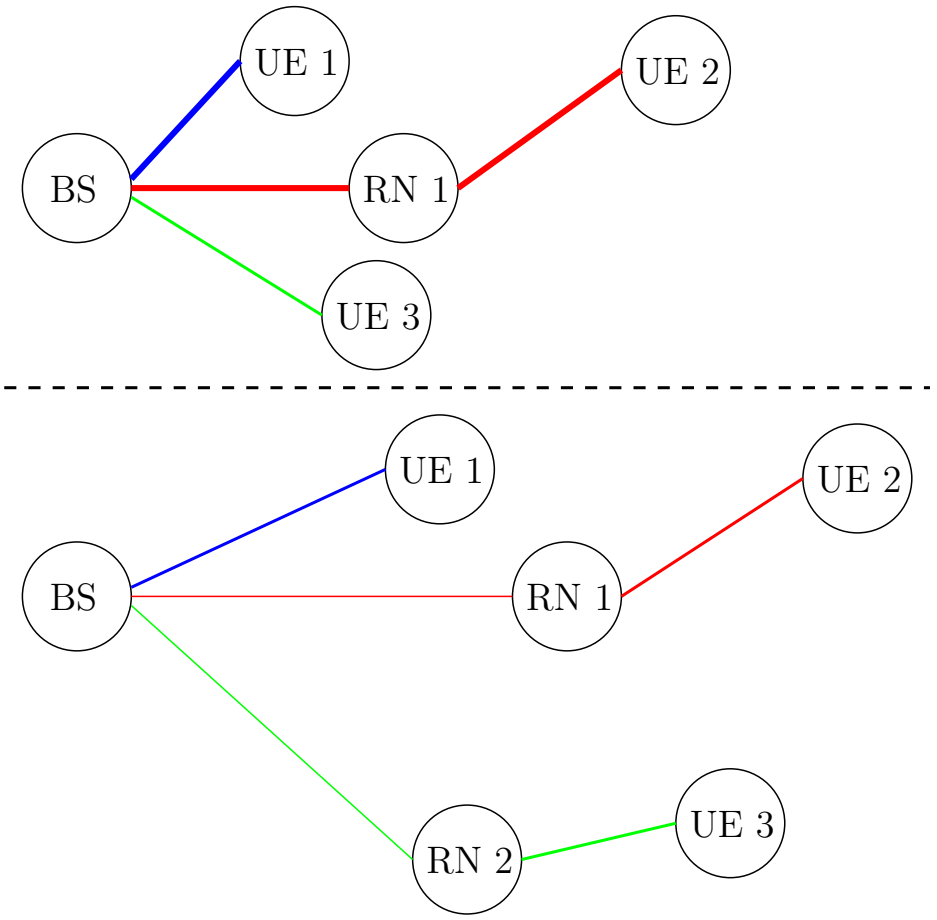


FIGURE 3.11: An illustration of the effect of increasing the cell radius. As the cell radius is increased more UEs are near the cell-edge, owing to their uniform distribution. Thus, relaying becomes more beneficial, when the cell radius is large.

entities. This phenomenon stems from the fact that, since the UEs are uniformly distributed across the cell, the UEs nearer the cell-center are more likely to be allocated resources for maximizing the SE or EE as they may benefit from the more-favorable direct transmission. Thus, increasing the number of RNs in the system brings a marginal benefit in terms of SE or EE.

### 3.7.5 Effect of the Relay's Position on the Attainable SE and EE

The effect of the RNs' position relative to the BS and the cell-edge is illustrated in Fig. 3.12, which clearly shows that the optimal SE and EE is obtained, when the RN is closer to the BS than to the UEs. This stems from the fact that the RN benefits from having a stronger LOS link to the BS, when it is placed closer to the BS, thus strengthening the AF links. However, it cannot be placed too close to the BS, since the benefits gleaned from having a stronger BS-to-RN link are then outweighed by having a more hostile RN-to-UE link.

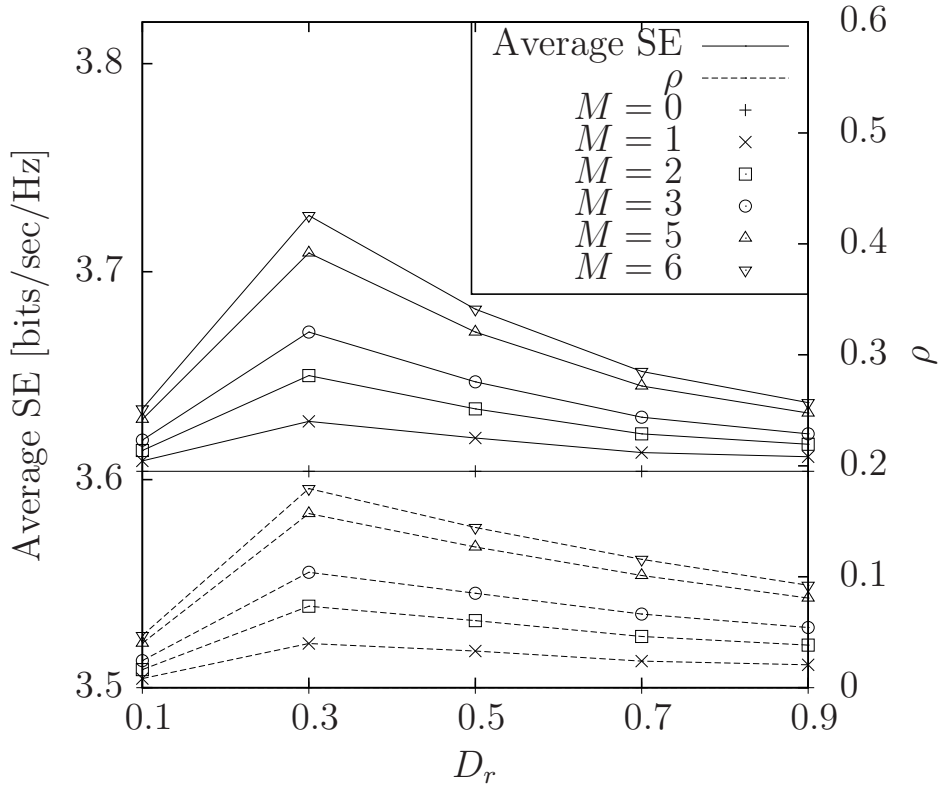


(a) Average SE and $\rho$ versus $P_{max}$ for $M = 0$, 1, 2, 3, 5 and 6.

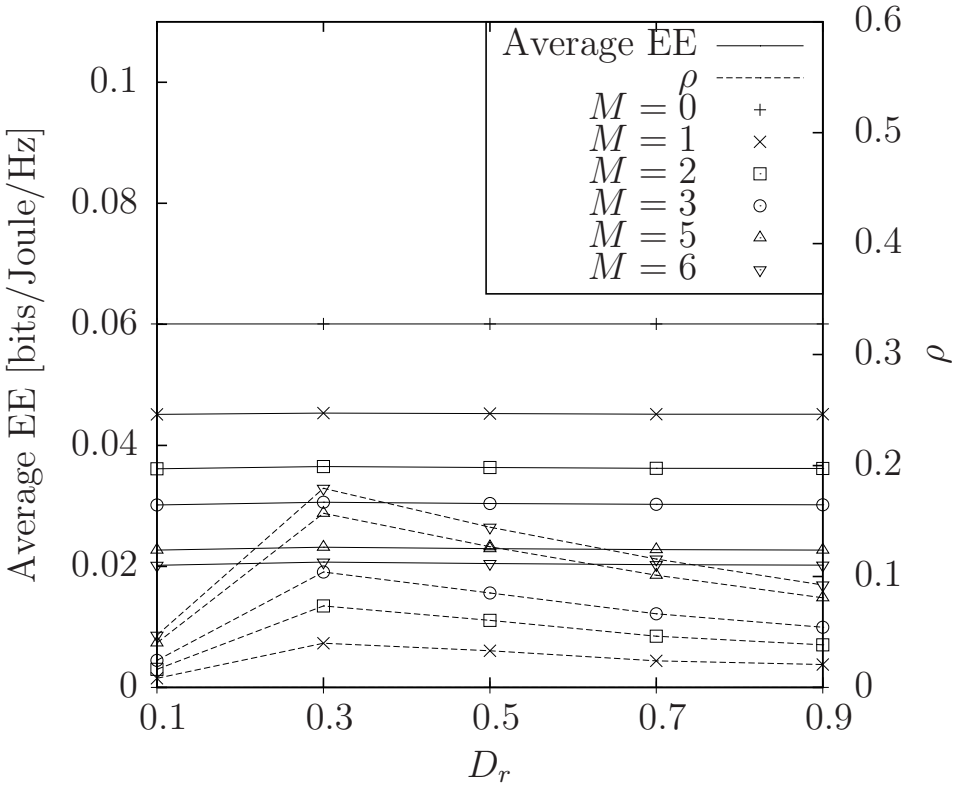


(b) Average EE and $\rho$ versus $P_{max}$ for $M = 0$, 1, 2, 3, 5 and 6.

FIGURE 3.12: Average SE, EE and $\rho$, and the effect of an increasing $D_r$, with simulation parameters from Table 3.4 with $K = 30$, $N = 128$, $M \in \{0, 1, 2, 3, 5, 6\}$, $P_{max} = 0$dBm and with a cell radius of 1.5km.

TABLE 3.5: Summary of the differences in complexities between each solution algorithm, as was depicted in Fig. 3.5.

| System parameters | Solution algorithm | Iterations required |
|---|---|---|
| $K = 2,\ N = 2$ | Bisection | 676 |
| | Dinkelbach's | 120 |
| | Charnes-Cooper | 11 |
| $K = 3,\ N = 2$ | Bisection | 521 |
| | Dinkelbach's | 140 |
| | Charnes-Cooper | 5 |
| $K = 2,\ N = 3$ | Bisection | 781 |
| | Dinkelbach's | 119 |
| | Charnes-Cooper | 13 |
| $K = 3,\ N = 3$ | Bisection | 625 |
| | Dinkelbach's | 138 |
| | Charnes-Cooper | 9 |

## 3.8 Chapter Summary and Conclusions

In this chapter, the joint power and subcarrier allocation problem was formulated for maximizing the EE in a multi-relay aided multi-user OFDMA cellular network. The objective function was proven to be quasi-concave and the three methods of Section 2.4.3 were employed for solving the associated optimization problem. Dinkelbach's method solved the optimization problem by converting it to a sequence of subtractive concave problems, the Charnes-Cooper transformation method converted the quasi-concave problem into a single concave problem with an additional linear constraint, while the bisection method solved the quasi-concave problem as a series of feasibility problems. All three methods relied on the dual decomposition approach described in Section 2.7 for solving their convex problems, hence their algorithmic complexities are comparable. All three methods were validated by comparing their EEM solutions to those found with the aid of an exhaustive search. The results presented in Section 3.7 demonstrate that although all three methods obtain the optimal solution, the bisection method requires many more iterations than either Dinkelbach's method or the Charnes-Cooper method, since several feasibility problems have to be solved. On the other hand, since only a single optimization problem has to be solved, the Charnes-Cooper method converges within much fewer iterations than Dinkelbach's method. Therefore, we can conclude that the Charnes-Cooper method is the least algorithmically complex method out of the three, and yet, it remains capable of finding the optimal results. A summary of the various complexities required by each solution algorithm is provided in Table 3.5.

Further simulation results show that when there is insufficient power for attaining the maximum achievable EE, both the EEM and the SEM algorithms have the same solution. As the system's total power is increased, the SEM algorithm continues to allocate more power

in order to achieve ever higher values of SE, whereas the EEM algorithm reaches an upper bound and does not make use of the additional available power. In the scenario considered, increasing the total power available to the system beyond 40dBm offers no benefits to EE.

Additionally, a comprehensive study of the effect of various system parameters on the achievable SE and EE is performed. To summarize, the achievable SE and EE is increased, when there is a larger number of UEs in the system owing to achieving a higher multi-user diversity. Increasing the number of available subcarriers, although increases the sum rate owing to frequency diversity, reduces the average SE and EE since not all subcarriers are effectively utilized. The benefit of introducing RNs into the network for improving the achievable SE becomes more significant as the cell-size increases or the number of relays increases. However, the EE is then degraded due to the increased overhead power consumption. Furthermore, relaying is more beneficial, when the RNs are placed closer to the BS, if there exists a LOS link between the RNs and BS, since the received SNR at the RNs is improved.

Chapter 4

# Spectral/Energy Efficient Resource Allocation for MIMO-Aided Single-Cell Networks

## 4.1 Introduction

We have seen in Chapter 3 that it is possible to formulate the problem of maximizing the EE of a relay-aided cellular network with the aid of a FP approach by employing methods described in Section 2.4.3. Furthermore, we have concluded from Section 3.7 that a RA scheme optimized for achieving a high SE is expected to perform poorly in terms of its EE, since the Shannon capacity increases only logarithmically with the SNR, i.e. with the transmit power. Nonetheless, we were able to demonstrate in Section 3 that the Charnes-Cooper variable transformation of Section 2.4.3.5 was capable of solving the optimization problem of (3.10)–(3.15) in fewer iterations than both Dinkelbach's method and the bisection method of Sections 2.4.3.3 and 2.4.3.1, respectively. As a further enhancement to the system model of Section 3.2, in this chapter MIMO techniques are introduced for increasing the attainable spatial multiplexing gain, thus increasing both the attainable SE and EE, because in contrast to the logarithmic Shannon-capacity, the capacity of MIMO systems may be increased linearly with the transmit power, provided that the extra power is assigned to additional antennas.

It is widely acknowledged that under the idealized simplifying condition of having perfect CSI at the transmitter, the DL or broadcast channel (BC) capacity [355, 356] may be approached with the aid of DPC [357]. However, the practical implementation of DPC is hampered by its excessive algorithmic complexity upon increasing the number of users. On the other hand, beamforming (BF) is an attractive suboptimal strategy for allowing mul-

tiple users to share the BC while resulting in reduced multi-user interference (MUI). A low-complexity transmit-BF technique is the ZF based BF (ZFBF), which can asymptotically achieve the BC capacity as the number of users tends to infinity [324]. Furthermore, ZFBF may be readily applied to a system with multiple-antenna receivers through the use of the SVD [358]. As a result, the associated MIMO channels may be mathematically decomposed into several *effective* MISO channels, which are termed SMCs in this chapter. Note that these effective MISO channels are different from the physical MISO channels directly composing the physical MIMO channel. For brevity, we coin the term SMC to emphasize that these effective MISOs will be used for the purpose of spatial multiplexing. A more in-depth discussion regarding the concept of SMCs will be provided in Section 4.4. Furthermore, in [359], these SMCs are specifically grouped so that the optimal grouping as well as the optimal allocation of the power may be found on each subcarrier block using convex optimization. In contrast to the channel-diagonalization methods of [77, 317, 360], the ZFBF approach does not enforce any specific relationship between the total numbers of transmit antennas and receive antennas. Therefore, ZFBF is more suitable for practical systems, since the number of transmit antennas at the BS is typically much lower than the total number of receive antennas of all the UEs. Compared to the random BF methods, such as that of [361], ZFBF is capable of completely avoiding the interference, allowing us to formulate our SEM/EEM problems as convex optimization problems. Due to its desirable performance versus complexity trade-off, in this chapter we employ ZFBF in the context of multi-relay aided MIMO-OFDMA systems, where the direct link between the BS and the UE may be exploited in conjunction with the relaying link for further improving the system's performance.

Although the EE metric of Chapter 3 was employed in [201, 224, 225, 330], these contributions did not consider RA in the context of a MIMO system, and only [330] incorporated relaying. On the other hand, although there are numerous contributions on optimal RA in MIMO systems, they typically only focused on either the SEM (equivalently, the sum-rate maximization) or the power minimization [202, 359, 362–364]. For example, the authors of [359] applied BF to a DL cellular system and aimed for minimizing the resultant total transmission power, while simultaneously satisfying the per-user rate requirements. The authors of [363] instead choose to minimize the per-antenna transmission powers, while satisfying both the maximum per-antenna power constraints as well as the per-user SINR requirements. Although there exists some literature studying the EE of relay-aided MIMO systems [365, 366], these contributions typically focus their attention on a simple three-node network consisting of the source, the destination and a single RN.

To summarize, there is a paucity of literature on the convex optimization approach to the EEM problem associated with both RA and joint transmit/receive BF in the context of multi-user multi-relay MIMO-OFDMA systems, which hence motivates this chapter. The most similar contribution to the work presented in this chapter is that of [359]. However, the

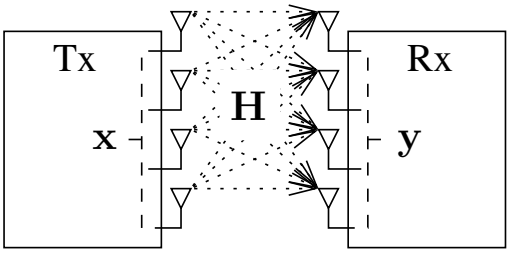


FIGURE 4.1: An illustration of a non-dispersive MIMO link, where the both transmitter and receiver have $N_T = N_R = 4$ antennas each. The transmitter sends the symbol vector $\mathbf{x}$ across channel $\mathbf{H}$. The receiver attempts to recover the transmitted symbol vector from $\mathbf{y}$.

authors of [359] only aimed for minimizing the total power, while we focus our attention on the EE objective function. Furthermore, we improve the system's SE and EE by invoking relaying, which imposes an increased complexity both on the transmission protocols and on the optimization algorithm.

As an additional contribution, the Charnes-Cooper transformation of Sections 2.4.3.5 and 3.5 is employed in this chapter for solving the associated EEM problem, in contrast to the scalarization approach of [347] that requires the weighting of multiple objectives. On the other hand, the employment of Dinkelbach's method detailed in Sections 2.4.3.3 and 3.4 is avoided, since it would require solving a series of parametric convex problems, rather than the resultant single convex problem of the Charnes-Cooper transformation, as demonstrated in Section 3.5. Although the latter approach does impose an additional linear constraint on the problem, our results provided in Section 3.7 demonstrated that it is capable of reaching the optimal solution at the cost of much fewer iterations than its rivals, and it is thus the preferred method. The authors of [227] employed the Charnes-Cooper variable transformation for the EEM of a simple point-to-point link. However, as far as we are aware, the Charnes-Cooper transformation has rarely been used in other contexts for solving the EEM problem.

### 4.1.1 Chapter Preliminaries

Let us examine the non-dispersive MIMO link exemplified in Fig. 4.1, where we have

$$\mathbf{x} = \begin{bmatrix} x_1 \\ x_2 \\ x_3 \\ x_4 \end{bmatrix}, \mathbf{H} = \begin{bmatrix} h_{11} & h_{12} & h_{13} & h_{14} \\ h_{21} & h_{22} & h_{23} & h_{24} \\ h_{31} & h_{32} & h_{33} & h_{34} \\ h_{41} & h_{42} & h_{43} & h_{44} \end{bmatrix}, \mathbf{y} = \begin{bmatrix} y_1 \\ y_2 \\ y_3 \\ y_4 \end{bmatrix}. \tag{4.1}$$

The complex-valued symbols of $x_i$ and $y_i$ correspond to the symbol transmitted to or received from the $i$th antenna at the transmitter or receiver, respectively. Additionally, $h_{ij}$ represents the channel coefficient between the $i$th receive antenna and the $j$th transmit

antenna. Therefore, this system can be represented by

$$\mathbf{y} = \mathbf{H}\mathbf{x} + \mathbf{n}, \tag{4.2}$$

where $\mathbf{n} = (n_1, n_2, n_3, n_4)^{\mathrm{T}}$ is the vector of noise components contaminating the symbols at the receiver. Observe that

$$\begin{aligned} y_1 &= h_{11}x_1 + h_{12}x_2 + h_{13}x_3 + h_{14}x_4 + n_1 && (4.3)\\ y_2 &= h_{21}x_1 + h_{22}x_2 + h_{23}x_3 + h_{24}x_4 + n_2 && (4.4)\\ y_3 &= h_{31}x_1 + h_{32}x_2 + h_{33}x_3 + h_{34}x_4 + n_3 && (4.5)\\ y_4 &= h_{41}x_1 + h_{42}x_2 + h_{43}x_3 + h_{44}x_4 + n_4 && (4.6) \end{aligned}$$

and each transmitted symbol is interfering with the reception of each other symbol. In order to eliminate this effect and hence to obtain interference-free symbols for the sake of achieving a *spatial multiplexing gain*, multiple antennas may be invoked for transmit and receive BF for the sake of *diagonalizing* the channel matrix. Hence we invoke the SVD of $\mathbf{H}$, which is assumed to have a full rank, yielding

$$\mathbf{H} = \mathbf{U}\mathbf{S}\mathbf{V}^{\mathrm{H}}, \tag{4.7}$$

where both $\mathbf{U} \in \mathbb{C}^{4\times4}$ and $\mathbf{V} \in \mathbb{C}^{4\times4}$ are unitary matrices, while

$$\mathbf{S} = \begin{bmatrix} s_1 & 0 & 0 & 0 \\ 0 & s_2 & 0 & 0 \\ 0 & 0 & s_3 & 0 \\ 0 & 0 & 0 & s_4 \end{bmatrix} \tag{4.8}$$

is a diagonal matrix of the singular values of $\mathbf{H}$. Since, both $\mathbf{U}$ and $\mathbf{V}$ are unitary, we have $\mathbf{U}^{\mathrm{H}}\mathbf{U} = \mathbf{I}_4$ and $\mathbf{V}^{\mathrm{H}}\mathbf{V} = \mathbf{I}_4$. Therefore, $\mathbf{U}^{\mathrm{H}}$ and $\mathbf{V}$ may be used as the receive and transmit BF matrices, respectively. Given the data symbols $\widetilde{\mathbf{x}} = (\widetilde{x}_1, \widetilde{x}_2, \widetilde{x}_3, \widetilde{x}_4)^{\mathrm{T}}$, the transmitted symbols are $\mathbf{x} = \mathbf{V}\widetilde{\mathbf{x}}$, while the decision vector is given by $\widetilde{\mathbf{y}} = (\widetilde{y}_1, \widetilde{y}_2, \widetilde{y}_3, \widetilde{y}_4)^{\mathrm{T}} = \mathbf{U}^{\mathrm{H}}\mathbf{y}$. Thus, the system may be represented by

$$\begin{aligned} \widetilde{\mathbf{y}} &= \mathbf{U}^{\mathrm{H}}\mathbf{y} && (4.9)\\ &= \mathbf{U}^{\mathrm{H}}(\mathbf{H}\mathbf{x} + \mathbf{n}) && (4.10)\\ &= \mathbf{U}^{\mathrm{H}}(\mathbf{H}\mathbf{V}\widetilde{\mathbf{x}} + \mathbf{n}) && (4.11)\\ &= \mathbf{U}^{\mathrm{H}}\mathbf{H}\mathbf{V}\widetilde{\mathbf{x}} + \mathbf{U}^{\mathrm{H}}\mathbf{n} && (4.12)\\ &= \mathbf{U}^{\mathrm{H}}\mathbf{U}\mathbf{S}\mathbf{V}^{\mathrm{H}}\mathbf{V}\widetilde{\mathbf{x}} + \mathbf{U}^{\mathrm{H}}\mathbf{n} && (4.13)\\ &= \mathbf{S}\widetilde{\mathbf{x}} + \mathbf{U}^{\mathrm{H}}\mathbf{n}. && (4.14) \end{aligned}$$

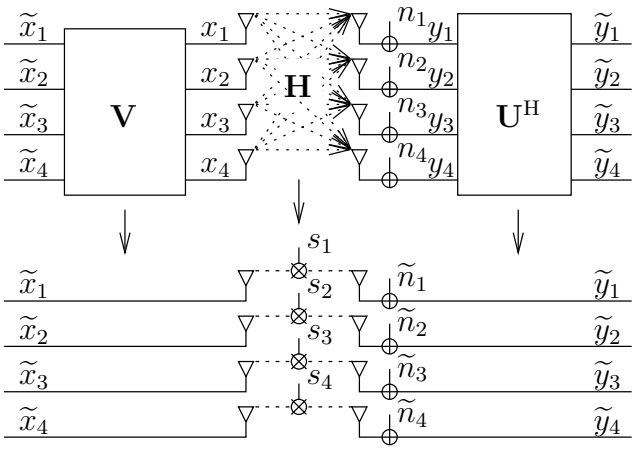


FIGURE 4.2: Parallel decomposition is applied to the top MIMO point-to-point link using both transmit and receive BF, which results in parallel channels with effective channel gains equal to the singular values of the original MIMO channel matrix, $\mathbf{H}$.

Introducing the notation of $\mathbf{U}^{\mathrm{H}}\mathbf{n} = (\widetilde{n}_1, \widetilde{n}_2, \widetilde{n}_3, \widetilde{n}_4)^{\mathrm{T}}$ allows us to write

$$\widetilde{y}_1 = s_1\widetilde{x}_1 + \widetilde{n}_1 \tag{4.15}$$

$$\widetilde{y}_2 = s_2\widetilde{x}_2 + \widetilde{n}_2 \tag{4.16}$$

$$\widetilde{y}_3 = s_3\widetilde{x}_3 + \widetilde{n}_3 \tag{4.17}$$

$$\widetilde{y}_4 = s_4\widetilde{x}_4 + \widetilde{n}_4. \tag{4.18}$$

Thus each symbol of $\widetilde{\mathbf{y}}$ is received without interference from other symbols. In effect, parallel decomposition [4] has been applied to the channel, as depicted in Fig. 4.2. In tangible physical terms, the MIMO link has been converted into non-interfering parallel channels having gains given by the singular values of the original MIMO matrix. It is important to note that the noise power imposed is not affected by the receive BF operator, since $\mathbf{U}$ is unitary.

In this chapter, the parallel decomposition concept of Fig. 4.2 is developed further and applied to a system relying on multiple transmitters and multiple receivers. Let us elaborate on the example of Fig. 4.2 using just two receivers for the sake of illustrating the core concept employed in this chapter - namely that of SMCs. The SVD is employed similarly in this case for decomposing the MIMO channel (assumed to be full-rank) between the Transmitter and Receiver 1, yielding $\mathbf{H}_1$, as well as between the Transmitter and Receiver 2, namely $\mathbf{H}_2$, as follows

$$\mathbf{H}_1 = \mathbf{U}_1\mathbf{S}_1\mathbf{V}_1^{\mathrm{H}} \tag{4.19}$$

$$\mathbf{H}_2 = \mathbf{U}_2\mathbf{S}_2\mathbf{V}_2^{\mathrm{H}}. \tag{4.20}$$

Similarly, the left unitary matrices $\mathbf{U}_1$ and $\mathbf{U}_2$ are employed as the receive beamformers for

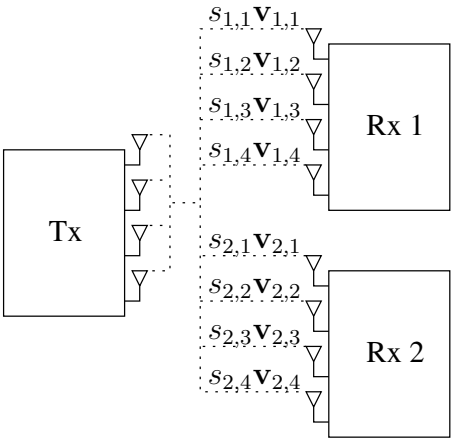


FIGURE 4.3: The total number of SMCs generated for $N_T = 4$ and $N_R = 4$, where we have $2 \cdot \min(N_T, N_R) = 8$ in this example.

Receiver 1 and 2, respectively, for deriving the effective channel matrices of

$$\underline{\mathbf{H}}_1 = \mathbf{S}_1 \mathbf{V}_1^{\mathrm{H}} \tag{4.21}$$

$$\underline{\mathbf{H}}_2 = \mathbf{S}_2 \mathbf{V}_2^{\mathrm{H}}. \tag{4.22}$$

Since both $\mathbf{V}_1$ and $\mathbf{V}_2$ are unitary matrices, these effective channel matrices contain rows, which are independent of each other. Furthermore, the norms of the orthogonal rows are equal to their corresponding singular values, which constitute the diagonal entries in $\mathbf{S}_1$ and $\mathbf{S}_2$, respectively. These rows are referred to as SMCs in this chapter. Given a transmitter relying on $N_T$ transmit antennas, and two receivers each having $N_R$ receive antennas, the total number of SMCs generated in this example is $2 \cdot \min(N_T, N_R)$. This is demonstrated in Fig. 4.3, where $s_{i,j}$ corresponds to the $j$th singular value of the channel matrix between the Transmitter and Receiver $i$, while $\mathbf{v}_{i,j}$ is its corresponding right singular vector. Since the transmitter can only transmit to $N_T$ SMCs without causing interference between them, a total of

$$\min[N_T, 2 \cdot \min(N_T, N_R)] \tag{4.23}$$

SMCs have to be selected for transmission. This is the purpose of the SMC grouping algorithms described in Section 4.5. The SMCs to serve are arranged as the rows of the transmission matrix $\widetilde{\mathbf{H}}$ and they are used for forming the ZF transmit BF matrix of

$$\mathbf{T} = \widetilde{\mathbf{H}}^{\mathrm{H}} \cdot \left[\widetilde{\mathbf{H}}\widetilde{\mathbf{H}}^{\mathrm{H}}\right]^{-1}. \tag{4.24}$$

Thus, each selected SMC becomes free from interference.

In the case of the multiple transmitters portrayed in Fig. 4.4, say Tx 1 transmits its data symbols intended for the receiver Rx, while Tx 2 also has to include its corresponding SMC, when computing its ZFBF matrix. With reference to Fig. 4.4, if the SMC $s_{1,1}\mathbf{v}_{1,1}$ is selected

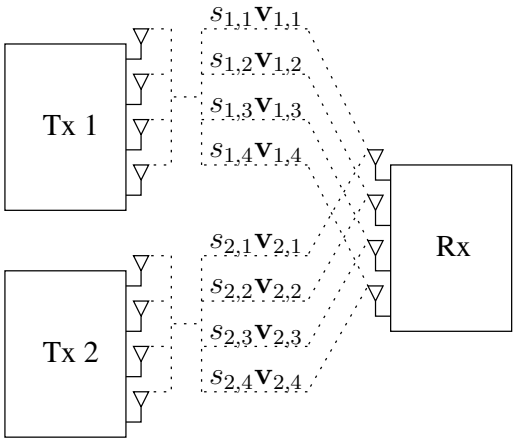


FIGURE 4.4: An example of SMCs, when multiple transmitters are used.

for transmission by Tx 1, then SMC $s_{2,1}\mathbf{v}_{2,1}$ must be selected for transmission by Tx 2 in order to avoid imposing interference at the receiver.

### 4.1.2 Novel Contributions

As stated above, the aim of this chapter is to formally optimize the SE or EE of a multi-relay MIMO-OFDMA cellular system by intelligently assigning the available power and frequency resources when employing both transmit and receive BF. A concise list of our novel contributions is as follows.

- This chapter focuses on a sophisticated DF [43] protocol aided multi-relay assisted MIMO-OFDMA cellular system model, whose network nodes are all equipped with multiple antennas. More specifically, this system model accounts for both the direct links between the BS and the UEs, as well as the relaying links employing the DF relaying protocol [43]. This system model is unlike that of [324, 359], which did not consider relaying, and it is also distinct from that of [365, 366], which only consider a single RN and a single UE. Additionally, we dispense with the constraint that the number of antennas at the BS needs to be greater or equal to the sum of the number of antennas at the UEs, which was assumed in [77, 317, 360]. Furthermore, this system model builds upon Section 3.2 as the network elements may now be equipped with an arbitrary number of antennas for improving the system's SE or EE performance.
- A novel transmission protocol is proposed. Since the multi-relay MIMO-OFDMA system model considered has not been studied in the context of the SEM/EEM problems before, we develop a novel transmission protocol that exploits spatial multiplexing in both transmission phases while allowing both the direct and relaying links to be simultaneously active. Although this protocol does not benefit from a higher spatial degree of freedom than that of the conventional half-duplex relay based cooperative system, we glean more

flexibility in choosing the best group of channels for each transmission phase, which leads to additional selection diversity. As a result, the achievable SE/EE performance may be improved. Again, this protocol is distinct from that presented in [324,359], since relaying is not considered in those works. Another benefit is that since spatial multiplexing is employed in conjunction with OFDMA, multiple data streams may be served using *the same* subcarrier block, while the transmit ZFBF is employed for avoiding the interference. Furthermore, the receive-BF matrices are designed with the aim of generating a number of SMCs that may be grouped for the purpose of increasing the attainable spatial multiplexing gain.

- Two SMC grouping algorithms are proposed. To elaborate, we present a pair of novel algorithms for grouping the SMCs transmissions. The possibility of relayed transmissions means that we have to partition each transmission period into two halves, one consisting of BS-to-UE and BS-to-RN links, and the other consisting of additional BS-to-UE as well as RN-to-UE links. As a result, the SMC-pairs of the two-hop relaying links are incomparable to the SMCs of the direct links in either the first or the second transmission phases. This is because, firstly the RNs are subject to their individual maximum transmission power constraints, and secondly they employ the DF protocol, which means that the information conveyed on the RN-to-UE link cannot be more than that conveyed on the BS-to-RN link. These challenging issues are resolved by the proposed grouping algorithms. The first grouping algorithm is optimal in the sense that it is based on exhaustive search over all the SMC groupings that satisfy the semi-orthogonality criterion, while the second algorithm constitutes a lower-complexity alternative. This complexity-reduction is achieved by a multi-stage SMC group construction process. In each stage, we firstly compute the orthogonal components with respect to the vectors contained in the tentative SMC group to be constructed using all the residual legitimate SMC vectors, and then insert the particular SMC vector that results in the orthogonal component having the highest norm into the SMC group to be constructed. In principle, this method is similar to that of [324, 359], but it has been appropriately adapted for the multi-relay cellular network considered under the above-mentioned particular constraints.
- The problems of choosing the SE- or EE-optimal SMC groupings and their associated power control values are formulated and solved using convex optimization. In contrast to [202,359,362–364], the crucial objective of maximizing the EE metric is employed, as motivated above. On the other hand, in contrast to [201,224,225], we consider a system that allows for *simultaneous* direct and relayed transmissions for the sake of increasing the attainable spatial multiplexing gain. Although there exist other methods of solving this EEM problem [200, 201, 330, 347], we employ the Charnes-Cooper transformation of Sections 2.4.3 and 3.5 for obtaining the maximum EE solution, since it exhibits a reduced complexity as a benefit of solving only a single convex optimization problem, as we demonstrated in Section 3.7.

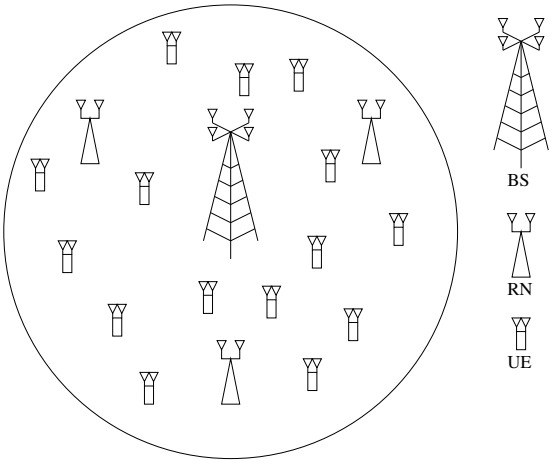


FIGURE 4.5: An example of a multi-relay MIMO-OFDMA cellular network, consisting of a single BS at the cell-center, 3 RNs and 15 UEs.

### 4.1.3 Chapter Organization

The rest of this chapter is organized as follows. Section 4.2 describes the multi-relay MIMO-OFDMA cellular network considered, while Section 4.4 characterizes our novel transmission protocol that allows for both direct and relayed links to be simultaneously activated. In Section 4.5, we elaborate on the aforementioned SMC grouping algorithms conceived for forming the sets of possible transmission groups. Finding the optimal transmission groups and the optimal power control variables is then formulated as an optimization problem in Section 4.6, which is then solved by using a number of variable transformations and relaxations. Our grouping algorithms and our SEM/EEM solver are characterized in Section 4.7. Finally, we present a summary in Section 4.8.

## 4.2 System Model

We focus our attention on the DL of a multi-relay MIMO-OFDMA cellular network, as shown in Fig. 4.5. The BS, $M$ DF-assisted RNs and $K$ UEs are each equipped with $N_B$, $N_R$ and $N_U$ antennas, respectively, in contrast to the system model of Section 3.2, which featured only single antenna nodes. The cellular system has access to $N$ subcarrier blocks, each encompassing $W$ Hertz of wireless bandwidth. The subcarrier blocks considered here are the resource blocks described in Section 1.3. The BS is located at the cell-center, while each of the RNs are located at a fixed distance from the BS on a circle and are positioned at identical angular rotations. The ratio of the distance between the BS and RNs to the cell radius is denoted by $D_r$. On the other hand, the UEs are uniformly distributed in the cell. The BS coordinates and synchronizes its own transmissions with that of the RNs, which employ the DF protocol and thus avoids the problem of noise amplification. As it will be shown in Section 4.6.3.1, this strategy results in a simple algorithm for finding the

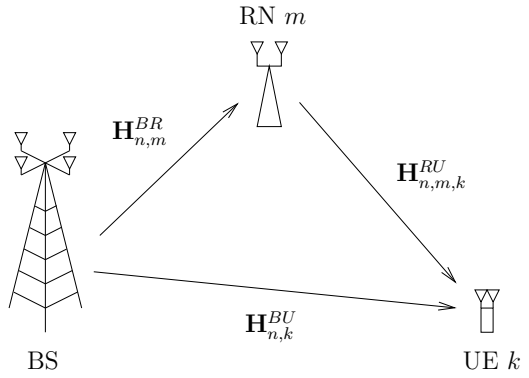


FIGURE 4.6: An illustration of the DL channels in the MIMO-OFDMA relay-aided cellular network.

optimal power control variables. For the subcarrier block $n \in \{1, \cdots, N\}$, let us define the complex-valued wireless channel matrices between the BS and UE $k \in \{1, \cdots, K\}$, between the BS and RN $m \in \{1, \cdots, M\}$, and between RN $m$ and UE $k$ as $\mathbf{H}_{n,k}^{BU} \in \mathbb{C}^{N_U \times N_B}$, $\mathbf{H}_{n,m}^{BR} \in \mathbb{C}^{N_R \times N_B}$ and $\mathbf{H}_{n,m,k}^{RU} \in \mathbb{C}^{N_U \times N_R}$, respectively, as shown in Fig. 4.6. These complex-valued channel matrices account for both the frequency-flat Rayleigh fading and the path-loss between the corresponding transceivers. The coherence bandwidth of each wireless link is assumed to be sufficiently high, so that each individual subcarrier block experiences frequency flat fading, although the level of fading may vary from one subcarrier block to another in each transmission period. Additionally, the transceivers are stationary or moving slowly enough so that the level of fading may be assumed to be fixed for the duration of a scheduled transmission period. Furthermore, the receive antennas are spaced sufficiently far apart, so that each transmit/receive antenna pair experiences independent and identically distributed (i.i.d.) fading. Since these channels are slowly varying, the system is capable of exploiting the benefits of channel reciprocity associated with time-division duplexing (TDD), so that the CSI becomes available at each BS- and RN-transmitter and at each possible RN- and UE-receiver. To elaborate, $\mathbf{H}_{n,k}^{BU}$ and $\mathbf{H}_{n,m}^{BR}$ are known at the BS, $\mathbf{H}_{n,m}^{BR}$ and $\mathbf{H}_{n,m,k}^{RU}$ are known at the RN $m$, while $\mathbf{H}_{n,k}^{BU}$ and $\mathbf{H}_{n,m,k}^{RU}$ are also known at UE $k$. Additionally, through the use of dedicated low-rate error-free feedback channels, $\mathbf{H}_{n,m,k}^{RU}$ is also assumed to be known at the BS so that the BS may perform network-wide scheduling. It is important to remember that, since our focus is on the resource allocation and the associated SE/EE optimization problems, the idealized simplifying assumption of the availability of perfect CSI is employed. At the current stage, accounting for erroneous CSI using, for example, robust optimization [342] is beyond the scope of this chapter and may be addressed in our future work. These channel matrices are assumed to have full row rank, which may be achieved with a high probability for typical DL wireless channel matrices.

Furthermore, each receiver suffers from AWGN having a power spectral density of $N_0$. The maximum instantaneous transmission power available to the BS and to each RN due to regulatory and health-constraints is $P_{max}^{B}$ and $P_{max}^{R}$, respectively. Since OFDMA modulation

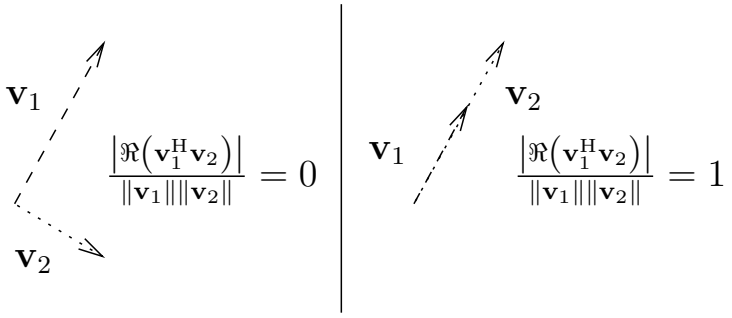


FIGURE 4.7: The 2-dimensional vectors on the left are orthogonal vectors, while the 2-dimensional vectors on the right are linearly dependent.

constitutes a linear operation, we focus our attention on a single subcarrier block and as usual, we employ the commonly-used equivalent baseband signal model. Furthermore, since the specific signal model expressions of each link is dependent on the transmission protocol to be designed, they are not presented here but instead detailed in Section 4.4.

## 4.3 The Definition of Semi-Orthogonality

The system can simultaneously use two transmission modes to convey information to the UEs, namely the BS-to-UE mode, and the relaying-based BS-to-RN and RN-to-UE mode. Note that although in classic OFDMA each data stream is orthogonal in frequency, for the sake of further improving the system's attainable SE or EE performance, our system employs spatial multiplexing in conjunction with ZFBF *so that multiple data streams may be served using the same subcarrier block, without suffering from interference*. Additionally, since the relaying-based transmission can be split into two phases, the design philosophy of the BF matrices in each phase are described separately, although for simplicity we have assumed that the respective channel matrices remain unchanged in both phases. Firstly, the definition of the semi-orthogonality criterion is given as follows [324].

A pair of MISO channels, represented by the complex-valued column vectors $\mathbf{v}_1$ and $\mathbf{v}_2$, are said to be semi-orthogonal to each other with parameter $\alpha \in [0, 1]$, when

$$\frac{\left|\Re\left(\mathbf{v}_1^{\mathrm{H}}\mathbf{v}_2\right)\right|}{\|\mathbf{v}_1\|\|\mathbf{v}_2\|} \leq \alpha. \tag{4.25}$$

To be more specific, a measure of the grade of orthogonality between $\mathbf{v}_1$ and $\mathbf{v}_2$ is given by the left-hand side of inequality (4.25), which ranges from 0 for orthogonal vectors to 1 for linearly dependent vectors. The authors of [324] demonstrated that employing the ZFBF strategy for MISO channels that satisfy $\alpha \to 0$, while the number of users $K \to \infty$, asymptotically achieves the DPC capacity, and it is therefore optimal for the BC channel. Similar principles are followed when maximizing the SE or EE of the system considered

in this chapter. Additionally, the effective channel gains of the $i$th SMC after applying transmit ZFBF is lower bounded by [324]

$$\frac{\|\mathbf{v}_i\|^2}{1+\frac{(N_*-1)^4\alpha^2}{1-(N_*-1)\alpha^2}}, \tag{4.26}$$

where $\mathbf{v}_i$ is the orthogonal component of the $i$th SMC with respect to the other SMCs chosen, while $N_*$ is the number of antennas at the transmitter. Therefore, one can see that imposing a lower value of $\alpha$ raises this lower bound on the effective channel gains after applying ZFBF. This is because the channel inversion operation of ZFBF then amounts to a simple matrix rotation operation, making the effective channel gains equal to the squared norms of the channel vectors. Although the effective channel gains may be improved when imposing a lower value of $\alpha$, the attainable multiplexing gain may decrease, because the probability of finding SMCs that satisfy this stricter semi-orthogonality criterion is reduced. Having said this, the derivation of an expression for this probability in the context of the considered system model is beyond the scope of this treatise.

On the other hand, a high value of $\alpha$ would increase the grouping algorithms' complexity, since there are more candidate SMCs to search through. At the same time, this would also decrease the lower bound on the effective channel gains, potentially leading to sub-optimal SMC groups. Clearly, a trade-off should be struck, but the optimal $\alpha$ cannot be found in a closed-form - in fact it would depend on several system parameters, such as $K$, $M$, $N$, $N_B$, $N_R$ and $N_U$. Hence in Section 4.7 the effect of varying the value of $\alpha$ on the system's attainable SE and EE is explored.

## 4.4 Transmission Protocol Design

For more explicit clarity, a schematic of the transmit and receive BF matrices in the first and second transmission phases is presented in Fig. 4.8.

### 4.4.1 BF Design for the First Transmission Phase

In the first transmission phase, only the BS is transmitting, while both the RNs and the UEs act as receivers. This is similar to the classic DL multi-user MIMO model. As described above, our aim is 1) to design a ZFBF matrix for the BS to avoid interference between data streams, and 2) to design receive BF matrices for the UEs and RNs so that the resultant *effective DL channel matrices* contain as many semi-orthogonal rows as possible that satisfy (4.25) for a given $\alpha$. Ideally, all receivers (UEs and RNs) should jointly compute their receive BF matrices to accomplish the second goal. The joint computation is required only for attaining the highest number of semi-orthogonal rows globally. However, it is generally

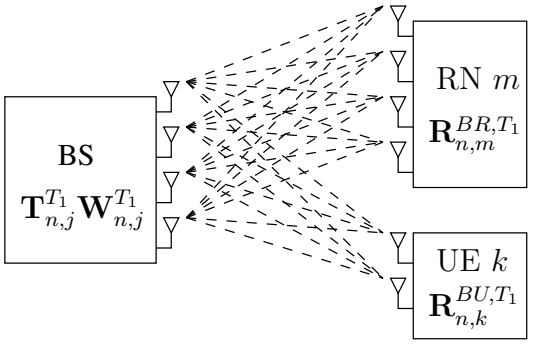


(a) Transmit and receive BF matrices employed in the first phase.

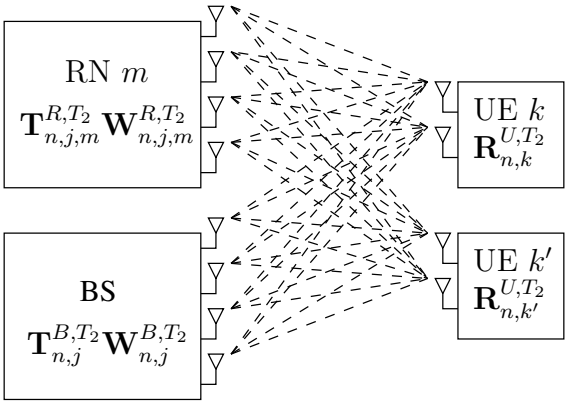


(b) Transmit and receive BF matrices employed in the second phase.

FIGURE 4.8: A conceptual schematic of the transmit- and receive-BF matrices employed in the first and second transmission phases. In the first phase, the BS applies the ZFBF matrix $\mathbf{T}_{n,j}^{T_1}$ in order to serve multiple data streams without imposing interference between them. In the second phase, the BS and RNs employ separate ZFBF matrices to distributively avoid interference between the data streams being served.

impossible, since we cannot realistically assume that the channel matrices associated with each UE and RN are shared among them, due to the geographically-distributed nature of the UEs and RNs. As a compromise, we opt for guaranteeing that each individual effective DL channel matrix contains locally orthogonal rows by employing the SVD [324, 359]. Although these locally orthogonal rows may not remain orthogonal globally, they can be characterized using the semi-orthogonality metric of (4.25).

Bearing this in mind, the channel matrices of all DL transmissions originating from the BS are decomposed at the BS, UEs and RNs using the SVD [34] as

$$\mathbf{H}_{n,k}^{BU} = \mathbf{U}_{n,k}^{BU}\mathbf{S}_{n,k}^{BU}\left(\mathbf{V}_{n,k}^{BU}\right)^{\mathrm{H}} \tag{4.27}$$

and

$$\mathbf{H}_{n,m}^{BR} = \mathbf{U}_{n,m}^{BR}\mathbf{S}_{n,m}^{BR}\left(\mathbf{V}_{n,m}^{BR}\right)^{\mathrm{H}}, \tag{4.28}$$

respectively. Thus, the receive-BF matrices for UE $k$ and RN $m$ are given by

$$\mathbf{R}_{n,k}^{BU,T_1} = \left(\mathbf{U}_{n,k}^{BU}\right)^{\mathrm{H}} \in \mathbb{C}^{N_U \times N_U} \tag{4.29}$$

and

$$\mathbf{R}_{n,m}^{BR,T_1} = \left(\mathbf{U}_{n,m}^{BR}\right)^{\mathrm{H}} \in \mathbb{C}^{N_R \times N_R}, \tag{4.30}$$

and the effective DL channel matrices are then given by

$$\underline{\mathbf{H}}_{n,k}^{BU,T_1} = \mathbf{R}_{n,k}^{BU,T_1}\mathbf{H}_{n,k}^{BU} = \mathbf{S}_{n,k}^{BU}\left(\mathbf{V}_{n,k}^{BU}\right)^{\mathrm{H}} \in \mathbb{C}^{N_U \times N_B} \tag{4.31}$$

and

$$\underline{\mathbf{H}}_{n,m}^{BR,T_1} = \mathbf{R}_{n,m}^{BR,T_1}\mathbf{H}_{n,m}^{BR} = \mathbf{S}_{n,m}^{BR}\left(\mathbf{V}_{n,m}^{BR}\right)^{\mathrm{H}} \in \mathbb{C}^{N_R \times N_B}, \tag{4.32}$$

respectively. Note that $T_1$ is used for indicating the first transmission phase, and underline is used to denote the effective DL channel matrices. Since $\mathbf{V}_{n,k}^{BU}$ and $\mathbf{V}_{n,m}^{BR}$ are both unitary, while $\mathbf{S}_{n,k}^{BU}$ and $\mathbf{S}_{n,m}^{BR}$ are both real and diagonal, these effective DL channel matrices respectively consist of $\min(N_B, N_U)$ and $\min(N_B, N_R)$ orthogonal nonzero rows with norms equal to their corresponding singular values. We refer to these nonzero orthogonal rows as the SMCs of their associated MIMO channel matrix. The reason why we use $\min(N_B, N_U)$ and $\min(N_B, N_R)$, instead of $N_U$ and $N_R$, is because the antenna configuration $N_B \leq N_U$ and/or $N_B \leq N_R$ is also covered. Furthermore, note that only when $N_B \geq N_U$ and $N_B \geq N_R$, a single SMC is generated for each receive antenna.

The $K$ BS-to-UE MIMO channel matrices and $M$ BS-to-RN channel matrices generate a total of

$$[K \cdot \min(N_B, N_U) + M \cdot \min(N_B, N_R)] \tag{4.33}$$

SMCs. Since these SMCs are generated from independent MIMO channel matrices associated with geographically distributed UEs and RNs, they are not all guaranteed to be orthogonal to each other. Furthermore, since each UE or RN has multiple antennas and $N_B$ might not be sufficiently large to simultaneously support all UEs and RNs, we have to determine which specific SMCs should be served. As a result, for each two-phase transmission period, we opt for selecting a SMC group accounting for both phases from the set of available SMC groups. This selection process is achieved by jointly using the SMC grouping algorithm and solving the optimization problem detailed below. For the sake of clarity, the concepts of the SMC, of the SMC group and of the set of SMC groups are illustrated in Fig. 4.9.

To elaborate a little further, a set of SMC groups, $\mathcal{G}_n$, which is associated with subcarrier block $n$, may be obtained using one of the grouping algorithms presented in Section 4.5.

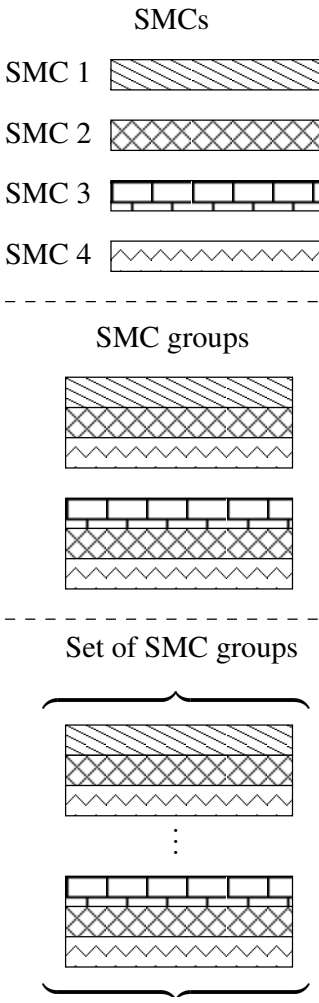


FIGURE 4.9: A conceptual illustration of the differences between SMCs, SMC groups and a set of SMC groups.

The BS selects a single group, $j \in \mathcal{G}_n$, containing (but not limited to $Q_j^{T_1}$ SMCs out of the

$$[K \cdot \min(N_B, N_U) + M \cdot \min(N_B, N_R)] \tag{4.34}$$

available SMCs to be supported by using ZFBF. Thus, we have

$$Q_j^{T_1} \leq \min[N_B, K \cdot \min(N_B, N_U) + M \cdot \min(N_B, N_R)] \tag{4.35}$$

and a multiplexing gain of $Q_j^{T_1}$ is achieved. The SMC group selection, as a part of the scheduling operation, is carried out at the BS before initiating the first transmission phase. Hence, the selected SMC group will also contain $Q_j^{T_2}$ SMCs selected by the BS for the second transmission phase, as detailed in Section 4.4.2. Let us denote the refined effective DL channel matrix with rows being the $Q_j^{T_1}$ selected SMCs as $\underline{\mathbf{H}}_{n,j}^{T_1} \in \mathbb{C}^{Q_j^{T_1} \times N_B}$. The ZFBF transmit matrix applied at the BS to subcarrier block $n$ is then given by the following right

inverse

$$\mathbf{T}_{n,j}^{T_1} = \left(\underline{\mathbf{H}}_{n,j}^{T_1}\right)^{\mathrm{H}} \cdot \left[\underline{\mathbf{H}}_{n,j}^{T_1}\left(\underline{\mathbf{H}}_{n,j}^{T_1}\right)^{\mathrm{H}}\right]^{-1} \in \mathbb{C}^{N_B \times Q_j^{T_1}}. \tag{4.36}$$

Since $\underline{\mathbf{H}}_{n,j}^{T_1}\mathbf{T}_{n,j}^{T_1} = \mathbf{I}_{N_B}$, the potential interference between the $Q_j^{T_1}$ selected SMCs is completely avoided. Furthermore, the columns of $\mathbf{T}_{n,j}^{T_1}$ are normalized by multiplying the diagonal matrix $\mathbf{W}_{n,j}^{T_1}$ on the right-hand side of $\mathbf{T}_{n,j}^{T_1}$ to ensure that each SMC transmission is initially set to unit power. This is accomplished by ensuring that each diagonal element of $\mathbf{W}_{n,j}^{T_1}$ is equal to the reciprocal of the norm of the column vector to be normalized. Then, $\mathbf{T}_{n,j}^{T_1}\mathbf{W}_{n,j}^{T_1}$ is used as the DL transmit-BF matrix for the BS in the first phase. Thus, the effective channel-to-noise ratios (CNRs) in the first transmission phase can be written as

$$G_{n,j,e_1}^{BU,T_1} = \frac{\left|w_{n,j,e_1}^{BU,T_1}\right|^2}{\Delta\gamma N_0 W} \tag{4.37}$$

and

$$G_{n,j,e}^{BR,T_1} = \frac{\left|w_{n,j,e}^{BR,T_1}\right|^2}{\Delta\gamma N_0 W}, \tag{4.38}$$

respectively, where $w_{n,j,e_1}^{BU,T_1}$ and $w_{n,j,e}^{BR,T_1}$ are the diagonal elements in $\mathbf{W}_{n,j}^{T_1}$. More specifically, these diagonal elements correspond to SMC group $j$ and subcarrier block $n$, and they are associated with either a direct BS-to-UE SMC or a BS-to-RN SMC. The additional subscripts $e_1 \in \{0, \cdots, \min[N_B, K \cdot \min(N_B, N_U)]\}$ and $e \in \{0, \cdots, \min[N_B, M \cdot \min(N_B, N_R), K \cdot \min(N_R, N_U)]\}$ are used for distinguishing the multiple selected SMCs of the direct links (i.e. those related to UEs), from the multiple selected SMC-pairs that may be associated with a particular RN $\mathcal{M}(e)$, respectively. A single SMC-pair consists of a SMC for the first phase and another for the second phase. Although these SMCs are generated separately in each phase, the SMC-pair associated with a common RN has to be considered as a single entity in the SMC grouping algorithms presented in Section 4.5. Note that $\mathcal{M}(e)$ is a function of $e$, representing the RN index (similar to $m$ used before) associated with the SMC-pair $e$, as further detailed in Section 4.5.

At a given BER requirement, $\Delta\gamma$ is the SNR gap between the lower-bound SNR required for achieving the DCMC capacity and the actual higher SNR required by the MCS of the practical physical layer transceivers employed. For example, making the simplifying assumption that idealized transceivers capable of achieving exactly the DCMC capacity are employed, then $\Delta\gamma = 0$dB. Although, strictly speaking, so far it is not possible to operate exactly at the DCMC channel capacity, there does exist several physical layer transceiver designs that operate very close to it [351]. Furthermore, the noise power received on each subcarrier block is given by $N_0 W$.

### 4.4.2 BF Design in the Second Transmission Phase

The second transmission phase may be characterized by the *MIMO interference channel*. A similar methodology is employed in the second transmission phase, except that now both the BS and the RNs are transmitters, while a number of UEs are receiving. In this phase, our aim is 1) to design ZFBF matrices for the BS and RNs to avoid interference between data streams, 2) and to design a receive-BF matrix for each UE so that the effective channel matrices associated with each of its transmitters contain rows which satisfy the semi-orthogonal condition (4.25) for a given $\alpha$. This means that more data streams may be served simultaneously, thus improving the attainable SE or EE performance. Since there are multiple *distributed* transmitters/MIMO channel matrices associated with each UE, the SVD method described in Section 4.4.1, which is performed in a centralized fashion, cannot be readily applied at the transmitter side. Instead, we aim for minimizing the resultant correlation between the generated SMCs, thus increasing the number of SMCs which satisfy (4.25) for a given $\alpha$. To accomplish this goal, we begin by introducing the shorthand of

$$\underline{\mathbf{H}}_{n,k}^{BU,T_2} = \mathbf{R}_{n,k}^{U,T_2}\mathbf{H}_{n,k}^{BU} \in \mathbb{C}^{N_U \times N_B} \tag{4.39}$$

and

$$\underline{\mathbf{H}}_{n,m,k}^{RU,T_2} = \mathbf{R}_{n,k}^{U,T_2}\mathbf{H}_{n,m,k}^{RU} \in \mathbb{C}^{N_U \times N_R} \tag{4.40}$$

as the effective channel matrices between the BS and UE $k$, and between RN $m$ and UE $k$, respectively, on subcarrier block $n$ in the second transmission phase, where $\mathbf{R}_{n,k}^{U,T_2} \in \mathbb{C}^{N_U \times N_U}$ is the yet-to-be-determined UE $k$'s receive-BF matrix. In light of the preceding discussions, one of our aims is to design $\mathbf{R}_{n,k}^{U,T_2}$ so that the off-diagonal values of the matrices given by

$$\mathbf{A}_0 = \underline{\mathbf{H}}_{n,k}^{BU,T_2}\left(\underline{\mathbf{H}}_{n,k}^{BU,T_2}\right)^{\mathrm{H}} = \mathbf{R}_{n,k}^{U,T_2}\mathbf{H}_{n,k}^{BU}\left(\mathbf{H}_{n,k}^{BU}\right)^{\mathrm{H}}\left(\mathbf{R}_{n,k}^{U,T_2}\right)^{\mathrm{H}} \tag{4.41}$$

and

$$\mathbf{A}_m = \underline{\mathbf{H}}_{n,m,k}^{RU,T_2}\left(\underline{\mathbf{H}}_{n,m,k}^{RU,T_2}\right)^{\mathrm{H}} = \mathbf{R}_{n,k}^{U,T_2}\mathbf{H}_{n,m,k}^{RU}\left(\mathbf{H}_{n,m,k}^{RU}\right)^{\mathrm{H}}\left(\mathbf{R}_{n,k}^{U,T_2}\right)^{\mathrm{H}}, \forall m \tag{4.42}$$

are as small as possible. For example, an $\mathbf{A}$ matrix of either (4.41) or (4.42) can be written as

$$\mathbf{A} = \begin{bmatrix} \mathbf{v}_1 \\ \mathbf{v}_2 \\ \mathbf{v}_3 \\ \mathbf{v}_4 \end{bmatrix}\left[\mathbf{v}_1^{\mathrm{H}}, \mathbf{v}_2^{\mathrm{H}}, \mathbf{v}_3^{\mathrm{H}}, \mathbf{v}_4^{\mathrm{H}}\right] = \begin{bmatrix} \mathbf{v}_1\mathbf{v}_1^{\mathrm{H}} & \mathbf{v}_1\mathbf{v}_2^{\mathrm{H}} & \mathbf{v}_1\mathbf{v}_3^{\mathrm{H}} & \mathbf{v}_1\mathbf{v}_4^{\mathrm{H}} \\ \mathbf{v}_2\mathbf{v}_1^{\mathrm{H}} & \mathbf{v}_2\mathbf{v}_2^{\mathrm{H}} & \mathbf{v}_2\mathbf{v}_3^{\mathrm{H}} & \mathbf{v}_2\mathbf{v}_4^{\mathrm{H}} \\ \mathbf{v}_3\mathbf{v}_1^{\mathrm{H}} & \mathbf{v}_3\mathbf{v}_2^{\mathrm{H}} & \mathbf{v}_3\mathbf{v}_3^{\mathrm{H}} & \mathbf{v}_3\mathbf{v}_4^{\mathrm{H}} \\ \mathbf{v}_4\mathbf{v}_1^{\mathrm{H}} & \mathbf{v}_4\mathbf{v}_2^{\mathrm{H}} & \mathbf{v}_4\mathbf{v}_3^{\mathrm{H}} & \mathbf{v}_4\mathbf{v}_4^{\mathrm{H}} \end{bmatrix}, \tag{4.43}$$

where $\mathbf{v}_i$, $i \in \{1,2,3,4\}$ are the generated SMCs organized as the rows of the equivalent channel matrix, $\underline{\mathbf{H}}$. The right hand side of (4.43) shows that the off-diagonal values quantify the grade of orthogonality between the SMCs generated. For the sake of maximizing the number of SMCs satisfying (4.25), these off-diagonal values should be minimized. This

design goal may be restated as

$$\begin{aligned}\min_{\mathbf{R}_{n,k}^{U,T_2},\mathbf{\Lambda}_0,\mathbf{\Lambda}_m} \quad & \left|\left|\mathbf{H}_{n,k}^{BU}\left(\mathbf{H}_{n,k}^{BU}\right)^{\mathrm{H}} - \left(\mathbf{R}_{n,k}^{U,T_2}\right)^{-1}\mathbf{\Lambda}_0\left(\mathbf{R}_{n,k}^{U,T_2}\right)^{-\mathrm{H}}\right|\right|_{\mathrm{F}}^2 \\ & + \sum_{m=1}^{M}\left|\left|\mathbf{H}_{n,m,k}^{RU}\left(\mathbf{H}_{n,m,k}^{RU}\right)^{\mathrm{H}}\right.\right. \\ & \left.\left. - \left(\mathbf{R}_{n,k}^{U,T_2}\right)^{-1}\mathbf{\Lambda}_m\left(\mathbf{R}_{n,k}^{U,T_2}\right)^{-\mathrm{H}}\right|\right|_{\mathrm{F}}^2, \end{aligned} \tag{4.44}$$

where $\mathbf{\Lambda}_0$ and $\mathbf{\Lambda}_m$ are diagonal matrices containing the diagonal elements of $\mathbf{A}_0$ and $\mathbf{A}_m$, respectively. Therefore, $\left(\mathbf{R}_{n,k}^{U,T_2}\right)^{-1}$ is the *jointly diagonalizing matrix* [367], when $\mathbf{H}_{n,k}^{BU}\left(\mathbf{H}_{n,k}^{BU}\right)^{\mathrm{H}}$ and $\mathbf{H}_{n,m,k}^{RU}\left(\mathbf{H}_{n,m,k}^{RU}\right)^{\mathrm{H}}$, $\forall m$ are the matrices to be diagonalized. Thus, the algorithm presented in [367] for solving (4.44) may be invoked at UE $k$ for obtaining $\mathbf{R}_{n,k}^{U,T_2}$, which may be further fed back to the BS and RNs. Hence, the BS and RNs do not have to share $\mathbf{H}_{n,k}^{BU}$ or $\mathbf{H}_{n,k}^{RU}$ via the wireless channel and do not have to solve (4.44) again. As a result, we accomplish the goal of creating effective channel matrices that contain rows aiming to satisfy (4.25). In fact, when there are only two matrices to diagonalize, say $\mathbf{A}_0$ and $\mathbf{A}_1$, the diagonalizing matrix may be obtained from the eigenvectors of $\mathbf{A}_0\left(\mathbf{A}_1\right)^{-1}$ [368]. This diagonalizing matrix is capable of fully diagonalizing both $\mathbf{A}_0$ and $\mathbf{A}_1$.

The algorithm involves iterating between two processing phases, namely the alternating-column (AC) and diagonal center (DC) phases, which is hence referred to as the AC-DC algorithm in [367]. Let us rewrite the objective function of (4.44) in the simplified form given by

$$\begin{aligned} & \sum_{k=1}^{K} w_k \left|\left|\mathbf{A}_k - \mathbf{B}\mathbf{\Lambda}_k\mathbf{B}^{\mathrm{H}}\right|\right|_{\mathrm{F}}^2 \\ = \quad & \sum_{k=1}^{K} w_k \left|\left|\mathbf{A}_k - \sum_{n=1}^{N}\lambda_n^{[k]}\mathbf{b}_n\mathbf{b}_n^{\mathrm{H}}\right|\right|_{\mathrm{F}}^2, \end{aligned} \tag{4.45}$$

where $\mathbf{A}_k \in \mathbb{C}^{N\times N}$, $\forall k$ represents the matrices to be diagonalized, $\mathbf{B} \in \mathbb{C}^{N\times N}$ is the jointly diagonalizing matrix, $\lambda_n^{[k]}$ is the $(n,n)$th entry of $\mathbf{\Lambda}_k$, and $\mathbf{b}_n$ is the $n$th column of $\mathbf{B}$. Additionally, the weighting factors $w_k$ of (4.45) may be invoked for assigning the required priorities to the matrices to be diagonalized.

The AC phase of the algorithm simply minimizes the objective function of (4.45) by optimizing each column of $\mathbf{B}$, while keeping the other columns constant, as described in Algorithm 1. This algorithm is applied once to each column of $\mathbf{B}$ in a sequential order, where the index of the column selected is given by $l$. Firstly, the matrix $\mathbf{P}$ is computed in line 3 of Algorithm 1. This matrix is Hermitian, therefore it can be decomposed using the symmetric eigendecomposition [34] in line 4 in order to give the ordered eigenvalues and eigenvectors

**Algorithm 1:** Algorithmic description of the AC phase

**inputs** : Matrices to be diagonalized $\mathbf{A}_k$,
Diagonal matrices $\mathbf{\Lambda}_k$,
Weights $w_k$,
Diagonalization matrix $\mathbf{B}$,
Selected column index $l$

**outputs**: none

1 void `ACPhase` $(\mathbf{A}_k, \mathbf{\Lambda}_k, w_k, \mathbf{B}, l)$

2 **begin**

3 $\quad \mathbf{P} \leftarrow \sum_{k=1}^{K} w_k \lambda_l^{[k]} \left[ \mathbf{A}_k - \sum_{\substack{n=1 \\ n \neq l}}^{N} \lambda_n^{[k]} \mathbf{b}_n \mathbf{b}_n^{\mathrm{H}} \right]$;

4 $\quad$ `eigen` $(\mathbf{P}, \boldsymbol{\beta}, \mathbf{V})$;

5 $\quad$ **if** $\beta_1 < 0$ **then**

6 $\quad\quad \mathbf{b}_l \leftarrow \mathbf{0}$;

7 $\quad$ **else**

8 $\quad\quad \mathbf{b}_l \leftarrow \frac{\mathbf{v}_1 \sqrt{\beta_1}}{\sqrt{\sum_{k=1}^{K} \omega_k \left(\lambda_l^{[k]}\right)^2}}$;

9 $\quad$ **end if**

10 $\quad$ **return**;

11 **end**

of $\mathbf{P}$ in $\boldsymbol{\beta}$ and $\mathbf{V}$, respectively. The highest eigenvalue, denoted by $\beta_1$ and the corresponding eigenvector, $\mathbf{v}_1$, are used for computing the updated column $\mathbf{b}_l$ of $\mathbf{B}$, in lines 5 to 9 of Algorithm 1. Additionally, the vector $\mathbf{v}_1$ must be rotated so that its first nonzero element becomes real-valued and positive.

**Algorithm 2:** Algorithmic description of the DC phase

**inputs** : Matrices to be diagonalized $\mathbf{A}_k$,
Diagonal matrices $\mathbf{\Lambda}_k$,
Diagonalization matrix $\mathbf{B}$

**outputs**: none

1 void `DCPhase` $(\mathbf{A}_k, \mathbf{\Lambda}_k, \mathbf{B})$

2 **begin**

3 $\quad \mathbf{G} \leftarrow \left[ \left(\mathbf{B}^{\mathrm{H}}\mathbf{B}\right)^* \odot \left(\mathbf{B}^{\mathrm{H}}\mathbf{B}\right) \right]^{-1}$;

4 $\quad$ **for** $k = 1$ **to** $K$ **do**

5 $\quad\quad \mathbf{\Lambda}_k \leftarrow \mathrm{diag}\left\{ \mathbf{G}\ \mathrm{diag}\left\{ \mathbf{B}^{\mathrm{H}}\mathbf{A}_k\mathbf{B} \right\} \right\}$;

6 $\quad$ **end for**

7 $\quad$ **return**;

8 **end**

The DC phase of the diagonalization algorithm attempts to minimize the objective function of (4.45) by updating $\mathbf{\Lambda}_k$, $\forall k$, which is described in Algorithm 2. The matrix $\mathbf{G}$ is computed

in line 3 with the aid of the Hadamard product (element-wise multiplication). This matrix is then used for updating the diagonal matrices $\mathbf{\Lambda}_k$, $\forall k$, in lines 4 to 6 of Algorithm 2.

The columns of $\mathbf{R}_{n,k}^{U,T_2}$ have been normalized for ensuring that the power assigned for each SMC remains unaffected. After obtaining the receive-BF matrix, the SMCs of the transmissions to UE $k$ on subcarrier block $n$ are given by the nonzero rows of the effective channel matrices $\underline{\mathbf{H}}_{n,k}^{BU,T_2}$ and $\underline{\mathbf{H}}_{n,m,k}^{RU,T_2}$, $\forall m$. Since the BS and the RNs act as distributed broadcasters during the second phase, they are only capable of employing *separate* ZFBF transmit matrices for ensuring that none of them imposes interference on the SMCs it does not explicitly intend to serve. As described with Fig. 4.4, when computing its ZFBF transmit matrix, each transmitter (either the BS or a RN) must take into account an auxiliary SMC, which is also selected from the legitimate SMC candidates and is required for nulling the interference that this particular transmitter imposes on each selected information-bearing SMC of the other transmitters. Furthermore, each auxiliary SMC is employed by its corresponding transmitter to transmit several additional zeros that are padded to the normal data symbols. As a beneficial result, no interference is received at each UE from the transmitter that does not serve this particular UE. For more details of the SMC-based transmission in the second phase, please refer to Algorithm 3 described in Section 4.5.1.

By employing one of the grouping algorithms described in Section 4.5, the BS schedules

$$Q_j^{T_2} \leq \min\left[\min\left(N_B, N_R\right), \sum_{k=1}^{K} L_k^B + L_k^R\right] \tag{4.46}$$

SMCs to be served simultaneously in the second phase, where $L_k^B$ and $L_k^R$ represent the number of SMCs of UE $k$ served by the BS and by RNs in this phase, respectively, where we have $L_k^B + L_k^R \leq N_U$, $L_k^B \leq \min(N_B, N_U)$, and $L_k^R \leq \min(N_R, N_U)$. Note that since UE $k$ may be simultaneously served both by the BS and by a RN (each of them serves a fraction of UE $k$'s SMCs), it is *possible* that the summation of the respective number of UEs served by the BS and by RNs may be higher than $K$. Note that, if at least one SMC of a UE is served by the BS (or a RN), we say that this UE is served by the BS (or the RN). Let us denote the *refined* effective DL channel matrices, from the perspectives of the BS and RN $m$, consisting of the $Q_j^{T_2}$ selected SMCs as $\underline{\mathbf{H}}_{n,j}^{B,T_2} \in \mathbb{C}^{Q_j^{T_2} \times N_B}$ and $\underline{\mathbf{H}}_{n,j,m}^{R,T_2} \in \mathbb{C}^{Q_j^{T_2} \times N_R}$, respectively. Since these are known to each transmitter, they may employ ZFBF transmit matrices in the second phase, given by the right inverses

$$\mathbf{T}_{n,j}^{B,T_2} = \left(\underline{\mathbf{H}}_{n,j}^{B,T_2}\right)^{\mathrm{H}} \cdot \left[\underline{\mathbf{H}}_{n,j}^{B,T_2}\left(\underline{\mathbf{H}}_{n,j}^{B,T_2}\right)^{\mathrm{H}}\right]^{-1} \in \mathbb{C}^{N_B \times Q_j^{T_2}} \tag{4.47}$$

for the BS, and

$$\mathbf{T}_{n,j,m}^{R,T_2} = \left(\underline{\mathbf{H}}_{n,j,m}^{R,T_2}\right)^{\mathrm{H}} \cdot \left[\underline{\mathbf{H}}_{n,j,m}^{R,T_2}\left(\underline{\mathbf{H}}_{n,j,m}^{R,T_2}\right)^{\mathrm{H}}\right]^{-1} \in \mathbb{C}^{N_R \times Q_j^{T_2}} \tag{4.48}$$

for RN $m$. Similar to the first transmission phase, these ZFBF transmit matrices are normalized by $\mathbf{W}_{n,j}^{BU,T_2}$ and $\mathbf{W}_{n,j,m}^{RU,T_2}$, respectively, to ensure that each SMC transmission is initially set to unit power. Upon obtaining the selected SMCs, we denote the effective CNRs in the second transmission phase as

$$G_{n,j,e_2}^{BU,T_2} = \frac{\left|w_{n,j,e_2}^{BU,T_2}\right|^2}{\Delta\gamma N_0 W} \tag{4.49}$$

and

$$G_{n,j,e}^{RU,T_2} = \frac{\left|w_{n,j,e}^{RU,T_2}\right|^2}{\Delta\gamma N_0 W}, \tag{4.50}$$

where $w_{n,j,e_2}^{BU,T_2}$ and $w_{n,j,e}^{RU,T_2}$ are the diagonal elements in $\mathbf{W}_{n,j}^{BU,T_2}$ and $\mathbf{W}_{n,j,\mathcal{M}(e)}^{RU,T_2}$, respectively, and the subscript $\mathcal{M}(e)$ has been defined in Section 4.4.1. To elaborate, for a second-phase BS-to-UE link, $w_{n,j,e_2}^{BU,T_2}$ corresponds to SMC group $j$ and subcarrier block $n$, while the subscript $e_2 \in \{0, \cdots, \min[N_B, K \cdot \min(N_B, N_U)]\}$ is employed for further distinguishing the multiple selected SMCs associated with UEs from the BS. Similarly, $w_{n,j,e}^{RU,T_2}$, which also corresponds to SMC group $j$ and subcarrier block $n$, is associated with the second-phase RN-to-UE link between RN $\mathcal{M}(e)$ and the particular UE determined by the SMC-pair $e$.

The sequence of matrix operations is illustrated in Fig. 4.10, where we have introduced the additional binary-valued matrices of $\mathbf{E}_{n,j}^{T_1}$ and $\mathbf{E}_{n,j}^{T_2}$, which represent the SMC selection matrices computed by the SMC grouping algorithms of Section 4.5, while the additional binary-valued row vectors $\mathbf{f}_{n,j,e_1}^{T_1}$, $\mathbf{f}_{n,j,e}^{T_1}$, $\mathbf{f}_{n,j,e_2}^{T_2}$ and $\mathbf{f}_{n,j,e}^{T_2}$ select the specific antenna corresponding to either SMC $e_1$, $e_2$ or $e$ for either UE $k$ or RN $m$ during either transmission phases. Furthermore, $\mathbf{n}_k^{T_1}$, $\mathbf{n}_{\mathcal{M}(e)}^{T_1}$ and $\mathbf{n}_k^{T_2}$ are the vectors constituting the complex-valued symbols representing the AWGN suffered by their respective antennas during their respective transmission phases. The vector of complex-valued modulated symbols is denoted by $\mathbf{d}_n^{T_1}$ and $\mathbf{d}_n^{T_2}$ for the first and second transmission phases, respectively, in Fig. 4.10. Furthermore, the diagonal real-valued normalization matrices precede their associated ZFBF matrices for both transmission phases. The ZFBF matrix $\mathbf{T}_{n,j}^{T_1}$ is given by (4.36), while $\mathbf{T}_{n,j}^{B,T_2}$ is given by (4.47) and $\mathbf{T}_{n,j,m}^{R,T_2}$ is given by (4.48). On the other hand, the receive BF matrices of $\mathbf{R}_{n,k}^{BU,T_1}$, $\mathbf{R}_{n,k}^{BR,T_1}$ and $\mathbf{R}_{n,k}^{U,T_2}$ are given by (4.29), (4.30) and (4.44), respectively. Furthermore, the transmit power allocation matrices of $\mathbf{P}_{n,j}^{B,T_1}$, $\mathbf{P}_{n,j}^{B,T_2}$ and $\mathbf{P}_{n,j,\mathcal{M}(e)}^{R,T_2}$ contain the power allocation values computed in Section 4.6.

### 4.4.3 Achievable SE and EE

For the sake of convenience, let us first denote the transmit power allocation policy as $\mathcal{P}$, which is a set composed by all transmit power control variables invoked at the BS and/or RNs in both transmission phases. Since receive-BF is employed in conjunction with ZFBF, each SMC transmission may be viewed as a SISO link. Therefore, on the direct links, the

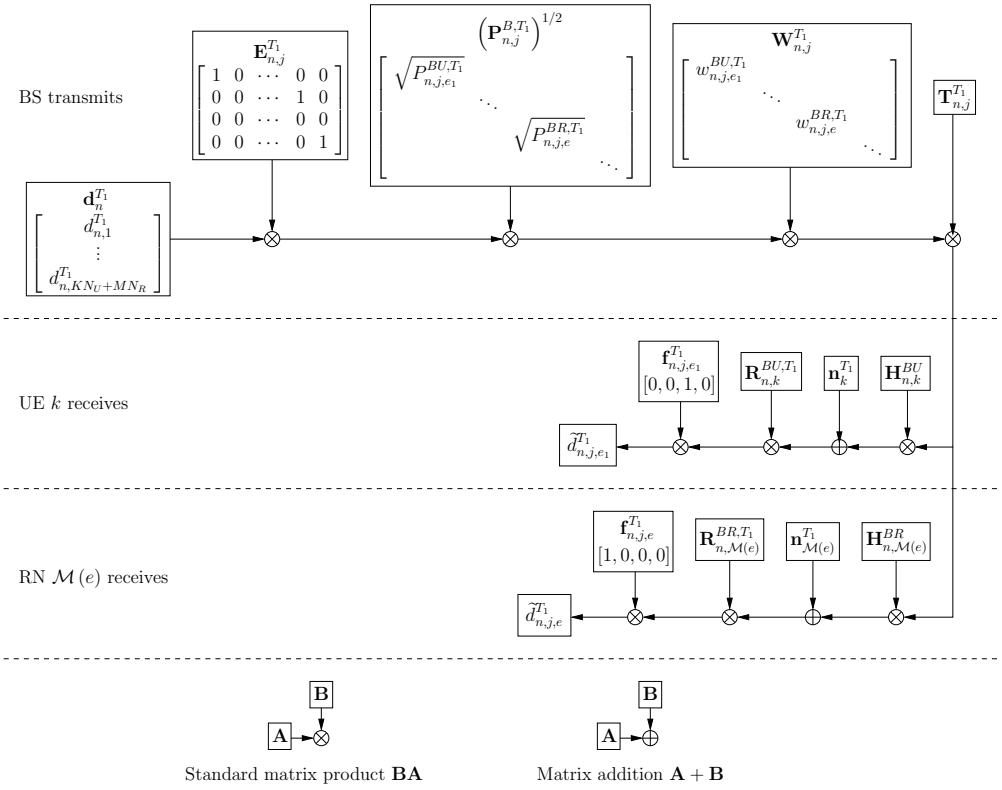


(a) Matrix operations required in the first transmission phase. Transmit BF is only applied at the BS.

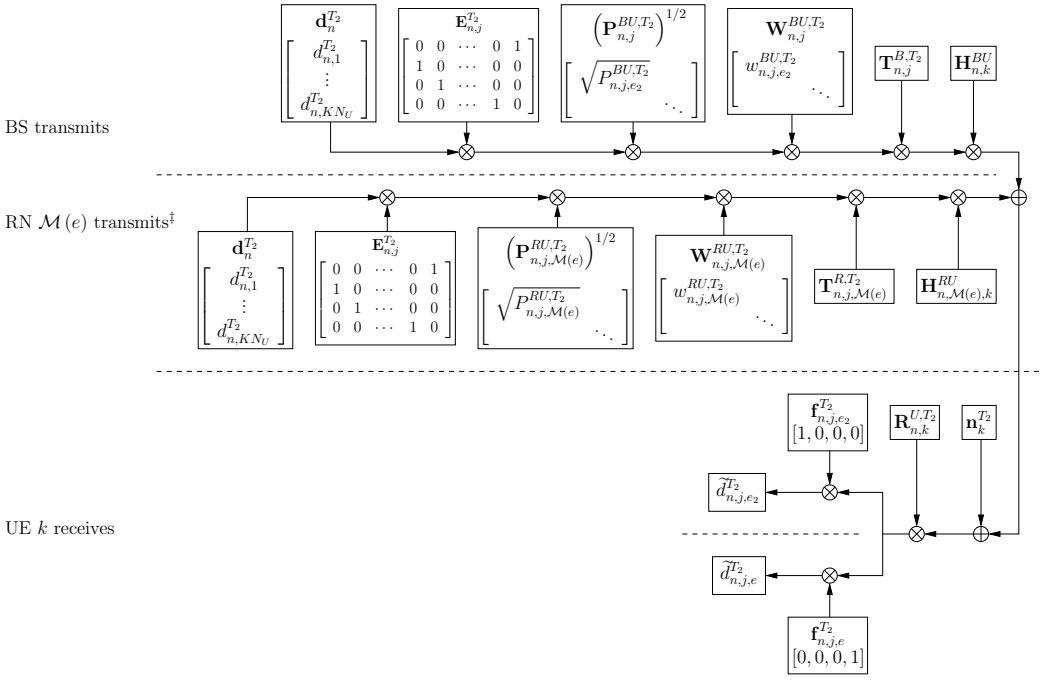


(b) In the second transmission phase, both the BS and all RNs are transmitting, and therefore they employ distributed ZFBF to ensure interference-free reception at the UEs. ‡For simplicity of illustration, both the BS and RN $\mathcal{M}(e)$ have access to $\mathbf{d}_n^{T_2}$ above. However, note that each RN only has access to the complex-valued modulated symbols that it received during the first transmission phase. Therefore, some entries in $\mathbf{d}_n^{T_2}$ at each RN will be zero, corresponding to symbols which that particular RN did not previously receive and decode.

FIGURE 4.10: Block diagrams illustrating the matrix operations required in the two transmission phases.

receiver's SNR at UE $k$ corresponding to SMCs $e_1$ and $e_2$ may be expressed as

$$\Gamma_{n,j,e_1}^{BU,T_1}(\mathcal{P}) = G_{n,j,e_1}^{BU,T_1} P_{n,j,e_1}^{BU,T_1} \tag{4.51}$$

and

$$\Gamma_{n,j,e_2}^{BU,T_2}(\mathcal{P}) = G_{n,j,e_2}^{BU,T_2} P_{n,j,e_2}^{BU,T_2} \tag{4.52}$$

for the first and second transmission phases, respectively. The scalar variables $P_{n,j,e_1}^{BU,T_1}$ and $P_{n,j,e_2}^{BU,T_2}$, which are elements of $\mathcal{P}$, determine the transmit power values for SMCs $e_1$ and $e_2$ on the direct links. As a result, the achievable instantaneous SE of the direct links is given by

$$C_{n,j,e_1}^{BU,T_1}(\mathcal{P}) = \frac{1}{2}\log_2\left(1+\Gamma_{n,j,e_1}^{BU,T_1}(\mathcal{P})\right) \tag{4.53}$$

and

$$C_{n,j,e_2}^{BU,T_2}(\mathcal{P}) = \frac{1}{2}\log_2\left(1+\Gamma_{n,j,e_2}^{BU,T_2}(\mathcal{P})\right), \tag{4.54}$$

which are normalized both by time and by frequency to give units of [bits/sec/Hz]. The factor of $\frac{1}{2}$ accounts for the fact that the transmission period is split into two phases.

Similarly, for the SMC-pair $e$ of the DF relaying links, the SNR at RN $\mathcal{M}(e)$ in the first transmission phase is given by

$$\Gamma_{n,j,e}^{BR,T_1}(\mathcal{P}) = G_{n,j,e}^{BR,T_1} P_{n,j,e}^{BR,T_1}$$

and the SNR at UE $k$ in the second transmission phase is formulated as

$$\Gamma_{n,j,e}^{RU,T_2}(\mathcal{P}) = G_{n,j,e}^{RU,T_2} P_{n,j,e}^{RU,T_2}.$$

Additionally, $P_{n,j,e}^{BR,T_1}$ and $P_{n,j,e}^{RU,T_2}$ are also elements of $\mathcal{P}$. Since the RNs employ the DF protocol, the achievable SE is limited by the weaker of the two RN-related links [43] and is given by

$$C_{n,j,e}^{BRU}(\mathcal{P}) = \min\left[\frac{1}{2}\log_2\left(1+\Gamma_{n,j,e}^{BR,T_1}(\mathcal{P})\right), \frac{1}{2}\log_2\left(1+\Gamma_{n,j,e}^{RU,T_2}(\mathcal{P})\right)\right].$$

Let us now introduce the SMC group selection variable $s_{n,j} \in \{0,1\}$, which indicates that SMC group $j$, as introduced in Sections 4.4.1 and 4.4.2, is selected for subcarrier block $n$, when $s_{n,j} = 1$, and $s_{n,j} = 0$ otherwise. All SMC group selection variables are scalars and are collected into a set denoted by $\mathcal{S}$. Once again, we emphasize that $\mathcal{G}_n$ denotes the set of possible SMC groups for subcarrier block $n$. Thus, the total achieved SE is given by

$$C_T(\mathcal{P},\mathcal{S}) = \sum_{n=1}^{N}\sum_{j\in\mathcal{G}_n} s_{n,j}\left[\sum_{e_1\in\mathcal{E}_{n,j}} C_{n,j,e_1}^{BU,T_1}(\mathcal{P}) + \sum_{e_2\in\mathcal{E}_{n,j}} C_{n,j,e_2}^{BU,T_2}(\mathcal{P}) + \sum_{e\in\mathcal{E}_{n,j}} C_{n,j,e}^{BRU}(\mathcal{P})\right], \tag{4.55}$$

where $\mathcal{E}_{n,j}$ is the set comprising the SMCs in the selected group $j$ on subcarrier block $n$.

In this chapter, we adopt the energy dissipation model presented in [369], where the total energy dissipation of the system is assumed to be dependent on several factors, including the number of transmit antennas, the energy dissipation of the RF and baseband circuits, and the efficiencies of the power amplifier, feeder cables, cooling system, mains power supply, and converters. For the sake of simplicity, the total energy dissipation as presented in [369] has been partitioned into a fixed term, and a term that varies with the transmission powers. Thus, the energy dissipation of the system may be characterized by

$$P_T(\mathcal{P},\mathcal{S}) = \left(P_C^B + M\cdot P_C^R\right) + \frac{1}{2}\sum_{n=1}^{N}\sum_{j\in\mathcal{G}_n} s_{n,j} \left[\xi^B\left(\sum_{e_1\in\mathcal{E}_{n,j}} P_{n,j,e_1}^{BU,T_1} + \sum_{e_2\in\mathcal{E}_{n,j}} P_{n,j,e_2}^{BU,T_2}\right) + \sum_{e\in\mathcal{E}_{n,j}}\left(\xi^B P_{n,j,e}^{BR,T_1} + \xi^R P_{n,j,e}^{RU,T_2}\right)\right], \tag{4.56}$$

where $P_C^B$ and $P_C^R$ represent the fixed energy dissipation of each BS and each RN, respectively, while $\xi^B > 1$ and $\xi^R > 1$ are the energy dissipation multipliers of the transmit powers for the BS and the RNs, respectively. The effect of multiple transmit antennas on the total energy dissipation has been included in the terms $P_C^B$, $P_C^R$, $\xi^B$ and $\xi^R$.

Finally, the EE of the system is expressed as

$$\eta_E(\mathcal{P},\mathcal{S}) = \frac{C_T(\mathcal{P},\mathcal{S})}{P_T(\mathcal{P},\mathcal{S})}. \tag{4.57}$$

The objective of this chapter is to maximize (4.57) by appropriately optimizing $\mathcal{P}$ and $\mathcal{S}$.

In the previous chapter, a simpler system model was featured, which allowed for simultaneous direct and AF relay-assisted transmission across different subcarriers, and did not require the grouping algorithms to be discussed in Section 4.5. By contrast, with the aid of the ZFBF described above, in this chapter both direct and DF relay-assisted transmissions can be conveyed by the same subcarriers. Moreover, the SMCs associated with either the direct or the relay-assisted transmissions are primarily selected based on the semi-orthogonality criterion. Hence the UEs are not restricted to be aided only by the RNs closest to them, as was the case in Chapter 3. A consequence of employing multiple antenna aided nodes in the system is the increased power cost imposed by the additional RF chains required. This has been accounted for in (4.56).

Furthermore, it is possible to employ adaptive antennas [370] in conjunction with the transmission protocol described above for the sake of improving the system's EE. For example, by deactivating some of the RF chains, the power consumption can reduced at the cost of a reduced resource allocation flexibility. Another consideration is the specific *combination*

of antennas in the system, which should be deactivated, since each combination naturally results in a unique set of SMCs. Generally speaking, considering *every* possible combination of activated antennas would result in an improved performance. However, this would lead to excessive complexity both in terms of the grouping algorithm and the optimization algorithm. Thus, adaptive antennas are not considered in this chapter.

## 4.5 Spatial Multiplexing Component Grouping Algorithms

As described in Section 4.2, the BS has to choose $Q_j^{T_1}$ and $Q_j^{T_2}$ SMCs for the first and second transmission phases, respectively. These selected SMCs collectively form the SMC group $j$, as exemplified in Fig. 4.9. Since the system supports both direct and relaying links, the grouping algorithms described in [324, 359], which were designed for MIMO systems dispensing with relays, may not be directly applied. Instead, we propose a pair of viable grouping algorithms, namely the exhaustive search-based grouping algorithm (ESGA), and the orthogonal component-based grouping algorithm (OCGA).

Note that because there are multiple distributed transmitters in the second transmission phase, each UE designs its receive-BF matrix by jointly considering all the MIMO channel matrices associated with it, as described in Section 4.4.2. However, before applying this method, we have to determine which particular transmitters (out of the BS and RNs) should actively transmit in the second transmission phase based on the results of SMC selection. Note that it is possible that the SMC candidates obtained may lead to higher effective CNRs when a subset of the transmitters are inactive. On the one hand, an additional effect of only activating a subset of transmitters is the reduced number of SMC candidates, which might in turn result in a reduced number of qualified SMCs that satisfy the semi-orthogonality criterion considered. As a result, the achievable spatial multiplexing gain and SE might be degraded. On the other hand, this SE-reduction effect may be counteracted by the improved CNRs gleaned from the fact that it is easier to generate SMCs that can satisfy a stricter semi-orthogonality criterion, specified by a smaller value of $\alpha$, when the number of transmitters is lower. For example, in the scenarios where only one or two active transmitters are selected, the UEs can employ receive-BF matrices that create effective DL channel matrices containing completely orthogonal rows by using the SVD or the exact diagonalization method described above, respectively. In order to account for this dilemma, for the second transmission phase, the proposed grouping algorithms evaluate a full list of SMCs, which consists of the SMCs obtained from the $2^{M+1}-1$ possible combinations of active transmitters (the BS and $M$ RNs, while ignoring the case when there are no active transmitters). Compared to using a smaller list of SMCs, using a full list of SMCs ensures that achieving a lower-bound SE is always guaranteed, while a higher SE can only be obtained upon increasing the number of transmitters in the system.

### 4.5.1 Spatial Multiplexing Component Checking Algorithm

Both grouping algorithms must evaluate a particular SMC before it may be included into the SMC group to be generated. This evaluating and SMC-group updating process is depicted in Algorithm 3. More specifically, the algorithm identifies the transmitters associated with each SMC of the current SMC group, denoted by $\mathcal{E}_{n,j}$, in lines 7 to 17. The transmitter associated with the candidate SMC, $e_c$, is identified in lines 18 to 28. Additionally, as briefly pointed out above, for an active transmitter, if the candidate SMC is associated with a transmission in the second phase, then the auxiliary SMCs, $e^{\varnothing}$ and $e_m^{\varnothing}$, are included for the other active transmitters in lines 23, 26 and 27, in order to ensure that these potentially interfering transmitters do not impose interference on the candidate SMC, as depicted in Fig. 4.4. For distributed transmitters encountered in the second transmission phase, it is not feasible to design a single ZFBF transmit matrix as we did for the BS in the first transmission phase. For the second transmission phase, when $N_B \leq N_U$ and $N_R \leq N_U$, each SMC is associated with a single receive antenna. Consider this case as an example, when the BS is transmitting on a SMC to a particular receive antenna of a UE, an active RN may be transmitting zeros on an auxiliary SMC, which is also selected from the legitimate SMC candidates, to the same receive antenna of that UE. As a beneficial result of this strategy, for each transmitter, the interference imposed by other active transmitters are nulled. Furthermore, observe that $e^{\varnothing}$ and $e_m^{\varnothing}$ represent auxiliary SMCs invoked by the BS and RNs, respectively. Having determined the transmitters associated with the SMCs, the algorithm checks that the SMCs associated with the same transmitter satisfy the semi-orthogonality criterion of (4.25) having parameter $\alpha$ in lines 20, 29 and 30. Furthermore, the algorithm ensures that the inclusion of the candidate SMC does not force any of the transmitters to transmit over its maximum number of transmit dimensions, as depicted in lines 29 and 30. Meanwhile, each UE should not receive more than its maximum number of receive dimensions, which is accomplished in lines 12, 32 and 33. Finally, the maximum achievable spatial multiplexing gain should not be exceeded in either the first or second phase, which is ensured by lines 35 and 36. If all of these checks are successful, the algorithm exits with a true condition in line 37.

### 4.5.2 Exhaustive Search and Orthogonal Component-Based Grouping Algorithms

We present our first grouping method in Algorithm 4. Simply put, the ESGA recursively creates new SMC groups by exhaustively searching through all the possible combinations of SMCs and including those that pass the SMC checking algorithm. To elaborate, in the loop ranging from line 3 to line 9, the algorithm searches through all the possible SMCs associated with subcarrier block $n$, which are collectively denoted by $\mathcal{E}_n$ and satisfy $e_c \in \mathcal{E}_n$. The specific SMCs that satisfy the checks performed in line 4 are appended to the current SMC group in line 5, and the resultant updated SMC group $\mathcal{E}'_{n,j'}$ is appended to the set of

**Algorithm 3:** SMC checking algorithm

**inputs** : candidate SMC $e_c$, current SMC group $\mathcal{E}_{n,j}$, semi-orthogonality parameter $\alpha$

**outputs**: **true** or **false**

bool `SMCCheck` $(e_c, \mathcal{E}_{n,j}, \alpha)$

**begin**

- $\mathcal{T}^{BS,T_1} \leftarrow \{\}$;
- $\mathcal{T}^{BS,T_2} \leftarrow \{\}$;
- $\mathcal{T}_m^{RN,T_2} \leftarrow \{\}$, $\forall m \in \{1, \cdots, M\}$;
- $\mathcal{R}_k^{UE,T_2} \leftarrow \{\}$, $\forall k \in \{1, \cdots, K\}$;
- **foreach** *SMC* $e_1 \in \mathcal{E}_{n,j}$ **do**
  - $\mathcal{T}^{BS,T_1} \leftarrow \mathcal{T}^{BS,T_1} \cup \{e_1\}$;
- **end foreach**
- **foreach** *SMC* $e_2 \in \mathcal{E}_{n,j}$ **do**
  - $\mathcal{T}^{BS,T_2} \leftarrow \mathcal{T}^{BS,T_2} \cup \{e_2\}$;
  - $\mathcal{R}_k^{UE,T_2} \leftarrow \mathcal{R}_k^{UE,T_2} \cup \{e_2\}$;
- **end foreach**
- **foreach** *SMC* $e \in \mathcal{E}_{n,j}$ **do**
  - $\mathcal{T}^{BS,T_2} \leftarrow \mathcal{T}^{BS,T_2} \cup \{e\}$;
  - $\mathcal{T}_{\mathcal{M}(e)}^{RN,T_2} \leftarrow \mathcal{T}_{\mathcal{M}(e)}^{RN,T_2} \cup \{e\}$;
- **end foreach**
- **if** $e_c$ *is BS transmission in* $T_1$ **then**
  - $\mathcal{T}^{BS,T_1} \leftarrow \mathcal{T}^{BS,T_1} \cup \{e_c\}$;
  - **if** $\mathcal{T}^{BS,T_1}$ *is not* $\alpha$*-semi-orthogonal* **or** $|\mathcal{T}^{BS,T_1}| > N_B$ **then return false**;
- **else if** $e_c$ *is BS transmission in* $T_2$ **then**
  - $\mathcal{T}^{BS,T_2} \leftarrow \mathcal{T}^{BS,T_2} \cup \{e_c\}$;
  - $\mathcal{T}_m^{RN,T_2} \leftarrow \mathcal{T}_m^{RN,T_2} \cup \{e_m^{\varnothing}\}$, $\forall m \in \{1, \cdots, M\}$;
- **else if** $e_c$ *is RN* $m$ *transmission in* $T_2$ **then**
  - $\mathcal{T}_m^{RN,T_2} \leftarrow \mathcal{T}_m^{RN,T_2} \cup \{e_c\}$;
  - $\mathcal{T}^{BS,T_2} \leftarrow \mathcal{T}^{BS,T_2} \cup \{e^{\varnothing}\}$;
  - $\mathcal{T}_{m'}^{RN,T_2} \leftarrow \mathcal{T}_{m'}^{RN,T_2} \cup \{e_{m'}^{\varnothing}\}$, $\forall m' \in \{1, \cdots, M\} \setminus m$;
- **end if**
- **if** $\mathcal{T}^{BS,T_2}$ *is not* $\alpha$*-semi-orthogonal* **or** $|\mathcal{T}^{BS,T_2}| > N_B$ **then return false**;
- **if** $\mathcal{T}_m^{RN,T_2}$ *is not* $\alpha$*-semi-orthogonal* **or** $|\mathcal{T}_m^{RN,T_2}| > N_R$, $m \in \{1, \cdots, M\}$ **then return false**;
- **if** $e_c$ *is UE* $k$ *reception in* $T_2$ **then**
  - $\mathcal{R}_k^{UE,T_2} \leftarrow \mathcal{R}_k^{UE,T_2} \cup \{e_c\}$;
  - **if** $|\mathcal{R}_k^{UE,T_2}| > N_U$, $k \in \{1, \cdots, K\}$ **then return false**;
- **end if**
- **if** $|\mathcal{T}^{BS,T_1}| > \min(N_B, KN_U + MN_R)$ **then return false**;
- **if** $\sum_{k=1}^{K} |\mathcal{R}_k^{UE,T_2}| > \min(N_B, N_R)$ **then return false**;
- **return true**;

**end**

**Algorithm 4:** Exhaustive search-based grouping algorithm (ESGA)

**inputs** : set of SMC groups associated with subcarrier block $n$ (initialized as empty set), $\mathcal{G}_n$
current SMC group (initialized as empty set), $\mathcal{E}_{n,j}$
SMCs associated with subcarrier block $n$, $\mathcal{E}_n$
semi-orthogonality parameter $\alpha$

**outputs**: none

1 void `ESGA` $(\mathcal{G}_n, \mathcal{E}_{n,j}, \mathcal{E}_n, \alpha)$
2 **begin**
3  **foreach** $e_c \in \mathcal{E}_n$ **do**
4  **if** `SMCCheck` $(e_c, \mathcal{E}_{n,j}, \alpha)$ **then**
5  $\mathcal{E}'_{n,j'} \leftarrow \mathcal{E}_{n,j} \cup \{e_c\}$;
6  $\mathcal{G}_n \leftarrow \mathcal{G}_n \cup \{\mathcal{E}'_{n,j'}\}$;
7  `ESGA` $\left(\mathcal{G}_n, \mathcal{E}'_{n,j'}, \mathcal{E}_n \setminus e_c, \alpha\right)$;
8  **end if**
9  **end foreach**
10  **return**;
11 **end**

SMC groups obtained for subcarrier block $n$ in line 6. Additionally, $\mathcal{E}'_{n,j'}$ is used recursively in line 7 for filling this group and for forming new groups. The computational complexity of ESGA is dependent on the number of SMCs which are semi-orthogonal to each other. The worst-case complexity is obtained when every SMC satisfies the checks performed in line 4, leading to a time-complexity (in terms of the number of SMC groups generated) upper-bounded (not necessarily tight) by $\mathcal{O}\left(\sum_{n=1}^{N} |\mathcal{E}_n|^{\theta}\right)$, where

$$\theta = \min\left[N_B, K \cdot \min\left(N_B, N_U\right) + M \cdot \min\left(N_B, N_R\right)\right] + \min\left[\min\left(N_B, N_R\right), \sum_{i=1}^{K} L_i^B + L_i^R\right]. \tag{4.58}$$

In other words, each subcarrier block may be treated independently. For each subcarrier block, $|\mathcal{E}_n|$ SMCs must be checked until the maximum multiplexing gain in both the first and second phases has been attained.

The second algorithm, OCGA, is presented in Algorithm 5, which aims to be a lower complexity alternative to ESGA. The OCGA commences by creating a SMC candidate set $\mathcal{E}_c$, whose elements satisfy the checks performed in Algorithm 3, in lines 4 to 16. More specifically, if the current SMC group $\mathcal{E}_{n,j}$ is empty, the algorithm can simply create a new SMC group containing only the candidate SMC that has passed the SMC checks of Algorithm 3 in lines 7 to 10. If the SMC group is not empty, the algorithm adds to it the particular SMC candidate that results in the highest norm of the orthogonal component (NOC), via the Gram-Schmidt procedure [324, 359], in line 20. This process is repeated until the maximum

**Algorithm 5:** Orthogonal component-based grouping algorithm (OCGA)

**inputs** : set of SMC groups associated with subcarrier block $n$ (initialized as empty set), $\mathcal{G}_n$
current SMC group (initialized as empty set), $\mathcal{E}_{n,j}$
SMCs associated with subcarrier block $n$, $\mathcal{E}_n$
semi-orthogonality parameter $\alpha$

**outputs**: none

```
1  void OCGA (G_n, E_{n,j}, E_n, α)
2  begin
3      complete ← true;
4      E_c ← {};
5      foreach e_c ∈ E_n do
6          if SMCCheck (e_c, E_{n,j}, α) then
7              if |E_{n,j}| == 0 then
8                  E'_{n,j'} ← E_{n,j} ∪ {e_c};
9                  OCGA (G_n, E'_{n,j'}, E_n \ e_c, α);
10                 return;
11             else
12                 E_c ← E_c ∪ {e_c};
13                 complete ← false;
14             end if
15         end if
16     end foreach
17     if complete then
18         G_n ← {E_{n,j}};
19     else
20         E'_{n,j'} ← E_{n,j} ∪ arg max_{e_c ∈ E_c} NOC (e_c, E_{n,j});
21         OCGA (G_n, E'_{n,j'}, E_n \ e_c, α);
22     end if
23     return;
24 end
```

multiplexing gain in both the first and second phases has been attained. When comparing the NOCs obtained for the relaying links, the minimum of the NOCs obtained from the BS-to-RN and RN-to-UE SMCs is used. This is because the information conveyed on the relaying link is limited by the weaker of the two transmissions, which is reflected in the effective channel gains quantified by these norms. If no SMCs satisfy the checks of line 6, the current SMC group is complete, and it is appended to the current set of SMC groups in line 18. Since new groups are only created when the current SMC group is empty, this algorithm results in much fewer groups than ESGA. The algorithmic time-complexity is given by $\mathcal{O}\left(\sum_{n=1}^{N}|\mathcal{E}_n|\right)$ as a single group is created for each initially-selected SMC.

Both grouping algorithms may be initialized with an empty SMC group, $\mathcal{E}_{n,j} \leftarrow \{\}$, and an empty set of SMC groups, $\mathcal{G}_n \leftarrow \{\}$, so that they recursively create and fill SMC groups according to their criteria. Additionally, a final step is performed to remove the specific groups, which result in effective channel gains that are less than or equal to that of another group, while having the same transmitters. Therefore, this final step does not reduce the attainable SE or EE, but reduces the number of possible groups, thus alleviating the computational complexity imposed by the optimization algorithms of Section 4.6.3.

### 4.5.3 The Norm of the Orthogonal Component Algorithm

**Algorithm 6:** Algorithm for computing the norm of the orthogonal component

**inputs** : Candidate SMC $e_c$, SMC group $\mathcal{E}_{n,j}$
**outputs**: The norm of the orthogonal component

1 double `NOC` $(e_c, \mathcal{E}_{n,j})$
2 **begin**
3 $\quad \mathcal{S} \leftarrow \{\}$;
4 $\quad$ **foreach** $e \in \mathcal{E}_{n,j}$ **do**
5 $\quad\quad \mathcal{S} \leftarrow \mathcal{S} \cup e - \sum_{s \in \mathcal{S}} \frac{es^*}{||s||^2} s$;
6 $\quad$ **end foreach**
7 $\quad$ **return** $\left|\left| e_c - \sum_{s \in \mathcal{S}} \frac{e_c s^*}{||s||^2} s \right|\right|$ ;
8 **end**

The NOC procedure is outlined in Algorithm 6, which aims for finding the norm of the orthogonal component of the candidate SMC $e_c$ with respect to the SMC group $\mathcal{E}_{n,j}$. Initially, the SMC group is orthogonalized using the Gram-Schmidt procedure in lines 3 to 6, which organizes the orthogonalized vectors of the SMC group into the set denoted by $\mathcal{S}$. The orthogonal component of $e_c$ with respect to the orthogonal components of the SMC group is then computed in line 7, where the algorithm returns its norm.

## 4.6 Problem Formulation and Solution

Having obtained the set of SMC groups $\mathcal{G}_n$ for each subcarrier block $n$, in this section our aim is to find the optimum power variables contained in $\mathcal{P}$ and optimum SMC-group selection variables contained in $\mathcal{S}$, so that (4.57) is maximized. We commence by formulating the

problem of maximizing the SE of the system as (4.59)–(4.65).

$$\underset{\mathcal{P},\mathcal{S}}{\text{maximize}} \quad C_T\left(\mathcal{P},\mathcal{S}\right) \tag{4.59}$$

$$\text{subject to} \quad \sum_{j\in\mathcal{G}_n} s_{n,j} \leq 1,\ \forall n, \tag{4.60}$$

$$\sum_{i=1}^{N}\sum_{j\in\mathcal{G}_n} s_{n,j}\left[\sum_{e_1\in\mathcal{E}_{n,j}} P_{n,j,e_1}^{BU,T_1} + \sum_{e\in\mathcal{E}_{n,j}} P_{n,j,e}^{BR,T_1}\right] \leq P_{max}^{B}, \tag{4.61}$$

$$\sum_{i=1}^{N}\sum_{j\in\mathcal{G}_n} s_{n,j}\sum_{e_2\in\mathcal{E}_{n,j}} P_{n,j,e_2}^{BU,T_2} \leq P_{max}^{B}, \tag{4.62}$$

$$\sum_{i=1}^{N}\sum_{j\in\mathcal{G}_n} s_{n,j}\sum_{\substack{e\in\mathcal{E}_{n,j}\\ \mathcal{M}(e)=m}} P_{n,j,e}^{RU,T_2} \leq P_{max}^{R},\ \forall m, \tag{4.63}$$

$$s_{n,j}\in\{0,1\},\ \forall n,j, \tag{4.64}$$

$$P_{n,j,e_1}^{BU,T_1}, P_{n,j,e}^{BR,T_1}, P_{n,j,e_2}^{BU,T_2}, P_{n,j,e}^{RU,T_2} \geq 0,\ \forall n,j,e_1,e_2,e. \tag{4.65}$$

To elaborate, (4.59) represents the sum SE of the system, which is formulated in more detail as (4.55). The constraints (4.61)–(4.63) ensure that the maximum instantaneous transmission power constraint is never exceeded in either of the two transmission phases for the BS and the RNs, while the constraints (4.60) and (4.64) ensure that only a single SMC group is selected for each subcarrier block. Finally, (4.65) restricts the power variables to be non-negative.

### 4.6.1 Relaxed Spectral Efficiency Maximization Problem

Although the constraint (4.65) is affine (hence convex) in the optimization variables contained in $\mathcal{P}$, (4.60)–(4.63) are nonconvex [34], because (4.64) imposes a binary constraint on the problem. Furthermore, the objective function given by (4.59) is not concave, since it is dependent on the binary variables given by $\mathcal{S}$. Thus, (4.59)–(4.65) may be classified as a *MINLP* problem, which may be solved using the classic branch-and-bound method described in Section 2.4.2. However, this method typically incurs a computational complexity that increases exponentially in the number of discrete variables, which is undesirable for practical implementations. To circumvent this initial setback, we introduce the following auxiliary variables

$$\widetilde{P}_{n,j,e_1}^{BU,T_1} = P_{n,j,e_1}^{BU,T_1}\widetilde{s}_{n,j},\ \forall n,j,e_1, \tag{4.66}$$

$$\widetilde{P}_{n,j,e}^{BR,T_1} = P_{n,j,e}^{BR,T_1}\widetilde{s}_{n,j},\ \forall n,j,e, \tag{4.67}$$

$$\widetilde{P}_{n,j,e_2}^{BU,T_2} = P_{n,j,e_2}^{BU,T_2}\widetilde{s}_{n,j},\ \forall n,j,e_2, \tag{4.68}$$

$$\widetilde{P}_{n,j,e}^{RU,T_2} = P_{n,j,e}^{RU,T_2}\widetilde{s}_{n,j},\ \forall n,j,e, \tag{4.69}$$

$$\widetilde{C}_{n,j,e_1}^{BU,T_1},\ \widetilde{C}_{n,j,e_2}^{BU,T_2} \text{ and } \widetilde{C}_{n,j,e}^{BRU},\ \forall n,j,e_1,e_2,e, \tag{4.70}$$

where we have relaxed the binary constraint of (4.64) to give

$$0 \leq \widetilde{s}_{n,j} \leq 1,\ \forall n,j, \tag{4.71}$$

as was performed in Section 3.3, so that we may write (4.59)–(4.65) in the hypograph form given by

$$\underset{\widetilde{\mathcal{C}},\widetilde{\mathcal{P}},\widetilde{\mathcal{S}}}{\text{maximize}} \quad \sum_{i=1}^{N}\sum_{j\in\mathcal{G}_n}\left[\sum_{e_1\in\mathcal{E}_{n,j}}\widetilde{C}_{n,j,e_1}^{BU,T_1}+\sum_{e_2\in\mathcal{E}_{n,j}}\widetilde{C}_{n,j,e_2}^{BU,T_2}\right]+\left[\sum_{e\in\mathcal{E}_{n,j}}\widetilde{C}_{n,j,e}^{BRU}\right] \tag{4.72}$$

$$\text{subject to} \quad \frac{\widetilde{s}_{n,j}}{2}\log_2\left(1+\frac{G_{n,j,e_1}^{BU,T_1}\widetilde{P}_{n,j,e_1}^{BU,T_1}}{\widetilde{s}_{n,j}}\right)\geq\widetilde{C}_{n,j,e_1}^{BU,T_1},\ \forall n,j,e_1, \tag{4.73}$$

$$\frac{\widetilde{s}_{n,j}}{2}\log_2\left(1+\frac{G_{n,j,e_2}^{BU,T_2}\widetilde{P}_{n,j,e_2}^{BU,T_2}}{\widetilde{s}_{n,j}}\right)\geq\widetilde{C}_{n,j,e_2}^{BU,T_2},\ \forall n,j,e_2, \tag{4.74}$$

$$\frac{\widetilde{s}_{n,j}}{2}\log_2\left(1+\frac{G_{n,j,e}^{BR,T_1}\widetilde{P}_{n,j,e}^{BR,T_1}}{\widetilde{s}_{n,j}}\right)\geq\widetilde{C}_{n,j,e}^{BRU},\ \forall n,j,e, \tag{4.75}$$

$$\frac{\widetilde{s}_{n,j}}{2}\log_2\left(1+\frac{G_{n,j,e}^{RU,T_2}\widetilde{P}_{n,j,e}^{RU,T_2}}{\widetilde{s}_{n,j}}\right)\geq\widetilde{C}_{n,j,e}^{BRU},\ \forall n,j,e, \tag{4.76}$$

$$\sum_{j\in\mathcal{G}_n}\widetilde{s}_{n,j}\leq 1,\ \forall n, \tag{4.77}$$

$$\sum_{i=1}^{N}\sum_{j\in\mathcal{G}_n}\left[\sum_{e_1\in\mathcal{E}_{n,j}}\widetilde{P}_{n,j,e_1}^{BU,T_1}+\sum_{e\in\mathcal{E}_{n,j}}\widetilde{P}_{n,j,e}^{BR,T_1}\right]\leq P_{max}^{B}, \tag{4.78}$$

$$\sum_{i=1}^{N}\sum_{j\in\mathcal{G}_n}\sum_{e_2\in\mathcal{E}_{n,j}}\widetilde{P}_{n,j,e_2}^{BU,T_2}\leq P_{max}^{B}, \tag{4.79}$$

$$\sum_{i=1}^{N}\sum_{j\in\mathcal{G}_n}\sum_{\substack{e\in\mathcal{E}_{n,j}\\ \mathcal{M}(e)=m}}\widetilde{P}_{n,j,e}^{RU,T_2}\leq P_{max}^{R},\ \forall m, \tag{4.80}$$

$$0\leq\widetilde{s}_{n,j}\leq 1,\ \forall n,j, \tag{4.81}$$

$$\widetilde{P}_{n,j,e_1}^{BU,T_1},\widetilde{P}_{n,j,e}^{BR,T_1},\widetilde{P}_{n,j,e_2}^{BU,T_2},\widetilde{P}_{n,j,e}^{RU,T_2}\geq 0,\ \forall n,j,e_1,e_2,e, \tag{4.82}$$

where $\widetilde{\mathcal{C}}$, $\widetilde{\mathcal{P}}$ and $\widetilde{\mathcal{S}}$ indicate the variable-sets containing their associated auxiliary variables.

Writing the original optimization problem in the hypograph form of (4.72)–(4.82) means that minimum per-link or system-wide SE constraints may be readily introduced. However, minimum SE constraints are not considered in this chapter as our goal is to find the maximum SE/EE solutions, which may not be equivalent to the solutions obtained when satisfying minimum SE constraints.

It can be seen that the objective function of (4.59) has been replaced by (4.72) using the

auxiliary rate variables given in (4.70), and by introducing the hypograph constraints (4.73)–(4.76). These additional constraints ensure that the feasible auxiliary rate variables do not exceed their counterparts calculated on each link before using relaxation. As a result, the sum rate given by (4.72) invoking the feasible auxiliary rate variables does not exceed the sum rate given by (4.55) either. Observe that obtaining separate constraints for the first- and second-phase power control variables associated with the relayed transmission is made possible using the DF protocol. This then allowed us to readily derive the optimal power control variables as the decoupled water-filling solutions in Section 4.6.3.1, which would not have been possible if the AF protocol was employed, as demonstrated in Section 3.5.

As our next step, we prove that the problem described by (4.72)–(4.82) is a concave programming problem. Clearly, (4.72) is affine, hence concave, while (4.77)–(4.82) are all affine, and hence convex. Therefore, what remains is to show that constraints (4.73)–(4.76) are convex as well. These remaining constraints may be written in the form of

$$C - \frac{s}{2}\log_2\left(1+\frac{GP}{s}\right) \leq 0, \tag{4.83}$$

where $s$, $P$ and $C$ are the decision variables. From Section 3.3, we know that functions of the form $f(P,s) = \frac{s}{2}\log_2\left(1+\frac{GP}{s}\right)$ are concave. Thus, it can be readily shown that $C - \frac{s}{2}\log_2\left(1+\frac{GP}{s}\right)$ is convex, since it is the sum of two convex functions. Since (4.83) is convex, it is clear that the constraints in (4.73)–(4.76) are convex and hence (4.72)–(4.82) is a concave programming problem, whose solution algorithm will be presented in Section 4.6.3.

### 4.6.2 Energy Efficiency Maximization Problem

The EE objective function, given by

$$\frac{(4.72)}{P_T\left(\widetilde{\mathcal{P}},\widetilde{\mathcal{S}}\right)}, \tag{4.84}$$

where

$$\begin{aligned} P_T\left(\widetilde{\mathcal{P}},\widetilde{\mathcal{S}}\right) &= \left(P_C^B + M\cdot P_C^R\right) + \frac{1}{2}\sum_{n=1}^{N}\sum_{j\in\mathcal{G}_n}\sum_{k=1}^{K}\xi^B\left(\sum_{e_1\in\mathcal{E}_{n,j}}\widetilde{P}_{n,j,e_1}^{BU,T_1} + \sum_{e_2\in\mathcal{E}_{n,j}}\widetilde{P}_{n,j,e_2}^{BU,T_2}\right) \\ &\quad \frac{1}{2}\sum_{n=1}^{N}\sum_{j\in\mathcal{G}_n}\sum_{k=1}^{K}\sum_{e\in\mathcal{E}_{n,j}}\left(\xi^B\widetilde{P}_{n,j,e}^{BR,T_1} + \xi^R\widetilde{P}_{n,j,e}^{RU,T_2}\right), \end{aligned} \tag{4.85}$$

which is obtained by substituting (4.66)–(4.69) into (4.56) and introducing the relaxed variables $\widetilde{s}_{n,j}$. The objective function (4.84) is a linear-fractional function, since it is a ratio of two affine functions. Thus the EEM problem can be solved using the Charnes-Cooper

transformation of [338], as given by

$$\widehat{C}_{n,j,e_1}^{BU,T_1} = \widetilde{C}_{n,j,e_1}^{BU,T_1} t,\ \forall n,j,e_1, \tag{4.86}$$
$$\widehat{C}_{n,j,e_2}^{BU,T_2} = \widetilde{C}_{n,j,e_2}^{BU,T_2} t,\ \forall n,j,e_2, \tag{4.87}$$
$$\widehat{C}_{n,j,,e}^{BRU} = \widetilde{C}_{n,j,e}^{BRU} t,\ \forall n,j,e, \tag{4.88}$$
$$\widehat{P}_{n,j,e_1}^{BU,T_1} = \widetilde{P}_{n,j,e_1}^{BU,T_1} t,\ \forall n,j,e_1, \tag{4.89}$$
$$\widehat{P}_{n,j,e_2}^{BU,T_2} = \widetilde{P}_{n,j,e_2}^{BU,T_2} t,\ \forall n,j,e_2, \tag{4.90}$$
$$\widehat{P}_{n,j,e}^{BR,T_1} = \widetilde{P}_{n,j,e}^{BR,T_1} t,\ \forall n,j,e, \tag{4.91}$$
$$\widehat{P}_{n,j,e}^{RU,T_2} = \widetilde{P}_{n,j,e}^{RU,T_2} t,\ \forall n,j,e, \tag{4.92}$$
$$\widehat{s}_{n,j} = \widetilde{s}_{n,j} t,\ \forall n,j, \tag{4.93}$$

where the auxiliary variable $t$ is given by

$$t = \frac{1}{P_T\left(\widetilde{\mathcal{P}},\widetilde{\mathcal{S}}\right)}. \tag{4.94}$$

Thus, the EEM problem may be written as

$$\underset{\widehat{\mathcal{C}},\widehat{\mathcal{P}},\widehat{\mathcal{S}},t}{\text{maximize}} \quad \sum_{i=1}^{N}\sum_{j\in\mathcal{G}_n}\left[\sum_{e_1\in\mathcal{E}_{n,j}}\widehat{C}_{n,j,e_1}^{BU,T_1}+\sum_{e_2\in\mathcal{E}_{n,j}}\widehat{C}_{n,j,e_2}^{BU,T_2}\right]+\left[\sum_{e\in\mathcal{E}_{n,j}}\widehat{C}_{n,j,e}^{BRU}\right] \tag{4.95}$$

$$\text{subject to} \quad \frac{\widehat{s}_{n,j}}{2}\log_2\left(1+\frac{G_{n,j,e_1}^{BU,T_1}\widehat{P}_{n,j,e_1}^{BU,T_1}}{\widehat{s}_{n,j}}\right)\geq\widehat{C}_{n,j,e_1}^{BU,T_1},\ \forall n,j,e_1, \tag{4.96}$$

$$\frac{\widehat{s}_{n,j}}{2}\log_2\left(1+\frac{G_{n,j,e_2}^{BU,T_2}\widehat{P}_{n,j,e_2}^{BU,T_2}}{\widehat{s}_{n,j}}\right)\geq\widehat{C}_{n,j,e_2}^{BU,T_2},\ \forall n,j,e_2, \tag{4.97}$$

$$\frac{\widehat{s}_{n,j}}{2}\log_2\left(1+\frac{G_{n,j,e}^{BR,T_1}\widehat{P}_{n,j,e}^{BR,T_1}}{\widehat{s}_{n,j}}\right)\geq\widehat{C}_{n,j,e}^{BRU},\ \forall n,j,e, \tag{4.98}$$

$$\frac{\widehat{s}_{n,j}}{2}\log_2\left(1+\frac{G_{n,j,e}^{RU,T_2}\widehat{P}_{n,j,e}^{RU,T_2}}{\widehat{s}_{n,j}}\right)\geq\widehat{C}_{n,j,e}^{BRU},\ \forall n,j,e, \tag{4.99}$$

$$\sum_{j\in\mathcal{G}_n}\widehat{s}_{n,j}\leq t,\ \forall n, \tag{4.100}$$

$$\sum_{i=1}^{N}\sum_{j\in\mathcal{G}_n}\left[\sum_{e_1\in\mathcal{E}_{n,j}}\widehat{P}_{n,j,e_1}^{BU,T_1}+\sum_{e\in\mathcal{E}_{n,j}}\widehat{P}_{n,j,e}^{BR,T_1}\right]\leq t\cdot P_{max}^{B}, \tag{4.101}$$

$$\sum_{i=1}^{N}\sum_{j\in\mathcal{G}_n}\sum_{e_2\in\mathcal{E}_{n,j}}\widehat{P}_{n,j,e_2}^{BU,T_2}\leq t\cdot P_{max}^{B}, \tag{4.102}$$

$$\sum_{i=1}^{N}\sum_{j\in\mathcal{G}_n}\sum_{\substack{e\in\mathcal{E}_{n,j}\\ \mathcal{M}(e)=m}}\widehat{P}_{n,j,e}^{RU,T_2}\leq t\cdot P_{max}^{R},\ \forall m, \tag{4.103}$$

$$0\leq\widehat{s}_{n,j}\leq t,\ \forall n,j, \tag{4.104}$$

$$\widehat{P}^{BU,T_1}_{n,j,e_1}, \widehat{P}^{BR,T_1}_{n,j,e}, \widehat{P}^{BU,T_2}_{n,j,e_2}, \widehat{P}^{RU,T_2}_{n,j,e} \geq 0, \forall n, j, e_1, e_2, e, \tag{4.105}$$

$$t \cdot \left(P^B_C + M \cdot P^R_C\right) + \frac{1}{2}\sum_{n=1}^{N}\sum_{j\in\mathcal{G}_n} \xi^B \left(\sum_{e_1\in\mathcal{E}_{n,j}} \widehat{P}^{BU,T_1}_{n,j,e_1} + \sum_{e_2\in\mathcal{E}_{n,j}} \widehat{P}^{BU,T_2}_{n,j,e_2}\right)$$
$$+\frac{1}{2}\sum_{n=1}^{N}\sum_{j\in\mathcal{G}_n}\sum_{e\in\mathcal{E}_{n,j}} \left(\xi^B \widehat{P}^{BR,T_1}_{n,j,e} + \xi^R \widehat{P}^{RU,T_2}_{n,j,e}\right) = 1 \tag{4.106}$$

where $\widehat{\mathcal{C}}$, $\widehat{\mathcal{P}}$ and $\widehat{\mathcal{S}}$ indicate the variable-sets containing their associated transformed variables. It is clear that the objective function (4.95) is affine, hence concave, while the constraints (4.100)–(4.106) are all affine, and hence convex. The constraints (4.96)–(4.99) are of the form (4.83) and are hence convex. Therefore, the problem described by (4.95)–(4.106) is a concave programming problem, which can be solved using the algorithm of Section 4.6.3.

In contrast to the optimization problem given by (3.55)–(3.61) of Chapter 3, the objective function of (4.95) is linear, since we have cast the problem in a hypograph form. However, here we have the additional inequality constraints given by (4.96)–(4.99). Furthermore, we now have separate maximum transmission power constraints for the BS and the RNs, which are given by (4.101)–(4.103), respectively. We inherit from (3.55)–(3.61) similar subcarrier indicator variable constraints, nonnegative power variable constraints, and the single linear constraint imposed by applying the Charnes-Cooper transformation. Explicitly, these constraints are given by (4.100), (4.104), (4.105) and (4.106), respectively.

### 4.6.3 Solution Algorithm Based on the Dual Decomposition Method

The dual decomposition method described in Section 2.7 and employed in Sections 3.4–3.6 can be used for conceiving solution algorithms for the SEM and EEM problems formulated as (4.72)–(4.82) and (4.95)–(4.106), respectively. We commence by describing the solution algorithm conceived for (4.95)–(4.106), which we term the EEM algorithm. The EEM algorithm, based on dual decomposition, iterates between calculating the tentative optima of the primal variables, namely of $\widehat{C}^{BU,T_1}_{n,j,e_1}$, $\widehat{C}^{BU,T_2}_{n,j,e_2}$, $\widehat{C}^{BRU}_{n,j,e}$, $\widehat{P}^{BU,T_1}_{n,j,e_1}$, $\widehat{P}^{BU,T_2}_{n,j,e_2}$, $\widehat{P}^{BR,T_1}_{n,j,e}$, $\widehat{P}^{RU,T_2}_{n,j,e}$, $\widehat{s}_{n,j}$ as well as $t$, and updating the dual variables $\lambda^{T_1}$, $\lambda^{T_2}$, $\nu_m$ as well as $\mu$, which will be defined later, until the objective function value converges.

#### 4.6.3.1 Obtaining the Optimal Primal Variables

Recall from Sections 2.8 and 3.5, that the transformed power control variables of the direct SMCs encountered in the problem of (4.95)–(4.106) may be formulated as the water-filling

solutions of

$$\begin{aligned}\widehat{P}_{n,j,e_1}^{BU,T_1} &= \widehat{s}_{n,j}\left[\frac{1}{\left(\xi^B\mu\left(i\right)+2\lambda^{T_1}\left(i\right)\right)\ln 2}-\frac{1}{G_{n,j,e_1}^{BU,T_1}}\right]^+ \\ &= \widehat{s}_{n,j}P_{n,j,e_1}^{BU,T_1} \end{aligned} \tag{4.107}$$

and

$$\begin{aligned}\widehat{P}_{n,j,e_2}^{BU,T_2} &= \widehat{s}_{n,j}\left[\frac{1}{\left(\xi^B\mu\left(i\right)+2\lambda^{T_2}\left(i\right)\right)\ln 2}-\frac{1}{G_{n,j,e_2}^{BU,T_2}}\right]^+ \\ &= \widehat{s}_{n,j}P_{n,j,e_2}^{BU,T_2}, \end{aligned} \tag{4.108}$$

where $i$ is the iteration index of the dual decomposition method. Additionally, the transformed power control variables of the relaying SMCs may be *initially* written as

$$\begin{aligned}\widehat{P}_{n,j,e}^{BR,T_1} &= \widehat{s}_{n,j}\left[\frac{1}{\left(\xi^B\mu\left(i\right)+2\lambda^{T_1}\left(i\right)\right)\ln 2}-\frac{1}{G_{n,j,e}^{BR,T_1}}\right]^+ \\ &= \widehat{s}_{n,j}P_{n,j,e}^{BR,T_1} \end{aligned} \tag{4.109}$$

and

$$\begin{aligned}\widehat{P}_{n,j,e}^{RU,T_2} &= \widehat{s}_{n,j}\left[\frac{1}{\left(\xi^R\mu\left(i\right)+2\nu_{\mathcal{M}(e)}\left(i\right)\right)\ln 2}-\frac{1}{G_{n,j,e}^{RU,T_2}}\right]^+ \\ &= \widehat{s}_{n,j}P_{n,j,e}^{RU,T_2}. \end{aligned} \tag{4.110}$$

Note that the value of $\widehat{s}_{n,j}$ in (4.107)–(4.110) is not yet known. Since the SE attainable for a relaying link is limited by the weaker of the BS-to-RN and RN-to-UE links, there is no need to transmit at a high power on the stronger link, if the other link is unable to support the high SE. Thus, the transformed power control variables provided for the relaying SMC $e$ may be refined by substituting (4.109)–(4.110) into the right-hand side of

$$\widehat{P}_{n,j,e}^{BR,T_1} = \min\left(\widehat{P}_{n,j,e}^{BR,T_1}, \frac{G_{n,j,e}^{RU,T_2}}{G_{n,j,e}^{BR,T_1}}\cdot\widehat{P}_{n,j,e}^{RU,T_2}\right) \tag{4.111}$$

and

$$\widehat{P}_{n,j,e}^{RU,T_2} = \min\left(\widehat{P}_{n,j,e}^{RU,T_2}, \frac{G_{n,j,e}^{BR,T_1}}{G_{n,j,e}^{RU,T_2}}\cdot\widehat{P}_{n,j,e}^{BR,T_1}\right). \tag{4.112}$$

As a result, the tentative estimates of the maximum values that $\widehat{C}_{n,j,e_1}^{BU,T_1}$, $\widehat{C}_{n,j,e_2}^{BU,T_2}$ and $\widehat{C}_{n,j,e}^{BRU}$

can attain are given by

$$\widehat{C}_{n,j,e_1}^{BU,T_1} = \frac{\widehat{s}_{n,j}}{2} \log_2 \left( 1 + \frac{G_{n,j,e_1}^{BU,T_1} \widehat{P}_{n,j,e_1}^{BU,T_1}}{\widehat{s}_{n,j}} \right), \tag{4.113}$$

$$\widehat{C}_{n,j,e_2}^{BU,T_2} = \frac{\widehat{s}_{n,j}}{2} \log_2 \left( 1 + \frac{G_{n,j,e_2}^{BU,T_2} \widehat{P}_{n,j,e_2}^{BU,T_2}}{\widehat{s}_{n,j}} \right), \tag{4.114}$$

and

$$\begin{aligned} \widehat{C}_{n,j,e}^{BRU} &= \frac{\widehat{s}_{n,j}}{2} \log_2 \left( 1 + \frac{G_{n,j,e}^{BR,T_1} \widehat{P}_{n,j,e}^{BR,T_1}}{\widehat{s}_{n,j}} \right) \\ &= \frac{\widehat{s}_{n,j}}{2} \log_2 \left( 1 + \frac{G_{n,j,e}^{RU,T_2} \widehat{P}_{n,j,e}^{RU,T_2}}{\widehat{s}_{n,j}} \right), \end{aligned} \tag{4.115}$$

where the value of $\widehat{s}_{n,j}$ remains unknown. However, it is plausible that for the purpose of maximizing the objective function value, $\widehat{s}_{n,j}, \forall n, j$ will always be given its maximum value $t$, if the single SMC group $j$ is selected for subcarrier block $n$. Thus, the chosen SMC group $j$ for subcarrier block $n$ is given by the group obtaining the highest value of

$$\sum_{j \in \mathcal{G}_n} \left[ \sum_{e_1 \in \mathcal{E}_{n,j}} \widehat{C}_{n,j,e_1}^{BU,T_1} + \sum_{e_2 \in \mathcal{E}_{n,j}} \widehat{C}_{n,j,e_2}^{BU,T_2} \right] + \sum_{e \in \mathcal{E}_{n,j}} \widehat{C}_{n,j,e}^{BRU}. \tag{4.116}$$

where $\widehat{s}_{n,j}$ inside the logarithm functions may be canceled out. Additionally, we can ignore the common positive multiplicative factor of $t$ without affecting the maximization of (4.116). The objective function (4.95) is maximized when choosing this particular group $j$ for subcarrier block $n$, while for the remaining groups associated with the same subcarrier block, we set the optimal values of $\widehat{P}_{n,j' \neq j,e_1}^{BU,T_1*} = \widehat{P}_{n,j' \neq j,e_2}^{BU,T_2*} = \widehat{P}_{n,j' \neq j,e}^{BR,T_1*} = \widehat{P}_{n,j' \neq j,e}^{RU,T_2*} = \widehat{s}_{n,j' \neq j}^{*} = \widehat{C}_{n,j' \neq j,e_1}^{BU,T_1*} = \widehat{C}_{n,j' \neq j,e_2}^{BU,T_2*} = \widehat{C}_{n,j' \neq j,e}^{BRU*} = P_{n,j' \neq j,e_1}^{BU,T_1*} = P_{n,j' \neq j,e_2}^{BU,T_2*} = P_{n,j' \neq j,e}^{BR,T_1*} = P_{n,j' \neq j,e}^{RU,T_2*} = 0$, as these remaining groups are not chosen. For the selected SMC group, we set $\widehat{P}_{n,j,e_1}^{BU,T_1*} = \widehat{P}_{n,j,e_1}^{BU,T_1}$, $\widehat{P}_{n,j,e_2}^{BU,T_2*} = \widehat{P}_{n,j,e_2}^{BU,T_2}$, $\widehat{P}_{n,j,e}^{BR,T_1*} = \widehat{P}_{n,j,e}^{BR,T_1}$ and $\widehat{P}_{n,j,e}^{RU,T_2*} = \widehat{P}_{n,j,e}^{RU,T_2}$.

Consequently, the optimal value of $t$ is given by

$$\begin{aligned} t^* = \Bigg[ & P_C^B + M \cdot P_C^R + \frac{1}{2} \sum_{n=1}^{N} \sum_{j \in \mathcal{G}_n} \xi^B \left( \sum_{e_1 \in \mathcal{E}_{n,j}} P_{n,j,e_1}^{BU,T_1*} + \sum_{e_2 \in \mathcal{E}_{n,j}} P_{n,j,e_2}^{BU,T_2*} \right) \\ & + \frac{1}{2} \sum_{n=1}^{N} \sum_{j \in \mathcal{G}_n} \sum_{e \in \mathcal{E}_{n,j}} \left( \xi^B P_{n,j,e}^{BR,T_1*} + \xi^R P_{n,j,e}^{RU,T_2*} \right) \Bigg]^{-1}. \end{aligned} \tag{4.117}$$

Note that this is possible without knowing the exact value of $\widehat{s}_{n,j}$, since the factor of $\widehat{s}_{n,j}$ may be canceled out, and thus (4.117) is only dependent on the dual variables and on the

SMC group selection.

Having identified the chosen SMC group, we set $\widehat{s}^{*}_{n,j} = t^{*}$ for this selected SMC group corresponding to each subcarrier block $n$, and we have

$$\widehat{C}^{BU,T_1*}_{n,j,e_1} = \frac{t}{2}\log_2\left(1 + G^{BU,T_1}_{n,j,e_1} P^{BU,T_1}_{n,j,e_1}\right), \tag{4.118}$$

$$\widehat{C}^{BU,T_2*}_{n,j,e_2} = \frac{t}{2}\log_2\left(1 + G^{BU,T_2}_{n,j,e_2} P^{BU,T_2}_{n,j,e_2}\right) \tag{4.119}$$

as well as

$$\begin{aligned}\widehat{C}^{BRU*}_{n,j,e} &= \frac{t}{2}\log_2\left(1 + G^{BR,T_1}_{n,j,e} P^{BR,T_1}_{n,j,e}\right) \\ &= \frac{t}{2}\log_2\left(1 + G^{RU,T_2}_{n,j,e} P^{RU,T_2}_{n,j,e}\right),\end{aligned} \tag{4.120}$$

for that selected SMC group. To summarize, given a set of dual variables, the values of power control variables are obtained, resulting in a chosen SMC group, which obtains the SE values for the corresponding subcarrier block. Therefore, all of the primal variables are obtained for a given set of dual variables. Thus, they are jointly optimized.

#### 4.6.3.2 Updating the Dual Variables

From the derivation of the optimal primal variables described in Section 4.6.3.1, we can see that the constraints (4.96)–(4.100) and (4.104)–(4.106) are implicitly satisfied. Therefore, we update the dual variables $\lambda^{T_1}$, $\lambda^{T_2}$ and $\nu_m$ which are associated with the remaining constraints (4.101)–(4.103), respectively. These may be viewed as pricing parameters to ensure that the optimal power control variables satisfy (4.101)–(4.103).

Since the Lagrangian of (4.95)–(4.106) is differentiable w.r.t. the dual variables, at each iteration $i$ of the solution algorithm, the gradient method described in Section 2.6 can be employed for updating these dual variables according to

$$\begin{aligned}\lambda^{T_1}(i) = \Bigg[&\lambda^{T_1}(i-1) - \delta_{\lambda^{T_1}}(i)\cdot \\ &\left(t^{*}\cdot P^{B}_{max} - \sum_{i=1}^{N}\sum_{j\in\mathcal{G}_n}\left[\sum_{e_1\in\mathcal{E}_{n,j}}\widehat{P}^{BU,T_1*}_{n,j,e_1} + \sum_{e\in\mathcal{E}_{n,j}}\widehat{P}^{BR,T_1*}_{n,j,e}\right]\right)\Bigg]^{+}\end{aligned} \tag{4.121}$$

$$\lambda^{T_2}(i) = \left[\lambda^{T_2}(i-1) - \delta_{\lambda^{T_2}}(i)\cdot\left(t^{*}\cdot P^{B}_{max} - \sum_{i=1}^{N}\sum_{j\in\mathcal{G}_n}\sum_{e_2\in\mathcal{E}_{n,j}}\widehat{P}^{BU,T_2*}_{n,j,e_2}\right)\right]^{+} \tag{4.122}$$

$$\nu_m(i) = \left[\nu_m(i-1) - \delta_{\nu_m}(i)\cdot\left(t^*\cdot P^R_{max} - \sum_{i=1}^{N}\sum_{j\in\mathcal{G}_n}\sum_{\substack{e\in\mathcal{E}_{n,j}\\ \mathcal{M}(e)=m}}\widehat{P}^{RU,T_2*}_{n,j,e}\right)\right]^+, \forall m, \tag{4.123}$$

where $\delta_{\lambda^{T_1}}(i)$, $\delta_{\lambda^{T_2}}(i)$ and $\delta_{\nu_m}(i)$ are appropriately chosen step sizes at iteration $i$.

The remaining dual variable, $\mu$, which is associated with (4.106) also has to be updated. However, the constraint given by (4.106) is implicitly satisfied since the value of $t$ is computed from (4.117). Therefore, we opt for the method employed in Section 3.5. We proceed by differentiating the Lagrangian w.r.t $t$ and substituting in the intermediate values of $\widehat{\mathcal{C}}$, $\widehat{\mathcal{P}}$, $\widehat{\mathcal{S}}$ and $t$. Thus, the updated value of $\mu$ is given by

$$\begin{aligned}\mu(i) = t^*\cdot\Bigg(&\sum_{i=1}^{N}\sum_{j\in\mathcal{G}_n}\left[\sum_{e_1\in\mathcal{E}_{n,j}}\widetilde{C}^{BU,T_1*}_{n,j,e_1} + \sum_{e_2\in\mathcal{E}_{n,j}}\widetilde{C}^{BU,T_2*}_{n,j,e_2}\right] + \left[\sum_{e\in\mathcal{E}_{n,j}}\widetilde{C}^{BRU*}_{n,j,e}\right]\\
&+\lambda^{T_1}(i-1)\cdot\left(P^B_{max} - \sum_{i=1}^{N}\sum_{j\in\mathcal{G}_n}\left[\sum_{e_1\in\mathcal{E}_{n,j}}\widetilde{P}^{BU,T_1*}_{n,j,e_1} + \sum_{e\in\mathcal{E}_{n,j}}\widetilde{P}^{BR,T_1*}_{n,j,e}\right]\right)\\
&+\lambda^{T_2}(i-1)\cdot\left(P^B_{max} - \sum_{i=1}^{N}\sum_{j\in\mathcal{G}_n}\sum_{e_2\in\mathcal{E}_{n,j}}\widetilde{P}^{BU,T_2*}_{n,j,e_2}\right)\\
&+\sum_{m=1}^{M}\nu_m(i-1)\cdot\left(P^R_{max} - \sum_{i=1}^{N}\sum_{j\in\mathcal{G}_n}\sum_{\substack{e\in\mathcal{E}_{n,j}\\ \mathcal{M}(e)=m}}\widetilde{P}^{RU,T_2*}_{n,j,e}\right)\Bigg).\end{aligned} \tag{4.124}$$

All primal variables are jointly optimized in Section 4.6.3.1 as the optimal power variables are determined by the related dual variables. This leads to the optimal group selection and rate variables, which then allow us to find the optimal $t$. Given the tentative optima of primal variables, the algorithm proceeds to update the dual variables, which are mostly to ensure that the maximum power constraints are not violated. Using these updated dual variables, the algorithm repeats this process until the objective function value $\widehat{\eta}_E(i)$ at iteration $i$ reaches the predefined convergence threshold, which is given by $|\widehat{\eta}_E(i) - \widehat{\eta}_E(i-1)| < \epsilon$. This process is illustrated in Algorithm 7.

The method presented in Section 4.6.3.1 and Section 4.6.3.2 solves the EEM problem described by (4.95)–(4.106). It may also be invoked for solving the SEM problem of (4.72)–(4.82), while fixing $\mu = 0$ and $t = 1$. This is because the EEM problem considered is simplified to the SEM problem, when we have $\mu = 0$ and $t = 1$.

In contrast to the solution algorithm described in Section 3.5, instead of allocating specific UEs to the subcarriers, we allocate SMC groups to subcarriers in this chapter. How-

**Algorithm 7:** EEM algorithm

**inputs** : All SMC groups, $\mathcal{G}_n, \forall n$, Number of subcarriers, $N$, Number of RNs, $M$
Maximum transmission power of the BS and RNs, $P^B_{max}, P^R_{max}$
Noise power, $N_0$
Fixed power dissipation of the BS and RNs, $P^B_C, P^R_C$
Transmission power dependent power dissipation of the BS and RNs, $\xi^B, \xi^R$
Algorithm convergence tolerance, $\epsilon$
Initial values of the dual variables, $\lambda^{T_1}(1), \lambda^{T_2}(1), \mu(1), \nu_m(1), \forall m$
Step sizes for the dual variables, $\delta_{\lambda^{T_1}}, \delta_{\lambda^{T_2}}, \delta_\mu, \delta_{\nu_m}, \forall m$

**outputs**: The optimal EEM value, $\widehat{\eta}^*_E$

```
1  double EEM
   (G_n, N, M, P^B_max, P^R_max, N_0, P^B_C, P^R_C, ξ^B, ξ^R, ϵ, λ^{T_1}(1), λ^{T_2}(1), μ(1), ν_m(1), δ_{λ^{T_1}}, δ_{λ^{T_2}}, δ_μ, δ_{ν_m})
2  begin
3      i ← 0;
4      η̂_E(0) ← 0;
5      repeat
6          i ← i + 1;
7          for n = 1 to N do
8              foreach E_{n,j} ∈ G_n do
9                  Update the power variables using (4.107), (4.108), (4.109), (4.110);
10                 Get adjusted relaying power variables with (4.111), (4.112);
11                 Compute obtainable SE values from (4.113), (4.114), (4.115);
12             end foreach
13             Select SMC group obtaining the highest value of (4.116);
14             Set remaining groups' power, selection, and SE values to zero;
15         end for
16         Compute the optimal t* value using (4.117);
17         Obtain optimal SE values from (4.118), (4.119), (4.120);
18         Update dual variables using (4.121), (4.122), (4.123), (4.124);
19         η̂_E(i) ← (4.95) · t*;
20     until |η̂_E(i) − η̂_E(i − 1)| < ϵ;
21     return;
22 end
```

ever, we still compute the optimal power values using the water-filling based solutions of (4.107), (4.108), (4.109) and (4.110). Furthermore, owing to the additional total power constraints on the RNs, we have to update additional dual variables in each iteration of Algorithm 7.

## 4.7 Numerical Results and Discussions

This section presents the numerical results obtained, when employing the SEM and EEM algorithms described in Section 4.6 to the MIMO-OFDMA multi-relay cellular network

TABLE 4.1: Simulation parameters used to obtain all results in Section 4.7 unless otherwise specified.

| **Simulation parameter** | **Value** |
|---|---|
| Subcarrier block bandwidth, $W$ [Hertz] | 180k |
| Number of RNs, $M$ | $\{0, 1, 2, 4\}$ |
| Number of subcarriers blocks, $N$ | $\{6, 12, 25, 50, 100\}$ |
| Number of UEs, $K$ | $\{2, 10\}$ |
| Antenna configuration, $(N_B, N_R, N_U)$ | $(4, 4, 2)$ |
| Cell radius, [km] | $\{0.75, 1.25, 1.75, 2.25\}$ |
| Ratio of BS-to-RN distance to the cell radius, $D_r$ | 0.5 |
| SNR gap of wireless transceivers, $\Delta\gamma$ [dB] | 0 |
| Maximum total transmission power of the BS and RNs, $P^B_{max}$ and $P^R_{max}$ [dBm] | $\{0, 10, 20, 30, 40, 50, 60\}$ |
| Fixed power rating of the BS, $P_C^{(B)}$ [Watts] [352, 369] | $32.306N_B$ |
| Fixed power rating of RNs, $P_C^{(R)}$ [Watts] [352, 369] | $21.874N_R$ |
| Reciprocal of the BS power amplifier's drain efficiency, $\xi^{(B)}$ [352, 369] | $3.24N_B$ |
| Reciprocal of the RNs' power amplifier's drain efficiency, $\xi^{(R)}$ [352, 369] | $4.04N_R$ |
| Noise power spectral density, $N_0$ [dBm/Hz] | $-174$ |
| Convergence threshold, $\epsilon$ | $10^{-6}$ |
| Number of channel samples | $10^4$ |

considered. In all cases, the step sizes and the initial values of the dual variables described in Section 4.6.3.2 are empirically optimized to give the optimal objective function value in as few iterations as possible, although the exact analytical method for determining the optimal step sizes and initial values still remains an open issue. In our experience, the algorithms converge within just 10 iterations when carefully chosen step sizes are employed, regardless of the size of the problem. The pertinent simulation parameters are given in Table 4.1. Additionally, the path-loss effect is characterized relying on the method and parameters of [354], where the BS-to-UE and RN-to-UE links are assumed to be non-line-of-sight (NLOS) links, since these links are typically blocked by buildings and other large obstructing objects, while the BS-to-RN links are realistically assumed to be LOS links, as the RNs may be strategically deployed on tall buildings to create strong wireless backhaul links. Furthermore, independently and randomly generated set of UE locations as well as fading channel realizations were used for each channel sample.

The results of a baseline algorithm is also presented to highlight the improved performance obtained from employing the SEM and EEM algorithms. This baseline algorithm consists of a random SMC grouping (RG) selection for each subcarrier block and then equal power allocation (EPA) across all the selected SMCs, and will be termed the RG-EPA algorithm.

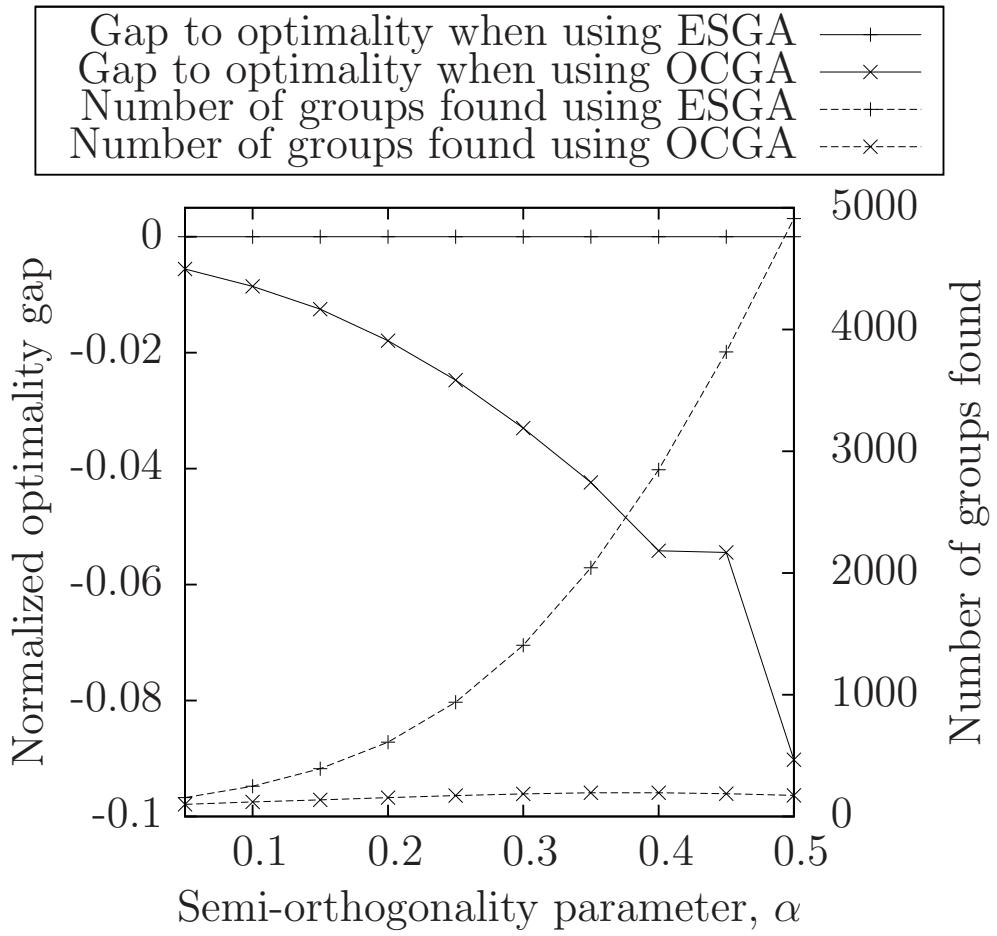


FIGURE 4.11: The optimality gap and total number of SMC groups found when employing the ESGA and OCGA, and using the parameters in Table 4.1 with $N = 6$, $K = 2$, $M = 2$, $P^B_{max} = 20$dBm, $P^R_{max} = 10$dBm and a cell radius of 0.75km.

### 4.7.1 On the Optimality and the Relative Complexity of ESGA and OCGA for Various $\alpha$ Values

Firstly, the behavior of the ESGA and OCGA as a function of $\alpha$ is examined. Note in Fig. 4.11 that since the ESGA is capable of enumerating all possible SMC groupings, which satisfy (4.25) for the corresponding $\alpha$, the optimal SE is attained. The 'normalized optimality gap' is then defined as $(\beta/\beta^*) - 1$, where $\beta^*$ is the optimal SE obtained from employing the ESGA algorithm, and $\beta$ is the SE obtained from any other algorithm. We can see from Fig. 4.11, that the normalized optimality gap of OCGA relative to ESGA is about $0.5\% \sim 1\%$ for the $\alpha$ values considered. However, the number of groups found using ESGA is exponentially increasing with $\alpha$. By contrast, for OCGA, this number is always significantly lower and gradually becomes less than 200, when $\alpha$ increases to 0.5. In fact, the number of groups found by OCGA is reduced to about 5% of that found by ESGA at $\alpha = 0.5$. This demonstrates the viability of using OCGA in the following simulations as a

reduced-complexity near-optimum alternative to ESGA. Under the conditions considered in Fig. 4.11, the optimal EE solution is the same as the optimal SE solution, as detailed in the next subsection. Therefore, as far as EEM is concerned, similar conclusions may be drawn regarding the optimality of the two grouping algorithms.

### 4.7.2 The Variation in Achievable SE and EE for Different Values of $P_{max}^{B}$ and $P_{max}^{R}$

As shown in Fig. 4.12(a), the achievable SE is monotonically increasing with $P_{max}^{B}$ and $P_{max}^{R}$ when using the SEM algorithm. This is not unexpected, since the SEM algorithm optimally allocates all the available power for the sake of achieving the maximum SE. By comparison, we observed from Fig. 4.12(a) and Fig. 4.12(b) that both the achievable SE and EE of the EEM algorithm saturate at some moderate values of $P_{max}^{B}$ and/or $P_{max}^{R}$, which mirrors the trend demonstrated in Fig. 3.6. This is because the EEM algorithm only allocates enough power (that may be lower than the power budget values of $P_{max}^{B}$ and/or $P_{max}^{R}$) for the sake of achieving the maximum EE. On the other hand, the EE performance of the SEM algorithm is severely degraded upon further increasing $P_{max}^{B}$ and/or $P_{max}^{R}$ after its EE performance reaches the peak, as shown in Fig. 4.12(b). This is because the EE metric is a quasiconcave function of the transmit powers – its numerator (i.e. the SE) increases logarithmically with the transmit powers, while its denominator increases linearly with the transmit powers. In fact, the peak EE of the SEM algorithm is attained at $P_{max}^{B} = 40$dBm and $P_{max}^{R} = 40$dBm, as seen in Fig. 4.12(b), and the associated normalized optimality gap is only $-0.074$. By contrast, the achievable EE when using the EEM algorithm also saturates at around $P_{max}^{B} = 40$dBm and $P_{max}^{R} = 40$dBm. Thus, the operating point of $P_{max}^{B} = 40$dBm and $P_{max}^{R} = 40$dBm may strike an attractive balance between SEM and EEM. Of course, the required trade-off may be struck on a case-by-case basis in practical systems. Observe that when $P_{max}^{B}$ and $P_{max}^{R}$ have low/moderate values, the SEM and EEM algorithms share the same solutions of $\mathcal{P}$ and $\mathcal{S}$.

Additionally, the RG-EPA algorithm performs significantly worse in terms of SE when compared to the SEM algorithm, and in terms of EE when compared to the EEM algorithm. Furthermore, the RG-EPA algorithm performs even worse than the SEM algorithm in terms of EE. Although the obtained SE when using the RG-EPA algorithm is, in some cases, higher than the SE obtained when using the EE algorithm, this performance improvement comes at a great cost to the EE performance of the RG-EPA algorithm.

Finally, note that although both the SE of the SEM algorithm, and the EE of the EEM algorithm are non-decreasing as either $P_{max}^{B}$ or $P_{max}^{R}$ is increased, the effect of increasing $P_{max}^{B}$ on the SE or EE is significantly more pronounced, than that of applying the same increase to $P_{max}^{R}$. The intuitive reasoning behind this is that the power available at the BS

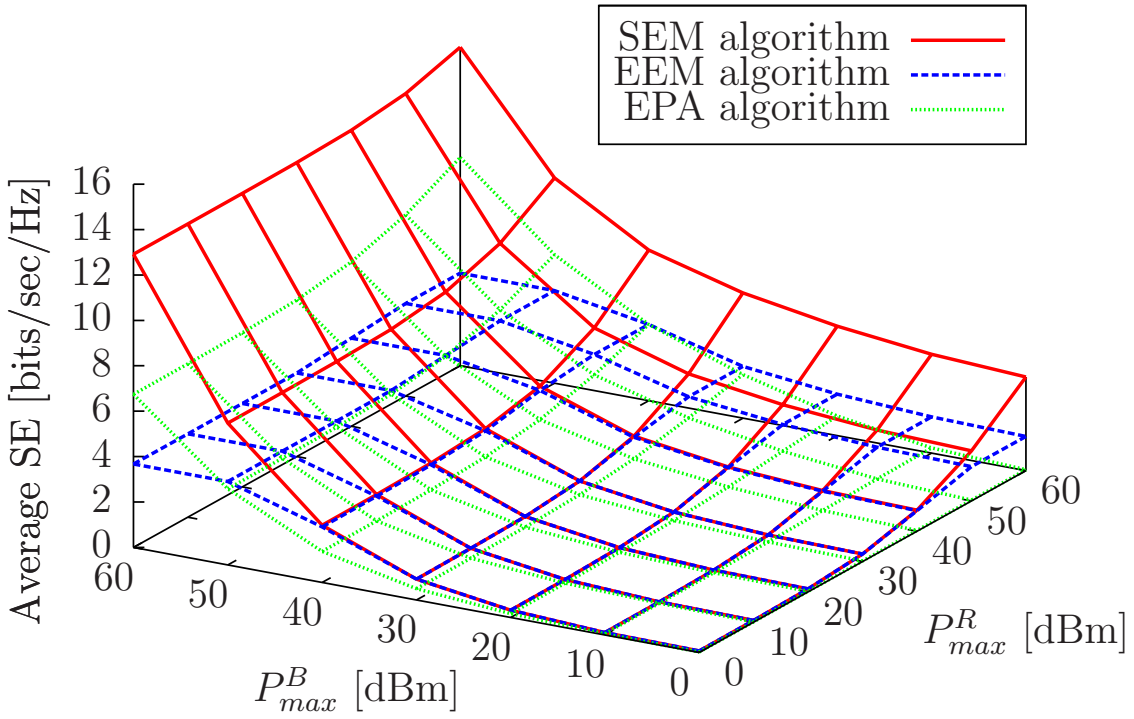


(a) Surface plots of the achievable SE when using the SEM and EEM algorithms.

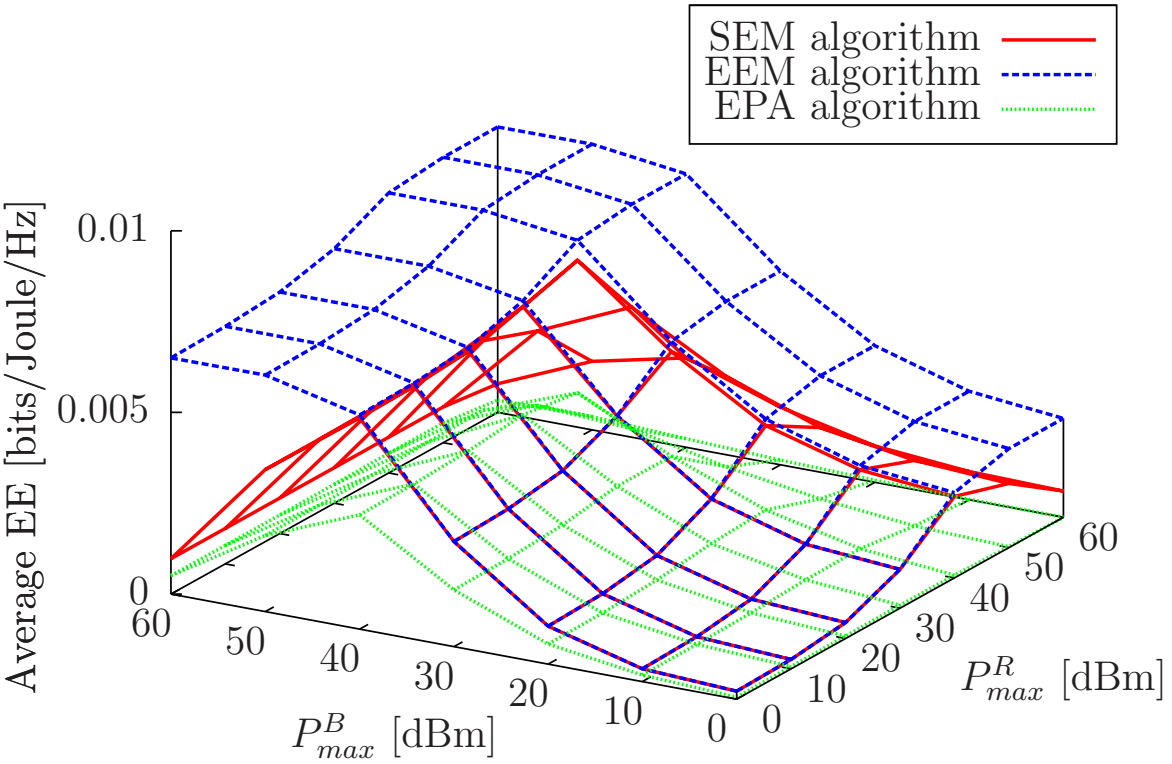


(b) Surface plots of the achievable EE when using the SEM and EEM algorithms.

FIGURE 4.12: The average achievable SE and EE of the SEM, EEM and RG-EPA algorithms upon varying $P^B_{max}$ and $P^R_{max}$. The parameters in Table 4.1 with $N = 6$, $K = 10$, $M = 2$, $\alpha = 0.1$ and a cell radius of 1.75km are used.

has a more pronounced effect on the system's performance, since the direct links and, more importantly, the BS-to-RN links rely on the BS. Therefore, increasing $P_{max}^{R}$ is futile if the BS-to-RN links are not allocated sufficient power to support the RN-to-UE links.

### 4.7.3 The Variation in Achievable SE and EE for Different Values of $M$ and the Cell Radius

Fig. 4.13 illustrates some advantages and disadvantages of employing RNs in the cellular system considered. We observe that the specific low values of the power constraints result in the same solutions for both the SEM and EEM algorithms. This phenomenon was also shown in Fig. 4.12.

As evidenced in Fig. 4.13(a), the attainable SE increases with $M$, which is a benefit of the additional selection diversity, when forming relaying links. However, in contrast to Fig. 3.10, the attainable SE does not increase substantially beyond $M = 2$. In fact, only an increase of 0.1% is attained for the SE, when $M$ is increased from 2 to 4 at a cell radius of 0.75km. On the other hand, the cost in terms of EE is significant (36.4%), as shown in Fig. 4.13(b). This suggests that employing RNs does not constitute an energy-efficient technique, although it increases the SE of a cellular system, which supports the conclusions drawn in Chapter 3. This may be attributed to both the power amplifier inefficiency and to the non-negligible fixed circuit energy dissipation of the RNs. Note furthermore that as in Chapter 3, both the attainable SE and EE are decreasing upon increasing the cell radius as a result of the increased path-loss of all the wireless links. However, this reduction is relatively small between a cell radius of 1.75km and 2.25km. The reason behind this phenomenon is that both the SEM and EEM algorithms will selectively serve the UEs nearer to the BS, so that a similar performance may be attained without suffering from a substantial path-loss. This is also the reason why the gain in SE gleaned by employing RNs at a cell radius of 2.25km seems negligible in Fig. 4.13(a). Once again, the RG-EPA algorithm performs worse both in terms of SE and EE performance.

### 4.7.4 The Achievable SE and EE as a Function of $N$ and $N_B$

Fig. 4.14 illustrates the effect of increasing $N$ and $N_B$ on the attainable SE and EE. Note that in a similar fashion to Fig. 4.13, the SEM and EEM algorithms attain the same solutions in the operating region considered.

Observe from both Figs. 4.14(a) and 4.14(b) that the attainable SE increases upon increasing $N_B$. This is due to the increased attainable spatial degrees of freedom at the BS in the first transmission phase, which allows for more direct transmissions overall. However, the attainable EE increases only slightly, or may even decrease upon increasing $N_B$, due to the

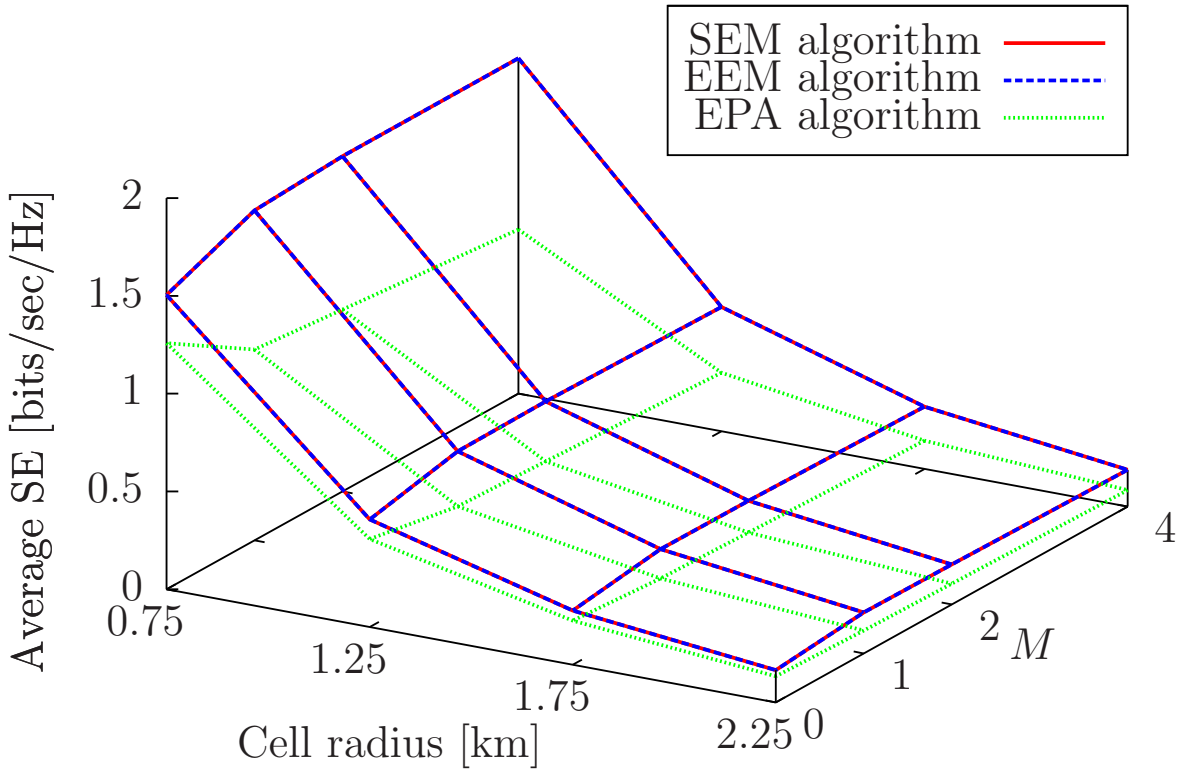


(a) Surface plots of the achievable SE when using the SEM and EEM algorithms.

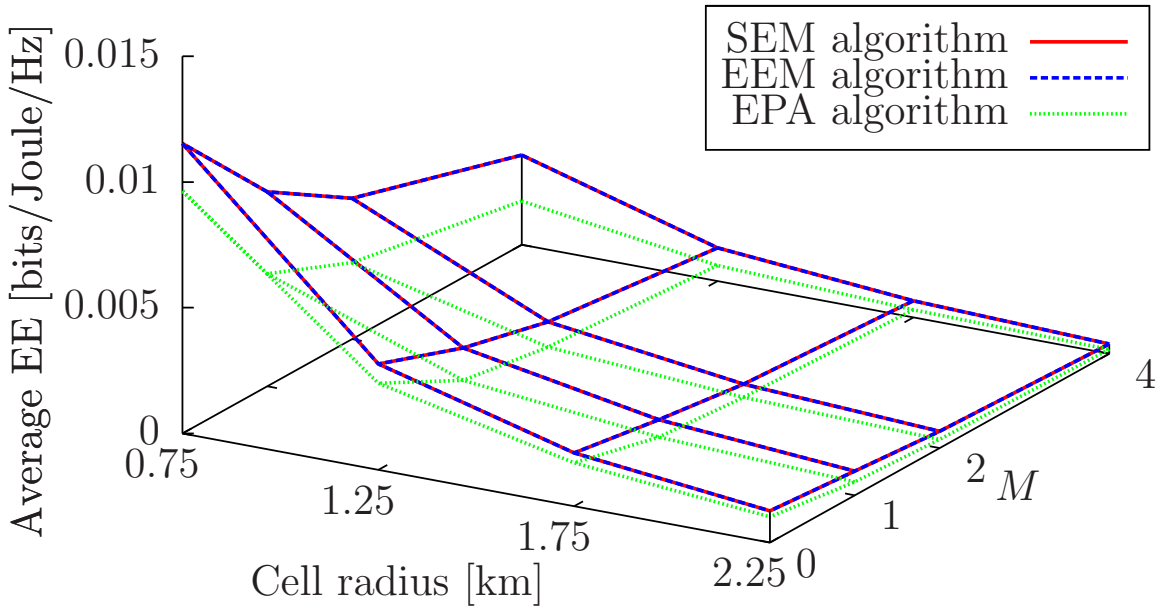


(b) Surface plots of the achievable EE when using the SEM and EEM algorithms.

FIGURE 4.13: The average achievable SE and EE when using the SEM and EEM algorithms, respectively, for varying $M$ and cell radius, and using the parameters in Table 4.1 with $N = 6$, $K = 10$, $\alpha = 0.1$, $P^B_{max} = 20$dBm and $P^R_{max} = 10$dBm.

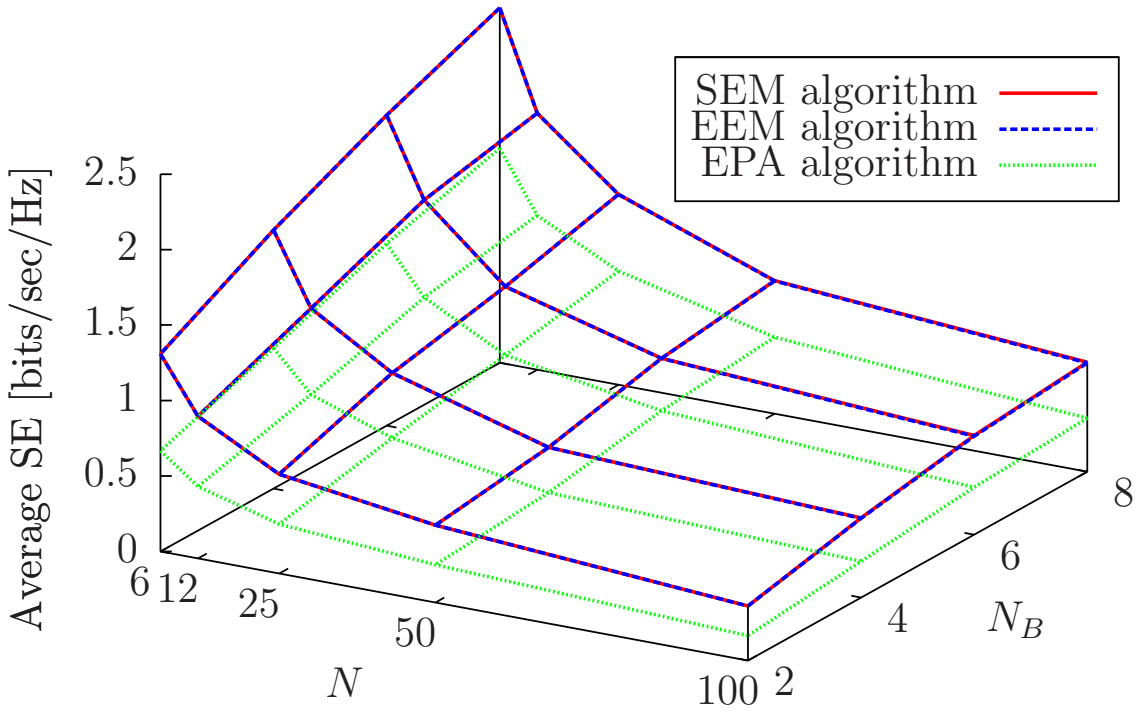


(a) Surface plots of the achievable SE when using the SEM and EEM algorithms.

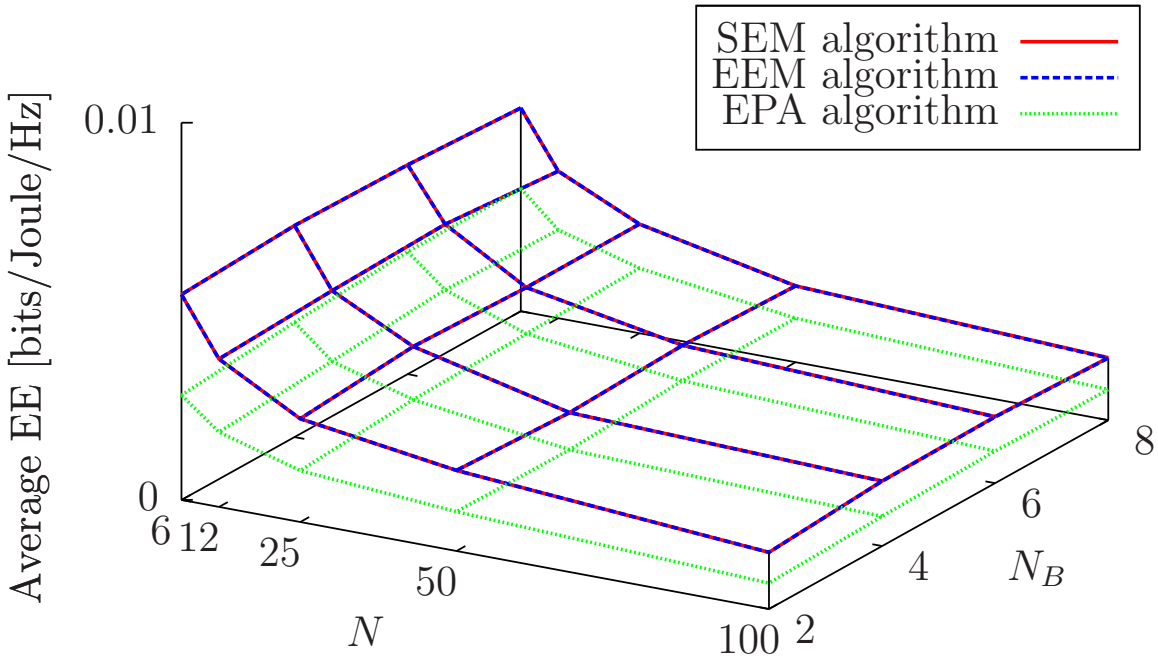


(b) Surface plots of the achievable EE when using the SEM and EEM algorithms.

FIGURE 4.14: The average achievable SE and EE when using the SEM and EEM algorithms, respectively, for varying $N$ and $N_B$, and using the parameters in Table 4.1 with $M = 2$, $K = 10$, $\alpha = 0.1$, $P^B_{max} = 20$dBm, $P^R_{max} = 10$dBm and a cell radius of 0.75km.

higher fixed power costs of supporting additional RF chains. Moreover, both the SE and EE are reduced upon increasing $N$, which suggests that increasing the number of subcarrier blocks does not increase the average efficiency of each block. This is because the power constraints are fixed and thus there is insufficient power for fully exploiting the additional subcarrier blocks. However, note that both total SE and EE do indeed increase upon increasing $N$, which may be explicitly seen upon multiplying the results of Figs. 4.14(a) and 4.14(b) by $NW$. The RG-EPA algorithm performs worse in both cases as expected.

## 4.8 Chapter Summary and Conclusions

In this chapter, firstly a novel transmission protocol based on joint transmit-BF and receive-BF was developed for the multi-relay MIMO-OFDMA cellular network considered. This protocol allows for achieving high-SE performance for the MIMO broadcast network consisting of a BS, multiple RNs and multiple UEs. The associated MIMO channel matrices were mathematically decomposed into multiple MISO channels, which we referred to as SMCs, using receive-BF. By applying ZFBF at the transmitter, the interference between SMC-based concurrent transmissions is completely eliminated, provided that perfect CSI-knowledge is available. For the purposes of obtaining a higher multiplexing gain, the SMCs may be grouped according to the semi-orthogonality criterion. Consequently, a pair of grouping algorithms were proposed, referred to as ESGA and OCGA. The former exhaustively enumerates all of the possible groupings, whereas the latter aims to be a lower-complexity design alternative. Finding the SE-optimal and EE-optimal SMC groupings as well as their associated optimal power control variables were formulated as optimization problems. With the aid of several variable relaxations and transformations, these optimization problems were transformed into concave optimization problems. Thus, the dual decomposition approach was employed for finding the optimal solutions.

We demonstrated that the OCGA constitutes an attractive alternative to ESGA, since it offers a near-optimal performance at a substantially reduced complexity across a range of $\alpha$-values, as summarized in Table 4.2. Furthermore, several numerical results were presented for characterizing the system's attainable SE and EE performance across a wide range of system parameters, such as the transmit power constraints, cell radius, the number of RNs, the number of BS antennas and the number of subcarrier blocks. To summarize, the maximum attainable SE of the system continues to rise as the power constraint on either the BS or RNs is loosened. However, this comes at a cost to EE, whose maximum is attained when roughly $P^B_{max} = 50$dBm and $P^R_{max} = 50$dBm in the scenarios considered. This results mirrors that of Section 3.7, however in this chapter we were also able to demonstrate that the BS's total power constraint has a greater effect on the attainable SE and EE of the system, when compared to the total power constraint of the RNs, which is likely the

TABLE 4.2: Summary of the reduction in complexity achieved versus the suboptimality cost for various values of $\alpha$, as was depicted in Fig. 4.11.

| Semi-orthogonality parameter, $\alpha$ | Suboptimality | Complexity reduction |
|---|---|---|
| 0.05 | 0.6% | 36.1% |
| 0.10 | 0.9% | 52.2% |
| 0.15 | 1.2% | 65.1% |
| 0.20 | 1.8% | 74.6% |
| 0.25 | 2.5% | 81.7% |
| 0.30 | 3.3% | 86.8% |
| 0.35 | 4.2% | 90.5% |
| 0.40 | 5.4% | 93.2% |
| 0.45 | 5.4% | 95.1% |
| 0.50 | 10.0% | 96.5% |

TABLE 4.3: Summary of the attainable gains in SE or EE, when employing their maximization algorithms compared to the RG-EPA algorithm, as depicted in Figs. 4.12 to 4.14.

| Figures | Max. gain in SE | Min. gain in SE | Max. gain in EE | Min. gain in EE |
|---|---|---|---|---|
| Fig. 4.12 | 103.7 | 4.0 | 995.5 | 3.9 |
| Fig. 4.13 | 2.0 | 1.2 | 2.2 | 1.2 |
| Fig. 4.14 | 2.2 | 1.7 | 2.2 | 1.7 |

effect of allowing both direct and relayed transmissions in the transmission protocol. On the other hand, increasing the number of RNs $M$ and the number of subcarrier blocks $N$ in the system negatively affects the attainable SE and EE, which was also confirmed in Section 3.7. However, increasing the number of antennas $N_B$ available at the BS does increase the attainable SE and EE, since these additional antennas provide an increased attainable spatial degrees of freedom at the BS in the first transmission phase. Moreover, we show that our SEM/EEM algorithms perform significantly better than the benchmark RG-EPA algorithm in Table 4.3.

It is important to highlight the differences in the attainable SE and EE values, when increasing either the number $K$ of UEs in the system, the number $N_B$ of antennas at the BS, or the number $M$ of RNs in the system. Since all of these parameters are directly related to the number of antennas in the system, it is expected that an additional selection diversity gain may be gleaned for increasing the attainable SE and EE upon increasing the number of any of these parameters.

As shown in Fig. 3.6, doubling the number of UEs results in a linear SE increase, which mirrors the trend demonstrated in Fig. 4.14. Although the EE does increase upon increasing $K$ in Fig. 3.6, the EE of Fig. 4.14 decreases as a result of the additional RF chains required at the BS, which were not present, when obtaining the results in Fig. 3.6.

On the other hand, increasing the number of RNs in the system only results in a marginal SE increase, as demonstrated in Figs. 3.10 and 4.13, while the EE erosion becomes severe.

Therefore, we can conclude that although increasing the aforementioned parameters may increase the SE, their effects on the EE are not equivalent.

Chapter 5

# Spectral/Energy Efficient Resource Allocation for MIMO-Aided Multi-Cell Networks

## 5.1 Introduction

Chapter 4 considered EEM in the context of a cellular system, which contained both multiple RNs as well as UEs, and expanded upon the system model of Chapter 3 by employing multiple antenna aided network nodes. A transmission protocol based on both BF and on the grouping of SMCs was presented in Section 4.4. However, in order to avoid interference between the BS's and RNs' transmission, the network had to coordinate its transmissions for the sake of reducing the total achievable spatial multiplexing gain. On the other hand, realistic cellular networks are heterogeneous and multi-cellular, hence leading to severe CCI, especially, when the networks aim for fully exploiting the precious wireless spectrum by relying on a unity frequency reuse factor [371]. Thus, a distributed method of coordinating the system's transmissions for the sake of avoiding the excessive interference is required. Furthermore, the system's EE remains still a major concern [10] and the optimization tools employed in Chapters 3 and 4 have to be invoked for maximizing the system's EE. Against this backdrop, in this chapter we aim for maximizing the EE of the DL of a DF relay-aided MIMO-OFDMA multi-cell network that employs the technique of IA.

IA has been advocated as a viable technique of managing the UL co-channel interference of multi-cell networks [372, 373]. Explicitly, IA is suitable for the UL, since the number of receive antennas at the BS is typically higher than the number of transmit antennas at each UE. Thus, the potentially higher number of signal dimensions available at the receiver can be exploited for aligning the CCI into a predetermined interference subspace, so that

the BS can receive the transmissions of its own UEs without CCI. However, this is not feasible in the DL, since each UE has access to a low number of receive dimensions. This challenge was successfully tackled by the DL transmission scheme of [374], which relies on specifically designing transmit precoding matrices for reducing the number of transmit dimensions at the BSs, thus facilitating DL IA at the UEs. In contrast to other IA techniques, such as [375–379], the technique presented in [374] does not require cooperation among the BSs for exchanging CSI, and IA is accomplished distributively. Furthermore, this technique facilitates IA in systems relying on arbitrary antenna configurations with the aid of frequency- or time-extension, which is capable of substantially expanding the total number of transmit and receive dimensions in a multicarrier system such as OFDMA. In [380], the technique of [374] was generalized to an arbitrary number of BSs and UEs, where each of them is equipped with an arbitrary number of antennas. Furthermore, the authors of [380] employed the semi-orthogonal user selection scheme of Yoo *et al.* [324] for maximizing the achievable SE. However, relaying was not considered in [380] and each UE was limited to receiving a single spatial stream.

The EE metric employed in Chapters 3 and 4 has also been utilized in [201,231,330–332,347]. The authors of [231] considered EEM of both the UL and the DL of a cellular network, while providing both the optimal solution method and a lower-complexity heuristic method. However, the effects of interference were not quantified in the system model of [231], since only a single cell was considered. Additionally, no relaying was employed. In [201], EEM was performed in a multi-cell setting, where the CCI was eliminated with the aid of BS cooperation [5] and ZFBF. However, the authors of [201] have not considered the benefits of multiple antenna aided nodes or relaying. As a further advance, the EE of a relay aided system was considered in [347], where the objective function of the optimization problem considered was formulated by incorporating both the SE and the energy dissipated. Nevertheless, these two metrics must be appropriately weighted, which is still an open challenge. Thus, the EE metric was not formally optimized.

The optimization problem considered in this chapter is formulated by maximizing the average EE of the system, which is given by a weighted sum of the fractional terms quantifying each cell's EE. Thus, it is possible to use the primal decomposition approach detailed in Section 2.7 for initially decomposing the problem into a single subproblem for each BS, requiring them to maximize each of their own cell's EE. Thus, each BS individually solves their own EEM problem without having to communicate with each other. The individual subproblems can then be converted into a concave maximization form using the Charnes-Cooper transformation of Sections 2.4.3.5, 3.5 and 4.6, so that the system can benefit from the associated low complexity solution method compared to other methods, as exemplified in Section 3.7.

The existing literature, which is most similar to the work presented in this chapter is that

of Suh *et al.* [372, 374] and of Yang *et al.* [380]. Suh *et al.* [372, 374] created IA-based transmission protocols for both the UL and DL of a cellular network. However, specific values were employed both for the number of BS and UE antennas, as well as both for the number of BSs and UEs in the system. Thus, the protocols cannot be readily generalized to a network of an arbitrary size and antenna configuration. On the other hand, Yang *et al.* [380] devised an IA-based transmission protocol for the DL of a cellular network of an arbitrary size and antenna configuration, although each UE was limited to receiving only a single data stream. Furthermore, Yang *et al.* [380] conceived a beneficial method for selecting which UEs to serve. In contrast to these existing works, we remove the restriction imposed on the number of UEs in the system and we support an arbitrary antenna configuration. Furthermore, we do not restrict the number of data streams that each UE can receive. However, the most notable difference is that we also invoke relaying for improving the system's SE and EE. Naturally, our transmission protocol has been designed with relaying in mind.

Let us now elaborate further by classifying the CCI as intra-cell interference (ICI) and OCI. In the DL considered, the former describes the interference that a RN or UE may receive from the BS within its own cell, where multiple concurrent transmissions are also intended for other RNs or UEs, while the latter describes the interference originating from sources located in other cells.

### 5.1.1 Chapter Preliminaries

IA was first introduced in [381–383] and it was further popularized in [384, 385]. In [385], Cadambe *et al.* described the main concept of IA and established the attainable degrees of freedom (DoF), when employing IA for completely avoiding interference in a network supporting three user-pairs as depicted in Fig. 5.1.

Three beneficial approaches conceived for interference management are described in [385], depending on the relative strength of the interference compared to the desired signal. If the interference is strong, it is possible to decode it and then, given the knowledge of the interference, distinguish the desired signal. Weak interference may simply be treated as noise. If the interference strength is comparable to the desired signal's strength, the traditional approach has been to orthogonalize the signals in the space-, time-, frequency- or code-domain. Thus, the attainable DoF per user in an example system with $K$ user-pairs scales with $1/K$ through orthogonalization. The principle of IA is that instead of judiciously partitioning the wireless resources amongst all users (often termed as orthogonalization), each user aligns his/her transmissions into a predetermined subspace, referred to as the interference subspace, at all the other receivers, so that the remaining subspace at all receivers becomes free of interference. Thus, the attainable DoFs in a system supporting $K$ user-pairs is $K/2$

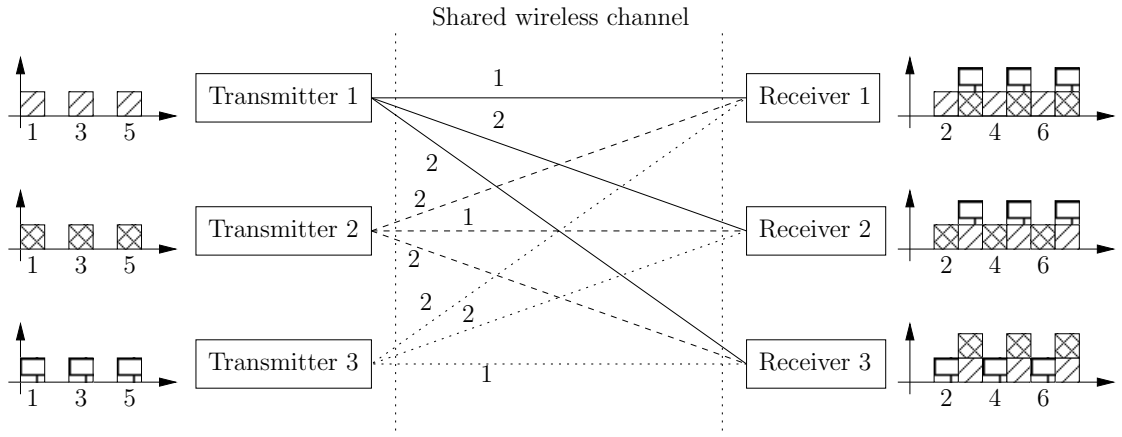


FIGURE 5.1: This illustrates how IA can be achieved via delay offsets. The propagation delay between each transmitter and their associated receiver is only 1 unit, whereas to other receivers, the delay is 2 units. Thus, each receiver is able to receive the desired signal free from interference, while all the interference is contained in the odd-index time slots.

when employing IA, instead of $1/K$ obtained through orthogonalization [385]. This becomes highly favorable, as $K$ increases.

A simple example is provided in Fig. 5.1, where each transmitter attempts to convey its data to their corresponding receivers without interfering with the transmissions of the other transmitters. Due to the differences in the propagation delay between different transmitter-receiver pairs, each transmitter may simply transmit during the odd-index time slots. Each receiver is then able to receive the desired data during the even-index time slots, while all interference is contained in the odd-index time slots. Thus, each receiver is able to receive useful data 1/2 of the time, which results in an achievable DoF per user of 1/2.

A more complex situation is illustrated in Fig. 5.3, which depicts users applying BF to align the interference signals into a subspace distinct from their desired signals. For example, let us assume that each transmitter is equipped with two antennas, while each receiver has access to five antennas, and examine how receiver 1 aligns the interference signals. Naturally, the other receivers can follow a similar process to achieve IA. The MIMO channel matrices associated with the links between transmitters 1, 2 and 3, to receiver 1 may be respectively written as $\mathbf{H}_{1,1}$, $\mathbf{H}_{2,1}$ and $\mathbf{H}_{3,1}$, which are each elements of $\mathbb{C}^{5\times 2}$. The channel matrices associated with the interference sources ($\mathbf{H}_{2,1}$ and $\mathbf{H}_{3,1}$) may be concatenated to form an interference channel matrix denoted by

$$\widehat{\mathbf{H}} = [\mathbf{H}_{2,1}|\,\mathbf{H}_{3,1}] \in \mathbb{C}^{5\times 4}. \tag{5.1}$$

The SVD, as exemplified in Fig. 5.2, is employed for finding the left nullspace of $\widehat{\mathbf{H}}$. It can be readily verified that $\widehat{\mathbf{H}}$ is guaranteed to have at least a one dimensional left nullspace corresponding to the rightmost column vector in $\mathbf{U}$, which is denoted as $\mathbf{u}_5 \in \mathbb{C}^{5\times 1}$. This is

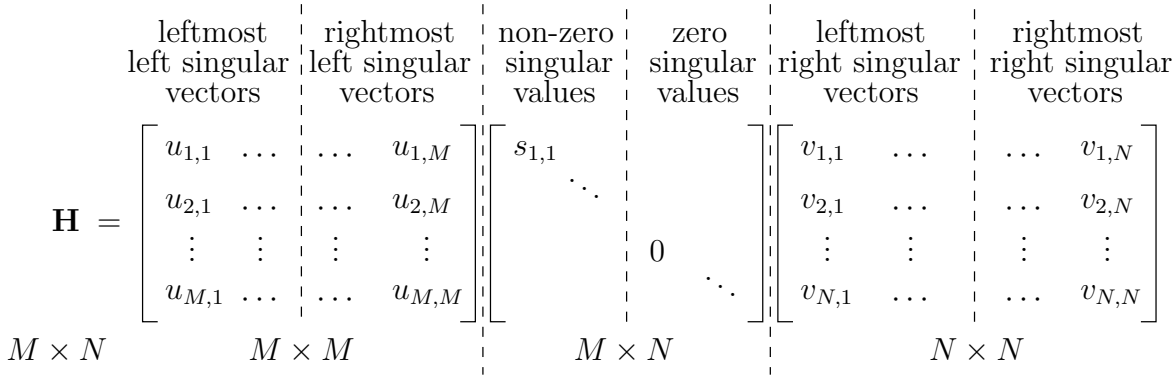


FIGURE 5.2: An illustration of the structure of the SVD. The leftmost left and right singular vectors correspond to the non-zero singular values, while the rightmost left and right singular vectors correspond to the zero singular vectors. Therefore, the rightmost left singular vectors span the left nullspace of $\mathbf{H}$.

a vector in both the left nullspace of $\mathbf{H}_{2,1}$ and the left nullspace of $\mathbf{H}_{3,1}$. In other words, if $\mathbf{u}_5$ is used as the receive beamformer weight-vector for receiver 1, then we have $\mathbf{u}_5^{\mathrm{H}}\mathbf{H}_{2,1} = \mathbf{u}_5^{\mathrm{H}}\mathbf{H}_{3,1} = \mathbf{0}$ and the interference emanating from transmitters 2 and 3 is completely avoided. On the other hand, typically we have $\mathbf{u}_5^{\mathrm{H}}\mathbf{H}_{1,1} \neq \mathbf{0}$ and, given that transmitter 1 appropriately designs its transmit beamformer weights, receiver 1 becomes capable of decoding its desired signal. This process may be repeated at the other receivers to achieve complete IA. The same IA technique will be employed in Section 5.3.

### 5.1.2 Novel Contributions

As stated above, the aim of this chapter is to formally optimize the EE of a multi-relay MIMO-OFDMA cellular system by intelligently assigning the available power and frequency resources, when employing both transmit and receive BF. A concise list of our novel contributions is as follows.

- We evaluate the EEM of IA employed in a realistic MIMO-OFDMA system involving multiple cells, multiple relays and multiple users. Although EEM has been studied intensely in recent years [201, 231, 347], these contributions typically consider single cells providing coverage without the assistance of relaying, or do not exploit the benefits of multiple antenna aided transceivers. Additionally, although IA was employed recently in [375, 386–389], these contributions focus on user-pair networks, rather than on multi-user cellular networks and the associated challenges of implementing IA require further research in the latter scenario. More importantly, previous contributions typically aim for investigating its SE benefits, while the achievable EE of using IA-based protocols has not been explored at all. Green communications has become increasingly important, but the quantitative benefits of IA have not been documented in the context of energy-efficient communications. Therefore, in this chapter we seek to deepen the research community's

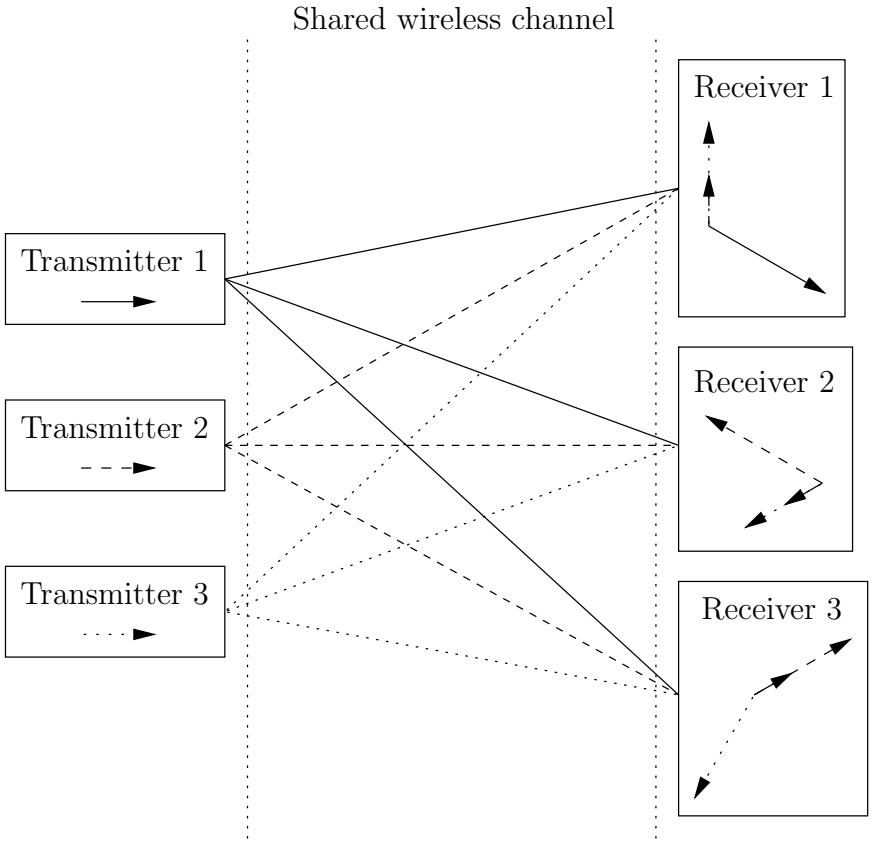


FIGURE 5.3: A network supporting three user-pairs. Each transmitter attempts to communicate with its corresponding receiver. Through the use of IA, each receiver is able to distinguish its intended signal from the overlapping interference signals.

understanding of IA from an EE perspective. Furthermore, a more realistic multi-cell MIMO-OFDMA relay-aided network is considered in this chapter, where multiple UEs are supported by each BS and multiple RNs. Therefore, the system model considered inevitably becomes challenging. As a beneficial result, the protocols and solutions provided in this chapter can be more readily applied to real network scenarios, when compared to the existing IA literature, which focuses only on the $K$-user interference network. In contrast to our previous contributions [330–332], this chapter investigates a multiple antenna aided multi-cell system. Although a multiple antenna assisted system was also studied in our previous contribution [332], only a single macrocell was considered and no IA was employed for avoiding the ICI imposed by both the simultaneously transmitting BS and RNs.

- We provide a sophisticated generalization of the IA protocol considered in [374]. Explicitly, in contrast to [374], the proposed IA protocols account for three cells, for an arbitrary number of UEs in each cell, for an arbitrary antenna configuration and for simultaneous direct as well as relay-aided transmissions. This is accomplished through the careful design of precoding-, transmit- and receive- beamforming matrices in order to ensure that IA is achieved. In particular, the number of guaranteed spatial dimensions available at

the BSs, RNs and UEs must be judiciously chosen. Furthermore, we conceive of two transmission protocols in this chapter, which may be implemented distributively at each BS. The first protocol is termed as full-IA, which invokes IA for avoiding the interference arriving from all transmitters. This is the intuitive choice, as advocated by the existing literature [372, 374, 390] highlighting its benefits in terms of achieving the optimal DoF. For example, it was also employed in [374], but for a simpler system model having no RNs. The second protocol proposed is unlike that of [374] and it is termed as partial-IA, which only aims for avoiding the ICI using IA, while ignoring the effect of OCI when making scheduling decisions. The partial-IA protocol therefore reduces the computational burden of having to estimate the DL CSI of the other-cell channel matrices at the receivers, albeit this might be expected to reduce the system's performance due to neglecting the OCI. We compared the performance of these two protocols and found that, as a surprise, the reduced-complexity partial-IA protocol is potentially capable of achieving a higher EE than the full-IA protocol. Explicitly, the partial-IA protocol achieves a higher EE, since more simultaneous transmissions may be scheduled due to its relaxed constraint on the number of transmit dimensions available. Furthermore, in contrast to the protocol proposed in [380], ours is a two-phase protocol, which is specifically designed for relay-aided networks and does not limit the number of spatial streams available to each UE.

- Employing the BF matrices calculated from either the full-IA or partial-IA protocols results in a list of SMCs as in Chapter 4, which correspond to the specific data streams that the BSs can choose to support. Finding the optimal SMCs as well as the optimal power control variables associated with these optimal SMCs is formally defined as a network-wide optimization problem. Unlike in our previous work [330–332], we decompose the network-wide multi-cell optimization problem in order to formulate a subproblem for each BS using the technique of primal decomposition [339], thus eliminating the need for the high-overhead backhaul-aided message passing amongst the BSs. Each of these subproblems is then converted into a convex form with the aid of various variable relaxations and transformations, which can then be optimally and distributively solved using the dual decomposition and subgradient methods of [339].

### 5.1.3 Chapter Organization

The organization of this chapter is as follows. We introduce our system model in Section 5.2 and describe the proposed transmission protocols in Section 5.3. Subsequently, the EEM optimization problem considered is formulated in Section 5.4, where the solution method is developed as well. Our numerical results along with our further discussions are presented in Section 5.5. Finally, our summary is presented in Section 5.6.

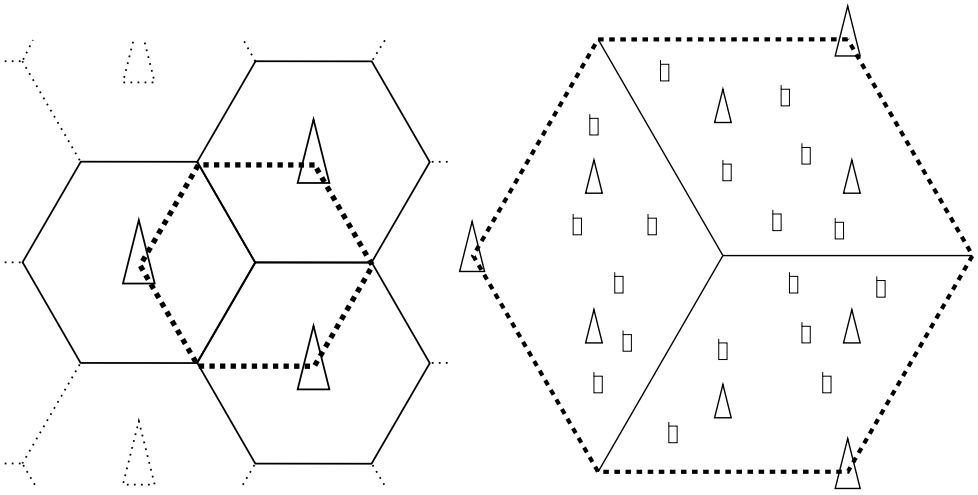

FIGURE 5.4: A multi-cell system is depicted on the left. Each cell is divided into three sectors, and one sector from each of the three neighboring cells are highlighted. This highlighted region is termed an OCI region. Through the use of directional antennas, it is assumed that the main source of OCI is caused when the neighboring BSs simultaneously transmit to a receiver located in its associated OCI region. On the right is a close-up view of the OCI region, with three BSs at the vertices of its perimeter. Furthermore, each sector is supported by two RNs and provides coverage for six UEs in this example.

## 5.2 System Model

In this chapter, a multi-cell DL MIMO-OFDMA network, relying on a radical unity frequency reuse factor is considered. The ubiquitous OFDMA technique is employed for avoiding the severe frequency-selective fading encountered in wideband communication systems. Additionally, OFDMA allows for transmission symbol extensions in the frequency-domain [374], which are required by the proposed IA-based transmission protocol described in Section 5.3.

As depicted in Fig. 5.4, each macrocell is divided into three sectors, and it is assumed that the employment of directional antennas and the NLOS path-loss attenuates the interference power, with the exception of the OCI received from the first tier of interfering cells and the ICI from the serving BS and RNs of each macrocell. Therefore, we may focus our attention on the central region seen at the left of Fig. 5.4, which we term as an OCI region. Thus, each DL transmission within an OCI region is subjected to OCI from two macrocells. Furthermore, each 120°-sector of Fig. 5.4 is supported by $M$ RNs, which are located at a fixed distance from its associated BS and evenly spaced within the sector, as seen at the right of Fig. 5.4. The ratio of the BS-RN distance to the cell radius is denoted by $D_r$. Additionally, $K$ UEs are uniformly distributed within each 120°-sector. The system has access to $L$ OFDMA subcarriers, each characterized by a wireless bandwidth of $W$ Hertz. The BSs, DF RNs, and UEs are respectively equipped with $N_B$, $N_R$ and $N_U$ antennas. It is assumed that all BSs and RNs are synchronized, and that the transceivers employ complex-valued symbol constellations to convey their data.

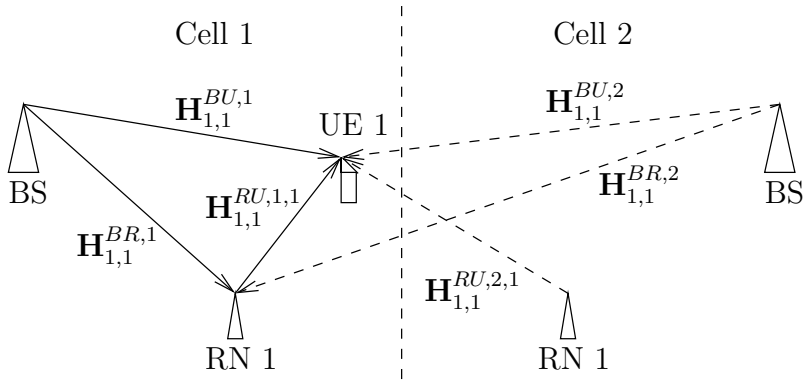


FIGURE 5.5: An illustration of the links that the channel matrices are associated with.

For each subcarrier $l \in \{1, \cdots, L\}$, the complex-valued channel matrix associated with the wireless link spanning from the BS of macrocell $n' \in \{1, 2, 3\}$ to RN $m \in \{1, \cdots, M\}$ belonging to macrocell $n \in \{1, 2, 3\}$ is denoted by $\mathbf{H}_{n,m}^{BR,l,n'} \in \mathbb{C}^{N_R \times N_B}$. The channel matrix associated with the link spanning from the BS of macrocell $n'$ to UE $k \in \{1, \cdots, K\}$ and belonging to macrocell $n$ on subcarrier $l$ is denoted by $\mathbf{H}_{n,k}^{BU,l,n'} \in \mathbb{C}^{N_U \times N_B}$. In this chapter, superscript indices refer to the transmitter, while subscript indices refer to the receiver. Additionally, a prime symbol $'$ refers to a potentially interfering transmission source. Furthermore, the channel matrix associated with the link between RN $m'$ belonging to macrocell $n'$ and UE $k$ belonging to macrocell $n$ on subcarrier $l$ is denoted by $\mathbf{H}_{n,k}^{RU,l,n',m'} \in \mathbb{C}^{N_U \times N_R}$. All channel matrices are assumed to have a full rank, as is often the case for wireless DL channels. For simplicity, the channel matrices associated with the same transceivers are combined across subcarriers to give the block-diagonal channel matrices $\mathbf{H}_{n,m}^{BR,n'} \in \mathbb{C}^{LN_R \times LN_B}$, $\mathbf{H}_{n,k}^{BU,n'} \in \mathbb{C}^{LN_U \times LN_B}$ and $\mathbf{H}_{n,k}^{RU,n',m'} \in \mathbb{C}^{LN_U \times LN_R}$, respectively. For example, we have

$$\mathbf{H}_{n,m}^{BR,n'} := \begin{bmatrix} \mathbf{H}_{n,m}^{BR,1,n'} & \mathbf{0} & \mathbf{0} \\ \mathbf{0} & \ddots & \mathbf{0} \\ \mathbf{0} & \mathbf{0} & \mathbf{H}_{n,m}^{BR,L,n'} \end{bmatrix}. \tag{5.2}$$

The links that these channel matrices are associated with are illustrated in Fig. 5.5. The channel matrices account for both the small-scale frequency-flat Rayleigh fading, as well as the large-scale path-loss between the corresponding transceivers. In this system model, the transceivers are either stationary or moving sufficiently slowly for ensuring that the channel matrices can be considered time-invariant for the duration of a scheduled transmission period. However, the channel matrices may evolve between each transmission period. Furthermore, it is assumed that the transceivers' antennas are spaced sufficiently far apart for ensuring that the associated transmissions experience i.i.d. small-scale fading, which are drawn from complex i.i.d. normal distributions having a zero mean and a unit variance. The system uses TDD and hence the associated channel reciprocity may be exploited for

predicting the CSI of the slowly varying DL channels from the received UL signal. Furthermore, by assuming the availability of low-rate error-free wireless backhaul channels, the CSI associated with the wireless intra-cell RN-UE links may be fed back to the particular BS in control, so that it may make the necessary scheduling decisions.

Additionally, each receiver suffers from complex-valued AWGN having a power spectral density of $N_0$. Due to both regulatory and safety concerns, the maximum instantaneous transmission power of each BS and each RN is limited, which are denoted by $P^B_{max}$ and $P^R_{max}$, respectively. We stipulate the idealized simplifying assumption that OFDMA modulation and demodulation is performed perfectly for all the information symbols.

In contrast to the single cell system models of Chapter 3 and Chapter 4, the model presented above is that of a multi-cell network. Unlike in the system model of Chapter 3, in this chapter the UEs may be supported by RNs positioned anywhere in the cell, rather than only by the specific RN that is located geographically closest to it. Furthermore, in contrast to the system model of Chapter 3, MIMO transceivers are employed in this chapter.

## 5.3 Transmission Protocol Design

Each BS may convey information to the UEs by either using a direct BS-UE link, or by utilizing a RN to create a two-hop BS-RN and RN-UE link, which requires two transmission phases. Thus, each transmission period is split into two halves. Due to the simultaneous transmissions from multiple sources, both the level of ICI and OCI in the network is likely to be detrimental to the achievable EE. In order to avoid both types of interference, the technique of IA is employed, which requires the careful design of both the transmit BF matrices of the BSs and of the RNs, as well as the receive BF matrices of the RNs and of the UEs. As relaying links may be utilized in this system, the design of these matrices is different for the two transmission phases. Hence they are described separately in the following. Additionally, both the full-IA and partial-IA protocols will be described side-by-side. To elaborate a little further, the full-IA protocol aims for completely avoiding both the ICI and OCI in both the first and second transmission phases by employing IA, while the partial-IA protocol only aims for avoiding the ICI in both transmission phases, thus dispensing with estimating the OCI channel matrices at each receiver.

### 5.3.1 Beamforming Design for the First Phase

In the first phase, only the BSs are transmitting to both the RNs and the UEs. Therefore, the only source of interference is constituted by the neighboring BSs associated with the same OCI region, which may be avoided by carefully designing the transmit BF matrices

at the BSs, as well as the receive BF matrices at the RNs and the UEs in a distributive manner. Initially, a trasmit precoding matrix, denoted by $\mathbf{A}^{B,n,T_1} \in \mathbb{C}^{LN_B \times S^{B,T_1}}$, is randomly-generated for each BS $n$, where $S^{B,T_1}$ is the number of symbols transmitted by each BS during the first phase, which is accurately defined in Section 5.3.1.3. The matrix $\mathbf{A}^{B,n,T_1}$ has a full column rank and its entries are complex-valued. These transmit precoding matrices are invoked for reducing the number of transmit dimensions for each BS from $LN_B$ to $S^{B,T_1}$, thus facilitating IA at the receivers. Furthermore, the columns of these transmit precoding matrices are normalized so that the power assigned to each transmission remains unaffected. By employing these transmit precoding matrices, the precoded channel matrices of the first phase are given by

$$\widetilde{\mathbf{H}}_{n,m}^{BR,n',T_1} := \mathbf{H}_{n,m}^{BR,n'} \mathbf{A}^{B,n',T_1} \in \mathbb{C}^{LN_R \times S^{B,T_1}} \tag{5.3}$$

and

$$\widetilde{\mathbf{H}}_{n,k}^{BU,n',T_1} := \mathbf{H}_{n,k}^{BU,n'} \mathbf{A}^{B,n',T_1} \in \mathbb{C}^{LN_U \times S^{B,T_1}}, \tag{5.4}$$

respectively for the BS-RN and BS-UE links.

We now define $S^R$ and $S^U$ as the minimum number of receive dimensions at each RN and each UE, respectively, which are chosen by the network operator. Furthermore, only the specific values of $S^R$ and $S^U$ along with the number of antennas at each network node and the number of available subcarrier blocks affect the feasibility of IA, while $M$ and $K$ have no effect.

#### 5.3.1.1 Full-IA Receiver Design

In order to completely avoid the interference arriving from the neighboring BSs during the first phase, it is necessary for the precoded OCI channel matrices given by (5.3) and (5.4), to have intersecting left nullspaces. Firstly, the precoded OCI channel matrices may be concatenated for forming the interference matrices, for example

$$\widehat{\mathbf{H}}_{1,m}^{R,T_1} := \left[ \widetilde{\mathbf{H}}_{1,m}^{BR,2,T_1} \middle| \widetilde{\mathbf{H}}_{1,m}^{BR,3,T_1} \right] \in \mathbb{C}^{LN_R \times 2S^{B,T_1}} \tag{5.5}$$

for RN $m$ in macrocell 1, and

$$\widehat{\mathbf{H}}_{2,k}^{U,T_1} := \left[ \widetilde{\mathbf{H}}_{2,k}^{BU,1,T_1} \middle| \widetilde{\mathbf{H}}_{2,k}^{BU,3,T_1} \right] \in \mathbb{C}^{LN_U \times 2S^{B,T_1}} \tag{5.6}$$

for UE $k$ in macrocell 2. Fig. 5.6 illustrates which links are associated with the OCI channel matrices. These precoded OCI matrices are associated with a left nullspace of at least $S^R$ and $S^U$ dimensions if

$$LN_R - 2S^{B,T_1} \geq S^R \tag{5.7}$$

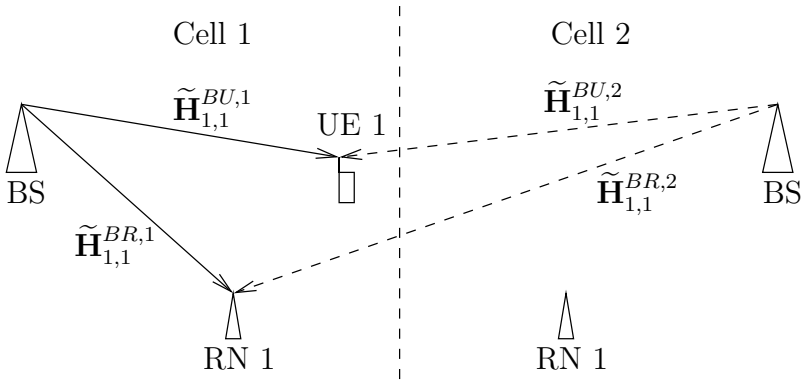


FIGURE 5.6: An illustration of the relevant channel matrices during the first transmission phase of the full-IA protocol. The solid arrows indicate the direct channels to the RN and UE of Macrocell 1, while the dashed arrows indicate the OCI channels.

and

$$LN_U - 2S^{B,T_1} \geq S^U, \tag{5.8}$$

respectively. Therefore, to guarantee $S^R$ and $S^U$ receive dimensions at the RNs and UEs, respectively, $S^{B,T_1}$ is derived as

$$S^{B,T_1} = \left\lfloor \min\left( \frac{LN_R - S^R}{2}, \frac{LN_U - S^U}{2} \right) \right\rfloor. \tag{5.9}$$

The intersecting left nullspace may be found using the SVD on $\widehat{\mathbf{H}}_{n,m}^{R,T_1}$ and $\widehat{\mathbf{H}}_{n,k}^{U,T_1}$, for RN $m$ and UE $k$ in macrocell $n$, respectively. For example, the SVD of $\widehat{\mathbf{H}}_{n,m}^{R,T_1}$ may be written as

$$\mathbf{U}_{n,m}^{R,T_1} \mathbf{S}_{n,m}^{R,T_1} \left(\mathbf{V}_{n,m}^{R,T_1}\right)^{\mathrm{H}}, \tag{5.10}$$

where $\mathbf{U}_{n,m}^{R,T_1} \in \mathbb{C}^{LN_R \times LN_R}$ is the left singular matrix containing, as its columns, the left singular vectors of $\widehat{\mathbf{H}}_{n,m}^{R,T_1}$, while $\mathbf{S}_{n,m}^{R,T_1} \in \mathbb{R}_{+}^{LN_R \times 2S^{B,T_1}}$ is a rectangular diagonal matrix whose diagonal entries are the singular values of $\widehat{\mathbf{H}}_{n,m}^{R,T_1}$ ordered in descending value, and $\mathbf{V}_{n,m}^{R,T_1} \in \mathbb{C}^{2S^{B,T_1} \times 2S^{B,T_1}}$ is the right singular matrix containing, as its columns, the right singular vectors of $\widehat{\mathbf{H}}_{n,m}^{R,T_1}$. The intersecting left nullspace may then be obtained as the $\left(LN_R - 2S^{B,T_1}\right)$ rightmost columns of $\mathbf{U}_{n,m}^{R,T_1}$ (corresponding to the zero singular values), and this is used as the receive BF matrices, $\mathbf{R}_{n,m}^{R,T_1}$, for RN $m$ in macrocell $n$. A similar procedure is performed for obtaining the receive BF matrices, $\mathbf{R}_{n,k}^{U,T_1}$, for UE $k$ in macrocell $n$ in the first phase, where the $\left(LN_U - 2S^{B,T_1}\right)$ rightmost columns of the corresponding left singular matrix are selected.

To summarize, the cost of implementing the full-IA protocol in the first transmission phase is the reduction of the number of available spatial transmission streams at each BS from $LN_B$ to $S^{B,T_1}$. Thus, if the RNs and UEs require a large number of spatial streams, the BSs have to substantially reduce the number of transmitted streams in order to accommodate IA. However, it is clear that $S^{B,T_1}$ should be higher than 0 to ensure that the BSs become

capable of transmitting. Following this procedure, the

$$3S^{B,T_1} - S^R \tag{5.11}$$

and

$$3S^{B,T_1} - S^U \tag{5.12}$$

total interference signal dimensions received at each RN and at each UE respectively have each been aligned to $2S^{B,T_1}$ dimensions, leaving

$$LN_R - 2S^{B,T_1} \geq S^R \tag{5.13}$$

and

$$LN_U - 2S^{B,T_1} \geq S^U \tag{5.14}$$

receive signal dimensions free from interference at the RNs and UEs, respectively. Thus, IA has been successfully employed for reducing the number of spatial dimensions that the interference signals occupy.

#### 5.3.1.2 Partial-IA Receiver Design

Using this design philosophy, the OCI encountered during the first phase is ignored when designing the receive BF matrices. However, since there is no ICI in the first phase since only the BSs are transmitting, there is no need to reduce the number of transmit dimensions at the BSs. Therefore,

$$S^{B,T_1} = LN_B \tag{5.15}$$

is chosen. Furthermore, the matched filter receiver design is adopted for maximizing the achievable SE [317]. In this case, the SVD is performed on the intra-cell precoded channel matrices, yielding for example

$$\widetilde{\mathbf{H}}_{n,m}^{BR,n,T_1} = \mathbf{U}_{n,m}^{BR,n,T_1} \mathbf{S}_{n,m}^{BR,n,T_1} \left(\mathbf{V}_{n,m}^{BR,n,T_1}\right)^{\mathrm{H}} \tag{5.16}$$

and

$$\widetilde{\mathbf{H}}_{n,k}^{BU,n,T_1} = \mathbf{U}_{n,k}^{BU,n,T_1} \mathbf{S}_{n,k}^{BU,n,T_1} \left(\mathbf{V}_{n,k}^{BU,n,T_1}\right)^{\mathrm{H}}, \tag{5.17}$$

respectively, and the $S^R$ (resp. $S^U$) leftmost left (thus corresponding to the highest singular values) singular vectors are selected as the receive BF matrices for the RNs (resp. UEs) in the first phase. Fig. 5.7 illustrates the channel matrices, which are employed for computing the receive BF matrices.

In summary, IA is not required during the first transmission phase of the partial-IA protocol, since the only transmitter within the same cell is the associated BS. Therefore, it is not

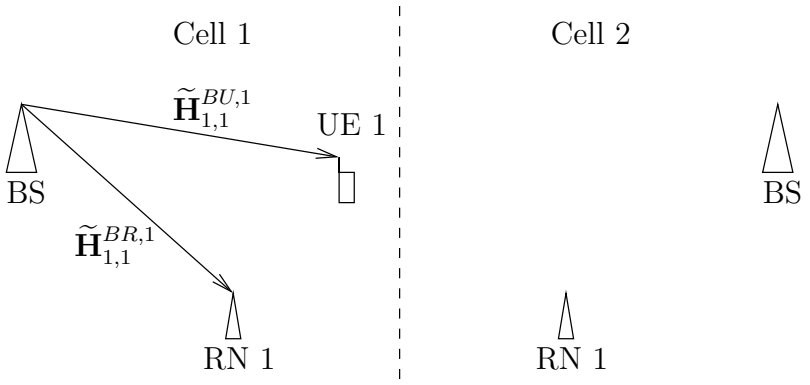


FIGURE 5.7: An illustration indicating the direct channel matrices employed for computing the receive BF matrices during the first transmission phase of the partial-IA protocol.

necessary for the BSs to reduce the number of transmit dimensions available to them for the sake of avoiding interference.

#### 5.3.1.3 Scheduling and Transmitter Design

Having designed the receive BF matrices, the effective DL channel matrices can be written as

$$\overline{\mathbf{H}}_{n,m}^{BR,n,T_1} := \left(\mathbf{R}_{n,m}^{R,T_1}\right)^{\mathrm{H}} \widetilde{\mathbf{H}}_{n,m}^{BR,n,T_1} \tag{5.18}$$

or

$$\overline{\mathbf{H}}_{n,k}^{BU,n,T_1} := \left(\mathbf{R}_{n,k}^{U,T_1}\right)^{\mathrm{H}} \widetilde{\mathbf{H}}_{n,k}^{BU,n,T_1} \tag{5.19}$$

for RN $m$ and UE $k$ in macrocell $n$, respectively. We term the rows of these matrices as the SMCs of the associated transceivers, since each SMC corresponds to a distinct *virtual* MISO channel between the associated transmitter as well as receiver, and then multiple MISOs can be multiplexed for composing a MIMO channel. A set of SMCs is generated for each of the two transmission phases, and each BS then distributively groups these SMCs according to the orthogonal component-based grouping algorithm of Section 4.5.2, given a semi-orthogonality parameter $\alpha$. For the first transmission phase, up to

$$\min\left(S^{B,T_1}, KLN_U + MLN_R\right) \tag{5.20}$$

SMCs may be served simultaneously by each BS, while avoiding ICI. The set of groupings available for BS $n$ is denoted by $\mathcal{G}^n$. Note that, each group additionally contains the SMCs selected for the second phase, as was discussed in Section 4.4. The SMCs belonging to group $j$, which are denoted by $\mathcal{E}^{n,j}$, are then the rows of the effective scheduled DL matrix, denoted by $\underline{\mathbf{H}}^{B,n,j,T_1}$ for macrocell $n$. In order to avoid ICI between these selected SMCs of group $j$, macrocell $n$ applies the normalized ZFBF matrix given by the normalized right

channel inverse

$$\mathbf{T}^{B,n,j,T_1} = \left(\underline{\mathbf{H}}^{B,n,j,T_1}\right)^{\mathrm{H}} \left[\underline{\mathbf{H}}^{B,n,j,T_1} \left(\underline{\mathbf{H}}^{B,n,j,T_1}\right)^{\mathrm{H}}\right]^{-1} \left(\mathbf{W}^{B,n,j,T_1}\right)^{\frac{1}{2}}, \tag{5.21}$$

before using its transmit precoding matrix $\mathbf{A}^{B,n}$. Furthermore, $\left(\mathbf{W}^{B,n,j,T_1}\right)^{\frac{1}{2}}$ is a real-valued diagonal matrix, which normalizes the columns of $\mathbf{T}^{B,n,j,T_1}$ for ensuring that the power assigned to each transmission remains unaffected.

The effective end-to-end channel power gains are then given by the squares of the diagonal entries in $\left(\mathbf{W}^{B,n,j,T_1}\right)^{\frac{1}{2}}$. For SMC $e_1$ in group $j$ of macrocell $n$ corresponding to a direct first phase BS-UE link, the effective channel power gain is denoted by $w_{n,e_1}^{BU,n,j,T_1}$, while the effective channel power gain of the OCI link, originating from macrocell $n'$ serving SMC group $j'$ to UE $k$ in macrocell $n$, is obtained from the element of

$$\left|\left(\mathbf{R}_{n,k}^{U,T_1}\right)^{\mathrm{H}} \widetilde{\mathbf{H}}_{n,k}^{BU,n',T_1} \mathbf{T}^{B,n',j',T_1}\right|^2 \tag{5.22}$$

corresponding to SMC $e_1$ at UE $k$ of macrocell $n$, and is denoted by $w_{n,e_1}^{BU,n',j',T_1}$. In the case of the full-IA protocol, all OCI is avoided, thus $w_{n,e_1}^{BU,n',j',T_1} = 0$, $\forall n' \neq n$. The effective channel power gains for the BS-to-RN links, corresponding to SMC-pair $e$, may be similarly obtained and are denoted by $w_{n,e}^{BR,n,j,T_1}$, whereas an OCI link is denoted by $w_{n,e}^{BR,n',j',T_1}$. Note that relaying links contain both a SMC for the BS-RN link and a SMC for the RN-UE link as discussed in Section 4.4.

### 5.3.2 Beamforming Design for the Second Phase

During the second phase, both the BSs and the RNs may transmit. Therefore, in a similar fashion to the first phase, the BS in cell $n$ adopts the precoding matrix $\mathbf{A}^{B,n,T_2} \in \mathbb{C}^{LN_B \times S^{B,T_2}}$, while RN $m$ in cell $n$ adopts the transmit precoding matrix $\mathbf{A}^{R,n,m,T_2} \in \mathbb{C}^{LN_R \times S^R}$, which are again complex-valued matrices having a full column-rank. Additionally, the columns of these transmit precoding matrices are normalized. Due to the additional interference imposed by the transmissions of the RNs, it is necessary to reduce the number of transmit dimensions at the BSs even further in order to facilitate IA at the DL receivers. Additionally, note that each transmit precoding matrix used at the RNs consist of $S^R$ columns, since the information received by each RN during the first phase must be conveyed to the intended UE. The precoded channel matrices used during the second phase are thus given by (note that the transmitter indices are $n'$ and $m'$, since these may be inter-cell channel matrices)

$$\widetilde{\mathbf{H}}_{n,k}^{RU,n',m',T_2} := \mathbf{H}_{n,k}^{RU,n',m'} \mathbf{A}^{R,n',m',T_2} \in \mathbb{C}^{LN_U \times S^R} \tag{5.23}$$

and

$$\widetilde{\mathbf{H}}_{n,k}^{BU,n',T_2} := \mathbf{H}_{n,k}^{BU,n'} \mathbf{A}^{B,n',T_2} \in \mathbb{C}^{LN_U \times S^{B,T_2}}. \tag{5.24}$$

#### 5.3.2.1 Full-IA Receiver Design

The receiver design used during the second phase depends on whether the BS or a RN is selected to serve each UE within the same macrocell. Each of the $(1+M)$ possible transmitters may be examined for the sake of finding the most beneficial choice. For example, assuming that BS 1 transmits to UE $k$ during the second phase, the OCI and ICI channel matrices may be concatenated to form

$$\begin{aligned}\widehat{\mathbf{H}}_{1,k}^{BU,1,T_2} : \; = \; & \left[\widetilde{\mathbf{H}}_{1,k}^{BU,2,T_2} \middle| \widetilde{\mathbf{H}}_{1,k}^{BU,3,T_2} \middle| \widetilde{\mathbf{H}}_{1,k}^{RU,1,1,T_2} \middle| \cdots \middle| \widetilde{\mathbf{H}}_{1,k}^{RU,1,M,T_2} \right. \\ & \left. \middle| \widetilde{\mathbf{H}}_{1,k}^{RU,2,1,T_2} \middle| \cdots \middle| \widetilde{\mathbf{H}}_{1,k}^{RU,2,M,T_2} \middle| \widetilde{\mathbf{H}}_{1,k}^{RU,3,1,T_2} \middle| \cdots \middle| \widetilde{\mathbf{H}}_{1,k}^{RU,3,M,T_2} \right] \in \mathbb{C}^{LN_U \times \left(2S^{B,T_2}+3MS^R\right)}.\end{aligned} \tag{5.25}$$

However, when assuming for example, that RN 1 of macrocell $n$ transmits to UE $k$, the combined interference matrix is defined by

$$\begin{aligned}\widehat{\mathbf{H}}_{n,k}^{RU,n,1,T_2} : \; = \; & \left[\widetilde{\mathbf{H}}_{n,k}^{BU,1,T_2} \middle| \widetilde{\mathbf{H}}_{n,k}^{BU,2,T_2} \middle| \widetilde{\mathbf{H}}_{n,k}^{BU,3,T_2} \middle| \widetilde{\mathbf{H}}_{n,k}^{RU,1,2,T_2} \middle| \cdots \middle| \widetilde{\mathbf{H}}_{n,k}^{RU,1,M,T_2} \right. \\ & \left. \middle| \widetilde{\mathbf{H}}_{n,k}^{RU,2,1,T_2} \middle| \cdots \middle| \widetilde{\mathbf{H}}_{n,k}^{RU,2,M,T_2} \middle| \widetilde{\mathbf{H}}_{n,k}^{RU,3,1,T_2} \middle| \cdots \middle| \widetilde{\mathbf{H}}_{n,k}^{RU,3,M,T_2} \right] \\ & \in \mathbb{C}^{LN_U \times \left[3S^{B,T_2}+(3M-1)S^R\right]}.\end{aligned} \tag{5.26}$$

Therefore, in order to guarantee having $S^U$ receive dimensions at each UE, we have

$$S^{B,T_2} = \left\lfloor \min\left( \frac{LN_U - S^U - 3MS^R}{2}, \frac{LN_U - S^U - (3M-1)S^R}{3} \right) \right\rfloor. \tag{5.27}$$

In both cases described above, the SVD may again be employed for finding the intersecting left nullspace of the precoded interference matrix. The receive BF matrix, $\mathbf{R}_{n,k}^{U,T_2}$, at UE $k$ in macrocell $n$ used during the second phase is then given by the rightmost (thus corresponding to its zero singular values) $LN_U - \left(2S^{B,T_2} + 3MS^R\right)$ number of columns in the left singular matrix of $\widehat{\mathbf{H}}_{1,k}^{BU,1,T_2}$, when the BS is the activated transmitter. By contrast, when assuming that RN 1 is the activated transmitter, the rightmost

$$\min\left(S^R, LN_U - \left[3S^{B,T_2} + (3M-1)S^R\right]\right) \tag{5.28}$$

number of columns in the ordered left singular matrix of $\widehat{\mathbf{H}}_{n,k}^{RU,n,1,T_2}$ specify the receive BF matrix. Fig. 5.8 illustrates the relevant interference links when either the BS or an RN is selected as the activated transmitter.

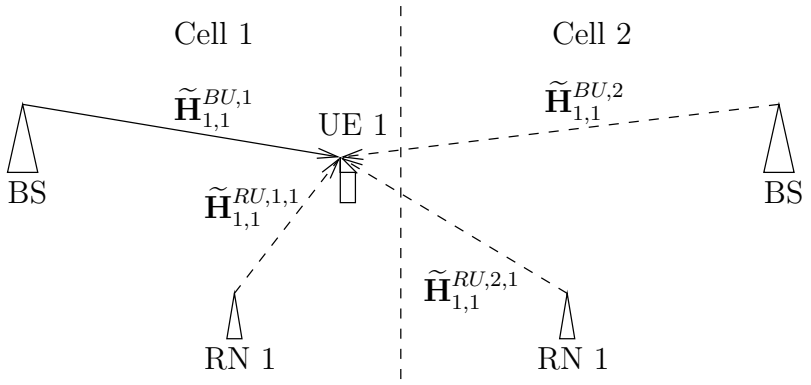


(a) When the BS is selected as the activated transmitter, the channel matrices associated with the links to all RNs and other BSs need to be considered when computing the IA receive BF matrix.

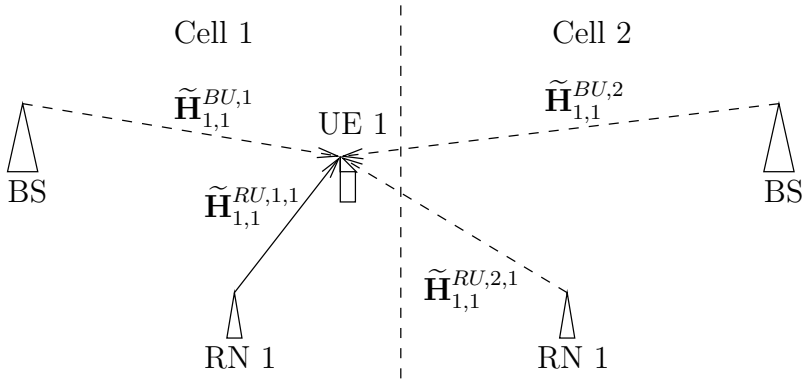


(b) When a RN is selected as the activated transmitter, the channel matrices associated with the links to all BSs and other RNs need to be considered when computing the IA receive BF matrix.

FIGURE 5.8: An illustration of the relevant links and their associated channel matrices when computing the receive BF matrices employed during the second phase of the full-IA protocol.

In conclusion, the BSs once again have to reduce the number of spatial transmission streams available to them in order to facilitate IA. In this case, their number is reduced from $LN_B$ to $S^{B,T_2}$. Additionally, each RN reduces the number of streams available for them to transmit from $LN_R$ to $S_R$. On one hand, when the BS is selected as the active transmitter for a particular UE using the full-IA protocol, a total of

$$3S^{B,T_2} + 3MS^R - S^U \tag{5.29}$$

interference signal dimensions are aligned to

$$2S^{B,T_2} + 3MS^R \tag{5.30}$$

signal dimensions, leaving

$$LN_U - \left(2S^{B,T_2} + 3MS^R\right) \geq S^U \tag{5.31}$$

signal dimensions free from interference. Thus, IA has been successfully employed. On the other hand, when a RN is selected as the activated transmitter for a particular UE, there is a total of

$$3S^{B,T_2} + 3MS^R - S^U \tag{5.32}$$

interference signal dimensions, which are aligned to

$$3S^{B,T_2} + 3MS^R - S^R \tag{5.33}$$

signal dimensions. Therefore, IA is only feasible at the UEs if we have $S^R > S^U$. The constraint given by

$$LN_U - \left(3S^{B,T_2} + 3MS^R\right) - S^R > S^R \tag{5.34}$$

is additionally enforced in the full-IA protocol, so that the CCI can still be nulled when $S^R \leq S^U$ and a RN is selected as the active transmitter. However, IA is not employed in this case.

#### 5.3.2.2 Partial-IA Receiver Design

Although the effects of OCI are ignored when using this protocol, the ICI must be avoided. Thus, the interference matrix, assuming for example that the BS is the selected transmitter for UE $k$ in macrocell 1, is then given by

$$\widehat{\mathbf{H}}_{1,k}^{BU,1,T_2} := \left[\widetilde{\mathbf{H}}_{1,k}^{RU,1,1,T_2} \middle| \cdots \middle| \widetilde{\mathbf{H}}_{1,k}^{RU,1,M,T_2}\right] \in \mathbb{C}^{LN_U \times MS^R}. \tag{5.35}$$

By contrast, if RN 1 of macrocell $n$ is selected as the transmitter for UE $k$, then the interference matrix is given by

$$\begin{aligned}\widehat{\mathbf{H}}_{n,k}^{RU,n,1,T_2} \quad := \quad & \left[\widetilde{\mathbf{H}}_{n,k}^{BU,1,T_2} \middle| \widetilde{\mathbf{H}}_{n,k}^{RU,n,2,T_2} \middle| \cdots \middle| \widetilde{\mathbf{H}}_{n,k}^{RU,n,M,T_2}\right] \\ & \in \mathbb{C}^{LN_U \times \left[S^{B,T_2} + (M-1)S^R\right]},\end{aligned} \tag{5.36}$$

which implies that

$$S^{B,T_2} = LN_U - S^U - (M-1)\,S^R \tag{5.37}$$

is satisfied for ensuring that the UEs are capable of finding approximate receive BF matrices, which completely null the ICI.

Thus, UE $k$ may employ the $LN_U - MS^R$ number of rightmost left singular columns in $\widehat{\mathbf{H}}_{1,k}^{BU,1,T_2}$ as its receive BF matrix, when the BS is the activated transmitter. By contrast, assuming that RN 1 is the activated transmitter, the

$$\min\left(S^R, LN_U - \left[S^{B,T_2} + (M-1)\,S^R\right]\right) \tag{5.38}$$

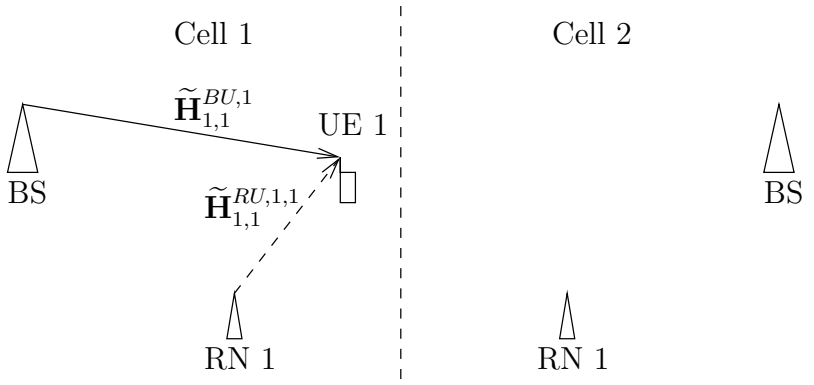


(a) When the BS is selected as the activated transmitter, the channel matrices associated with the links to all RNs within the same macrocell need to be considered when computing the IA receive BF matrix.

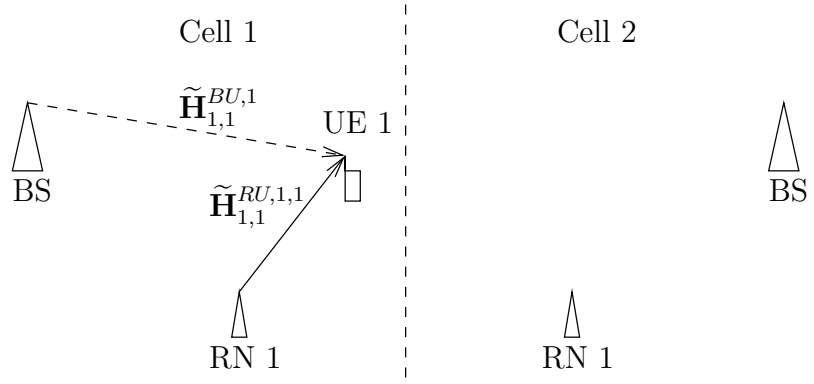


(b) When a RN is selected as the activated transmitter, the channel matrix associated with the links to the BS and other RNs with the same macrocell need to be considered when computing the IA receive BF matrix.

FIGURE 5.9: An illustration of the relevant links and their associated channel matrices when computing the receive BF matrices employed during the second phase of the partial-IA protocol.

number of rightmost left singular columns in $\widehat{\mathbf{H}}_{n,k}^{RU,n,1,T_2}$ specify the receive BF matrix. Fig. 5.9 illustrates the relevant interference links when either the BS or an RN is selected as the activated transmitter.

To summarize, the BSs reduce the number of spatial streams available to them from $LN_B$ to $S^{B,T_2}$, while the RNs reduce the number of their spatial streams from $LN_R$ to $S^R$. On one hand, when the BS is selected as the active transmitter for the partial-IA protocol, a total of

$$S^{B,T_2} + MS^R - S^U \tag{5.39}$$

interference signal dimensions are aligned to $MS^R$ signal dimensions, leaving

$$LN_U - MS^R \geq S^U \tag{5.40}$$

signal dimensions free from interference. Thus, IA has been successfully employed. On the

other hand, when a RN is selected as the activated transmitter, there are a total of

$$S^{B,T_2} + MS^R - S^U \tag{5.41}$$

interference signal dimensions, which are aligned to

$$S^{B,T_2} + MS^R - S^R \tag{5.42}$$

signal dimensions. Therefore, IA is only feasible for $S^R > S^U$. However, the aforementioned receive BF matrices are still capable of nulling the CCI, when a RN is selected as the active transmitter in the partial-IA protocol and we have $S^R \leq S^U$. But in this case the constraint given by (5.34) is not required, since it is already satisfied by (5.37).

#### 5.3.2.3 Scheduling and Transmitter Design

In a similar fashion to the first phase, the effective DL channel matrices are given by

$$\overline{\mathbf{H}}_{n,k}^{RU,n,m,T_2} := \left(\mathbf{R}_{n,k}^{U,T_2}\right)^{\mathrm{H}} \widetilde{\mathbf{H}}_{n,k}^{RU,n,m,T_2} \tag{5.43}$$

and

$$\overline{\mathbf{H}}_{n,k}^{BU,n,T_2} := \left(\mathbf{R}_{n,k}^{U,T_2}\right)^{\mathrm{H}} \widetilde{\mathbf{H}}_{n,k}^{BU,n,T_2}, \tag{5.44}$$

when the BS or RN $m$ is activated as the transmitter for UE $k$ belonging to macrocell $n$, respectively. The rows of the DL transmit BF matrices corresponding to each transmitter form the SMCs for that transmitter, and they may be grouped at each BS according to the semi-orthogonal user selection algorithm described above. Furthermore, in the second phase, each BS can select up to $\min\left(S^{B,T_2}, KLN_U\right)$ number of SMCs to serve simultaneously while avoiding ICI, whereas each RN may select $\min\left(S^R, KLN_U\right)$ number of SMCs. At BS $n$ (or RN $m$ of macrocell $n$), the selected SMCs of group $j$ form the rows of its effective scheduled DL matrix, denoted by $\underline{\mathbf{H}}^{B,n,j,T_2}$ (or $\underline{\mathbf{H}}^{R,n,m,j,T_2}$). The ZFBF matrix employed by BS $n$ or by RN $m$ of macrocell $n$ in the second phase is then given by the right inverse

$$\mathbf{T}^{B,n,j,T_2} = \left(\underline{\mathbf{H}}^{B,n,j,T_2}\right)^{\mathrm{H}} \left[\underline{\mathbf{H}}^{B,n,j,T_2} \left(\underline{\mathbf{H}}^{B,n,j,T_2}\right)^{\mathrm{H}}\right]^{-1} \left(\mathbf{W}^{B,n,j,T_2}\right)^{\frac{1}{2}} \tag{5.45}$$

or

$$\mathbf{T}^{R,n,m,j,T_2} = \left(\underline{\mathbf{H}}^{R,n,m,j,T_2}\right)^{\mathrm{H}} \left[\underline{\mathbf{H}}^{R,n,m,j,T_2} \left(\underline{\mathbf{H}}^{R,n,m,j,T_2}\right)^{\mathrm{H}}\right]^{-1} \left(\mathbf{W}^{R,n,m,j,T_2}\right)^{\frac{1}{2}}, \tag{5.46}$$

respectively, where the real-valued diagonal matrices of $\left(\mathbf{W}^{B,n,j,T_2}\right)^{\frac{1}{2}}$ and $\left(\mathbf{W}^{R,n,m,j,T_2}\right)^{\frac{1}{2}}$ are required for normalizing the columns of $\mathbf{T}^{B,n,j,T_2}$ and $\mathbf{T}^{R,n,m,j,T_2}$, respectively.

The effective channel power gains in the second phase are thus given by the squares of the

diagonal entries in $\left(\mathbf{W}^{B,n,j,T_2}\right)^{\frac{1}{2}}$ and $\left(\mathbf{W}^{R,n,m,j,T_2}\right)^{\frac{1}{2}}$. The effective channel power gain of a BS-UE SMC $e_2$ of group $j$ associated with macrocell $n$ and UE $k$ is denoted by $w_{n,e_2}^{BU,n,j,T_2}$, while the RN-UE effective channel power gain of SMC-pair $e$ associated with RN $m$ of macrocell $n$ and UE $k$ may be denoted by $w_{n,e}^{RU,n,m,j,T_2}$. Similar to the first phase, the effective channel power gain of the OCI link originating from the BS of macrocell $n'$ serving group $j'$ to UE $k$ in macrocell $n$, is obtained from the specific element of

$$\left|\left(\mathbf{R}_{n,k}^{U,T_2}\right)^{\mathrm{H}} \widetilde{\mathbf{H}}_{n,k}^{BU,n',T_2} \mathbf{T}^{B,n',j',T_2}\right|^2 \tag{5.47}$$

corresponding to SMC $e_2$ at UE $k$ of macrocell $n$, which is denoted by $w_{n,e_2}^{BU,n',j',T_2}$. On the other hand, the effective channel power gain of the OCI link, originating from RN $m'$ of macrocell $n'$ serving group $j'$ to UE $k$ of macrocell $n$, is obtained from the element of

$$\left|\left(\mathbf{R}_{n,k}^{U,T_2}\right)^{\mathrm{H}} \widetilde{\mathbf{H}}_{n,k}^{RU,n',m',T_2} \mathbf{T}^{R,n',m',j,T_2}\right|^2 \tag{5.48}$$

corresponding to SMC $e$ at UE $k$ of macrocell $n$, and is denoted by $w_{n,e}^{RU,n',m',j',T_2}$. In the case of the full-IA protocol, all OCI is avoided, thus we have $w_{n,e_2}^{BU,n',j',T_2} = w_{n,e}^{RU,n',m',j',T_2} = 0$, $\forall n' \neq n$. The procedures for the full-IA and the partial-IA protocols are outlined in Tables 5.1 and 5.2. Furthermore, an illustration of the transmit BF matrices and receive BF matrices employed in both transmission phases is presented in Fig. 5.10.

### 5.3.3 Achievable Spectral Efficiency and Energy Efficiency

Since we have mathematically decomposed the MIMO channels into effective SISO channels, we may directly employ the Shannon capacity bound for characterizing the achievable EE performance, rather than relying on bounds derived for MIMO channels [391]. We begin by defining the SINR of the direct link SMCs belonging to group $j$ and intended for UE $k$ of macrocell $n$ during the first and the second phase as

$$\Gamma_{n,e_1}^{BU,n,j,T_1}(\mathcal{P},\mathcal{S}) = \frac{w_{n,e_1}^{BU,n,j,T_1} P_{n,e_1}^{B,n,j,T_1}}{\Delta\gamma\left(N_0 LW + I_{n,e_1}^{U,T_1}\right)} \tag{5.49}$$

and

$$\Gamma_{n,e_2}^{BU,n,j,T_2}(\mathcal{P},\mathcal{S}) = \frac{w_{n,e_2}^{BU,n,j,T_2} P_{n,e_2}^{B,n,j,T_2}}{\Delta\gamma\left(N_0 LW + I_{n,e_2}^{U,T_2}\right)}, \tag{5.50}$$

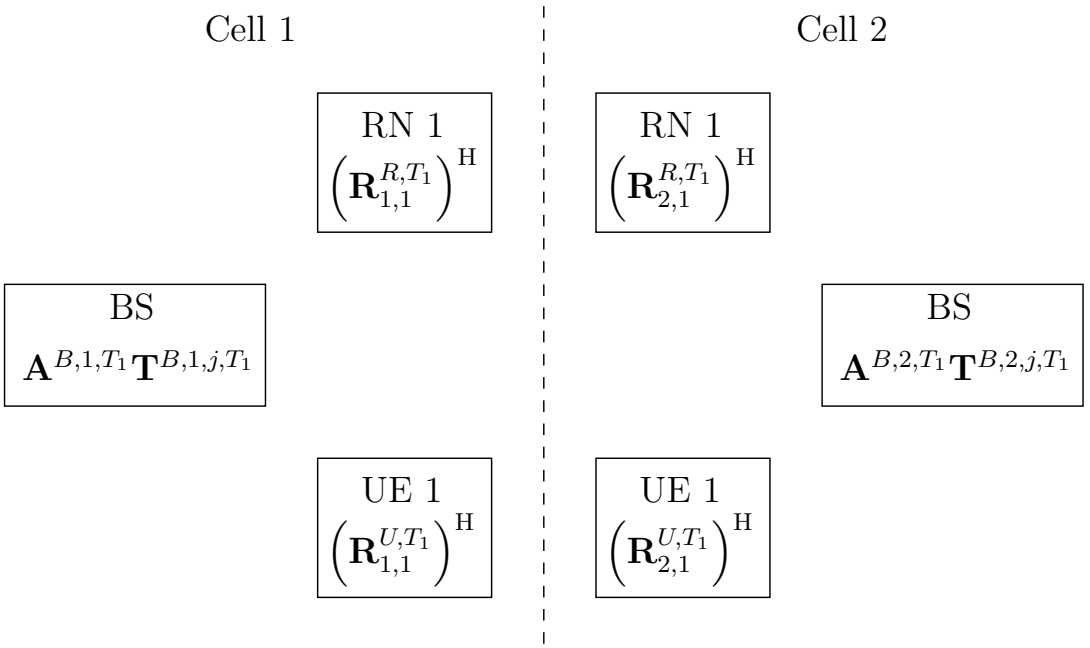


(a) Transmit BF matrices and receive BF matrices employed in the first transmission phase.

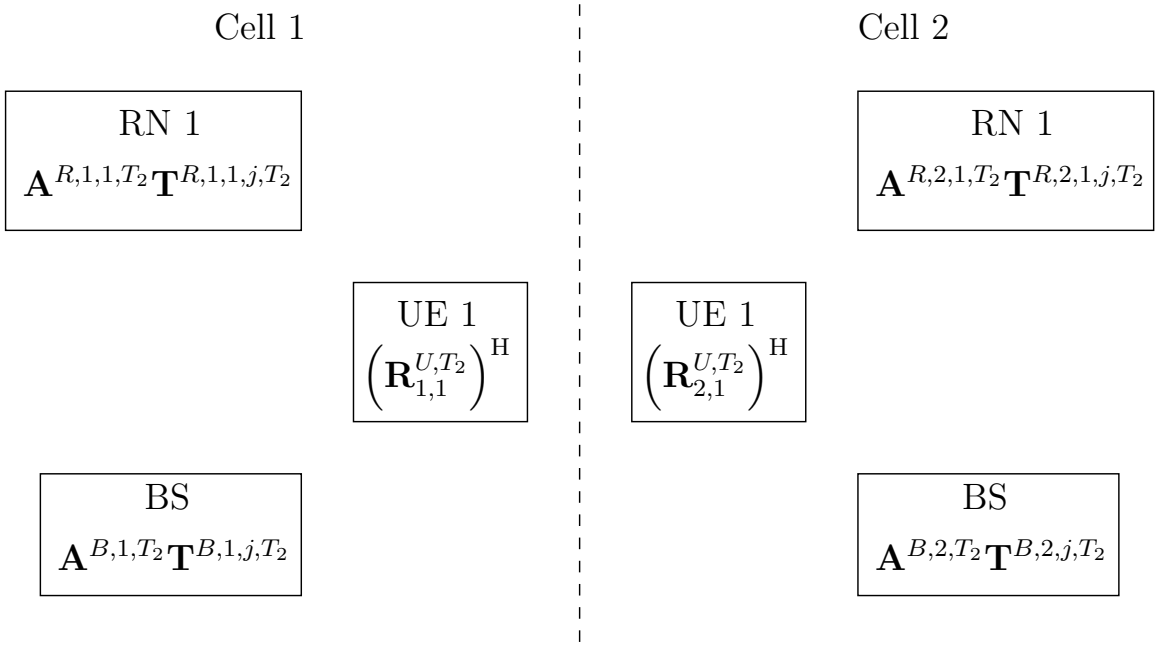


(b) Transmit BF matrices and receive BF matrices employed in the second transmission phase.

FIGURE 5.10: An illustration of the transmit BF matrices and receive BF matrices employed in both transmission phases.

TABLE 5.1: The procedure of the full-IA protocol.

**Algorithm 1** Full-IA protocol

**for** $n$ **from** 1 **to** 3
  Create precoding matrices for the BS, $\mathbf{A}^{B,n,T_1}$ and $\mathbf{A}^{B,n,T_2}$.
  **for** $m$ **from** 1 **to** $M$
    Compute the OCI matrix, $\widehat{\mathbf{H}}_{n,m}^{R,T_1}$, for the first phase.
    Using the SVD, find the left nullspace of $\widehat{\mathbf{H}}_{n,m}^{R,T_1}$ for use as the receive BF matrix, $\mathbf{R}_{n,m}^{R,T_1}$, in the first phase. Compute the effective DL channel matrix, $\overline{\mathbf{H}}_{n,m}^{BR,n,T_1}$.
    Create precoding matrix, $\mathbf{A}^{R,n,m,T_2}$.
  **end for**
  **for** $k$ **from** 1 **to** $K$
    Compute the OCI matrix, $\widehat{\mathbf{H}}_{n,k}^{U,T_1}$, for the first phase.
    Using the SVD, find the left nullspace of $\widehat{\mathbf{H}}_{n,k}^{U,T_1}$ for use as the receive BF matrix, $\mathbf{R}_{n,m}^{U,T_1}$. Compute the effective DL matrix, $\overline{\mathbf{H}}_{n,k}^{BU,n,T_1}$.
    Compute the ICI plus OCI matrix for the second phase assuming the BS is chosen as the transmitter, $\widehat{\mathbf{H}}_{n,k}^{BU,n,T_2}$. Use the SVD to compute the receive BF matrix, $\mathbf{R}_{n,k}^{U,T_2}$. Compute the effective DL channel matrix, $\overline{\mathbf{H}}_{n,k}^{BU,n,T_2}$.
    Compute the ICI plus OCI matrix for the second phase assuming the RN $m$ is chosen as the transmitter, $\widehat{\mathbf{H}}_{n,k}^{RU,n,m,T_2}$. Use the SVD to compute the receive BF matrix, $\mathbf{R}_{n,k}^{U,T_2}$. Compute the effective DL channel matrix, $\overline{\mathbf{H}}_{n,k}^{RU,n,m,T_2}$.
  **end for**
  Use the semi-orthogonal user selection algorithm [324, 359] to compute SMC groups, $\mathcal{G}^n$.
  **for each** $j$ **in** $\mathcal{G}^n$
    Compute the ZFBF matrices, $\mathbf{T}^{B,n,j,T_1}$, $\mathbf{T}^{B,n,j,T_2}$ and $\mathbf{T}^{R,n,m,j,T_2}$. Compute the effective channel power gains.
  **end for each**
**end for**

respectively, where the total received OCI in the first and second phase has been denoted by

$$I_{n,e_1}^{U,T_1}(\mathcal{P},\mathcal{S}) = \sum_{\substack{n'=1\\n'\neq n}} \sum_{j'\in\mathcal{G}^{n'}} s^{n',j'} w_{n,e_1}^{BU,n',j',T_1} \left[ \sum_{e_1'\in\mathcal{E}^{n',j'}} P_{n',e_1'}^{B,n',j',T_1} + \sum_{e'\in\mathcal{E}^{n',j'}} P_{n',e'}^{B,n',j',T_1} \right] \tag{5.51}$$

and

$$\begin{aligned} I_{n,e_2}^{U,T_2}(\mathcal{P},\mathcal{S}) &= \sum_{\substack{n'=1\\n'\neq n}} \sum_{j'\in\mathcal{G}^{n'}} s^{n',j'} w_{n,e_2}^{BU,n',j',T_2} \sum_{e_2'\in\mathcal{E}^{n',j'}} P_{n',e_2'}^{B,n',j',T_2} \\ &\quad + \sum_{\substack{n'=1\\n'\neq n}} \sum_{j'\in\mathcal{G}^{n'}} s^{n',j'} \sum_{e'\in\mathcal{E}^{n',j'}} w_{n,e_2}^{RU,n',\mathcal{M}(e'),j',T_2} P_{n,e'}^{R,n',\mathcal{M}(e'),j',T_2}, \end{aligned} \tag{5.52}$$

TABLE 5.2: The procedure of the partial-IA protocol.

**Algorithm 2** Partial-IA protocol

**for** $n$ **from** 1 **to** 3
  Create precoding matrices for the BS, $\mathbf{A}^{B,n,T_1}$ and $\mathbf{A}^{B,n,T_2}$.
  **for** $m$ **from** 1 **to** $M$
    Compute the DL channel matrix, $\widetilde{\mathbf{H}}_{n,m}^{BR,n,T_1}$.
    Using the SVD, find the leftmost left singular vectors of $\widehat{\mathbf{H}}_{n,m}^{R,T_1}$ for use as the receive BF matrix, $\mathbf{R}_{n,m}^{R,T_1}$, in the first phase. Compute the effective DL channel matrix, $\overline{\mathbf{H}}_{n,m}^{BR,n,T_1}$.
    Create precoding matrix $\mathbf{A}^{R,n,m,T_2}$.
  **end for**
  **for** $k$ **from** 1 **to** $K$
    Compute the DL channel matrix $\widetilde{\mathbf{H}}_{n,k}^{BU,n,T_1}$.
    Using the SVD, find the left nullspace of $\widehat{\mathbf{H}}_{n,k}^{U,T_1}$ for use as the receive BF matrix, $\mathbf{R}_{n,m}^{U,T_1}$. Compute the effective DL matrix, $\overline{\mathbf{H}}_{n,k}^{BU,n,T_1}$.
    Compute the ICI matrix for the second phase assuming the BS is chosen as the transmitter, $\widehat{\mathbf{H}}_{n,k}^{BU,n,T_2}$. Use the SVD to compute the receive BF matrix, $\mathbf{R}_{n,k}^{U,T_2}$. Compute the effective DL channel matrix, $\overline{\mathbf{H}}_{n,k}^{BU,n,T_2}$.
    Compute the ICI matrix for the second phase assuming the RN $m$ is chosen as the transmitter, $\widehat{\mathbf{H}}_{n,k}^{RU,n,m,T_2}$. Use the SVD to compute the receive BF matrix, $\mathbf{R}_{n,k}^{U,T_2}$. Compute the effective DL channel matrix, $\overline{\mathbf{H}}_{n,k}^{RU,n,m,T_2}$.
  **end for**
  Use the semi-orthogonal user selection algorithm [324, 359] to compute SMC groups, $\mathcal{G}^n$.
  **for each** $j$ **in** $\mathcal{G}^n$
    Compute the ZFBF matrices, $\mathbf{T}^{B,n,j,T_1}$, $\mathbf{T}^{B,n,j,T_2}$ and $\mathbf{T}^{R,n,m,j,T_2}$. Compute the effective channel power gains.
  **end for each**
**end for**

respectively. As in Chapter 4, $\mathcal{M}(e)$ is a function of $e$, representing the RN index (similar to $m$ used before) associated with the SMC-pair $e$. For simplicity, the interference that was not avoided using IA is treated as noise. Although not the case in this chapter, if the level of interference is strong enough, then more sophisticated methods, such as multiuser detection, may be employed. The set $\mathcal{P}$ contains the power control variables denoted by $P_{n,e_1}^{B,n,j,T_1}$, $P_{n,e}^{B,n,j,T_1}$, $P_{n,e_2}^{B,n,j,T_2}$, and $P_{n,e}^{R,n,m,j,T_2}$, $\forall n, e_1, e_2, e$. On the other hand, the set $\mathcal{S}$ contains the group selection indicator variables, $s^{n,j}$, $\forall n, j$, where $s^{n,j} = 1$, when the SMC group $j$ has been selected for macrocell $n$, and $s^{n,j} = 0$ otherwise. The total noise power across all subcarriers is given by $N_0LW$, while $\Delta\gamma$ is the SNR difference between the SNR at the DCMC capacity and the actual SNR required by the specific MCS of the practical physical layer transceivers employed [351].

The SINR of the BS-RN SMC $e$ belonging to group $j$ of macrocell $n$ and intended for RN

$m$ may be expressed as

$$\Gamma_{n,e}^{BR,n,j,T_1}\left(\mathcal{P},\mathcal{S}\right)=\frac{w_{n,e}^{BR,n,j,T_1}P_{n,e}^{B,n,j,T_1}}{\Delta\gamma\left(N_0LW+I_{n,e}^{R,T_1}\right)}, \tag{5.53}$$

while the SINR of the corresponding RN-UE link may be formulated as

$$\Gamma_{n,e}^{RU,n,m,j,T_2}\left(\mathcal{P},\mathcal{S}\right)=\frac{w_{n,e}^{RU,n,m,j,T_2}P_{n,e}^{R,n,m,j,T_2}}{\Delta\gamma\left(N_0LW+I_{n,e}^{U,T_2}\right)}, \tag{5.54}$$

where the total received OCI of the BS-RN and RN-UE links are given by

$$I_{n,e}^{R,T_1}\left(\mathcal{P},\mathcal{S}\right)=\sum_{\substack{n'=1\\n'\neq n}}\sum_{j'\in\mathcal{G}^{n'}}s^{n',j'}w_{n,e}^{BR,n',j',T_1}\left[\sum_{e'_1\in\mathcal{E}^{n',j'}}P_{n',e'_1}^{B,n',j',T_1}+\sum_{e'\in\mathcal{E}^{n',j'}}P_{n',e'}^{B,n',j',T_1}\right] \tag{5.55}$$

and

$$\begin{aligned}I_{n,e}^{U,T_2}\left(\mathcal{P},\mathcal{S}\right) &= \sum_{\substack{n'=1\\n'\neq n}}\sum_{j'\in\mathcal{G}^{n'}}s^{n',j'}w_{n,e}^{BU,n',j',T_2}\sum_{e'_2\in\mathcal{E}^{n',j'}}P_{n',e'_2}^{B,n',j',T_2}\\ &\quad+\sum_{\substack{n'=1\\n'\neq n}}\sum_{j'\in\mathcal{G}^{n'}}s^{n',j'}\sum_{e'\in\mathcal{E}^{n',j'}}w_{n,e}^{RU,n',\mathcal{M}(e'),j',T_2}P_{n',e'}^{R,n',\mathcal{M}(e'),j',T_2},\end{aligned} \tag{5.56}$$

respectively.

The achievable SE of the direct first and second phase transmissions can be respectively written as

$$C_{n,e_1}^{BU,n,j,T_1}\left(\mathcal{P},\mathcal{S}\right)=\frac{1}{2}\log_2\left(1+\Gamma_{n,e_1}^{BU,n,j,T_1}\right) \tag{5.57}$$

and

$$C_{n,e_2}^{BU,n,j,T_2}\left(\mathcal{P},\mathcal{S}\right)=\frac{1}{2}\log_2\left(1+\Gamma_{n,e_2}^{BU,n,j,T_2}\right), \tag{5.58}$$

where the pre-log factor of $\frac{1}{2}$ accounts for the fact that the transmission period has been split into two phases. When using the DF protocol, the achievable SE of the relaying link is limited by the weaker of the BS-RN and RN-UE links as described in Section 1.4, and is given by

$$C_{n,e}^{BRU,n,m,j}\left(\mathcal{P},\mathcal{S}\right)=\min\left[\frac{1}{2}\log_2\left(1+\Gamma_{n,e}^{BR,n,j,T_1}\right),\frac{1}{2}\log_2\left(1+\Gamma_{n,e}^{RU,n,m,j,T_2}\right)\right]. \tag{5.59}$$

Thus, the total achievable SE of macrocell $n$ is given by

$$C_T^n\left(\mathcal{P},\mathcal{S}\right)=\sum_{j\in\mathcal{G}^n}s^{n,j}\left[\sum_{e_1\in\mathcal{E}^{n,j}}C_{n,e_1}^{BU,n,j,T_1}+\sum_{e_2\in\mathcal{E}^{n,j}}C_{n,e_2}^{BU,n,j,T_2}+\sum_{e\in\mathcal{E}^{n,j}}C_{n,e}^{BRU,n,\mathcal{M}(e),j}\right]. \tag{5.60}$$

Furthermore, we adopt the simplified energy dissipation model of Section 4.4 in order to formulate the total energy dissipation in macrocell $n$ as

$$P_T^n(\mathcal{P},\mathcal{S}) = \left(P_C^B + MP_C^R\right) + \frac{1}{2}\sum_{j\in\mathcal{G}^n} s^{n,j}\xi^B \left(\sum_{e_1\in\mathcal{E}^{n,j}} P_{n,e_1}^{B,n,j,T_1} + \sum_{e_2\in\mathcal{E}^{n,j}} P_{n,e_2}^{B,n,j,T_2}\right) + \frac{1}{2}\sum_{j\in\mathcal{G}^n} s^{n,j} \sum_{e\in\mathcal{E}^{n,j}} \left(\xi^B P_{n,e}^{B,n,j,T_1} + \xi^R P_{n,e}^{R,n,\mathcal{M}(e),j,T_2}\right). \quad (5.61)$$

The effect of the number of transmit antennas, of the energy dissipation of the RF as well as of the baseband circuits, and the efficiencies of the power amplifier, feeder cables, cooling system, mains power supply, and converters has been accounted for in the fixed energy dissipation terms of $P_C^B$ and $P_C^R$, while the transmit power dependent terms $\xi^B$ and $\xi^R$ are associated with the BS $n$ and its RNs, respectively.

Thus, the EE of macrocell $n$ is given by

$$\eta_E^n(\mathcal{P},\mathcal{S}) = \frac{C_T^n(\mathcal{P},\mathcal{S})}{P_T^n(\mathcal{P},\mathcal{S})}. \quad (5.62)$$

In the sequel, our aim is to maximize (5.62) for each macrocell $n$ by the careful optimization of the variables contained within $\mathcal{P}$ and $\mathcal{S}$. We define the average EE of the multicell system as

$$\eta_E(\mathcal{P},\mathcal{S}) = \frac{1}{3}\sum_{n=1}^{3} \eta_E^n(\mathcal{P},\mathcal{S}), \quad (5.63)$$

so that the average EE of the system can be optimized by individually maximizing each macrocell's EE, as it will be discussed in the following.

In contrast to the MIMO transmission protocol of Chapter 4, in this chapter we have employed the IA technique for the sake of avoiding some or all of the CCI present in the network. This was accomplished by using interference-nulling beamforming matrices at the receivers instead of the SVD-based beamforming matrices of Chapter 4, which were designed for increasing the number of SMCs satisfying the semi-orthogonality constraint of (4.25). Furthermore, in order to facilitate IA at the receivers, the transmitters in the network employ precoding matrices, which reduce the number of spatial dimensions available to them. Then, in a similar fashion to the transmission protocol presented in Chapter 4, the transmitters employ ZFBF and normalization matrices for the sake of avoiding inter-stream interference.

The objective function of (5.63) is formulated as the average of each cell's EE, whereas in Chapter 4, the objective function was formed as the EE of a single cell. Moreover, (5.63) features interference terms, which were not present in the previous chapters.

## 5.4 Optimization Problem Formulation and Solution Algorithm

In this section, our aim is to optimize the objective function (5.63). We formally describe the optimization problem as

$$\underset{\mathcal{P},\mathcal{S}}{\text{maximize}} \quad (5.63) \tag{5.64}$$

$$\text{subject to} \quad \sum_{j\in\mathcal{G}^n} s^{n,j} \leq 1,\ \forall n, \tag{5.65}$$

$$\sum_{j\in\mathcal{G}^n} s^{n,j} \left[ \sum_{e_1\in\mathcal{E}^{n,j}} P_{n,e_1}^{B,n,j,T_1} + \sum_{e\in\mathcal{E}^{n,j}} P_{n,e}^{B,n,j,T_1} \right] \leq P_{max}^{B},\ \forall n, \tag{5.66}$$

$$\sum_{j\in\mathcal{G}^n} s^{n,j} \sum_{e_2\in\mathcal{E}^{n,j}} P_{n,e_2}^{B,n,j,T_2} \leq P_{max}^{B},\ \forall n, \tag{5.67}$$

$$\sum_{j\in\mathcal{G}^n} s^{n,j} \sum_{\substack{e\in\mathcal{E}^{n,j} \\ \mathcal{M}(e)=m}} P_{n,e}^{R,n,m,j,T_2} \leq P_{max}^{R},\ \forall n,m, \tag{5.68}$$

$$s^{n,j} \in \{0,1\},\ \forall n,j, \tag{5.69}$$

$$P_{n,e_1}^{B,n,j,T_1},\ P_{n,e}^{B,n,j,T_1},\ P_{n,e_2}^{B,n,j,T_2},\ P_{n,e}^{R,n,m,j,T_2} \geq 0,\ \forall n,j,e_1,e_2,e. \tag{5.70}$$

To elaborate, (5.63) is maximized by appropriately optimizing the decision variables contained within the sets $\mathcal{P}$ and $\mathcal{S}$. The constraint (5.65) ensures that each macrocell only serves a single SMC group, thus the ICI is completely avoided. The constraints (5.66)–(5.68) require that none of the transmitters exceeds its maximum transmission power constraint. Observe that two constraints are needed for each BS, since each BS transmits in both phases, whereas the RNs only transmit during the second phase. Furthermore, the constraint (5.69) reflects the binary constraint imposed on the $s^{n,j}$ variables, while the constraints (5.70) ensures that the power control variables are non-negative.

### 5.4.1 Concave Problem Formulation

Observe that in both the full-IA and partial-IA protocols, the OCI terms are negligible or zero, if perfect CSI is available. Therefore, each macrocell's EE is independent of the decision variables associated with other macrocells, and the optimization problem can be split using the primal decomposition method described in Section 2.7, and solved distributively, where each macrocell optimizes its own EE. It can be readily proven that the objective function is nonlinear and involves binary variables. Thus, the optimization problem of (5.64)–(5.70) is a MINLP problem, which can be solved using the branch-and-bound method of Section 2.4.2. In order to mitigate the heavy computational burden that this method entails, we relax the

binary constraint (5.69) imposed on the variables $s^{n,j}$ by replacing it with

$$0 \leq s^{n,j} \leq 1, \forall n, j, \tag{5.71}$$

as it was similarly performed in Sections 3.3 and 4.6. Additionally, we introduce the auxiliary variables

$$\begin{aligned}
\widetilde{P}^{B,n,j,T_1}_{n,e_1} &= t^n s^{n,j} P^{B,n,j,T_1}_{n,e_1}, && (5.72)\\
\widetilde{P}^{B,n,j,T_1}_{n,e} &= t^n s^{n,j} P^{B,n,j,T_1}_{n,e}, && (5.73)\\
\widetilde{P}^{B,n,j,T_2}_{n,e_2} &= t^n s^{n,j} P^{B,n,j,T_2}_{n,e_2}, && (5.74)\\
\widetilde{P}^{R,n,m,j,T_2}_{n,e} &= t^n s^{n,j} P^{R,n,m,j,T_2}_{n,e}, && (5.75)\\
\widetilde{s}^{n,j} &= t^n s^{n,j}, \forall n, j, e_1, e_2, e, && (5.76)
\end{aligned}$$

where $t^n$ is given by

$$\begin{aligned}
t^n = \Bigg[ & \left(P^B_C + M P^R_C\right) + \frac{1}{2} \sum_{j \in \mathcal{G}^n} \xi^B \left( \sum_{e_1 \in \mathcal{E}^{n,j}} \widetilde{P}^{B,n,j,T_1}_{n,e_1} + \sum_{e_2 \in \mathcal{E}^{n,j}} \widetilde{P}^{B,n,j,T_2}_{n,e_2} \right) \\
& + \frac{1}{2} \sum_{j \in \mathcal{G}^n} \sum_{e \in \mathcal{E}^{n,j}} \left( \xi^B \widetilde{P}^{B,n,j,T_1}_{n,e} + \xi^R \widetilde{P}^{R,n,m,j,T_2}_{n,e} \right) \Bigg]^{-1}. \qquad (5.77)
\end{aligned}$$

Note that we have applied the Charnes-Cooper variable transformation of Section 2.4.3.5 using the variable $t^n$ for each BS $n$. In a similar manner to Section 4.6, the auxiliary SE variables $\widetilde{C}^{BU,n,j,T_1}_{n,e_1}$, $\widetilde{C}^{BU,n,j,T_2}_{n,e_2}$ and $\widetilde{C}^{BRU,n,m,j}_{n,e}$ are introduced, so that we may rewrite the optimization problem of (5.64)–(5.70) in the hypograph form given by

$$\begin{aligned}
\underset{\widetilde{\mathcal{P}}^n, \widetilde{\mathcal{S}}^n, \widetilde{\mathcal{C}}^n}{\text{maximize}} \quad & \sum_{j \in \mathcal{G}^n} \left[ \sum_{e_1 \in \mathcal{E}^{n,j}} \widetilde{C}^{BU,n,j,T_1}_{n,k,e_1} + \sum_{e_2 \in \mathcal{E}^{n,j}} \widetilde{C}^{BU,n,j,T_2}_{n,k,e_2} + \sum_{e \in \mathcal{E}^{n,j}} \widetilde{C}^{BRU,n,\mathcal{M}(e),j}_{n,k,e} \right] && (5.78)\\
& \frac{\widetilde{s}^{n,j}}{2} \log_2 \left( 1 + \frac{w^{BU,n,j,T_1}_{n,e_1} \widetilde{P}^{B,n,j,T_1}_{n,e_1}}{\widetilde{s}^{n,j} \Delta\gamma N_0 LW} \right) \geq \widetilde{C}^{BU,n,j,T_1}_{n,e_1}, \forall j, e_1, && (5.79)\\
& \frac{\widetilde{s}^{n,j}}{2} \log_2 \left( 1 + \frac{w^{BU,n,j,T_2}_{n,e_2} \widetilde{P}^{B,n,j,T_2}_{n,e_2}}{\widetilde{s}^{n,j} \Delta\gamma N_0 LW} \right) \geq \widetilde{C}^{BU,n,j,T_2}_{n,e_2}, \forall j, e_2, && (5.80)\\
& \frac{\widetilde{s}^{n,j}}{2} \log_2 \left( 1 + \frac{w^{BR,n,j,T_1}_{n,e} \widetilde{P}^{B,n,j,T_1}_{n,e}}{\widetilde{s}^{n,j} \Delta\gamma N_0 LW} \right) \geq \widetilde{C}^{BRU,n,\mathcal{M}(e),j}_{n,e}, \forall j, e, && (5.81)\\
& \frac{\widetilde{s}^{n,j}}{2} \log_2 \left( 1 + \frac{w^{RU,n,\mathcal{M}(e),j,T_2}_{n,e} \widetilde{P}^{R,n,\mathcal{M}(e),j,T_2}_{n,e}}{\widetilde{s}^{n,j} \Delta\gamma N_0 LW} \right) \geq \widetilde{C}^{BRU,n,\mathcal{M}(e),j}_{n,e}, \forall j, e, && (5.82)\\
& \sum_{j \in \mathcal{G}^n} \widetilde{s}^{n,j} \leq t^n, && (5.83)
\end{aligned}$$

$$\sum_{j\in\mathcal{G}^n}\left[\sum_{e_1\in\mathcal{E}^{n,j}}\widetilde{P}_{n,e_1}^{B,n,j,T_1}+\sum_{e\in\mathcal{E}^{n,j}}\widetilde{P}_{n,e}^{B,n,j,T_1}\right]\leq t^n\cdot P_{max}^B, \tag{5.84}$$

$$\sum_{j\in\mathcal{G}^n}\sum_{e_2\in\mathcal{E}^{n,j}}\widetilde{P}_{n,e_2}^{B,n,j,T_2}\leq t^n\cdot P_{max}^B, \tag{5.85}$$

$$\sum_{j\in\mathcal{G}^n}\sum_{\substack{e\in\mathcal{E}^{n,j}\\ \mathcal{M}(e)=m}}\widetilde{P}_{n,e}^{R,n,m,j,T_2}\leq t^n\cdot P_{max}^R,\ \forall m, \tag{5.86}$$

$$0\leq\widetilde{s}^{n,j}\leq t,\ \forall j, \tag{5.87}$$

$$\widetilde{P}_{n,e_1}^{B,n,j,T_1},\widetilde{P}_{n,e_2}^{B,n,j,T_2},\widetilde{P}_{n,e}^{B,n,j,T_1}\widetilde{P}_{n,e}^{R,n,m,j,T_2}\geq 0,\ \forall j,e_1,e_2,e, \tag{5.88}$$

$$t^n\cdot\left(P_C^B+M\cdot P_C^R\right)+\frac{1}{2}\sum_{j\in\mathcal{G}^n}\xi^B\left(\sum_{e_1\in\mathcal{E}^{n,j}}\widetilde{P}_{n,e_1}^{B,n,j,T_1}+\sum_{e_2\in\mathcal{E}^{n,j}}\widetilde{P}_{n,e_2}^{B,n,j,T_2}\right)$$
$$+\frac{1}{2}\sum_{j\in\mathcal{G}^n}\sum_{e\in\mathcal{E}^{n,j}}\left(\xi^B\widetilde{P}_{n,e}^{B,n,j,T_1}+\xi^R\widetilde{P}_{n,e}^{R,n,m,j,T_2}\right)=1, \tag{5.89}$$

$\forall n$, where $\widetilde{\mathcal{P}}^n$, $\widetilde{\mathcal{S}}^n$ and $\widetilde{\mathcal{C}}^n$ denote the variable sets containing the auxiliary variables that are associated with macrocell $n$. To elaborate further, the constraints (5.79) and (5.80) ensure that the auxiliary SE variables given by $\widetilde{C}_{n,e_1}^{BU,n,j,T_1}$ and $\widetilde{C}_{n,e_2}^{BU,n,j,T_2}$ do not exceed the direct link SEs obtained from (5.57) and (5.58), respectively, while the constraints (5.81) and (5.82) have to be combined to guarantee that (5.59) is adhered to. The constraints (5.83)–(5.88) are simply the equivalents of the constraints (5.65)–(5.70), when employing the auxiliary variables, while the constraint (5.89) is the result of the Charnes-Cooper variable transformation. Finally, the objective function (5.78) defines the EE of macrocell $n$.

Let us now aim for proving that (5.78)–(5.89) is a concave maximization problem. It can be readily shown that the objective function (5.78) is linear, hence concave. Similarly, the constraints (5.83)–(5.89) are all linear. Therefore, what remains for us to prove is that the constraints (5.79)–(5.82) are all convex. Observe that the constraints (5.79)–(5.82) are all of the form

$$\frac{s}{2}\log_2\left(1+\frac{aP}{s}\right)\geq C, \tag{5.90}$$

which was already shown to be a convex constraint in Section 4.6. Thus, we have proven that (5.78)–(5.89) is a concave programming problem, which may be solved using efficient algorithms. Let us now proceed with the portrayal of the algorithm employed in this work for solving the above problem.

### 5.4.2 Solution Algorithm

Observe that the optimization problem of (5.78)–(5.89) is akin to a sum-rate maximization problem, which is optimally solved using the well-known water-filling method of Section 2.8. The dual decomposition technique was used in Sections 3.5 and 4.6.3, which can similarly

be employed here, leading to

$$\widetilde{P}_{n,e_1}^{B,n,j,T_1} = \widetilde{s}^{n,j}\left[\frac{1}{\left(\xi^B\mu\left(i\right)+2\lambda^{n,T_1}\left(i\right)\right)\ln 2}-\frac{\Delta\gamma N_0 LW}{w_{n,e_1}^{BU,n,j,T_1}}\right]^+ \tag{5.91}$$

and

$$\widetilde{P}_{n,e_2}^{B,n,j,T_2} = \widetilde{s}^{n,j}\left[\frac{1}{\left(\xi^B\mu\left(i\right)+2\lambda^{n,T_2}\left(i\right)\right)\ln 2}-\frac{\Delta\gamma N_0 LW}{w_{n,e_2}^{BU,n,j,T_2}}\right]^+, \tag{5.92}$$

where $\widetilde{s}^{n,j}$ is yet to be determined, while $[\cdot]^+$ is equivalent to $\max(0,\cdot)$. At iteration $i$ of the dual decomposition method, $\mu\left(i\right)$ is the Lagrangian dual variable associated with the constraint (5.89), while $\lambda^{n,T_1}\left(i\right)$ and $\lambda^{n,T_2}\left(i\right)$ are respectively the Lagrangian dual variables associated with the constraints (5.84) and (5.85) for macrocell $n$. The Lagrangian dual variables are updated using the subgradient algorithm of Section 2.6 at each iteration of the dual decomposition method.

It may be shown that the power control variables of the relaying links may be formulated as

$$\widetilde{P}_{n,e}^{B,n,j,T_1} = \widetilde{s}^{n,j}\left[\frac{1}{\left(\xi^B\mu\left(i\right)+2\lambda^{n,T_1}\left(i\right)\right)\ln 2}-\frac{\Delta\gamma N_0 LW}{w_{n,e}^{BR,n,j,T_1}}\right]^+ \tag{5.93}$$

and

$$\widetilde{P}_{n,e}^{R,n,\mathcal{M}(e),j,T_2} = \widetilde{s}^{n,j}\left[\frac{1}{\left(\xi^R\mu\left(i\right)+2\nu^{n,\mathcal{M}(e),T_2}\left(i\right)\right)\ln 2}-\frac{\Delta\gamma N_0 LW}{w_{n,e}^{RU,n,\mathcal{M}(e),j,T_2}}\right]^+, \tag{5.94}$$

where $\nu^{n,\mathcal{M}(e),T_2}\left(i\right)$ is the Lagrangian dual variable associated with the constraint (5.86) for RN $\mathcal{M}\left(e\right)$ belonging to macrocell $n$. Since the attainable SE of a relaying link is limited by the weaker of the BS-RN and RN-UE links, there is no need to transmit at a higher power than necessary, if the other link is unable to support the higher SE. Thus, the power control variables for the relaying link are given by

$$\widetilde{P}_{n,e}^{B,n,j,T_1} = \min\left(\frac{w_{n,e}^{RU,n,\mathcal{M}(e),j,T_2}}{w_{n,e}^{BR,n,j,T_1}}\cdot\widetilde{P}_{n,e}^{R,n,\mathcal{M}(e),j,T_2},\widetilde{P}_{n,e}^{B,n,j,T_1}\right) \tag{5.95}$$

and

$$\widetilde{P}_{n,e}^{R,n,\mathcal{M}(e),j,T_2} = \min\left(\frac{w_{n,e}^{BR,n,j,T_1}}{w_{n,e}^{RU,n,\mathcal{M}(e),j,T_2}}\cdot\widetilde{P}_{n,e}^{B,n,j,T_1},\widetilde{P}_{n,e}^{R,n,\mathcal{M}(e),j,T_2}\right). \tag{5.96}$$

Thus, the maximum values of $\widetilde{C}_{n,e_1}^{BU,n,j,T_1}$, $\widetilde{C}_{n,e_2}^{BU,n,j,T_2}$ and $\widetilde{C}_{n,e}^{BRU,n,\mathcal{M}(e),j}$ are given by

$$\widetilde{C}_{n,e}^{BU,n,j,T_1} = \frac{\widetilde{s}^{n,j}}{2}\log_2\left(1+\frac{w_{n,e}^{BU,n,j,T_1}\widetilde{P}_{n,e}^{B,n,j,T_1}}{\Delta\gamma N_0 LW}\right), \tag{5.97}$$

$$\widetilde{C}_{n,e}^{BU,n,j,T_2} = \frac{\widetilde{s}^{n,j}}{2} \log_2 \left( 1 + \frac{w_{n,e}^{BU,n,j,T_2} \widetilde{P}_{n,e}^{B,n,j,T_2}}{\Delta \gamma N_0 L W} \right) \tag{5.98}$$

and

$$\begin{aligned} \widetilde{C}_{n,e}^{BRU,n,\mathcal{M}(e),j} &= \frac{\widetilde{s}^{n,j}}{2} \log_2 \left( 1 + \frac{w_{n,e}^{BR,n,j,T_1} \widetilde{P}_{n,e}^{B,n,j,T_1}}{\Delta \gamma N_0 L W} \right) \\ &= \frac{\widetilde{s}^{n,j}}{2} \log_2 \left( 1 + \frac{w_{n,e}^{RU,n,\mathcal{M}(e),j,T_2} \widetilde{P}_{n,e}^{R,n,\mathcal{M}(e),j,T_2}}{\Delta \gamma N_0 L W} \right), \end{aligned} \tag{5.99}$$

where the value of $\widetilde{s}^{n,j}$ is not yet known. However, regardless of the exact value of $\widetilde{s}^{n,j}$, macrocell $n$ may choose the specific SMC group $j$ that obtains the highest value of

$$\left[ \sum_{e_1 \in \mathcal{E}^{n,j}} \widetilde{C}_{n,e_1}^{BU,n,j,T_1} + \sum_{e_2 \in \mathcal{E}^{n,j}} \widetilde{C}_{n,e_2}^{BU,n,j,T_2} + \sum_{e \in \mathcal{E}^{n,j}} \widetilde{C}_{n,e}^{BRU,n,\mathcal{M}(e),j} \right] \tag{5.100}$$

in order to maximize the objective function (5.78) by setting

$$\widetilde{s}^{n,j} = t^n, \tag{5.101}$$

where the value of $t^n$ is not yet known. As a result, the SMC groups $j' \neq j$ are not chosen and we may set the optimal values of $\widetilde{s}^{n,j'*} = \widetilde{P}_{n,e_1}^{B,n,j',T_1*} = \widetilde{P}_{n,e_2}^{B,n,j',T_2*} = \widetilde{P}_{n,e}^{B,n,j',T_1*} = \widetilde{P}_{n,e}^{R,n,\mathcal{M}(e),j',T_2*} = \widetilde{C}_{n,e_1}^{BU,n,j',T_1*} = \widetilde{C}_{n,e_2}^{BU,n,j',T_2*} = \widetilde{C}_{n,e}^{BRU,n,\mathcal{M}(e),j'*} = 0$, $\forall e_1, e_2, e, j' \neq j$. On the other hand, $\widetilde{P}_{n,e_1}^{B,n,j,T_1*} = \widetilde{P}_{n,e_1}^{B,n,j,T_1}$, $\widetilde{P}_{n,e_2}^{B,n,j,T_2*} = \widetilde{P}_{n,e_2}^{B,n,j,T_2}$, $\widetilde{P}_{n,e}^{B,n,j,T_1*} = \widetilde{P}_{n,e}^{B,n,j,T_1}$ and $\widetilde{P}_{n,e}^{R,n,\mathcal{M}(e),j,T_2*} = \widetilde{P}_{n,e}^{R,n,\mathcal{M}(e),j,T_2}$ for the selected SMC group.

The optimal value of $t^n$ is then given by

$$\begin{aligned} t^{n*} = \Bigg( & P_C^B + M \cdot P_C^R + \sum_{j \in \mathcal{G}^n} \frac{1}{2\widetilde{s}^{n,j}} \xi^B \left( \sum_{e_1 \in \mathcal{E}^{n,j}} \widetilde{P}_{n,e_1}^{B,n,j,T_1*} + \sum_{e_2 \in \mathcal{E}^{n,j}} \widetilde{P}_{n,e_2}^{B,n,j,T_2*} \right) \\ & + \sum_{j \in \mathcal{G}^n} \frac{1}{2\widetilde{s}^{n,j}} \sum_{e \in \mathcal{E}^{n,j}} \left( \xi^B \widetilde{P}_{n,e}^{B,n,j,T_1*} + \xi^R \widetilde{P}_{n,e}^{R,n,m,j,T_2*} \right) \Bigg)^{-1}. \end{aligned} \tag{5.102}$$

Observe that this is possible, since (5.102) is only dependent on the dual variables. Furthermore, determining the value of $t^{n*}$ gives the optimal values of $\widetilde{s}^{n,j*}$, and consequently $\widetilde{P}_{n,e_1}^{B,n,j,T_1*}$, $\widetilde{P}_{n,e_2}^{B,n,j,T_2*}$, $\widetilde{P}_{n,e}^{B,n,j,T_1*}$, $\widetilde{P}_{n,e}^{R,n,m,j,T_2*}$, $\widetilde{C}_{n,e}^{BU,n,j,T_1*}$, $\widetilde{C}_{n,e}^{BU,n,j,T_2*}$ and $\widetilde{C}_{n,e}^{BRU,n,\mathcal{M}(e),j*}$ for the selected SMC group.

By following the above derivations, the constraints (5.79)–(5.83) and (5.87)–(5.89) are implicitly satisfied and there is no need to introduce dual variables for them. This EEM solution algorithm may be implemented distributively, and iterates between obtaining the optimal primal variables and applying the subgradient method of Section 2.6 for updating

TABLE 5.3: The EEM algorithm based on dual decomposition and the subgradient method.

**Algorithm 1** EEM algorithm

$i \leftarrow 0$
**do while** $|\lambda^{n,T_1}(i) - \lambda^{n,T_1}(i-1)| > \epsilon$ **or**
$|\lambda^{n,T_1}(i) - \lambda^{n,T_1}(i-1)| > \epsilon$ **or**
$|\nu^{n,m,T_2}(i) - \nu^{n,m,T_2}(i-1)| > \epsilon$ **or**
$|\mu(i) - \mu(i-1)| > \epsilon$
  $i \leftarrow i+1$
  **if** $i > I_{max}$
    **break**
  **end if**
  **for** $n$ **from** 1 **to** 3
    **for each** $j$ **in** $\mathcal{G}^n$
      Obtain the optimal power allocation using (5.91)–(5.96)
      Compute their achievable SE using (5.97)–(5.99)
    **end for**
    Find the optimal SMCs, which obtains the maximum (5.100)
    Compute the optimal $t$ using (5.102)
  **end for**
  Update the dual variables $\lambda^{n,T_1}(i)$, $\lambda^{n,T_2}(i)$, $\nu^{n,m,T_2}(i)$
  and $\mu(i)$ using the subgradient method of Section 2.6
**end do**
**return**

the dual variables, until the change in the dual variable values becomes less than $\epsilon$ or the maximum number of iterations, $I_{max}$, has been reached. The EEM algorithm is summarized in Table 5.3, where $\lambda^{n,T_1}(i)$, $\lambda^{n,T_2}(i)$, $\nu^{n,m,T_2}(i)$ and $\mu(i)$ indicate the value of their respective dual variables at the $i$th iteration.

In contrast to the previous chapter, we aim for optimizing the network-wide EE metric. However, since we have employed the primal decomposition of [339] for the sake of solving the EE optimization problem distributively at each cell, the optimal power variables, SMC groups and the solution algorithm follow a similar form to those presented in Chapter 4.

## 5.5 Numerical Results and Discussions

This section presents the numerical results obtained, when the solution algorithm presented in Section 5.4.2 is employed for the EEM problem of (5.78)–(5.89), where the simulation parameters are given in Table 5.4. In all cases, the step sizes and the initial values of the dual variables described in Section 5.4.2 are empirically optimized so that the algorithm converges in as few iterations as possible, although the exact analytical method for achieving this still remains an open issue. In our experience, the algorithm converges within just 10 iterations when carefully chosen step sizes are employed, regardless of the size of the problem.

TABLE 5.4: Simulation parameters used to obtain all results in this section unless otherwise specified.

| Simulation parameter | Value |
|---|---|
| Subcarrier block bandwidth, $W$ [Hertz] | 180k |
| Number of RNs per macrocell, $M$ | $\{0, 1, 2, 3\}$ |
| Number of subcarriers blocks, $N$ | 12 |
| Number of UEs, $K$ | 6 |
| Antenna configuration, $(N_B, N_R, N_U)$ | $(4, 4, 4)$ |
| Semi-orthogonality parameter, $\alpha$ | 0.1 |
| Inter-site distance (ISD), [km] | $\{1.5, 2.5, 3.5, 4.5\}$ |
| Minimum number of receive dimensions at the RNs and UEs, $S^R$ and $S^U$ | 1 and 2 |
| Ratio of BS-to-RN distance to the cell radius, $D_r$ | 0.7 |
| SNR gap of wireless transceivers, $\Delta\gamma$ [dB] | 0 |
| Maximum total transmission power of the BS and RNs, $P^B_{max}$ and $P^R_{max}$ [dBm] | $\{0, 12, 24, 36, 48, 60\}$ |
| Fixed power rating of the BS, $P^B_C$ [Watts] [352, 369] | $32.306N_B$ |
| Fixed power rating of RNs, $P^R_C$ [Watts] [352, 369] | $21.874N_R$ |
| Reciprocal of the BS power amplifier's drain efficiency, $\xi^B$ [352, 369] | $3.24N_B$ |
| Reciprocal of the RNs' power amplifier's drain efficiency, $\xi^R$ [352, 369] | $4.04N_R$ |
| Noise power spectral density, $N_0$ [dBm/Hz] | $-174$ |
| Convergence threshold, $\epsilon$ | $10^{-8}$ |
| Number of channel samples | $10^4$ |

Furthermore, we employed the path-loss model of [354] and assumed that all BS-UE and RN-UE links are NLOS links, since they are typically blocked by buildings and other large obstructing objects, while all BS-RN links may realistically be assumed to be LOS links, since the RNs may be strategically positioned on tall buildings to create strong wireless backhaul links. Furthermore, independently and randomly generated set of UE locations as well as fading channel realizations were used. Again, for benchmarking we employ a baseline algorithm, which relies on random SMC selections and equal power allocation across the selected SMCs. This algorithm is termed as the EPA algorithm.

The attainable performance of both the full-IA and partial-IA protocols is explored and these results are obtained by employing the optimized power control variables and group selection variables in the actual system model. Therefore, the results reflect the actual EE achieved rather than the optimized objective value of (5.78), which is optimistic, since it does not account for any potential OCI remaining after employing the partial-IA protocol.

### 5.5.1 The Variation of SE and EE for Different Values of $P^B_{max}$ and $P^R_{max}$

The effects of varying both $P^B_{max}$ and $P^R_{max}$ are demonstrated in Fig. 5.11. Observe that the partial-IA protocol outperforms the full-IA protocol for all the power constraints considered. This is due to the requirements of (5.9), (5.15), (5.27) and (5.37), which restrict the number of data streams that the BSs can transmit simultaneously in each phase. The full-IA protocol imposes more restrictive constraints than the partial-IA protocol, since the partial-IA protocol only requires that the receive BF matrices has to eliminate the ICI, rather than both the ICI and OCI that the full-IA protocol has to null. Observe furthermore that the EPA algorithms achieve higher SE values than their EEM algorithmic counterparts at high $P^B_{max}$ values. However, this is achieved at a higher cost to the EE obtained from using the EPA algorithms, when compared to their EEM counterparts. In fact, in the low to medium $P^B_{max}$ regime, both the SEM and EEM correspond to the same solution, as demonstrated in Chapters 3 and 4. This results in a higher SE for the EEM algorithm than for the heuristic EPA algorithm. As the value of $P^B_{max}$ increases, the EPA continues to allocate more power, which increases the SE obtained, without any cognizance to the EE performance.

In comparison to the results presented in Section 4.7, the SE and EE obtained does not increase significantly upon increasing $P^R_{max}$. This can be attributed to the low multiplexing gain specified in these experiments, given that $S^R = 1$. The results of the next subsection explore the effects of varying the requirements imposed on $S^U$ and $S^R$.

### 5.5.2 The Variation of SE and EE for Different Values of $S^U$ and $S^R$

Fig. 5.12 shows the results obtained upon varying $S^U$ and $S^R$. Once again, the partial-IA protocol outperforms the full-IA protocol in terms of both its SE and EE performances. Additionally, we observe that the EPA algorithm performs worse than the EEM algorithm for all cases. Increasing $S^U$ has a marginal effect on the SE and EE obtained for both protocols. However, increasing $S^R$ does lead to an increase in SE, when employing the partial-IA protocol, albeit at a cost to EE resulting from the fixed power dissipation costs of the RNs. Observe that increasing $S^R$ reduces the SE attained when using the full-IA protocol. This may be explained by the detrimental effects of the constraints imposed on the multiplexing gain of the BSs' transmissions when employing the full-IA protocol, because increasing $S^R$ imposes a substantial reduction on both (5.9) and (5.27), when multiple RNs are operated in each macrocell. This reduction in SE is not so dominant for the partial-IA protocol, since the increase in the multiplexing gain of the RNs' transmissions outweighs the detrimental effects of imposing a multiplexing gain restriction at the BSs due to (5.37). Additionally, the potential multiplexing gain attained at the BSs in the first transmission phase, given by (5.15), is not affected by the increase of $S^R$.

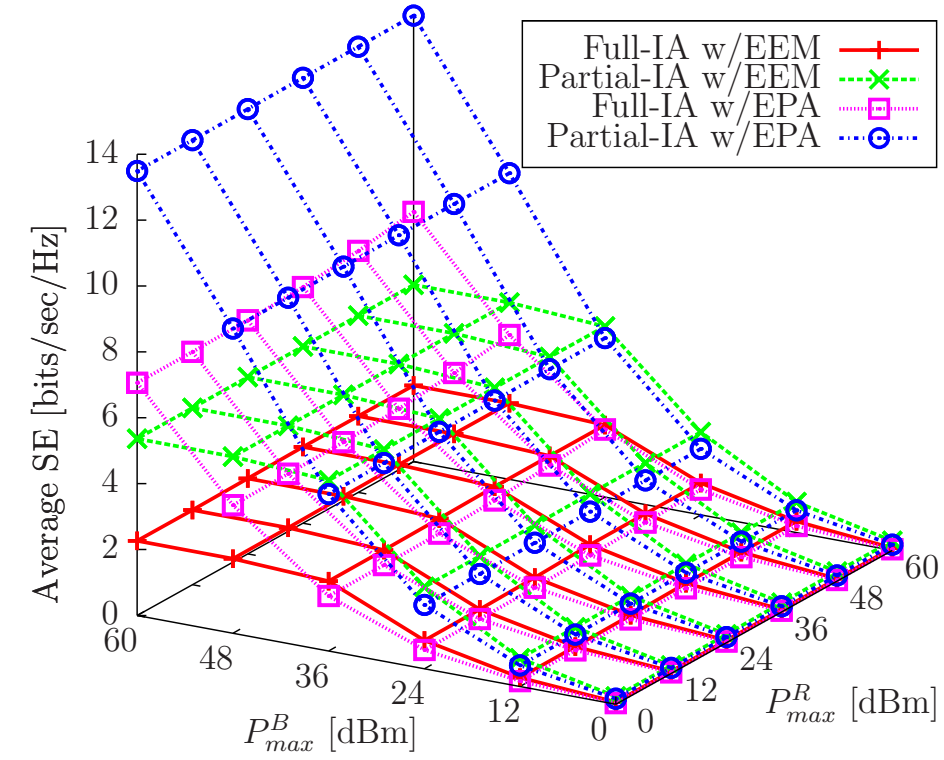


(a) Surface plots of the achievable SE when using the EEM and EPA algorithms.

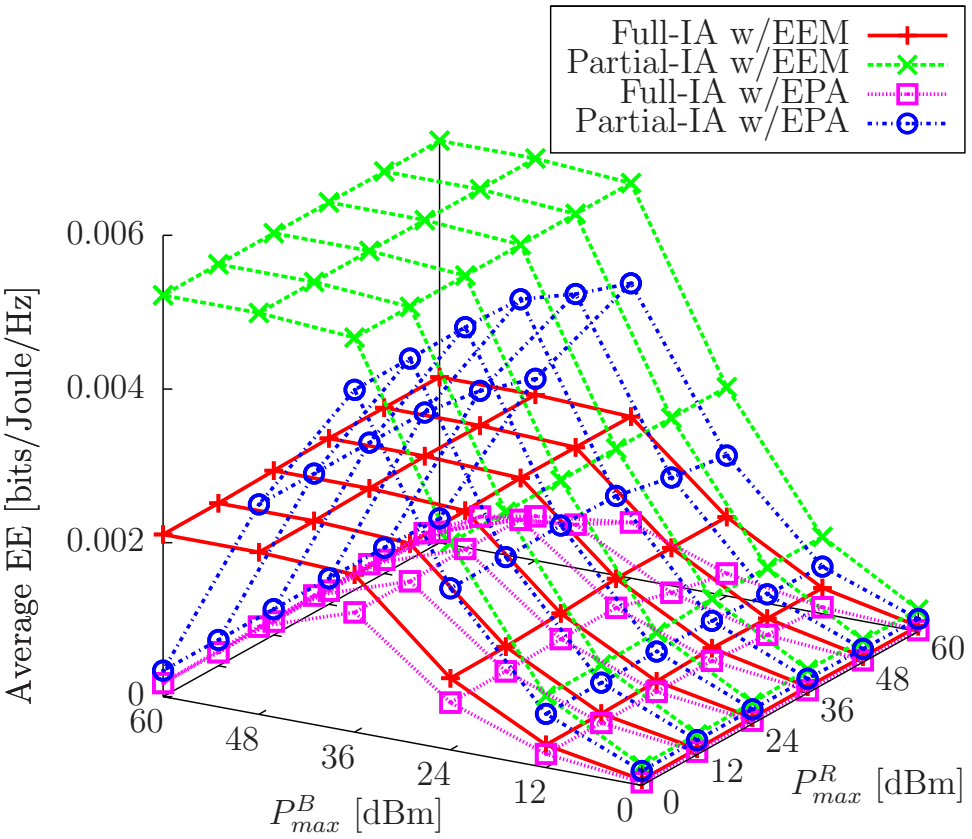


(b) Surface plots of the achievable EE when using the EEM and EPA algorithms.

FIGURE 5.11: The average achievable SE and EE when using the EEM and EPA algorithms with either full-IA or partial-IA, for varying $P^B_{max}$ and $P^R_{max}$, and using the parameters in Table 5.4 with $M = 2$ and an ISD of 1.5km.

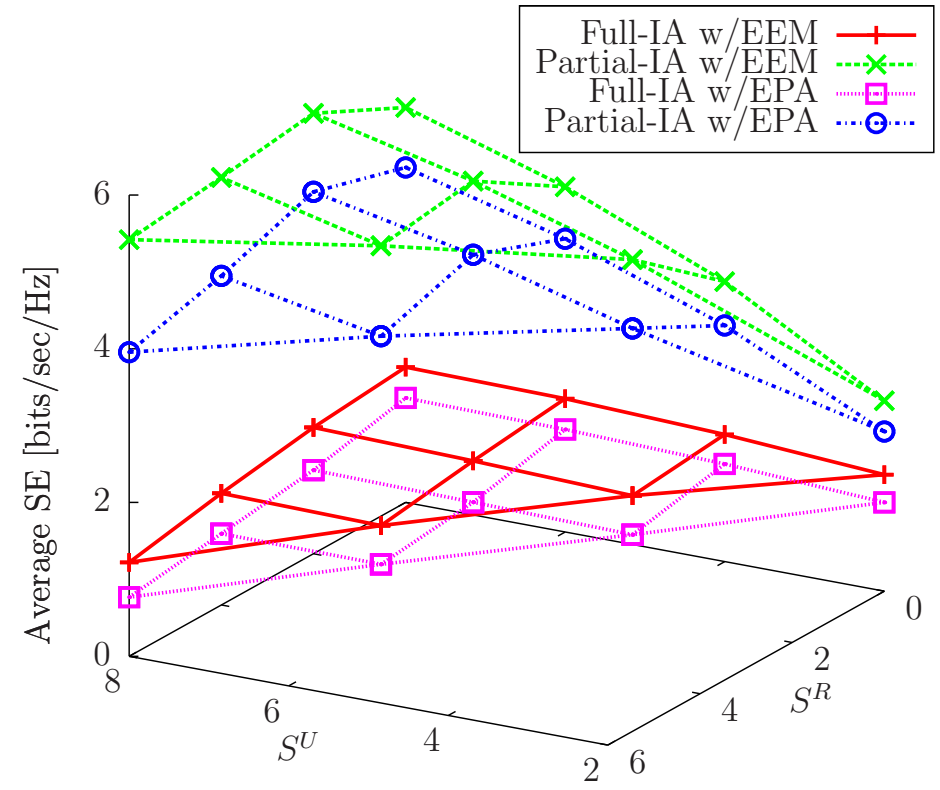


(a) Surface plots of the achievable SE when using the EEM and EPA algorithms.

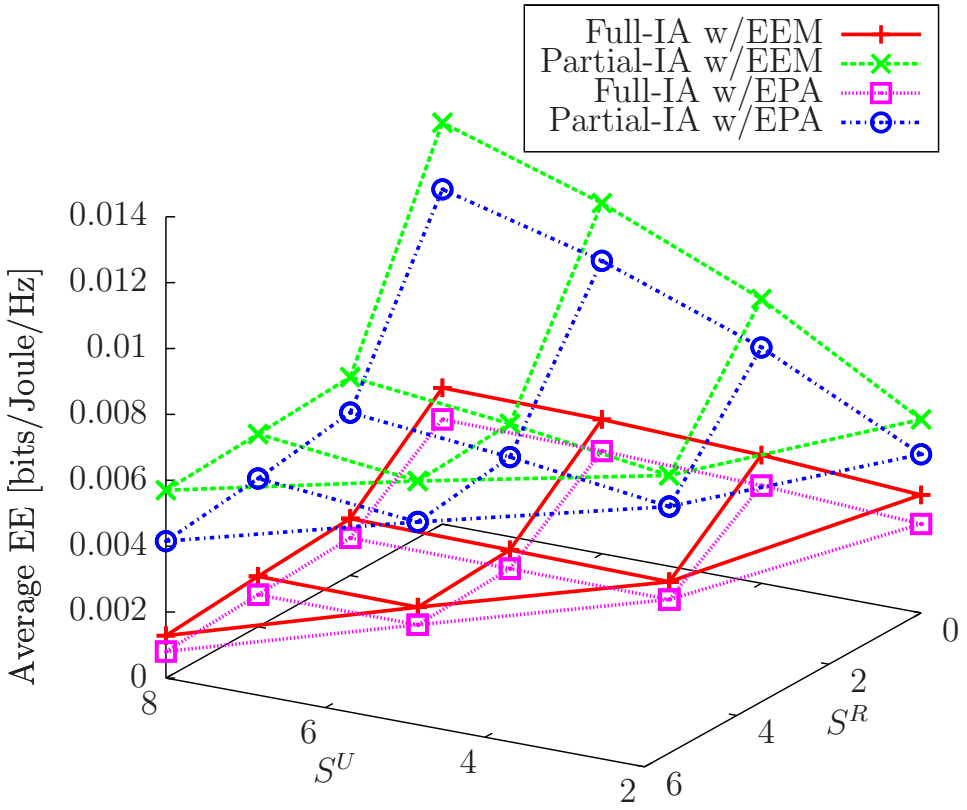


(b) Surface plots of the achievable EE when using the EEM and EPA algorithms.

FIGURE 5.12: The average achievable SE and EE when using the EEM and EPA algorithms with either full-IA or partial-IA, for varying $S^U$ and $S^R$, and using the parameters in Table 5.4 with $M = 2$, $P^B_{max} = 30$dBm, $P^R_{max} = 20$dBm and an ISD of 1.5km.

### 5.5.3 The Variation of SE and EE for Different Values of $M$ and Inter-Site Distance

As shown in Fig. 5.13, both the achievable SE and EE decreases as the ISD is increased, indicating that the effect of a higher path-loss on the channel gains has a more grave detrimental effect on both the SE and EE than the beneficial effects of the reduced interference levels. Once again, the EPA algorithm performs worse than their EEM algorithmic counterparts. Additionally, the SE attained, when using the full-IA protocol is slightly reduced upon increasing $M$ due to both (5.9) and (5.27), while the EE achieved is reduced, as the power dissipation of the system is increased upon increasing $M$. Furthermore, the SE obtained when using the partial-IA protocol peaks for $M = 1$, but decreases slightly, upon increasing $M$ further, since then the multiplexing gain of the experienced during the second phase is reduced as indicated by (5.37). By contrast, the EEM of the partial-IA protocol only decreases upon increasing $M$.

In fact, when $M = 0$ or $S^R = 0$ we arrive at a special case of the partial-IA protocol, which is similar to the conventional single cell multi-user ZFBF in the absence of RNs. However, the proposed partial-IA protocol represents a sophisticated extension of classic ZFBF to the broad class of multi-relay aided multi-cell networks, which have been combined with intelligent user selection.

### 5.5.4 The Variation of SE and EE for Different Values of $K$ and Inter-Site Distance

Fig. 5.14 shows that both the achievable SE and EE increase, when $K$ increases, which was also demonstrated in Fig. 3.6. This happens owing to the increased multi-user diversity attained, when multiple UEs are active in the system, which allows the EEM algorithm to allocate power and choose SMC groups resulting in greater EE values. Note that both the SE and EE values also increase upon increasing $K$, when using the EPA algorithm, even though it randomly selects the SMC groups to serve. This happens owing to the increased number of available SMC groups as well as due to the increase in the number of SMCs in each group as a result of the higher number of UEs, which in turn generate more SMCs satisfying the semi-orthogonality constraint of (4.25). Note also that the partial-IA protocol outperforms the full-IA protocol in all cases, as we demonstrated in Figs. 5.12 and 5.13.

### 5.5.5 The Sensitivity of the IA Protocols to CSI Errors

Furthermore, we may explore the effects of CSI errors on the achieved EE when using either transmission protocol. For example, the CSI errors are introduced into the BS-RN channel

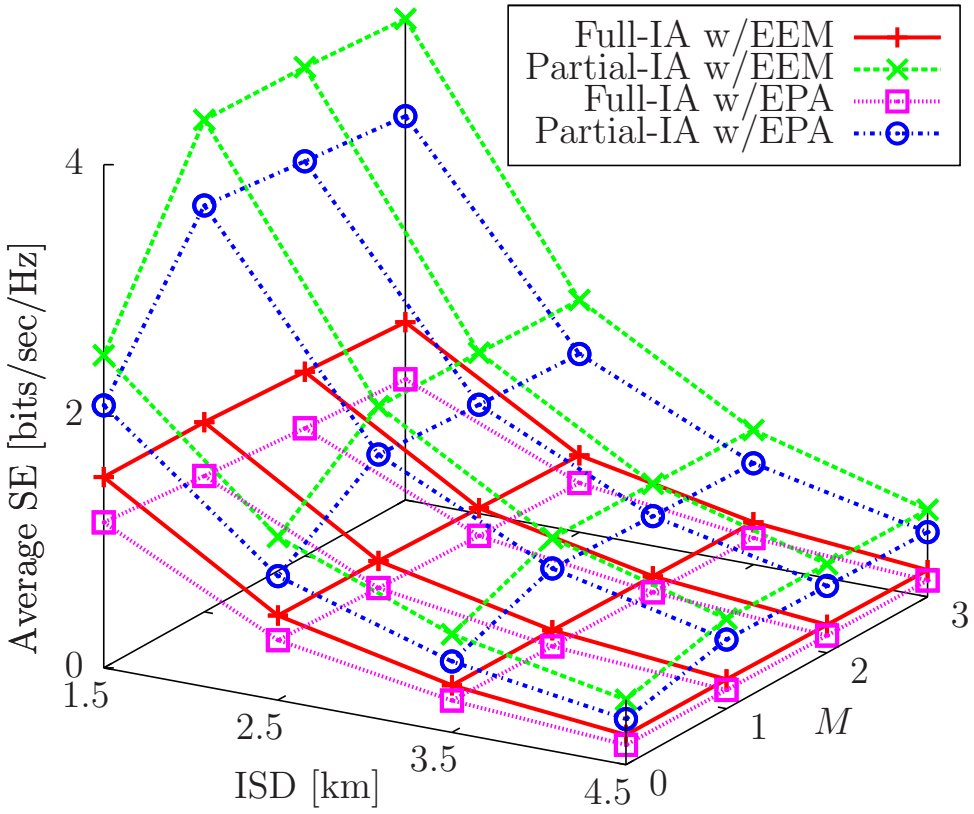


(a) Surface plots of the achievable SE when using the EEM and EPA algorithms.

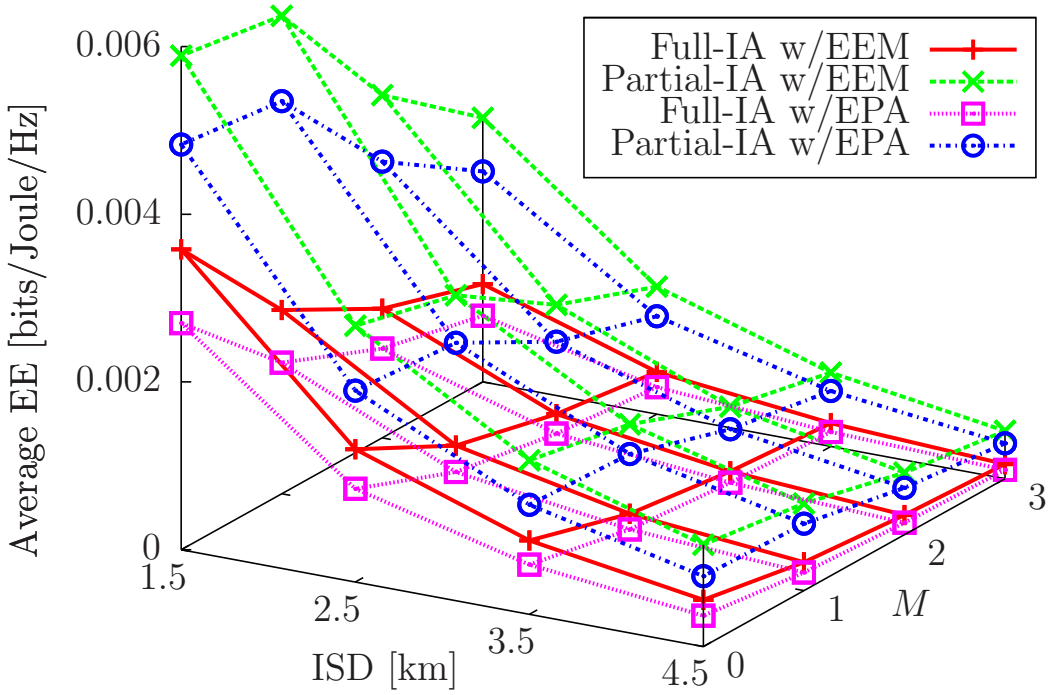


(b) Surface plots of the achievable EE when using the EEM and EPA algorithms.

FIGURE 5.13: The average achievable SE and EE when using the EEM and EPA algorithms with either full-IA or partial-IA, for varying $M$ and ISD, and using the parameters in Table 5.4 with $P^B_{max} = 30$dBm, $P^R_{max} = 20$dBm and an ISD of 1.5km.

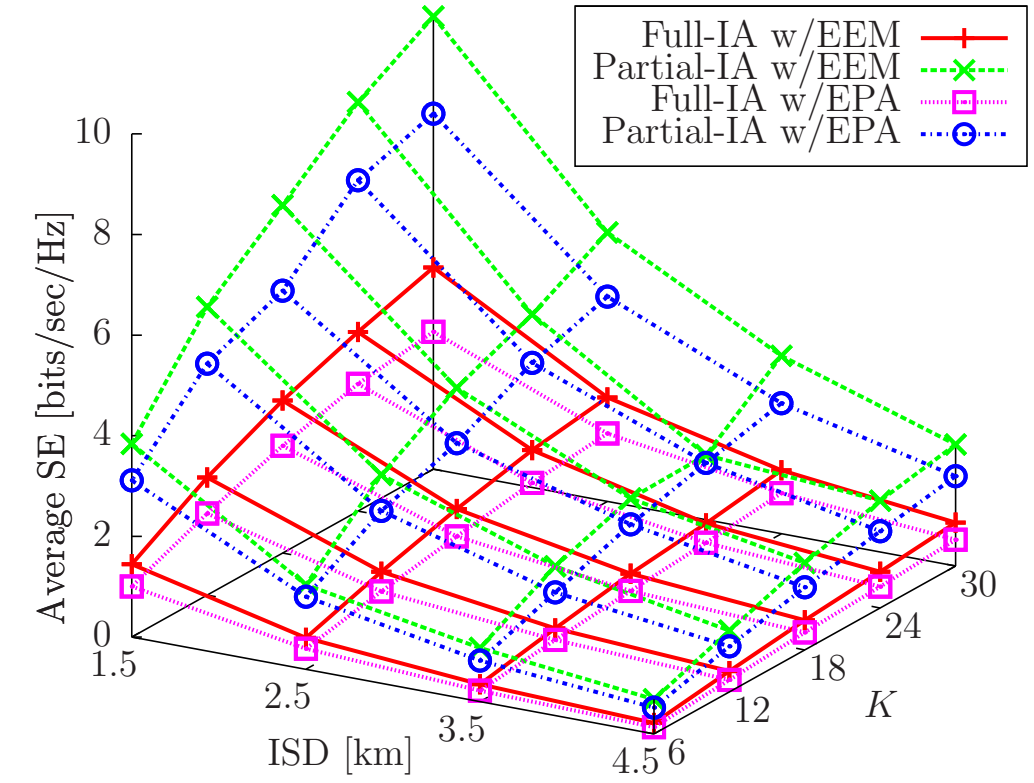


(a) Surface plots of the achievable SE when using the EEM and EPA algorithms.

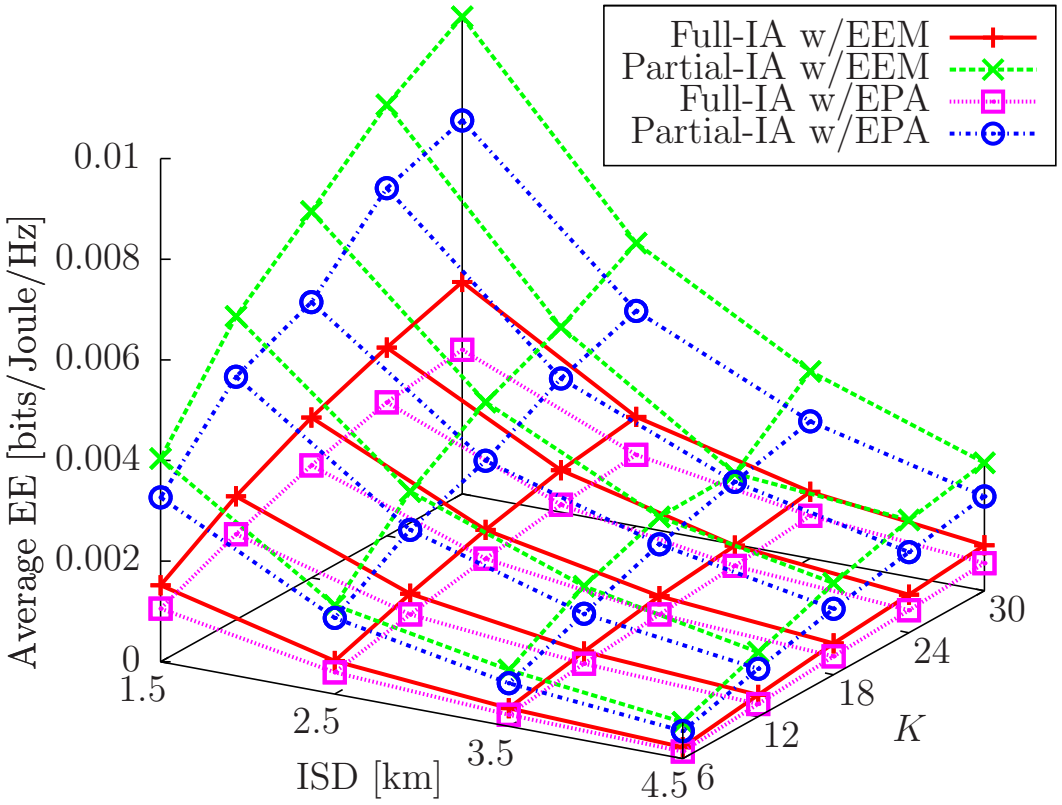


(b) Surface plots of the achievable EE when using the EEM and EPA algorithms.

FIGURE 5.14: The average achievable SE and EE when using the EEM and EPA algorithms with either full-IA or partial-IA, for varying $K$ and ISD, and using the parameters in Table 5.4 with $P^B_{max} = 30$dBm, $P^R_{max} = 20$dBm and $M = 2$.

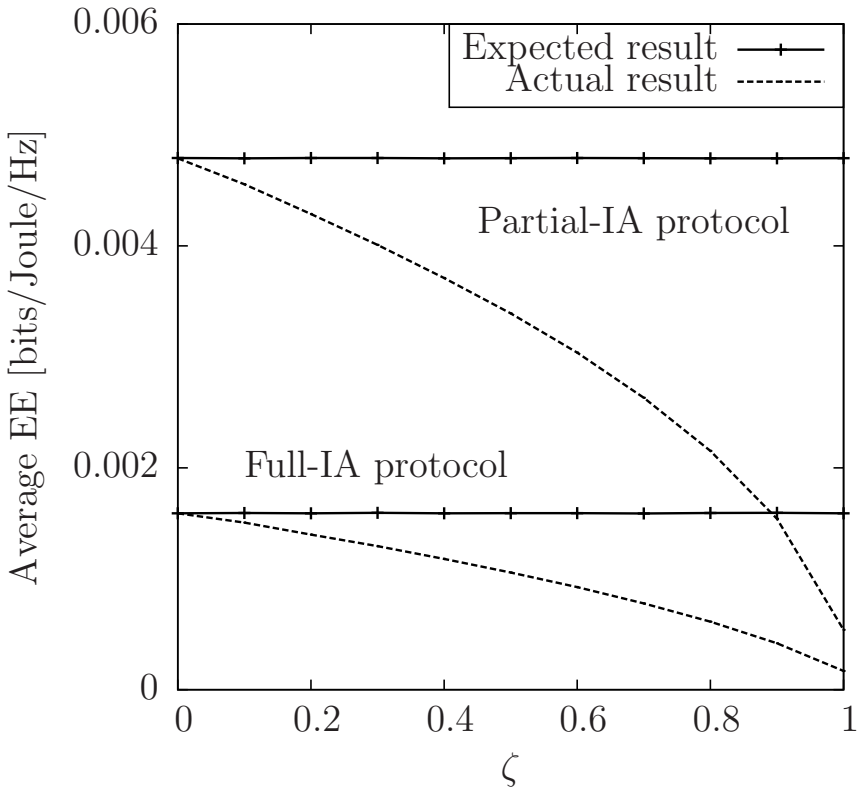


FIGURE 5.15: The average expected EE versus the actually achieved EE when using the EEM algorithm with either full-IA or partial-IA, for varying values of $\zeta$, and using the parameters in Table 5.4 with $M = 2$, $P^B_{max} = 30$dBm, $P^R_{max} = 20$dBm and an ISD of 1.5km.

matrices as follows

$$\breve{\mathbf{H}}^{BR,l,n'}_{n,m} = \sqrt{1-\zeta^2}\breve{\mathbf{H}}^{BR,l,n'}_{n,m} + \zeta\Delta\breve{\mathbf{H}}^{BR,l,n'}_{n,m} \tag{5.103}$$

where $\breve{\mathbf{H}}^{BR,l,n'}_{n,m}$ denotes the channel estimate assuming perfect CSI, $\Delta\breve{\mathbf{H}}^{BR,l,n'}_{n,m}$ denotes the random error in the channel estimate, and $\breve{\mathbf{H}}^{BR,l,n'}_{n,m}$ denotes the true channel estimate with the CSI error. The matrix $\breve{\mathbf{H}}^{BR,l,n'}_{n,m}$ is combined with pathloss to form $\mathbf{H}^{BR,1,n'}_{n,m}$, which may then be employed for computing the BF matrices and scheduling decisions as described in Section 5.3. The matrix $\Delta\breve{\mathbf{H}}^{BR,l,n'}_{n,m}$ is randomly generated for each channel matrix and its entries are drawn from complex normal distributions having a zero mean and a unit variance. Thus, the parameter, $\zeta$, denotes the relative magnitude of the CSI error.

Fig. 5.15 characterizes the effects of different values of $\zeta$ on the achieved EE. Since the optimization algorithm is oblivious to the effect of CSI errors, the optimized EE remains constant for each protocol independent of the value of $\zeta$. However, the actual EE, obtained from employing the BF matrices and scheduling decisions created when assuming that the erroneous channel matrices are correct, reduces as $\zeta$ increases. As expected, the greater the value of $\zeta$, the greater the difference between the expected EE and the actual EE, regardless of the transmission protocol. When $\zeta = 1.0$, both protocols obtain actual EE values of roughly 11% of the expected EE values.

TABLE 5.5: Summary of the EE reduction caused by CSI errors, as was depicted in Fig. 5.15.

| Magnitude of CSI error, $\zeta$ | Reduction in EE achieved with the full-IA protocol | Reduction in EE achieved with the partial-IA protocol |
|---|---|---|
| 0.0 | 0.0% | 0.0% |
| 0.1 | 5.4% | 4.9% |
| 0.2 | 12.1% | 10.5% |
| 0.3 | 18.9% | 16.4% |
| 0.4 | 25.9% | 22.5% |
| 0.5 | 33.7% | 29.2% |
| 0.6 | 41.9% | 36.6% |
| 0.7 | 51.0% | 45.1% |
| 0.8 | 61.5% | 55.0% |
| 0.9 | 73.8% | 67.8% |
| 1.0 | 89.4% | 88.7% |

## 5.6 Chapter Summary and Conclusions

In this chapter, a multi-user, multi-relay, multi-cell MIMO system model is studied. In order to avoid the excessive interference inflicted by the multiple transmission sources, a pair of distributed IA protocols were designed. The first, termed as full-IA, completely avoids any interference by finding receive BF matrices, which entirely eliminate the interference imposed at the receivers. However, this comes at a cost to the spatial multiplexing gain of the BSs, which limits the number of DL transmission streams. The second transmission protocol, namely partial-IA, aims for striking a balance between the spatial multiplexing gain and interference contamination by finding receive BF matrices, which only null the interference emerging from sources within the same macrocell. Employing the receive BF matrices created by either of these transmission protocols results in a list of SMCs, which correspond to data streams that may be conveyed by the BS. We formally defined the problem of maximizing the EE by optimally choosing the SMCs as well as by appropriately choosing their power control variables. The resultant nonconvex optimization problem was converted into a convex optimization problem with the aid of carefully chosen variable relaxations and transformations, which was then solved using the classic dual decomposition and subgradient methods [339], that may be implemented distributively at each BS. We characterized the attainable SE and EE performances of both protocols for a range of system parameters, while comparing the performance of our EEM algorithm to that of a baseline EPA algorithm. Additionally, we explored the effect of CSI errors on the achievable EE of either IA protocol and found that any CSI errors severely reduce the attainable EE, as summarized in Table 5.5.

To summarize, the EEM algorithm of Section 5.4.2 outperforms the EPA algorithm described in Section 5.5 in most cases. Moreover, the EEM algorithm outperforms the EPA algorithm

TABLE 5.6: Summary of the attainable gains in EE, when employing the EEM algorithm compared to the EPA algorithm, as depicted in Figs. 5.11 to 5.13.

| Figures | Max. gain in EE using full-IA | Min. gain in EE using full-IA | Max. gain in EE using partial-IA | Min. gain in EE using partial-IA |
|---|---|---|---|---|
| Fig. 5.11 | 15.3 | 1.9 | 16.5 | 1.4 |
| Fig. 5.12 | 1.6 | 1.3 | 1.4 | 1.2 |
| Fig. 5.13 | 1.6 | 1.3 | 1.4 | 1.2 |

TABLE 5.7: Summary of the attainable gains in EE, when employing the partial-IA protocol compared to the full-IA protocol, as depicted in Figs. 5.11 to 5.13.

| Figures | Max. gain in EE using full-IA | Min. gain in EE using full-IA |
|---|---|---|
| Fig. 5.11 | 4.1 | 2.4 |
| Fig. 5.12 | 4.4 | 1.6 |
| Fig. 5.13 | 3.3 | 1.6 |

in all cases, when considering only the attainable EE metric, as shown in Table 5.6. On the other hand, the partial-IA protocol of Sections 5.3.1.2 and 5.3.2.2 surprisingly outperforms the full-IA protocol of Sections 5.3.1.1 and 5.3.2.1 in all cases as shown in Table 5.7. For the cell sizes considered, the path-loss mitigates the majority of the OCI, and thus the full-IA protocol actually over-compensates, when reducing the available number of transmit dimensions at the transmitters to facilitate IA. However, in denser wireless networks the CCI may become strong enough to warrant using the full-IA protocol. Furthermore, the maximum transmission power constraint imposed on the RNs has only a marginal effect on the attainable EE, which is however strongly dependent on the maximum power constraint of the BS. For the scenario considered, $P^B_{max} = 36$dBm is sufficiently high to attain the maximum EE. When employing the full-IA protocol, increasing $S^R$ only reduces the attainable SE and EE, since the multiplexing gain achieved by either the BSs or RNs is severely reduced in order to accommodate IA. However, when employing the partial-IA protocol, the maximum SE is attained when $S^R = 2$, albeit at a substantial reduction of the EE. Furthermore, employing a single RN within each sector is sufficient for maximizing the SE for the cell sizes considered, when employing the partial-IA protocol. On the other hand, the SE does not benefit from employing RNs, when using the full-IA protocol. However, employing additional RNs in conjunction with either protocol reduces the attainable EE.

Chapter 6

# Conclusions and Future Research

## 6.1 Summary and Conclusions

This thesis has motivated and studied the DL EE maximization problem in the context of relay-aided cellular networks. We firstly described the relevant convex optimization tools, which were then extensively employed in later chapters for the sake of formulating and solving the formally defined problems associated with progressively more complex system models. We developed sophisticated transmission protocols relying on powerful signal processing techniques, such as spatial multiplexing and IA, for the sake of formulating a tractable optimization problem for each system. Thus, we were capable of obtaining the optimal RA with the aid of low-complexity iterative algorithms. To elaborate further:

- **Chapter 1**
  We justified the importance of EEM as a concern for current and future cellular networks, which was complemented by discussing some rudimentary issues of the discrete channel capacity, channel fading, the OFDMA method, relaying protocols and of RA in Sections 1.1 to 1.4. A state-of-the-art review was provided in Section 1.5, where an overview of RA was given, before delving into contributions in the area of RA conceived for OFDMA systems, which specifically aim for EE optimization. Additionally, the coverage of the literature review was progressively expanded to include more complex systems, such as relay-aided and MIMO-aided systems in Sections 1.5.6 and 1.5.7, respectively. Brief summaries of the pertinent references related to these topics were provided in Tables 1.1 to 1.3. Furthermore, we observed that much effort has been devoted to EE optimization of OFDMA cellular networks. However, most papers were concerned with minimizing the total energy, rather than optimizing the fractional EE metric. In particular, the EEM of relay-aided and MIMO-aided relaying systems has rarely been studied. In Section 1.6, we concluded the chapter with an overview of the organization of this thesis, as well as listed

its novel contributions. An illustration of the organization of this thesis was provided in Fig. 1.8.

- **Chapter 2**

  In Section 2.3, we presented the basics of convex sets and functions, along with intuitive geometric examples for the sake of determining whether they are convex or not in Figs. 2.2 and 2.3. Some well-known convex functions were listed and the specific method by which they can be combined to form more complex functions was elucidated in Section 2.3.4. In Section 2.4, we formally defined the classic convex optimization problem structure. Although some problems, such as MINLPs and FP problems do not readily fall within the convex problem framework, in Sections 2.4.2 and 2.4.3 we presented methods capable of reformulating them, so that the conventional convex optimization solution algorithms can still be applied.

  The solution algorithms described later crucially rely on the concept of duality for the sake of ensuring that the optimal solution is indeed obtained. As described in Section 2.5, duality is a method derived for obtaining bounds on the optimal objective function value. Thus, if a solution obtains an objective function value close enough to these bounds, the conclusion is that the problem has been solved to an acceptable degree of accuracy. The difference between strong and weak dualities as well as their implications were elucidated in Section 2.5.3. In Section 2.5.4, we presented the KKT conditions, which are the necessary and sufficient optimality conditions to be satisfied in order to optimally solve convex optimization problems. They form the basis of the solution algorithms which followed. We began by describing iterative algorithms conceived for solving simple unconstrained optimization problems using the so-called descent methods in Section 2.6.1. On the other hand, the family of equality-constrained problems requires that each iteration should be feasible, which is guaranteed by initializing the algorithm to a feasible point, and only progressing along feasible descent directions. In Section 2.6.3, we then discussed interior point methods proposed for solving problems featuring both equality and inequality constraints. The logarithmic barrier function was presented in Fig. 2.20, and its application in combining the inequality constraints into the associated objective function was highlighted in Section 2.6.3.1. Thus, it is possible that the solution to the general optimization problem presented in Section 2.4 is obtained by solving a series of equality constrained problems. Furthermore, a simple primal-dual interior point method was provided in Section 2.6.3.2. We then explored decomposition theory in Section 2.7 and considered how either primal or dual decomposition can be applied to any decomposable problem.

  The chapter was then concluded with some intuitive examples of convex optimization applied in the wireless communications field in Section 2.8. Specifically, the well-known classical water-filling method was depicted in Fig. 2.22 and was reviewed, as well as its relation to duality. We then expanded upon the water-filling principle applied to more

complex systems.

- **Chapter 3** [330, 331]

  A multiuser multi-relay OFDMA cellular network was considered in this chapter. In Section 3.3, we formulated the problem of maximizing the EE of the system with the aid of optimal subcarrier and power allocation, where both simultaneous direct and AF relaying links were permitted. As described in Section 3.2, each UE was associated with the specific RN that is geographically nearest to itself, hence relay selection was implicitly performed. We applied several variable relaxations to the optimization problem and proved that the result is the fractional quasi-concave maximization problem of (3.10)–(3.15), as detailed in Section 3.3. Thus, all of the methods described in Section 2.4.3 can be invoked for reformulating the quasi-concave problem as a series of efficiently solvable convex problems. In Section 3.4, Dinkelbach's method reformulated the problem in the subtractive form of (3.23) by introducing a parameter related to the objective function value. As detailed in Section 2.4.3.3, the solution to the subtractive problem approaches that of the original quasi-concave problem, when progressively increasing the value of this parameter. On the other hand, the Charnes-Cooper transformation of Section 3.5 introduced an additional variable, which converted the quasi-concave problem of (3.10)–(3.15) to the equivalent convex problem of (3.55)–(3.61) under an extra linear constraint. Solving only this single convex problem results in the solution of the original quasi-concave problem, as discussed in Section 2.4.3.5. In Section 3.6, the bisection method was employed for writing the problem in a subtractive form with the aid of an additional parameter. However, as detailed in Section 2.4.3.1, the solution to a series of feasibility problems is required. For all three methods, dual decomposition and gradient methods were respectively invoked for developing iterative algorithms for solving their resultant problems. Notably, each algorithm relied on inner iterations, which exhibited comparable complexities in terms of the number of operations imposed. Thus, the number of inner iterations required by each algorithm can be used in a complexity versus performance comparison in Section 3.7.

  The three algorithms were evaluated in Section 3.7 by comparing them to the results obtained from an exhaustive search method. As shown in Fig. 3.5, all algorithms were capable of reaching the optimal objective values. In particular, the algorithm of Section 3.5 based on the Charnes-Cooper transformation reached the optimal solution in less than 20 iterations, while the algorithm of Section 3.4 based on Dinkelbach's method typically required 30 or more iterations. Both of these algorithms vastly outperformed the one based on the bisection search of Section 3.6, which required more than 200 iterations. We concluded that the Charnes-Cooper transformation offered the most beneficial performance versus complexity trade-off, which makes it the preferred method in later Chapters. A summary of the required complexities was provided in Table 3.5.

  The additional simulation results provided in Section 3.7 showed that both the EEM

and SEM algorithms reached the same SE/EE values when there is insufficient power for attaining the maximum EE. Fig. 3.6(b) showed that, when the power constraint became sufficientl relaxed, the EEM obtained the maximum EE value for the specific network scenario considered, which cannot be increased further. For our particular system model, Fig. 3.6(b) shows that increasing the total power available to the system in excess of 40dBm no longer offers additional EE benefits. On the other hand, the SEM algorithm continued to allocate more power for the sake of achieving ever-higher SE results, which was however detrimental to in terms of the system's EE, as seen in Fig. 3.6(b).

Furthermore, results obtained in Figs. 3.6(a) and 3.6(b) upon varying other system parameters revealed that increasing the number of UEs in the system benefits both the SE and EE, which is due to the increased multiuser diversity. Observe in Figs. 3.8(a) and 3.8(b) that increasing the number of available subcarriers reduces both the SE and EE, since the subcarriers are not all efficiently utilized. Additionally, relaying is beneficial when the RNs are placed close to the BS, since that improves their SNRs. Although it is observed in Fig. 3.12(a) that increasing the number of RNs benefits the SE, which is due to increased relay selection diversity, the EE is negatively impacted in Fig. 3.12(b), since each additional RN requires a fixed operating power.

- **Chapter 4** [332]
  We extended the system model of Chapter 3 to include MIMO transceivers. For the sake of exploiting the additional antennas, in Section 4.4 we developed a novel transmission protocol that is applicable to any arbitrary multiuser multi-relay MIMO-OFDMA cellular network. This transmission protocol relies on spatial multiplexing, which is facilitated by ZF transmit BF. In Section 4.4, the receive BF matrices of the RNs and UEs are designed so that their associated MIMO channel matrices can be decomposed into multiple MISO channels, which we termed as SMCs in this thesis. Thus, the interference between transmissions using SMCs associated with the same subcarrier can be completely eliminated with the aid of ZFBF at the transmitter.

  For the sake of improving the effective channel gains resulting from employing the above-mentioned transmit and receive BF matrices, a pair of beneficial algorithms was designed in Section 4.5 for grouping the SMCs for each subcarrier. The main grouping criterion of (4.25) was based on the concept of semi-orthogonality, which was motivated in Section 4.3. The ZF transmit BF operation involves channel inversion, which is simply a matrix rotation and does not affect the norms of each SMC, if the selected SMCs are orthogonal to each other. Thus, selecting SMCs, which are orthogonal or nearly-orthogonal, hence results in higher channel gains overall. In Section 4.5, we described our two grouping algorithms, which are termed as ESGA and OCGA. ESGA relies on an exhaustive search of all the possible grouping combinations, while OCGA is a lower-complexity approach, which forms a fixed number of groups that are then iteratively improved.

Finding the EE-optimal groupings across all subcarriers as well as their associated power allocation values was formulated as an optimization problem in Section 4.6. Once again, the binary constraints of (4.64) were relaxed to obtain a fractional quasi-concave problem. Thus, in Section 4.6.2 we opted for employing the Charnes-Cooper transformation for converting the problem into the convex form of (4.95)–(4.106). Dinkelbach's method of Section 2.4.3.3 and the bisection method of Section 2.4.3.1 were not considered, since our previous results of Fig. 3.5 indicated that algorithms based on those methods require more iterations for reaching the same solution as the Charnes-Cooper transformation based algorithm. The resultant convex problem of (4.95)–(4.106) was solved by utilizing an algorithm based on dual decomposition and the gradient method, as detailed in 4.6.3.

In Section 4.7, our results demonstrated that OCGA is capable of producing groups, which result in SE values close to those obtained by the ESGA, but much fewer groups are needed. Since the number of available groups dictates the complexity imposed by the optimization algorithm of Section 5.4.2, this result indicates that OCGA is an attractive lower-complexity alternative to ESGA. As expected, our joint optimal power allocation and group selection optimization algorithm is capable of outperforming the equal power allocation and random group selection algorithm. The simulation results of Fig. 4.12 indicated that the maximum EE of our system was obtained at $P^B_{max} = 50$dBm and $P^R_{max} = 50$dBm. Further increasing the available power reduced the EE, when employing the SEM algorithm of Section 4.6, but the power constraint imposed on the BS was shown to have a more dominant effect on the achievable SE and EE values, when compared to the power constraint imposed on the RNs. However, increasing either the number of RNs or the number of available subcarriers reduced the attainable EE in Figs. 4.13 and 4.14, since these additional resources cannot be efficiently exploited. On the other hand, increasing the number of antennas available at the BS increased the SE and EE in Fig. 4.14 as a result of the higher potential spatial multiplexing gain achieved by the BS.

- **Chapter 5 [333]**

  The system model of Chapter 4 was then further extended to multi-cell systems. In Section 5.3, we developed a pair of transmission protocols based on the concept of IA for the sake of avoiding the excessive interference caused by multiple simultaneously active transmitters. These are the full-IA and partial-IA protocols of Sections 5.3.1.1 and 5.3.2.1, and Sections 5.3.1.2 and 5.3.2.2, respectively. Since simultaneous direct and relaying links are possible, we designed separate transmit and receive BF matrices for the first and second phases of each scheduled frame. When employing the full-IA protocol of Sections 5.3.1.1 and 5.3.2.1, all potential sources of interference are considered for designing the interference-nulling BF matrix at each receiver. On the other hand, the partial-IA protocol of Sections 5.3.1.2 and 5.3.2.2 only aims for avoiding the interference caused by transmitters within each receiver's own cell. Therefore, based on the IA principle,

the partial-IA protocol of Sections 5.3.1.2 and 5.3.2.2 is capable of supporting a higher multiplexing gain, while requiring less exchange of channel knowledge between BSs than the full-IA protocol, albeit this results in an increased interference contaminating each transmission. Having obtained the interference-nulling receive BF matrices in Section 5.3, their associated MIMO channel matrices can be decomposed into several effective MISO channels, which constitute the SMCs of the system. Once again, the concept of semi-orthogonality is considered and the OCGA of Section 4.5 is employed for grouping the SMCs. Thus, we were able to form the fractional quasi-concave EE optimization problem of Section 5.4, which we solved using a distributed algorithm based on dual decomposition and the gradient method.

We compared the performance of the full-IA and partial-IA protocols for a wide range of system parameters in Section 5.5. Somewhat surprisingly, the partial-IA protocol consistently outperformed the full-IA protocol, since the interference imposed by the neighboring cells was mitigated by pathloss of the cell sizes considered. Furthermore, we demonstrated that our power allocation and group selection optimization algorithm of Section 5.4.2 outperforms the equal-power allocation algorithm. In particular, we observed in Fig. 5.11 that the achievable EE is again more strongly dependent on the power constraint imposed on the BSs, rather than that imposed on the RNs, and the EE is maximized in Fig. 5.11 when $P^B_{max} = 36$dBm. Furthermore, increasing the number of spatial streams available at each RN reduced the achievable EE when using the full-IA protocol due to the resultant reduced multiplexing gain at the BSs. On the other hand, the EE was increased in Fig. 5.12 by using the partial-IA protocol, when supporting a pair of spatial streams at each RN. Most importantly, having a single RN in each sector was seen in Fig. 5.13 to be sufficient for maximizing the SE, when using partial-IA, although the EE was reduced in all cases, when additional RNs were deployed.

## 6.2 Future Research Ideas

In this section, we present a range of future research ideas, some of which are related to the literature review performed in Chapter 1.

- **Subcarrier pairing**
  In this thesis, we assumed that both the first-hop and the second-hop of a relaying link share the same subcarrier. This is not necessarily the case, and a potentially higher performance could be obtained if the relaying data was remapped to different subcarriers at the RNs [298,306]. For example, this could be modeled using a single allocation matrix for the first-hop and second-hop subcarriers. The goal would then be to maximize the utility improvement resulting from pairing specific allocations, which can be obtained by

using the Hungarian algorithm [240]. Furthermore, the performance enhancement versus additional complexity of employing subcarrier pairing can also be analyzed.

- **Low-complexity algorithms**
  The protocols and algorithms employed in this thesis only aimed for maximizing the EE performance and did not consider the practicality of their implementation. Thus, low-complexity alternatives should be developed, either based on reformulating the problem to the weighted-average form proposed in [223, 225], or by opting for heuristic methods for some allocation variables, as advocated in [201].
- **Cross-layer optimization**
  In this thesis, we only consider power allocation and subcarrier/group assignment, which restricts the optimization to the physical and MAC layers. Real communication networks operate on data packets and suffer from delays in queuing or from erroneous reception in the case of high BERs. Future efforts can be invested in designing holistic transmission protocols and formulating problems, which take this into account. Although there exist some contributions on cross-layer EE optimization in cellular systems [247, 392], their extension to MIMO multi-cell systems has rarely been performed.
- **Effective capacity maximization [269, 270]**
  The ratio of the effective capacity over the energy consumption was previously maximized in [269, 270]. This metric naturally imposes constraints on the statistical properties of the packet delay and can be employed in the relay-aided networks studied in this thesis.
- **Robust optimization**
  In realistic communication systems, perfect CSI is never available, but it is typically only statistically known or outdated. Furthermore, Section 5.5 demonstrated that our optimization algorithms perform poorly, even when small errors are present in the CSI. Robust optimization [22, 199, 341, 343] can be a beneficial tool under these circumstances. To elaborate, the objective function can be optimized under the assumption of only first-order and second-order statistics of the CSI. Thus, the performance is often degraded, but it is resistant to changes in the actual channel state. Furthermore, robust optimization is important, since the realistic CSI suffers from the associated quantization error [22, 199] as well as delays.
- **Joint DL/UL optimization**
  This thesis only considered the optimization of the DL transmissions. However, the UL can also be considered, especially the trade-off between DL and UL EEs [271], when assigning subcarriers for either transmissions. Extensions can be made to the relay-aided case, when employing two-way relaying [303–305] or full-duplex relaying [307].
- **Deployment optimization**
  The result of EE optimization is not limited to RA. Further progress can be made, when considering deployment optimization [393, 394] of the RNs. Typically, the statistical properties of the UEs and their associated channels will have to be considered, since it is not possible to optimize the location of the RNs, when the cellular network is active.

Thus, stochastic optimization is preferred. Additionally, the joint optimization of the BSs and RNs as well as their numbers can be performed.

- **Energy harvesting**
  Although a relatively new concept in wireless communications, energy harvesting [271,281] can be considering when optimizing the EE of a system. The energy harvested can additionally by reused in the reverse link, thus lessening the need to rely on the non-renewable energy source. This effect can be modeled as part of the optimization problem, as demonstrated in [281].

# Glossary

| | |
|---|---|
| 3GPP | Third Generation Partnership Project. |
| AC | alternating-column. |
| AF | amplify-and-forward. |
| AMC | adaptive modulation and coding. |
| ARQ | automatic repeat-request. |
| ASE | area spectral efficiency. |
| AWGN | additive white Gaussian noise. |
| BC | broadcast channel. |
| BER | bit error rate. |
| BF | beamforming. |
| BLP | binary linear programming. |
| BS | base station. |
| CCI | co-channel interference. |
| CDMA | code-division multiple-access. |
| CNR | channel-to-noise ratio. |
| CoV | calculus of variations. |
| CSI | channel state information. |
| DC | diagonal center. |
| DCMC | discrete-input continuous-output memoryless channel. |
| DF | decode-and-forward. |
| DL | downlink. |
| DN | destination node. |
| DoF | degrees of freedom. |
| DPC | dirty paper coding. |

| | |
|---|---|
| EARTH | energy aware radio and network technologies. |
| EE | energy-efficiency. |
| EPA | equal power allocation . |
| EPG | energy-per-goodbit. |
| EPSRC | Engineering & Physical Sciences Research Council. |
| EEM | energy efficiency maximization. |
| ESGA | exhaustive search-based grouping algorithm. |
| FD | frequency-domain. |
| FFT | fast Fourier transform. |
| FP | fractional programming. |
| GP | geometric programming. |
| IA | interference alignment. |
| ICI | intra-cell interference. |
| IEEE | Institute of Electrical and Electronics Engineers. |
| IFFT | inverse fast Fourier transform. |
| ILP | integer linear programming. |
| ISD | inter-site distance. |
| IWF | iterative water-filling. |
| KKT | Karush-Kuhn-Tucker. |
| LOS | line-of-sight. |
| LP | linear programming. |
| LPF | low pass filter. |
| LTE-A | Long Term Evolution-Advanced. |
| MAC | medium access control. |
| MCS | modulation and coding scheme. |
| MF | matched filter. |
| MI | mutual information. |
| MIMO | multiple-input–multiple-output. |
| MINLP | mixed integer nonlinear programming. |
| MISO | multiple-input–single-output. |
| ML | maximum likelihood. |
| MMSE | minimum mean-square error. |
| MRC | maximum ratio combining. |
| MRT | maximum ratio transmission. |
| MUI | multi-user interference. |

| | |
|---|---|
| NLOS | non-line-of-sight. |
| NOC | norm of the orthogonal component. |
| OCGA | orthogonal component-based grouping algorithm. |
| OCI | other-cell interference. |
| OFDM | orthogonal frequency division multiplexing. |
| OFDMA | orthogonal frequency division multiple access. |
| PER | packet error rate. |
| PF | proportional fair. |
| PSO | particle swarm optimization. |
| QAM | quadrature amplitude modulation. |
| QoE | quality-of-experience. |
| QoS | quality-of-service. |
| RA | resource allocation. |
| RAT | radio access technology. |
| RB | resource block. |
| RF | radio frequency. |
| RG | random SMC grouping. |
| RG-EPA | random SMC grouping equal power allocation. |
| RN | relay node. |
| RR | round-robin. |
| RRM | radio resource management. |
| SE | spectral-efficiency. |
| SEM | spectral-efficiency maximization. |
| SER | symbol error rate. |
| SINR | signal-to-interference-plus-noise ratio. |
| SISO | single-input–single-output. |
| SMC | spatial multiplexing component. |
| SN | source node. |
| SNR | signal-to-noise ratio. |
| STBC | space-time block code. |
| SVD | singular value decomposition. |
| TD | time-domain. |
| TDD | time-division duplexing. |
| TDMA | time-division multiple access. |

| | |
|---|---|
| UE | user equipment. |
| UL | uplink. |
| WiMAX | Worldwide Interoperability for Microwave Access. |
| WLAN | wireless local area network. |
| XOR | exclusive or. |
| ZF | zero-forcing. |
| ZFBF | zero-forcing beamforming. |

# List of Figures

# List of Tables

# Bibliography


[1] "Cisco visual networking index: Global mobile data traffic forecast update, 2012–2017," White paper, Cisco, Feb. 2013. [Online]. Available: http://www.cisco.com/en/US/solutions/collateral/ns341/ns525/ns537/ns705/ns827/white_paper_c11-520862.pdf

[2] R. Wood, "Wireless network traffic worldwide: forecasts and analysis 2013–2018," Research Forecast Report, Analysis Mason, Oct. 2013. [Online]. Available: analysysmason.com/Research/Content/Reports/Wireless-traffic-forecasts-Oct2013-RDTN0

[3] "Semi-annual wireless industry survey," CTIA - The Wireless Association, 2013. [Online]. Available: http://files.ctia.org/pdf/CTIA_Survey_YE_2012_Graphics-FINAL.pdf

[4] A. Goldsmith, *Wireless Communications*. Cambridge University Press, New York, NY, USA, 2005.

[5] D. Gesbert, S. Hanly, H. Huang, S. Shamai Shitz, O. Simeone, and W. Yu, "Multi-cell MIMO cooperative networks: A new look at interference," *IEEE Journal on Selected Areas in Communications*, vol. 28, no. 9, pp. 1380–1408, Dec. 2010.

[6] U. Madhow, "Wireless communications research: The next two decades," in *International Conference on Computers and Devices for Communication*, Kolkata, India, Dec. 2012.

[7] "The 1000x mobile data challenge: More small cells, more spectrum, higher efficiency," Qualcomm, Nov. 2013. [Online]. Available: http://www.qualcomm.com/media/documents/files/web_1000x-mobile-data-challenge.pdf

[8] F. Cardoso, S. Petersson, M. Boldi, S. Mizuta, G. Dietl, R. Torrea-Duran, C. Desset, J. Leinonen, and L. Correia, "Energy efficient transmission techniques for LTE," *IEEE Communications Magazine*, vol. 51, no. 10, pp. 182–190, Oct. 2013.

[9] G. Fettweis and E. Zimmermann, "ICT energy consumption - trends and challenges," in *International Symposium on Wireless Personal Multimedia Communications*, Lapland, Finland, Sept. 2008.

[10] C. Han, T. Harrold, S. Armour, I. Krikidis, S. Videv, P. Grant, H. Haas, J. Thompson, I. Ku, C.-X. Wang, T. A. Le, M. Nakhai, J. Zhang, and L. Hanzo, "Green radio: radio techniques to enable energy-efficient wireless networks," *IEEE Communications Magazine*, vol. 49, no. 6, pp. 46–54, Jun. 2011.

[11] G. Li, Z. Xu, C. Xiong, C. Yang, S. Zhang, Y. Chen, and S. Xu, "Energy-efficient wireless communications: tutorial, survey, and open issues," *IEEE Wireless Communications Magazine*, vol. 18, no. 6, pp. 28–35, Dec. 2011.

[12] M. Gruber, O. Blume, D. Ferling, D. Zeller, M. Imran, and E. Strinati, "EARTH - energy aware radio and network technologies," in *IEEE International Symposium on Personal, Indoor and Mobile Radio Communications*, Tokyo, Japan, Sep. 2009.

[13] L. Correia, D. Zeller, O. Blume, D. Ferling, Y. Jading, I. Gódor, G. Auer, and L. Van Der Perre, "Challenges and enabling technologies for energy aware mobile radio networks," *IEEE Communications Magazine*, vol. 48, no. 11, pp. 66–72, Nov. 2010.

[14] F. Meshkati, H. Poor, and S. Schwartz, "Energy-efficient resource allocation in wireless networks," *IEEE Signal Processing Magazine*, vol. 24, no. 3, pp. 58–68, May 2007.

[15] L. Collins, "Greening the global network," *Engineering Technology*, vol. 5, no. 4, pp. 64–65, Mar. 2010.

[16] "EARTH (Energy Aware Radio and neTwork tecHnologies), EU Funded Research Project FP7-ICT-2009-4- 247733-EARTH," 2010–2012. [Online]. Available: https://www.ict-earth.eu

[17] Y. Yang, H. Hu, J. Xu, and G. Mao, "Relay technologies for WiMAX and LTE-advanced mobile systems," *IEEE Communications Magazine*, vol. 47, no. 10, pp. 100–105, Oct. 2009.

[18] L. Hanzo, Y. Akhtman, L. Wang, and M. Jiang, *MIMO-OFDM for LTE, WIFI and WIMAX: Coherent Versus Non-Coherent and Cooperative Turbo-Transceivers*. Wiley-IEEE Press, 2010.

[19] T. Keller and L. Hanzo, "Adaptive multicarrier modulation: a convenient framework for time-frequency processing in wireless communications," *Proceedings of the IEEE*, vol. 88, no. 5, pp. 611–640, May 2000.

[20] G. Li and H. Liu, "Resource allocation for OFDMA relay networks with fairness constraints," *IEEE Journal on Selected Areas in Communications*, vol. 24, no. 11, pp. 2061–2069, Nov. 2006.

[21] T. C.-Y. Ng and W. Yu, "Joint optimization of relay strategies and resource allocations in cooperative cellular networks," *IEEE Journal on Selected Areas in Communications*, vol. 25, no. 2, pp. 328–339, Feb. 2007.

[22] D. Ng and R. Schober, "Cross-layer scheduling for OFDMA amplify-and-forward relay networks," *IEEE Transactions on Vehicular Technology*, vol. 59, no. 3, pp. 1443–1458, Mar. 2010.

[23] C. Y. Wong, R. Cheng, K. Letaief, and R. Murch, "Multiuser OFDM with adaptive subcarrier, bit, and power allocation," *IEEE Journal on Selected Areas in Communications*, vol. 17, no. 10, pp. 1747–1758, Oct. 1999.

[24] L. Piazzo, "Fast algorithm for power and bit allocation in OFDM systems," *Electronics Letters*, vol. 35, no. 25, pp. 2173–2174, Dec. 1999.

[25] L. Xiao and L. Cuthbert, "Adaptive power allocation scheme for energy efficient OFDMA relay networks," in *IEEE Singapore International Conference on Communication Systems*, Guangzhou, China, Nov. 2008, pp. 637–641.

[26] L. Piazzo, "Optimal fast algorithm for power and bit allocation in OFDM systems," *IEEE Transactions on Vehicular Technology*, vol. 60, no. 3, pp. 1263–1265, Mar. 2011.

[27] J. Joung and S. Sun, "Power efficient resource allocation for downlink OFDMA relay cellular networks," *IEEE Transactions on Signal Processing*, vol. 60, no. 5, pp. 2447–2459, May 2012.

[28] G. Zhang, K. Yang, and H.-H. Chen, "Resource allocation for wireless cooperative networks: a unified cooperative bargaining game theoretic framework," *IEEE Wireless Communications*, vol. 19, no. 2, pp. 38–43, Apr. 2012.

[29] S. Ali, K.-D. Lee, and V. C. Leung, "Dynamic resource allocation in OFDMA wireless metropolitan area networks," *IEEE Wireless Communications Magazine*, vol. 14, no. 1, pp. 6–13, Feb. 2007.

[30] S. Srikanth, P. Murugesa Pandian, and X. Fernando, "Orthogonal frequency division multiple access in WiMAX and LTE: a comparison," *IEEE Communications Magazine*, vol. 50, no. 9, pp. 153–161, Sept. 2012.

[31] A. Asadi and V. Mancuso, "A survey on opportunistic scheduling in wireless communications," *IEEE Communications Surveys & Tutorials*, vol. 15, no. 4, pp. 1671–1688, 4th Quarter 2013.

[32] J. Huang, V. Subramanian, R. Agrawal, and R. Berry, "Downlink scheduling and resource allocation for OFDM systems," *IEEE Transactions on Wireless Communications*, vol. 8, no. 1, pp. 288–296, Jan. 2009.

[33] K. Letaief and Y. Zhang, "Dynamic multiuser resource allocation and adaptation for wireless systems," *IEEE Wireless Communications Magazine*, vol. 13, no. 4, pp. 38–47, Aug. 2006.

[34] S. Boyd and L. Vandenberghe, *Convex Optimization*. Cambridge University Press, New York, NY, USA, 2004.

[35] M. Chiang, "Geometric programming for communication systems," *Foundations and Trends of Communications and Information Theory*, vol. 2, no. 1–2, pp. 1–156, May 2005.

[36] M. Chiang, C. wei Tan, D. Palomar, D. O'Neill, and D. Julian, "Power control by geometric programming," *IEEE Transactions on Wireless Communications*, vol. 6, no. 7, pp. 2640–2651, Jul. 2007.

[37] W. Yu, W. Rhee, S. Boyd, and J. Cioffi, "Iterative water-filling for Gaussian vector multiple-access channels," *IEEE Transactions on Information Theory*, vol. 50, no. 1, pp. 145–152, Jan. 2004.

[38] T. Cover and A. Gamal, "Capacity theorems for the relay channel," *IEEE Transactions on Information Theory*, vol. 25, no. 5, pp. 572–584, Sep. 1979.

[39] G. Kramer, M. Gastpar, and P. Gupta, "Cooperative strategies and capacity theorems for relay networks," *IEEE Transactions on Information Theory*, vol. 51, no. 9, pp. 3037–3063, Sep. 2005.

[40] A. Host-Madsen and J. Zhang, "Capacity bounds and power allocation for wireless relay channels," *IEEE Transactions on Information Theory*, vol. 51, no. 6, pp. 2020–2040, Jun. 2005.

[41] B. Wang, J. Zhang, and A. Host-Madsen, "On the capacity of MIMO relay channels," *IEEE Transactions on Information Theory*, vol. 51, no. 1, pp. 29–43, Jan. 2005.

[42] A. Nosratinia, T. Hunter, and A. Hedayat, "Cooperative communication in wireless networks," *IEEE Communications Magazine*, vol. 42, no. 10, pp. 74–80, Oct. 2004.

[43] J. Laneman, D. Tse, and G. Wornell, "Cooperative diversity in wireless networks: Efficient protocols and outage behavior," *IEEE Transactions on Information Theory*, vol. 50, no. 12, pp. 3062–3080, Dec. 2004.

[44] O. Oyman, "Opportunistic scheduling and spectrum reuse in relay-based cellular networks," *IEEE Transactions on Wireless Communications*, vol. 9, no. 3, pp. 1074–1085, Mar. 2010.

[45] J. Zander, "Radio resource management in future wireless networks: requirements and limitations," *IEEE Communications Magazine*, 1997.

[46] S. Grandhi, R. Yates, and D. Goodman, "Resource allocation for cellular radio systems," *IEEE Transactions on Vehicular Technology*, vol. 46, no. 3, pp. 581–587, Aug. 1997.

[47] M. Bohge, J. Gross, A. Wolisz, and M. Meyer, "Dynamic resource allocation in OFDM systems: an overview of cross-layer optimization principles and techniques," *IEEE Network Magazine*, vol. 21, no. 1, pp. 53–59, Jan. 2007.

[48] J. Louhi, "Energy efficiency of modern cellular base stations," in *IEEE International Telecommunications Energy Conference*, Rome, Italy, Sep. 2007, pp. 475–476.

[49] S. Chieochan and E. Hossain, "Adaptive radio resource allocation in OFDMA systems: a survey of the state-of-the-art approaches," *Wiley Wireless Communications and Mobile Computing*, vol. 9, no. 4, pp. 513–527, Apr. 2009.

[50] G. Miao, N. Himayat, G. Li, and A. Swami, "Cross-layer optimization for energy-efficient wireless communications: a survey," *Wiley Wireless Communications and Mobile Computing*, vol. 9, no. 4, pp. 529–542, Apr. 2009.

[51] E. Strinati and L. Hrault, "Holistic approach for future energy efficient cellular networks," *Springer-Verlag Elektrotechnik und Informationstechnik*, vol. 127, no. 11, pp. 314–320, Nov. 2010.

[52] M. Salem, A. Adinoyi, M. Rahman, H. Yanikomeroglu, D. Falconer, Y.-D. Kim, E. Kim, and Y.-C. Cheong, "An overview of radio resource management in relay-enhanced OFDMA-based networks," *IEEE Communications Surveys & Tutorials*, vol. 12, no. 3, pp. 422–438, Apr. 2010.

[53] S. Mclaughlin, P. Grant, J. Thompson, H. Haas, D. Laurenson, C. Khirallah, Y. Hou, and R. Wang, "Techniques for improving cellular radio base station energy efficiency," *IEEE Wireless Communications Magazine*, vol. 18, no. 5, pp. 10–17, Oct. 2011.

[54] V. Mancuso and S. Alouf, "Reducing costs and pollution in cellular networks," *IEEE Communications Magazine*, vol. 49, no. 8, pp. 63–71, Aug. 2011.

[55] Y. Chen, S. Zhang, S. Xu, and G. Li, "Fundamental trade-offs on green wireless networks," *IEEE Communications Magazine*, vol. 49, no. 6, pp. 30–37, Jun. 2011.

[56] T. Chen, Y. Yang, H. Zhang, H. Kim, and K. Horneman, "Network energy saving technologies for green wireless access networks," *IEEE Wireless Communications Magazine*, vol. 18, no. 5, pp. 30–38, Oct. 2011.

[57] Z. Hasan, H. Boostanimehr, and V. Bhargava, "Green cellular networks: A survey, some research issues and challenges," *IEEE Communications Surveys & Tutorials*, vol. 13, no. 4, pp. 524–540, 4th Quarter 2011.

[58] G. Auer, V. Giannini, C. Desset, I. Godor, P. Skillermark, M. Olsson, M. Imran, D. Sabella, M. Gonzalez, O. Blume, and A. Fehske, "How much energy is needed to run a wireless network?" *IEEE Wireless Communications Magazine*, vol. 18, no. 5, pp. 40–49, Oct. 2011.

[59] Z. Chong and E. Jorswieck, "Analytical foundation for energy efficiency optimisation in cellular networks with elastic traffic," in *Mobile Lightweight Wireless Systems*, ser. Lecture Notes of the Institute for Computer Sciences, Social Informatics and Telecommunications Engineering. Springer Berlin Heidelberg, 2012, vol. 81, pp. 18–29.

[60] A. Zappone, S. Buzzi, E. Jorswieck, and M. Meo, "A survey on game-theoretic approaches to energy-efficient relay-assisted communications," in *IEEE Tyrrhenian International Workshop on Digital Communications - Green ICT*, Genoa, Italy, Sep. 2013.

[61] D. Quintas and V. Friderikos, "Robust cross layer optimization in relay aided cellular networks," *Springer Wireless Networks*, vol. 19, no. 6, pp. 1361–1373, Aug. 2013.

[62] D. Feng, C. Jiang, G. Lim, L. Cimini, G. Feng, and G. Li, "A survey of energy-efficient wireless communications," *IEEE Communications Surveys & Tutorials*, vol. 15, no. 1, pp. 167–178, 1st Quarter 2013.

[63] J. Rao and A. Fapojuwo, "A survey of energy efficient resource management techniques for multicell cellular networks," *IEEE Communications Surveys & Tutorials*, vol. 16, no. 1, pp. 154–180, 1st Quarter 2014.

[64] C. e Souza, A. Ricieri, A. de Almeida, J. Roberto, and T. Abrão, "Energy-efficiency maximisation for cooperative and non-cooperative OFDMA cellular networks - a survey," *Wiley Transactions on Emerging Telecommunications Technologies*, Early Access 2014.

[65] M. Kaneko, P. Popovski, and K. Hayashi, "Throughput-guaranteed resource-allocation algorithms for relay-aided cellular OFDMA system," *IEEE Transactions on Vehicular Technology*, vol. 58, no. 4, pp. 1951–1964, May 2009.

[66] T. Wang and L. Vandendorpe, "Iterative resource allocation for maximizing weighted sum min-rate in downlink cellular OFDMA systems," *IEEE Transactions on Signal Processing*, vol. 59, no. 1, pp. 223–234, Jan. 2011.

[67] S.-J. Kim and G. Giannakis, "Optimal resource allocation for MIMO ad hoc cognitive radio networks," *IEEE Transactions on Information Theory*, vol. 57, no. 5, pp. 3117–3131, May 2011.

[68] M.-S. Alouini and A. Goldsmith, "Area spectral efficiency of cellular mobile radio systems," *IEEE Transactions on Vehicular Technology*, vol. 48, no. 4, pp. 1047–1066, Jul. 1999.

[69] F. Meshkati, H. Poor, S. Schwartz, and R. Balan, "Energy-efficient resource allocation in wireless networks with quality-of-service constraints," *IEEE Transactions on Communications*, vol. 57, no. 11, pp. 3406–3414, Nov. 2009.

[70] R. Xie, F. R. Yu, H. Ji, and Y. Li, "Energy-efficient resource allocation for heterogeneous cognitive radio networks with femtocells," *IEEE Transactions on Wireless Communications*, vol. 11, no. 11, pp. 3910–3920, Nov. 2012.

[71] D. Ng, E. Lo, and R. Schober, "Energy-efficient resource allocation in OFDMA systems with large numbers of base station antennas," *IEEE Transactions on Wireless Communications*, vol. 11, no. 9, pp. 3292–3304, Sept. 2012.

[72] Z. Han, Z. Ji, and K. Liu, "Power minimization for multi-cell OFDM networks using distributed non-cooperative game approach," in *IEEE Global Telecommunications Conference*, vol. 6, Dallas, Texas, USA, Nov. 2004, pp. 3742–3747.

[73] M. Olfat, F. Farrokhi, and K. Liu, "Power allocation for OFDM using adaptive beamforming over wireless networks," *IEEE Transactions on Communications*, vol. 53, no. 3, pp. 505–514, Mar. 2005.

[74] Z. Han, Z. Ji, and K. Liu, "Non-cooperative resource competition game by virtual referee in multi-cell OFDMA networks," *IEEE Journal on Selected Areas in Communications*, vol. 25, no. 6, pp. 1079–1090, Aug. 2007.

[75] X. Wang and G. Giannakis, "Power-efficient resource allocation for time-division multiple access over fading channels," *IEEE Transactions on Information Theory*, vol. 54, no. 3, pp. 1225–1240, Mar. 2008.

[76] M. Chen, S. Serbetli, and A. Yener, "Distributed power allocation strategies for parallel relay networks," *IEEE Transactions on Wireless Communications*, vol. 7, no. 2, pp. 552–561, Feb. 2008.

[77] W. Ho and Y.-C. Liang, "Optimal resource allocation for multiuser MIMO–OFDM systems with user rate constraints," *IEEE Transactions on Vehicular Technology*, vol. 58, no. 3, pp. 1190–1203, Mar. 2009.

[78] X. Kang, Y.-C. Liang, A. Nallanathan, H. Garg, and R. Zhang, "Optimal power allocation for fading channels in cognitive radio networks: Ergodic capacity and outage capacity," *IEEE Transactions on Wireless Communications*, vol. 8, no. 2, pp. 940–950, Feb. 2009.

[79] H. Ahmadi and Y. H. Chew, "Subcarrier-and-bit allocation in multiclass multiuser single-cell OFDMA systems using an ant colony optimization based evolutionary algorithm," in *IEEE Wireless Communications and Networking Conference*, Sydney, Australia, Apr. 2010.

[80] F. Chiti, R. Fantacci, L. Pierucci, and N. Privitera, "An energy efficient antennas allocation method for MIMO multicast communications using network coding," in *IEEE International Conference on Communications*, Ottawa, Ontario, Canada, Jun. 2012, pp. 5249–5293.

[81] D. Julian, M. Chiang, D. O'Neill, and S. Boyd, "QoS and fairness constrained convex optimization of resource allocation for wireless cellular and ad hoc networks," in *IEEE International Conference on Computer Communications*, vol. 2, New York, New York, USA, Jun. 2002, pp. 477–486.

[82] Y. Zhang and K. Letaief, "An efficient resource-allocation scheme for spatial multiuser access in MIMO/OFDM systems," *IEEE Transactions on Communications*, vol. 53, no. 1, pp. 107–116, Jan. 2005.

[83] A. Eryilmaz and R. Srikant, "Fair resource allocation in wireless networks using queue-length-based scheduling and congestion control," in *IEEE International Conference on Computer Communications*, vol. 3, Miami, Florida, USA, Mar. 2005, pp. 1794–1803.

[84] Z. Shen, J. Andrews, and B. Evans, "Adaptive resource allocation in multiuser OFDM systems with proportional rate constraints," *IEEE Transactions on Wireless Communications*, vol. 4, no. 6, pp. 2726–2737, Nov. 2005.

[85] L. Xu, X. Shen, and J. Mark, "Fair resource allocation with guaranteed statistical QoS for multimedia traffic in wideband CDMA cellular network," *IEEE Transactions on Mobile Computing*, vol. 4, no. 2, pp. 166–177, Mar. 2005.

[86] A. Eryilmaz and R. Srikant, "Joint congestion control, routing, and MAC for stability and fairness in wireless networks," *IEEE Journal on Selected Areas in Communications*, vol. 24, no. 8, pp. 1514–1524, Aug. 2006.

[87] J. Luo, L. Lin, R. Yates, and P. Spasojevic, "Service outage based power and rate allocation," *IEEE Transactions on Information Theory*, vol. 49, no. 1, pp. 323–330, Jan. 2003.

[88] Y. Zhao, R. Adve, and T. J. Lim, "Improving amplify-and-forward relay networks: Optimal power allocation versus selection," in *IEEE International Symposium on Information Theory*, Seattle, Washington, USA, Jul. 2006, pp. 1234–1238.

[89] S. Deb and R. Srikant, "Congestion control for fair resource allocation in networks with multicast flows," *IEEE/ACM Transactions on Networking*, vol. 12, no. 2, pp. 274–285, Apr. 2004.

[90] L. Chen, S. H. Low, and J. Doyle, "Joint congestion control and media access control design for ad hoc wireless networks," in *IEEE International Conference on Computer Communications*, vol. 3, Miami, Florida, USA, Mar. 2005, pp. 2212–2222.

[91] M. Chiang, "Balancing transport and physical layers in wireless multihop networks: jointly optimal congestion control and power control," *IEEE Journal on Selected Areas in Communications*, vol. 23, no. 1, pp. 104–116, Jan. 2005.

[92] S. Merlin, N. Vaidya, and M. Zorzi, "Resource allocation in multi-radio multi-channel multi-hop wireless networks," in *IEEE International Conference on Computer Communications*, Phoenix, Arizona, USA, Apr. 2008.

[93] A. Elwalid, D. Mitra, and R. Wentworth, "A new approach for allocating buffers and bandwidth to heterogeneous, regulated traffic in an ATM node," *IEEE Journal on Selected Areas in Communications*, vol. 13, no. 6, pp. 1115–1127, Aug. 1995.

[94] N. Damji and T. Le-Ngoc, "Dynamic downlink OFDM resource allocation with interference mitigation and macro diversity for multimedia services in wireless cellular systems," *IEEE Transactions on Vehicular Technology*, vol. 55, no. 5, pp. 1555–1564, Sep. 2006.

[95] M. Tao, Y.-C. Liang, and F. Zhang, "Resource allocation for delay differentiated traffic in multiuser OFDM systems," *IEEE Transactions on Wireless Communications*, vol. 7, no. 6, pp. 2190–2201, Jun. 2008.

[96] S. Chakrabarti and A. Mishra, "QoS issues in ad hoc wireless networks," *IEEE Communications Magazine*, vol. 39, no. 2, pp. 142–148, Feb. 2001.

[97] E.-S. El-Alfy, Y.-D. Yao, and H. Heffes, "Adaptive resource allocation with prioritized handoff in cellular mobile networks under QoS provisioning," in *IEEE Vehicular Technology Conference Fall*, vol. 4, Atlantic City, New Jersey, USA, Oct. 2001, pp. 2113–2117.

[98] W. Pattara-Atikom, P. Krishnamurthy, and S. Banerjee, "Distributed mechanisms for quality of service in wireless LANs," *IEEE Wireless Communications Magazine*, vol. 10, no. 3, pp. 26–34, Jun. 2003.

[99] M. Ergen, S. Coleri, and P. Varaiya, "QoS aware adaptive resource allocation techniques for fair scheduling in OFDMA based broadband wireless access systems," *IEEE Transactions on Broadcasting*, vol. 49, no. 4, pp. 362–370, Nov. 2003.

[100] S. Pietrzyk and G. Janssen, "Radio resource allocation for cellular networks based on OFDMA with QoS guarantees," in *IEEE Global Telecommunications Conference*, vol. 4, Dallas, Texas USA, Nov. 2004, pp. 2694–2699.

[101] L. Huang, S. Kumar, and C.-C. Kuo, "Adaptive resource allocation for multimedia QoS management in wireless networks," *IEEE Transactions on Vehicular Technology*, vol. 53, no. 2, pp. 547–558, Mar. 2004.

[102] J. Yao, J. Mark, T. C. Wong, Y. H. Chew, K. M. Lye, and K.-C. Chua, "Virtual partitioning resource allocation for multiclass traffic in cellular systems with QoS constraints," *IEEE Transactions on Vehicular Technology*, vol. 53, no. 3, pp. 847–864, May 2004.

[103] L. Lee, C.-J. Chang, Y.-S. Chen, and S. Shen, "A utility-approached radio resource allocation algorithm for downlink in OFDMA cellular systems," in *IEEE Vehicular Technology Conference Spring*, vol. 3, Stockholm, Sweden, May 2005, pp. 1798–1802.

[104] J. Tang and X. Zhang, "Cross-layer resource allocation over wireless relay networks for quality of service provisioning," *IEEE Journal on Selected Areas in Communications*, vol. 25, no. 4, pp. 645–656, May 2007.

[105] ——, "Cross-layer modeling for quality of service guarantees over wireless links," *IEEE Transactions on Wireless Communications*, vol. 6, no. 12, pp. 4504–4512, Dec. 2007.

[106] ——, "Cross-layer-model based adaptive resource allocation for statistical QoS guarantees in mobile wireless networks," *IEEE Transactions on Wireless Communications*, vol. 7, no. 6, pp. 2318–2328, Jun. 2008.

[107] G. Aristomenopoulos, T. Kastrinogiannis, V. Kaldanis, G. Karantonis, and S. Papavassiliou, "A novel framework for dynamic utility-based QoE provisioning in wireless networks," in *IEEE Global Telecommunications Conference*, Miami, Florida, USA, Dec. 2010.

[108] J. Zhang and N. Ansari, "On assuring end-to-end QoE in next generation networks: challenges and a possible solution," *IEEE Communications Magazine*, vol. 49, no. 7, pp. 185–191, Jul. 2011.

[109] C. Sacchi, F. Granelli, and C. Schlegel, "A QoE-oriented strategy for OFDMA radio resource allocation based on min-MOS maximization," *IEEE Communications Letters*, vol. 15, no. 5, pp. 494–496, May 2011.

[110] P. Janis, V. Koivunen, C. Ribeiro, J. Korhonen, K. Doppler, and K. Hugl, "Interference-aware resource allocation for device-to-device radio underlaying cellular networks," in *IEEE Vehicular Technology Conference Spring*, Barcelona, Spain, Apr. 2009.

[111] S. Almalfouh and G. Stuber, "Interference-aware radio resource allocation in OFDMA-based cognitive radio networks," *IEEE Transactions on Vehicular Technology*, vol. 60, no. 4, pp. 1699–1713, May 2011.

[112] C. Xu, L. Song, Z. Han, Q. Zhao, X. Wang, and B. Jiao, "Interference-aware resource allocation for device-to-device communications as an underlay using sequential second price auction," in

*IEEE International Conference on Communications*, Ottawa, Ontario, Canada, Jun. 2012, pp. 445–449.

[113] L. Jorguseski, E. Fledderus, J. Farserotu, and R. Prasad, "Radio resource allocation in third generation mobile communication systems," *IEEE Communications Magazine*, vol. 39, no. 2, pp. 117–123, Feb. 2001.

[114] W. Song, H. Jiang, W. Zhuang, and X. Shen, "Resource management for QoS support in cellular/WLAN interworking," *IEEE Network Magazine*, vol. 19, no. 5, pp. 12–18, Sep. 2005.

[115] G. Li and H. Liu, "Downlink radio resource allocation for multi-cell OFDMA system," *IEEE Transactions on Wireless Communications*, vol. 5, no. 12, pp. 3451–3459, Dec. 2006.

[116] J.-W. Lee, R. Mazumdar, and N. Shroff, "Joint resource allocation and base-station assignment for the downlink in CDMA networks," *IEEE/ACM Transactions on Networking*, vol. 14, no. 1, pp. 1–14, Feb. 2006.

[117] A. Abrardo, A. Alessio, P. Detti, and M. Moretti, "Centralized radio resource allocation for OFDMA cellular systems," in *IEEE International Conference on Communications*, Glasgow, Scotland, June 2007, pp. 5738–5743.

[118] C.-H. Yu, O. Tirkkonen, K. Doppler, and C. Ribeiro, "Power optimization of device-to-device communication underlaying cellular communication," in *IEEE International Conference on Communications*, Dresden, Germany, Jun. 2009.

[119] R. Kwan, C. Leung, and J. Zhang, "Resource allocation in an LTE cellular communication system," in *IEEE International Conference on Communications*, Dresden, Germany, Jun. 2009.

[120] N. Ksairi, P. Bianchi, P. Ciblat, and W. Hachem, "Resource allocation for downlink cellular OFDMA systems part I: Optimal allocation," *IEEE Transactions on Signal Processing*, vol. 58, no. 2, pp. 720–734, Feb. 2010.

[121] R. Madan, S. Boyd, and S. Lall, "Fast algorithms for resource allocation in wireless cellular networks," *IEEE/ACM Transactions on Networking*, vol. 18, no. 3, pp. 973–984, Jun. 2010.

[122] K. Zheng, F. Hu, W. Wang, W. Xiang, and M. Dohler, "Radio resource allocation in LTE-advanced cellular networks with M2M communications," *IEEE Communications Magazine*, vol. 50, no. 7, pp. 184–192, Jul. 2012.

[123] E. Yaacoub and Z. Dawy, "A survey on uplink resource allocation in OFDMA wireless networks," *IEEE Communications Surveys & Tutorials*, vol. 14, no. 2, pp. 322–337, Second Quarter 2012.

[124] S. Lal and E. Sousa, "Distributed resource allocation for DS–CDMA–based multimedia ad hoc wireless LANs," *IEEE Journal on Selected Areas in Communications*, vol. 17, no. 5, pp. 947–967, May 1999.

[125] S. W. Kim, B.-S. Kim, and Y. Fang, "Downlink and uplink resource allocation in IEEE 802.11 wireless LANs," *IEEE Transactions on Vehicular Technology*, vol. 54, no. 1, pp. 320–327, Jan. 2005.

[126] H. Zhang, H. Ji, and X. Li, "RAU allocation for secondary users in cognitive WLAN over fiber system: A HMM approach," in *IEEE Wireless Communications and Networking Conference*, Shanghai, China, Apr. 2012, pp. 1416–1421.

[127] P. Björklund, P. Varbrand, and D. Yuan, "Resource optimization of spatial TDMA in ad hoc radio networks: a column generation approach," in *IEEE International Conference on Computer Communications*, vol. 2, San Francisco, California, USA, Mar. 2003, pp. 818–824.

[128] Z. Fang and B. Bensaou, "Fair bandwidth sharing algorithms based on game theory frameworks for wireless ad-hoc networks," in *IEEE International Conference on Computer Communications*, vol. 2, Hong Kong, Mar. 2004, pp. 1284–1295.

[129] Y. Xue, B. Li, and K. Nahrstedt, "Optimal resource allocation in wireless ad hoc networks: a price-based approach," *IEEE Transactions on Mobile Computing*, vol. 5, no. 4, pp. 347–364, Apr. 2006.

[130] W. Grover, "Self-organizing broad-band transport networks," *Proceedings of the IEEE*, vol. 85, no. 10, pp. 1582–1611, Oct. 1997.

[131] C. Prehofer and C. Bettstetter, "Self-organization in communication networks: principles and design paradigms," *IEEE Communications Magazine Magazine*, vol. 43, no. 7, pp. 78–85, Jul. 2005.

[132] D. Lopez-Perez, A. Valcarce, G. de la Roche, and J. Zhang, "OFDMA femtocells: A roadmap on interference avoidance," *IEEE Communications Magazine*, vol. 47, no. 9, pp. 41–48, Sept. 2009.

[133] D. Lopez-Perez, A. Ladanyi, A. Juttner, and J. Zhang, "OFDMA femtocells: A self-organizing approach for frequency assignment," in *IEEE International Symposium on Personal, Indoor and Mobile Radio Communications*, Tokyo, Japan, Sep. 2009, pp. 2202–2207.

[134] A. Stolyar and H. Viswanathan, "Self-organizing dynamic fractional frequency reuse for best-effort traffic through distributed inter-cell coordination," in *IEEE International Conference on Computer Communications*, Rio de Janeiro, Brazil, Apr. 2009, pp. 1287–1295.

[135] K. Lee, H. Lee, and D.-H. Cho, "Collaborative resource allocation for self-healing in self-organizing networks," in *IEEE International Conference on Communications*, Kyoto, Japan, Jun. 2011.

[136] W. Yu and J. Yuan, "Joint source coding, routing and resource allocation for wireless sensor networks," in *IEEE International Conference on Communications*, vol. 2, Seoul, Korea, May 2005, pp. 737–741.

[137] H. Nama, M. Chiang, and N. Mandayam, "Utility-lifetime trade-off in self-regulating wireless sensor networks: A cross-layer design approach," in *IEEE International Conference on Communications*, vol. 8, Istanbul, Turkey, Jun. 2006, pp. 3511–3516.

[138] N. Pantazis and D. Vergados, "A survey on power control issues in wireless sensor networks," *IEEE Communications Surveys and Tutorials*, vol. 9, no. 4, pp. 86–107, 4th Quarter 2007.

[139] J. Zhu, S. Chen, B. Bensaou, and K.-L. Hung, "Tradeoff between lifetime and rate allocation in wireless sensor networks: A cross layer approach," in *IEEE International Conference on Computer Communications*, Anchorage, Alaska, USA, May 2007, pp. 267–275.

[140] M. Hasna and M.-S. Alouini, "Optimal power allocation for relayed transmissions over rayleigh-fading channels," *IEEE Transactions on Wireless Communications*, vol. 3, no. 6, pp. 1999–2004, Nov. 2004.

[141] Y. Liu, R. Hoshyar, X. Yang, and R. Tafazolli, "Integrated radio resource allocation for multihop cellular networks with fixed relay stations," *IEEE Journal on Selected Areas in Communications*, vol. 24, no. 11, pp. 2137–2146, Nov. 2006.

[142] L. B. Le and E. Hossain, "Multihop cellular networks: Potential gains, research challenges, and a resource allocation framework," *IEEE Communications Magazine*, vol. 45, no. 9, pp. 66–73, Sep. 2007.

[143] M. Kaneko and P. Popovski, "Radio resource allocation algorithm for relay-aided cellular OFDMA system," in *IEEE International Conference on Communications*, Glasgow, Scotland, Jun. 2007, pp. 4831–4836.

[144] ——, "Adaptive resource allocation in cellular OFDMA system with multiple relay stations," in *IEEE Vehicular Technology Conference Spring*, Dublin, Ireland, Apr. 2007, pp. 3026–3030.

[145] L. Huang, M. Rong, L. Wang, Y. Xue, and E. Schulz, "Resource allocation for OFDMA based relay enhanced cellular networks," in *IEEE Vehicular Technology Conference Spring*, Dublin, Ireland, Apr. 2007, pp. 3160–3164.

[146] ——, "Resource scheduling for OFDMA/TDD based relay enhanced cellular networks," in *IEEE Wireless Communications and Networking Conference*, Kowloon, Hong Kong, Mar. 2007, pp. 1544–1548.

[147] B. Wang, Z. Han, and K. Liu, "Distributed relay selection and power control for multiuser cooperative communication networks using buyer/seller game," in *IEEE International Conference on Computer Communications*, Barcelona, Spain, May 2007, pp. 544–552.

[148] J. Huang, Z. Han, M. Chiang, and H. Poor, "Auction-based resource allocation for cooperative communications," *IEEE Journal on Selected Areas in Communications*, vol. 26, no. 7, pp. 1226–1237, Sep. 2008.

[149] L. You, M. Song, J. Song, Q. Miao, and Y. Zhang, "Adaptive resource allocation in OFDMA relay-aided cooperative cellular networks," in *IEEE Vehicular Technology Conference Spring*, Singapore, May 2008, pp. 1925–1929.

[150] E. Calvo, J. Vidal, and J. Fonollosa, "Optimal resource allocation in relay-assisted cellular networks with partial CSI," *IEEE Transactions on Signal Processing*, vol. 57, no. 7, pp. 2809–2823, Jul. 2009.

[151] G. Zhang, H. Zhang, L. Zhao, W. Wang, and L. Cong, "Fair resource sharing for cooperative relay networks using nash bargaining solutions," *IEEE Communications Letters*, vol. 13, no. 6, pp. 381–383, Jun. 2009.

[152] B. Wang, Z. Han, and K. Liu, "Distributed relay selection and power control for multiuser cooperative communication networks using stackelberg game," *IEEE Transactions on Mobile Computing*, vol. 8, no. 7, pp. 975–990, Jul. 2009.

[153] I. Maric and R. Yates, "Bandwidth and power allocation for cooperative strategies in gaussian relay networks," *IEEE Transactions on Information Theory*, vol. 56, no. 4, pp. 1880–1889, Apr. 2010.

[154] S. Kadloor and R. Adve, "Relay selection and power allocation in cooperative cellular networks," *IEEE Transactions on Wireless Communications*, vol. 9, no. 5, pp. 1676–1685, May 2010.

[155] Y. Liu, M. Tao, B. Li, and H. Shen, "Optimization framework and graph-based approach for relay-assisted bidirectional OFDMA cellular networks," *IEEE Transactions on Wireless Communications*, vol. 9, no. 11, pp. 3490–3500, Nov. 2010.

[156] G. Li and H. Liu, "Downlink dynamic resource allocation for multi-cell OFDMA system," in *IEEE Vehicular Technology Conference Fall*, vol. 3, Orlando, Florida, USA, Oct. 2003, pp. 1698–1702.

[157] K. Navaie and H. Yanikomeroglu, "Optimal downlink resource allocation for non-real time traffic in cellular CDMA/TDMA networks," *IEEE Communications Letters*, vol. 10, no. 4, pp. 278–280, Apr. 2006.

[158] M. Feng, L. Chen, and X. She, "Uplink adaptive resource allocation mitigating inter-cell interference fluctuation for future cellular systems," in *IEEE International Conference on Communications*, Glasgow, Scotland, Jun. 2007, pp. 5519–5524.

[159] D. Gesbert, S. Kiani, A. Gjendemsjo, and G. Øien, "Adaptation, coordination, and distributed resource allocation in interference-limited wireless networks," *Proceedings of the IEEE*, vol. 95, no. 12, pp. 2393–2409, Dec. 2007.

[160] X. Wang, Q. Liu, and G. Giannakis, "Analyzing and optimizing adaptive modulation-coding jointly with ARQ for QoS-guaranteed traffic," *IEEE Transactions on Vehicular Technology*, vol. 56, no. 2, pp. 710–720, Mar. 2006.

[161] D. Niyato and E. Hossain, "A cooperative game framework for bandwidth allocation in 4G heterogeneous wireless networks," in *IEEE International Conference on Communications*, vol. 9, Istanbul, Turkey, Jun. 2006, pp. 4357–4362.

[162] ——, "A noncooperative game-theoretic framework for radio resource management in 4G heterogeneous wireless access networks," *IEEE Transactions on Mobile Computing*, vol. 7, no. 3, pp. 332–345, Mar. 2008.

[163] S. Bashar and Z. Ding, "Admission control and resource allocation in a heterogeneous OFDMA wireless network," *IEEE Transactions on Wireless Communications*, vol. 8, no. 8, pp. 4200–4210, Aug. 2009.

[164] E. J. Hong, S. Y. Yun, and D.-H. Cho, "Decentralized power control scheme in femtocell networks: A game theoretic approach," in *IEEE International Symposium on Personal, Indoor and Mobile Radio Communications*, Tokyo, Japan, Sep. 2009, pp. 415–419.

[165] Y. Choi, H. Kim, S.-w. Han, and Y. Han, "Joint resource allocation for parallel multi-radio access in heterogeneous wireless networks," *IEEE Transactions on Wireless Communications*, vol. 9, no. 11, pp. 3324–3329, Nov. 2010.

[166] M. Ismail and W. Zhuang, "A distributed multi-service resource allocation algorithm in heterogeneous wireless access medium," *IEEE Journal on Selected Areas in Communications*, vol. 30, no. 2, pp. 425–432, Feb. 2012.

[167] Q. Qu, L. Milstein, and D. Vaman, "Cognitive radio based multi-user resource allocation in mobile ad hoc networks using multi-carrier CDMA modulation," *IEEE Journal on Selected Areas in Communications*, vol. 26, no. 1, pp. 70–82, Jan. 2008.

[168] L. B. Le and E. Hossain, "Resource allocation for spectrum underlay in cognitive radio networks," *IEEE Transactions on Wireless Communications*, vol. 7, no. 12, pp. 5306–5315, Dec. 2008.

[169] C.-g. Yang, J.-d. Li, and Z. Tian, "Optimal power control for cognitive radio networks under coupled interference constraints: A cooperative game-theoretic perspective," *IEEE Transactions on Vehicular Technology*, vol. 59, no. 4, pp. 1696–1706, May 2010.

[170] R. Zhang, Y.-C. Liang, and S. Cui, "Dynamic resource allocation in cognitive radio networks," *IEEE Signal Processing Magazine*, vol. 27, no. 3, pp. 102–114, May 2010.

[171] H. Xu and B. Li, "Efficient resource allocation with flexible channel cooperation in OFDMA cognitive radio networks," in *IEEE International Conference on Computer Communications*, San Diego, California, USA, Mar. 2010.

[172] R. Xie, F. R. Yu, and H. Ji, "Dynamic resource allocation for heterogeneous services in cognitive radio networks with imperfect channel sensing," *IEEE Transactions on Vehicular Technology*, vol. 61, no. 2, pp. 770–780, Feb. 2012.

[173] C. Saraydar, N. Mandayam, and D. Goodman, "Pricing and power control in a multicell wireless data network," *IEEE Journal on Selected Areas in Communications*, vol. 19, no. 10, pp. 1883–1892, Oct. 2001.

[174] ——, "Efficient power control via pricing in wireless data networks," *IEEE Transactions on Communications*, vol. 50, no. 2, pp. 291–303, Feb. 2002.

[175] Z. Han, Z. Ji, and K. Liu, "Fair multiuser channel allocation for OFDMA networks using nash bargaining solutions and coalitions," *IEEE Transactions on Communications*, vol. 53, no. 8, pp. 1366–1376, Aug. 2005.

[176] H. Ahmadi, Y. H. Chew, and C. C. Chai, "Multicell multiuser OFDMA dynamic resource allocation using ant colony optimization," in *IEEE Vehicular Technology Conference Spring*, Yokohama, Japan, May 2011.

[177] Q. Zhang, W. Zhu, and Y.-Q. Zhang, "Resource allocation for multimedia streaming over the internet," *IEEE Transactions on Multimedia*, vol. 3, no. 3, pp. 339–355, Sep. 2001.

[178] P. Pahalawatta, R. Berry, T. Pappas, and A. Katsaggelos, "Content-aware resource allocation and packet scheduling for video transmission over wireless networks," *IEEE Journal on Selected Areas in Communications*, vol. 25, no. 4, pp. 749–759, May 2007.

[179] H. Zhu, S. Karachontzitis, and D. Toumpakaris, "Low-complexity resource allocation and its application to distributed antenna systems," *IEEE Wireless Communications Magazine*, vol. 17, no. 3, pp. 44–50, Jun. 2010.

[180] I. Toufik and R. Knopp, "Multiuser channel allocation algorithms achieving hard fairness," in *IEEE Global Telecommunications Conference*, vol. 1, Dallas, Texas, USA, Nov. 2004, pp. 146–150.

[181] D. Ng and R. Schober, "Spectral efficiency in large-scale MIMO–OFDM systems with per-antenna power cost," in *IEEE Asilomar Conference on Signals, Systems and Computers*, Pacific Grove, California, USA, Nov. 2012, pp. 289–294.

[182] G. de Veciana, G. Kesidis, and J. Walrand, "Resource management in wide-area ATM networks using effective bandwidths," *IEEE Journal on Selected Areas in Communications*, vol. 13, no. 6, pp. 1081–1090, Aug. 1995.

[183] Z. Dziong and L. Mason, "Fair-efficient call admission control policies for broadband networks - a game theoretic framework," *IEEE/ACM Transactions on Networking*, vol. 4, no. 1, pp. 123–136, Feb. 1996.

[184] C. Leong, W. Zhuang, Y. Cheng, and L. Wang, "Optimal resource allocation and adaptive call admission control for voice/data integrated cellular networks," *IEEE Transactions on Vehicular Technology*, vol. 55, no. 2, pp. 654–669, Mar. 2006.

[185] Y. Xing, R. Chandramouli, S. Mangold, and N. Sai Shankar, "Dynamic spectrum access in open spectrum wireless networks," *IEEE Journal on Selected Areas in Communications*, vol. 24, no. 3, pp. 626–637, Mar. 2006.

[186] P. Ramanathan, K. Sivalingam, P. Agrawal, and S. Kishore, "Dynamic resource allocation schemes during handoff for mobile multimedia wireless networks," *IEEE Journal on Selected Areas in Communications*, vol. 17, no. 7, pp. 1270–1283, Jul. 1999.

[187] R. Berry and E. Yeh, "Cross-layer wireless resource allocation," *IEEE Signal Processing Magazine*, vol. 21, no. 5, pp. 59–68, Sep. 2004.

[188] G. Song and G. Li, "Cross-layer optimization for OFDM wireless networks-part I–II," *IEEE Transactions on Wireless Communications*, vol. 4, no. 2, pp. 614–634, Mar. 2005.

[189] ——, "Utility-based resource allocation and scheduling in OFDM-based wireless broadband networks," *IEEE Communications Magazine*, vol. 43, no. 12, pp. 127–134, Dec. 2005.

[190] X. Lin, N. Shroff, and R. Srikant, "A tutorial on cross-layer optimization in wireless networks," *IEEE Journal on Selected Areas in Communications*, vol. 24, no. 8, pp. 1452–1463, Aug. 2006.

[191] N. Ksairi, P. Bianchi, P. Ciblat, and W. Hachem, "Resource allocation for downlink cellular OFDMA systems part II: Practical algorithms and optimal reuse factor," *IEEE Transactions on Signal Processing*, vol. 58, no. 2, pp. 735–749, Feb. 2010.

[192] M. Sherif, I. Habib, M. Nagshineh, and P. Kermani, "Adaptive allocation of resources and call admission control for wireless ATM using genetic algorithms," *IEEE Journal on Selected Areas in Communications*, vol. 18, no. 2, pp. 268–282, Feb. 2000.

[193] S. Patra, K. Roy, S. Banerjee, and D. Vidyarthi, "Improved genetic algorithm for channel allocation with channel borrowing in mobile computing," *IEEE Transactions on Mobile Computing*, vol. 5, no. 7, pp. 884–892, Jul. 2006.

[194] F. Dressler and O. Akan, "Bio-inspired networking: from theory to practice," *IEEE Communications Magazine*, vol. 48, no. 11, pp. 176–183, Nov. 2010.

[195] Y.-J. Gong, J. Zhang, H. Chung, W.-N. Chen, Z.-H. Zhan, Y. Li, and Y.-H. Shi, "An efficient resource allocation scheme using particle swarm optimization," *IEEE Transactions on Evolutionary Computation*, vol. 16, no. 6, pp. 801–816, Dec. 2012.

[196] L. Su, Y. Ji, P. Wang, and F. Liu, "Resource allocation using particle swarm optimization for D2D communication underlay of cellular networks," in *IEEE Wireless Communications and Networking Conference*, Shanghai, China, Apr. 2013, pp. 129–133.

[197] L. B. Le and E. Hossain, "Cross-layer optimization frameworks for multihop wireless networks using cooperative diversity," *IEEE Transactions on Wireless Communications*, vol. 7, no. 7, pp. 2592–2602, Jul. 2008.

[198] J. Huang, V. Subramanian, R. Agrawal, and R. Berry, "Joint scheduling and resource allocation in uplink OFDM systems for broadband wireless access networks," *IEEE Journal on Selected Areas in Communications*, vol. 27, no. 2, pp. 226–234, Feb. 2009.

[199] D. Ng and R. Schober, "Resource allocation and scheduling in multi-cell OFDMA systems with decode-and-forward relaying," *IEEE Transactions on Wireless Communications*, vol. 10, no. 7, pp. 2246–2258, Jul. 2011.

[200] D. Ng, E. Lo, and R. Schober, "Energy-efficient resource allocation for secure OFDMA systems," *IEEE Transactions on Vehicular Technology*, vol. 61, no. 6, pp. 2572–2585, Jul. 2012.

[201] ——, "Energy-efficient resource allocation in multi-cell OFDMA systems with limited backhaul capacity," *IEEE Transactions on Wireless Communications*, vol. 11, no. 10, pp. 3618–3631, Oct. 2012.

[202] ——, "Dynamic resource allocation in MIMO-OFDMA systems with full-duplex and hybrid relaying," *IEEE Transactions on Communications*, vol. 60, no. 5, pp. 1291–1304, May 2012.

[203] G. Scutari, D. Palomar, F. Facchinei, and J.-S. Pang, "Convex optimization, game theory, and variational inequality theory," *IEEE Signal Processing Magazine*, vol. 27, no. 3, pp. 35–49, May 2010.

[204] X. Kang, R. Zhang, and M. Motani, "Price-based resource allocation for spectrum-sharing femtocell networks: A stackelberg game approach," *IEEE Journal on Selected Areas in Communications*, vol. 30, no. 3, pp. 538–549, Apr. 2012.

[205] H. Kwon and B. G. Lee, "Distributed resource allocation through noncooperative game approach in multi-cell OFDMA systems," in *IEEE International Conference on Communications*, vol. 9, Istanbul, Turkey, Jun. 2006, pp. 4345–4350.

[206] L. Wang, Y. Xue, and E. Schulz, "Resource allocation in multicell OFDM systems based on noncooperative game," in *IEEE International Symposium on Personal, Indoor and Mobile Radio Communications*, Helsinki, Finland, Sep. 2006.

[207] M. Felegyhazi, M. Cagalj, S. Bidokhti, and J.-P. Hubaux, "Non-cooperative multi-radio channel allocation in wireless networks," in *IEEE International Conference on Computer Communications*, Anchorage, Alaska, USA, May 2007, pp. 1442–1450.

[208] G. Zhang, K. Yang, P. Liu, E. Ding, and Y. Zhong, "Joint channel bandwidth and power allocation game for selfish cooperative relaying networks," *IEEE Transactions on Vehicular Technology*, vol. 61, no. 9, pp. 4142–4156, Nov. 2012.

[209] S.-L. Hew and L. White, "Cooperative resource allocation games in shared networks: symmetric and asymmetric fair bargaining models," *IEEE Transactions on Wireless Communications*, vol. 7, no. 11, pp. 4166–4175, Nov. 2008.

[210] W. Saad, Z. Han, M. Debbah, A. Hjorungnes, and T. Basar, "Coalitional game theory for communication networks," *IEEE Signal Processing Magazine*, vol. 26, no. 5, pp. 77–97, Sep. 2009.

[211] C. Singh, S. Sarkar, A. Aram, and A. Kumar, "Cooperative profit sharing in coalition-based resource allocation in wireless networks," *IEEE/ACM Transactions on Networking*, vol. 20, no. 1, pp. 69–83, Feb. 2012.

[212] J. Hui, "Resource allocation for broadband networks," *IEEE Journal on Selected Areas in Communications*, vol. 6, no. 9, pp. 1598–1608, Dec. 1988.

[213] M. Neely, E. Modiano, and C. Rohrs, "Dynamic power allocation and routing for time-varying wireless networks," *IEEE Journal on Selected Areas in Communications*, vol. 23, no. 1, pp. 89–103, Jan. 2005.

[214] C. Y. Wong, C.-Y. Tsui, R. Cheng, and K. Letaief, "A real-time sub-carrier allocation scheme for multiple access downlink OFDM transmission," in *IEEE Vehicular Technology Conference Fall*, vol. 2, Amsterdam, Netherlands, Sep. 1999, pp. 1124–1128.

[215] D. Kivanc and H. Liu, "Subcarrier allocation and power control for OFDMA," in *Asilomar Conference on Signals, Systems and Computers*, vol. 1, Pacific Grove, California, USA, Oct. 2000, pp. 147–151.

[216] D. Kivanc, G. Li, and H. Liu, "Computationally efficient bandwidth allocation and power control for OFDMA," *IEEE Transactions on Wireless Communications*, vol. 2, no. 6, pp. 1150–1158, Nov. 2003.

[217] I. Kim, H. L. Lee, B. Kim, and Y. H. Lee, "On the use of linear programming for dynamic subchannel and bit allocation in multiuser OFDM," in *IEEE Global Telecommunications Conference*, vol. 6, San Antonio, Texas, USA, Nov. 2001, pp. 3648–3652.

[218] I. Kim, I.-S. Park, and Y. H. Lee, "Use of linear programming for dynamic subcarrier and bit allocation in multiuser OFDM," *IEEE Transactions on Vehicular Technology*, vol. 55, no. 4, pp. 1195–1207, Jul. 2006.

[219] K. Seong, M. Mohseni, and J. Cioffi, "Optimal resource allocation for OFDMA downlink systems," in *IEEE International Symposium on Information Theory*, Seattle, Washington, USA, Jul. 2006, pp. 1394–1398.

[220] G. Miao, N. Himayat, G. Li, and D. Bormann, "Energy efficient design in wireless OFDMA," in *IEEE International Conference on Communications*, Beijing, China, May 2008, pp. 3307–3312.

[221] G. Miao, N. Himayat, and G. Li, "Energy-efficient transmission in frequency-selective channels," in *IEEE Global Telecommunications Conference*, New Orleans, Louisiana, USA, Nov. 2008.

[222] G. Miao, N. Himayat, G. Li, A. Koc, and S. Talwar, "Interference-aware energy-efficient power optimization," in *IEEE International Conference on Communications*, Dresden, Germany, Jun. 2009.

[223] G. Miao, N. Himayat, G. Li, and S. Talwar, "Low-complexity energy-efficient OFDMA," in *IEEE International Conference on Communications*, Dresden, Germany, Jun. 2009.

[224] G. Miao, N. Himayat, and G. Li, "Energy-efficient link adaptation in frequency-selective channels," *IEEE Transactions on Communications*, vol. 58, no. 2, pp. 545 –554, Feb. 2010.

[225] G. Miao, N. Himayat, G. Li, and S. Talwar, "Low-complexity energy-efficient scheduling for uplink OFDMA," *IEEE Transactions on Communications*, vol. 60, no. 1, pp. 112–120, Jan. 2012.

[226] C. Isheden and G. Fettweis, "Energy-efficient multi-carrier link adaptation with sum rate-dependent circuit power," in *IEEE Global Telecommunications Conference*, Miami, Florida, USA, Dec. 2010.

[227] C. Isheden, Z. Chong, E. Jorswieck, and G. Fettweis, "Framework for link-level energy efficiency optimization with informed transmitter," *IEEE Transactions on Wireless Communications*, vol. 11, no. 8, pp. 2946–2957, Aug. 2012.

[228] C. Xiong, G. Li, S. Zhang, Y. Chen, and S. Xu, "Energy- and spectral-efficiency tradeoff in downlink OFDMA networks," *IEEE Transactions on Wireless Communications*, vol. 10, no. 11, pp. 3874–3886, Nov. 2011.

[229] ——, "Energy- and spectral-efficiency tradeoff in downlink OFDMA networks," in *IEEE International Conference on Communications*, Kyoto, Japan, Jun. 2011.

[230] ——, "Energy-efficient resource allocation in OFDMA networks," in *IEEE Global Telecommunications Conference*, Houston, Texas, USA, Dec. 2011.

[231] ——, "Energy-efficient resource allocation in OFDMA networks," *IEEE Transactions on Communications*, vol. 60, no. 12, pp. 3767–3778, Dec. 2012.

[232] H. Kwon and T. Birdsall, "Channel capacity in bits per joule," *IEEE Journal of Oceanic Engineering*, vol. 11, no. 1, pp. 97–99, Jan. 1986.

[233] R. Gallager, "Energy limited channels: Coding, multiaccess, and spread spectrum," Tech. Rep., 1987.

[234] S. Verdú, "On channel capacity per unit cost," *IEEE Transactions on Information Theory*, vol. 36, no. 5, pp. 1019–1030, Sep. 1990.

[235] K.-L. Wu, P. Yu, and M.-S. Chen, "Energy-efficient caching for wireless mobile computing," in *International Conference on Data Engineering*, New Orleans, Louisiana, USA, Feb. 1996, pp. 336–343.

[236] J. Rulnick and N. Bambos, "Mobile power management for maximum battery life in wireless communication networks," in *IEEE International Conference on Computer Communications*, vol. 2, San Francisco, California, USA, Mar. 1996, pp. 443–450.

[237] ——, "Performance evaluation of power-managed mobile communication devices," in *IEEE International Conference on Communications*, vol. 3, Dallas, Texas, USA, Jun. 1996, pp. 1477–1481.

[238] M. Zorzi and R. Rao, "Energy-constrained error control for wireless channels," *IEEE Personal Communications Magazine*, vol. 4, no. 6, pp. 27–33, Dec. 1997.

[239] S.-M. Lee, Y.-S. Park, and D.-J. Park, "Fast bit and power allocation algorithm for OFDM systems," in *IEEE Vehicular Technology Conference Fall*, vol. 1, Los Angeles, California, USA, Sep. 2004, pp. 503–506.

[240] S. Pietrzyk and G. Janssen, "Multiuser subcarrier allocation for QoS provision in the OFDMA systems," in *IEEE Vehicular Technology Conference Fall*, vol. 2, Vancouver, Canada, Sep. 2002, pp. 1077–1081.

[241] C. Papadimitriou and K. Steiglitz, *Combinatorial Optimization: Algorithms and Complexity*. Dover Publications, Inc., Mineola, NY, USA, 1998.

[242] Z. Liang, Y. H. Chew, and C. C. Ko, "A linear programming solution to the subcarrier-and-bit allocation of multiclass multiuser OFDM systems," in *IEEE Vehicular Technology Conference Spring*, Dublin, Ireland, Apr. 2007, pp. 2682–2686.

[243] J. Li, H. Kim, Y. Lee, and Y. Kim, "A novel broadband wireless OFDMA scheme for downlink in cellular communications," in *IEEE Wireless Communications and Networking Conference*, vol. 3, New Orleans, Louisiana, USA, Mar. 2003, pp. 1907–1911.

[244] L. Xiaowen and Z. Jinkang, "An adaptive subcarrier allocation algorithm for multiuser OFDM system," in *IEEE Vehicular Technology Conference Fall*, vol. 3, Orlando, Florida, USA, Oct. 2003, pp. 1502–1506.

[245] Y. Zhang and K. Letaief, "Adaptive resource allocation and scheduling for multiuser packet-based OFDM networks," in *IEEE International Conference on Communications*, vol. 5, Paris, France, Jun. 2004, pp. 2949–2953.

[246] ——, "Energy-efficient MAC–PHY resource management with guaranteed QoS in wireless OFDM networks," in *IEEE International Conference on Communications*, vol. 5, Seoul, Korea, May 2005, pp. 3127–3131.

[247] ——, "Cross-layer adaptive resource management for wireless packet networks with OFDM signaling," *IEEE Transactions on Wireless Communications*, vol. 5, no. 10, pp. 3244–3254, Nov. 2006.

[248] Q. Bai and J. Nossek, "On energy efficient cross-layer assisted resource allocation in multiuser multicarrier systems," in *IEEE International Symposium on Personal, Indoor and Mobile Radio Communications*, Tokyo, Japan, Sept 2009, pp. 2603–2607.

[249] C. Han and S. Armour, "Energy efficient radio resource management strategies for green radio," *IET Communications*, vol. 5, no. 18, pp. 2629–2639, Dec. 2011.

[250] C. Zarakovitis, Q. Ni, D. Skordoulis, and M. Hadjinicolaou, "Power-efficient cross-layer design for OFDMA systems with heterogeneous QoS, imperfect CSI, and outage considerations," *IEEE Transactions on Vehicular Technology*, vol. 61, no. 2, pp. 781–798, Feb. 2012.

[251] Z. Mao and X. Wang, "Efficient optimal and suboptimal radio resource allocation in OFDMA system," *IEEE Transactions on Wireless Communications*, vol. 7, no. 2, pp. 440–445, Feb. 2008.

[252] Y.-B. Lin, T.-H. Chiu, and Y.-T. Su, "Optimal and near-optimal resource allocation algorithms for OFDMA networks," *IEEE Transactions on Wireless Communications*, vol. 8, no. 8, pp. 4066–4077, Aug. 2009.

[253] A. Akbari, R. Hoshyar, and R. Tafazolli, "Energy-efficient resource allocation in wireless OFDMA systems," in *IEEE International Symposium on Personal Indoor and Mobile Radio Communications*, Istanbul, Turkey, Sep. 2010, pp. 1731–1735.

[254] S. Khakurel, L. Musavian, and T. Le-Ngoc, "Energy-efficient resource and power allocation for uplink multi-user OFDM systems," in *IEEE International Symposium on Personal Indoor and Mobile Radio Communications*, Sydney, Australia, Sep. 2012, pp. 357–361.

[255] Q. Xu, X. Li, and H. Ji, "Multiple resource allocation in OFDMA downlink networks: End-to-end energy-efficient approach," in *IEEE International Conference on Communications*, Sydney, Australia, Jun. 2014, pp. 3957–3962.

[256] G. Lim, C. Xiong, L. Cimini, and G. Li, "Energy-efficient resource allocation for OFDMA-based multi-RAT networks," *IEEE Transactions on Wireless Communications*, vol. 13, no. 5, pp. 2696–2705, May 2014.

[257] T. Thanabalasingham, S. Hanly, L. Andrew, and J. Papandriopoulos, "Joint allocation of subcarriers and transmit powers in a multiuser OFDM cellular network," in *IEEE International Conference on Communications*, vol. 1, Istanbul, Turkey, Jun. 2006, pp. 269–274.

[258] A. Abrardo, A. Alessio, P. Detti, and M. Moretti, "Radio resource allocation problems for OFDMA cellular systems," *Elsevier Computers & Operations Research*, vol. 36, no. 5, pp. 1572–1581, May 2009.

[259] M. Moretti and A. Todini, "A resource allocator for the uplink of multi-cell OFDMA systems," *IEEE Transactions on Wireless Communications*, vol. 6, no. 8, pp. 2807–2812, Aug. 2007.

[260] S. Hanly, L. Andrew, and T. Thanabalasingham, "Dynamic allocation of subcarriers and transmit powers in an OFDMA cellular network," *IEEE Transactions on Information Theory*, vol. 55, no. 12, pp. 5445–5462, Dec. 2009.

[261] I. Bang, S. H. Kim, S. M. Kim, and D. K. Sung, "Energy-efficient subchannel allocation scheme based on adaptive base station cooperation in downlink cellular networks," in *IEEE Wireless Communications and Networking Conference*, Shanghai, China, Apr. 2012, pp. 2434–2439.

[262] S. Buzzi, G. Colavolpe, D. Saturnino, and A. Zappone, "Potential games for energy-efficient power control and subcarrier allocation in uplink multicell OFDMA systems," *IEEE Journal of Selected Topics in Signal Processing*, vol. 6, no. 2, pp. 89–103, Apr. 2012.

[263] L. Venturino, C. Risi, S. Buzzi, and A. Zappone, "Energy-efficient coordinated user scheduling and power control in downlink multi-cell OFDMA networks," in *IEEE International Symposium on Personal Indoor and Mobile Radio Communications*, London, UK, Sep. 2013, pp. 1655–1659.

[264] L. Venturino, A. Zappone, C. Risi, and S. Buzzi, "Energy-efficient scheduling and power allocation in downlink OFDMA networks with base station coordination," *accepted for publication in IEEE Transactions on Wireless Communications*, 2014.

[265] H. Liu, W. Zheng, H. Zhang, Z. Zhang, and X. Wen, "An iterative two-step algorithm for energy efficient resource allocation in multi-cell OFDMA networks," in *IEEE Wireless Communications and Networking Conference*, Shanghai, China, Apr. 2013, pp. 608–613.

[266] S. Andreev, P. Gonchukov, N. Himayat, Y. Koucheryavy, and A. Turlikov, "Energy efficient communications for future broadband cellular networks," *Elsevier Computer Communications*, vol. 35, no. 14, pp. 1662–1671, Aug. 2012, special issue: Wireless Green Communications and Networking.

[267] F. Héliot, M. Imran, and R. Tafazolli, "Energy-efficiency based resource allocation for the orthogonal multi-user channel," in *IEEE Vehicular Technology Conference Fall*, Québec City, Québec, Canada, Sep. 2012.

[268] ——, "Low-complexity energy-efficient resource allocation for the downlink of cellular systems," *IEEE Transactions on Communications*, vol. 61, no. 6, pp. 2271–2281, Jun. 2013.

[269] C. Xiong, G. Li, Y. Liu, and S. Xu, "Qos driven energy-efficient design for downlink OFDMA networks," in *IEEE Global Communications Conference*, Anaheim, California, USA, Dec. 2012, pp. 4320–4325.

[270] C. Xiong, G. Li, Y. Liu, Y. Chen, and S. Xu, "Energy-efficient design for downlink OFDMA with delay-sensitive traffic," *IEEE Transactions on Wireless Communications*, vol. 12, no. 6, pp. 3085–3095, Jun. 2013.

[271] C. Xiong, L. Lu, and G. Li, "Energy efficiency tradeoff in downlink and uplink TDD OFDMA with simultaneous wireless information and power transfer," in *IEEE International Conference on Communications*, Sydney, Australia, Jun. 2014, pp. 5383–5388.

[272] D. Tsilimantos, J.-M. Gorce, and K. Jaffrès-Runser, "Spectral and energy efficiency trade-off with joint power-bandwidth allocation in OFDMA networks," *submitted to IEEE Transactions on Communications*, 2013. [Online]. Available: http://arxiv.org/abs/1311.7302

[273] Z. Zheng, L. Dan, Y. Xiao, G. Wu, and S. Hu, "Low-complexity energy-efficient resource allocation for uplink OFDMA systems," in *IEEE Vehicular Technology Conference Fall*, Las Vegas, Nevada, USA, Sep. 2013.

[274] Z. Zheng, L. Dan, S. Gong, and S. Li, "Energy-efficient resource allocation for downlink OFDMA systems," in *IEEE International Conference on Communications Workshops*, Budapest, Hungary, Jun. 2013, pp. 391–395.

[275] J. Tang, D. So, E. Alsusa, and K. Hamdi, "Resource efficiency: A new paradigm on energy efficiency and spectral efficiency tradeoff," *IEEE Transactions on Wireless Communications*, vol. 13, no. 8, pp. 4656–4669, Aug. 2014.

[276] Z. Li, H. Jiang, Z. Pan, N. Liu, and X. You, "Energy spectral efficiency tradeoff in downlink OFDMA network," *accepted for publication in Wiley International Journal of Communication Systems*, 2014.

[277] F. Haider, C.-X. Wang, H. Haas, E. Hepsaydir, and X. Ge, "Energy-efficient subcarrier-and-bit allocation in multi-user OFDMA systems," in *IEEE Vehicular Technology Conference Spring*, Yokohama, May 2012.

[278] R. Loodaricheh, S. Mallick, and V. Bhargava, "Energy-efficient resource allocation for OFDMA cellular networks with user cooperation and QoS provisioning," *IEEE Transactions on Wireless Communications*, vol. 13, no. 11, pp. 6132–6146, Nov. 2014.

[279] X. Xiao, X. Tao, and J. Lu, "QoS-aware energy-efficient radio resource scheduling in multi-user OFDMA systems," *IEEE Communications Letters*, vol. 17, no. 1, pp. 75–78, Jan. 2013.

[280] Q. Shi, W. Xu, D. Li, Y. Wang, X. Gu, and W. Li, "On the energy efficiency optimality of OFDMA for SISO–OFDM downlink system," *IEEE Communications Letters*, vol. 17, no. 3, pp. 541–544, Mar. 2013.

[281] D. Ng, E. Lo, and R. Schober, "Energy-efficient resource allocation in OFDMA systems with hybrid energy harvesting base station," *IEEE Transactions on Wireless Communications*, vol. 12, no. 7, pp. 3412–3427, Jul. 2013.

[282] A. Klein, F. Wegner, M. Kuipers, and B. Raaf, "Dynamic subcarrier, bit and power allocation in OFDMA-based relay networks," in *IEEE International OFDM Workshop*, Hamburg, Germany, Aug. 2007.

[283] Y. Ma, N. Yi, and R. Tafazolli, "Bit and power loading for OFDM-based three-node relaying communications," *IEEE Transactions on Signal Processing*, vol. 56, no. 7, pp. 3236–3247, Jul. 2008.

[284] T. Girici, C. Zhu, J. Agre, and A. Ephremides, "Optimal radio resource management in multihop relay networks," in *IEEE International Symposium on Modeling and Optimization in Mobile, Ad Hoc, and Wireless Networks and Workshops*, Berlin, Germany, Apr. 2008, pp. 443–451.

[285] T. Girici, "Joint power, subcarrier and subframe allocation in multihop relay networks," *Wiley International Journal of Communication Systems*, vol. 22, no. 7, pp. 835–855, Jul. 2009.

[286] C. Y. Ho and C.-Y. Huang, "Energy efficient subcarrier-power allocation and relay selection scheme for OFDMA-based cooperative relay networks," in *IEEE International Conference on Communications*, Kyoto, Japan, Jun. 2011.

[287] J. Joung and S. Sun, "A simple network-power-saving resource allocation method for OFDMA cellular networks with multiple relays," in *IEEE International Conference on Acoustics, Speech and Signal Processing*, Prague, Czech Republic, May 2011, pp. 2504–2507.

[288] J. Zhang, Y. Jiang, and X. Li, "Energy-efficient resource allocation in multiuser relay-based OFDMA networks," *Wiley Concurrency and Computation: Practice and Experience*, vol. 25, no. 9, pp. 1113–1125, Jun. 2013.

[289] Y. Chen, X. Fang, and B. Huang, "Energy-efficient relay selection and resource allocation in nonregenerative relay OFDMA systems," *IEEE Transactions on Vehicular Technology*, vol. 63, no. 8, pp. 3689–3699, Oct. 2014.

[290] T. Wang, Y. Fang, and L. Vandendorpe, "Power minimization for OFDM transmission with subcarrier-pair based opportunistic DF relaying," *IEEE Communications Letters*, vol. 17, no. 3, pp. 471–474, Mar. 2013.

[291] G. Song and H. Liu, "A low complexity resource allocation method for relay OFDMA systems," in *IEEE International Conference on Information Theory and Information Security*, Beijing, China, Dec. 2010, pp. 1054–1057.

[292] A. Ahmad and M. Assaad, "Joint resource optimization and relay selection in cooperative cellular networks with imperfect channel knowledge," in *IEEE International Workshop on Signal Processing Advances in Wireless Communications*, Marrakech, Morocco, Jun. 2010.

[293] L. Xiao, L. Cuthbert, and T. Zhang, "Distributed multi-cell power allocation algorithm for energy efficiency in OFDMA relay systems," in *IEEE International Conference on Communications Workshops*, Dresden, Germany, Jun. 2009.

[294] D. Wang, Z. Li, and X. Wang, "Joint optimal subcarrier and power allocation for wireless cooperative networks over OFDM fading channels," *IEEE Transactions on Vehicular Technology*, vol. 61, no. 1, pp. 249–257, Jan. 2012.

[295] H. Banizaman and S. Almodarresi, "Dynamic resource allocation algorithm in multi-user cooperative OFDMA systems: Considering QoS and fairness constraints," *Springer Journal of Wireless Networks*, vol. 18, no. 4, pp. 365–380, May 2012.

[296] B. Huang, X. Fang, and Y. Chen, "Joint energy saving resource allocation and user scheduling in OFDMA relay networks," in *IEEE/CIC International Conference on Communications in China*, Xi'an, China, Aug. 2013, pp. 484–490.

[297] Y. Jiang, J. Zhang, X. Li, and W. Xu, "Energy-efficient resource optimization for relay-aided uplink OFDMA systems," in *IEEE Vehicular Technology Conference Spring*, Yokohama, Japan, May 2012.

[298] W. Hao, S. Yang, and W. Hao, "Relay selection and subcarrier-pair based energy-efficient resource allocation for multirelay cooperative ofdma networks," *Hindawi International Journal of Antennas and Propagation*, vol. 2014, 2014.

[299] H. Yu, H. Qin, Y. Li, Y. Zhao, X. Xu, and J. Wang, "Energy-efficient power allocation for non-regenerative OFDM relay links," *Springer Science China Information Sciences*, vol. 56, no. 2, pp. 1–8, Feb. 2013.

[300] J. Kazemi, M. Omidi, and K. Navaie, "Energy-efficient resource allocation for amplify-and-forward relaying in OFDM systems," *Wiley Transactions on Emerging Telecommunications Technologies*, Early Access 2014.

[301] Y. Chen, X. Fang, and Y. Zhao, "Energy-efficient adaptive power allocation in orthogonal frequency division multiplexing-based amplify-and-forward relay link," *IET Communications*, vol. 7, no. 15, pp. 1676–1687, Oct. 2013.

[302] C. Sun, Y. Cen, and C. Yang, "Energy efficient OFDM relay systems," *IEEE Transactions on Communications*, vol. 61, no. 5, pp. 1797–1809, May 2013.

[303] Z. Chen, T. J. Lim, and M. Motani, "Energy minimization in two-way relay networks with digital network coding," in *IEEE International Conference on Communications in China*, Beijing, Aug. 2012, pp. 7–11.

[304] T.-S. Chang, K.-T. Feng, J.-S. Lin, and L.-C. Wang, "Green resource allocation schemes for relay-enhanced MIMO-OFDM networks," *IEEE Transactions on Vehicular Technology*, vol. 62, no. 9, pp. 4539–4554, Nov. 2013.

[305] Y. Chen and X. Fang, "Energy-efficient dynamic resource allocation with opportunistic network coding in OFDMA relay networks," *Elsevier Computer Networks*, vol. 56, no. 15, pp. 3446–3455, Oct. 2012.

[306] Y. Liu, S. Yan, X. Li, and Y. Shang, "Energy-efficient resource allocation for multi-user two-way relay-assisted OFDM system," in *IEEE International Conference on Telecommunications*, Lisbon, Portugal, May 2014, pp. 150–154.

[307] G. Liu, H. Ji, F. R. Yu, Y. Li, and R. Xie, "Energy-efficient resource allocation in full-duplex relaying networks," in *IEEE International Conference on Communications*, Sydney, Australia, Jun. 2014, pp. 2400–2405.

[308] Z. Hu, G. Zhu, Y. Xia, and G. Liu, "Adaptive subcarrier and bit allocation for multiuser MIMO-OFDM transmission," in *IEEE Vehicular Technology Conference Spring*, vol. 2, Milan, Italy, May 2004, pp. 779–783.

[309] ——, "Multiuser subcarrier and bit allocation for MIMO-OFDM systems with perfect and partial channel information," in *IEEE Wireless Communications and Networking Conference*, vol. 2, Atlanta, Georgia, USA, Mar. 2004, pp. 1188–1193.

[310] Y. Zhang and K. Letaief, "Optimizing power and resource management for multiuser MIMO/OFDM systems," in *IEEE Global Telecommunications Conference*, vol. 1, San Francisco, California, USA, Dec. 2003, pp. 179–183.

[311] ——, "Adaptive resource allocation for multiaccess MIMO/OFDM systems with matched filtering," *IEEE Transactions on Communications*, vol. 53, no. 11, pp. 1810–1816, Nov. 2005.

[312] W. Ho and Y.-C. Liang, "Efficient resource allocation for power minimization in MIMO-OFDM downlink," in *IEEE Vehicular Technology Conference Fall*, Calgary, Canada, Sep. 2008.

[313] H. S. Kim and B. Daneshrad, "Energy-aware link adaptation for MIMO-OFDM based wireless communication," in *IEEE Military Communications Conference*, San Diego, California, USA, Nov. 2008.

[314] ——, "Energy-constrained link adaptation for MIMO OFDM wireless communication systems," *IEEE Transactions on Wireless Communications*, vol. 9, no. 9, pp. 2820–2832, Sep. 2010.

[315] R. S. Prabhu and B. Daneshrad, "Energy-efficient power loading for a MIMO-SVD system and its performance in flat fading," in *IEEE Global Telecommunications Conference*, Miami, Florida, USA, Dec. 2010.

[316] Z. Xu, C. Yang, G. Li, S. Zhang, Y. Chen, and S. Xu, "Energy-efficient configuration of spatial and frequency resources in MIMO-OFDMA systems," *IEEE Transactions on Communications*, vol. 61, no. 2, pp. 564–575, Feb. 2013.

[317] G. Raleigh and J. Cioffi, "Spatio-temporal coding for wireless communication," *IEEE Transactions on Communications*, vol. 46, no. 3, pp. 357–366, Mar. 1998.

[318] T.-S. Chang, K.-T. Feng, J.-S. Lin, and L.-C. Wang, "Green resource allocation for MIMO-OFDM relay networks," in *IEEE Wireless Communications and Networking Conference*, Shanghai, China, Apr. 2012, pp. 1386–1391.

[319] Y. Zhao, X. Li, X. Zhang, Y. Li, and H. Ji, "Multidimensional resource allocation strategy for high-speed railway MIMO-OFDM system," in *IEEE Global Communications Conference*, Anaheim, California, USA, Dec. 2012, pp. 1653–1657.

[320] X. Xiao, X. Tao, and J. Lu, "QoS-guaranteed energy-efficient power allocation in downlink multi-user MIMO-OFDM systems," in *IEEE International Conference on Communications*, Sydney, Australia, Jun. 2014, pp. 3945–3950.

[321] ——, "Energy-efficient resource allocation in LTE-based MIMO-OFDMA systems with user rate constraints," *accepted for publication in IEEE Transactions on Vehicular Technology*, no. 99, 2014.

[322] G. Liu, F. R. Yu, H. Ji, and V. C. Leung, "Energy-efficient resource allocation in cellular networks with shared full-duplex relaying," *accepted for publication in IEEE Transactions on Vehicular Technology*, no. 99, 2014.

[323] Y.-i. Shin, T.-s. Kang, and H.-M. Kim, "An efficient resource allocation for multiuser MIMO-OFDM systems with zero-forcing beamformer," in *IEEE International Symposium on Personal, Indoor and Mobile Radio Communications*, Athens, Greece, Sep. 2007.

[324] T. Yoo and A. Goldsmith, "On the optimality of multiantenna broadcast scheduling using zero-forcing beamforming," *IEEE Journal on Selected Areas in Communications*, vol. 24, no. 3, pp. 528–541, Mar. 2006.

[325] F. She, W. Chen, H. Luo, T. Huang, and X. Wang, "Joint power allocation and scheduling of multi-antenna OFDM system in broadcast channel," in *IEEE International Conference on Communications*, Dresden, Germany, Jun. 2009.

[326] E. Eraslan and B. Daneshrad, "Practical energy efficient link adaptation for MIMO-OFDM systems," in *IEEE Wireless Communications and Networking Conference*, Shanghai, China, Apr. 2012, pp. 480–485.

[327] ——, "Low-complexity energy efficiency maximization protocol for MIMO-OFDM systems," in *IEEE Global Communications Conference*, Atlanta, Georgia, USA, Dec 2013, pp. 2484–2490.

[328] E. Eraslan, C.-Y. Wang, and B. Daneshrad, "Practical energy-aware link adaptation for MIMO-OFDM systems," *IEEE Transactions on Wireless Communications*, vol. 13, no. 1, pp. 246–258, Jan. 2014.

[329] A. Zappone, G. Alfano, S. Buzzi, and M. Meo, "Energy-efficient non-cooperative resource allocation in multi-cell OFDMA systems with multiple base station antennas," in *IEEE Online Conference on Green Communications*, Sep. 2011, pp. 82–87.

[330] K. T. K. Cheung, S. Yang, and L. Hanzo, "Achieving maximum energy-efficiency in multi-relay OFDMA cellular networks: A fractional programming approach," *IEEE Transactions on Communications*, vol. 61, no. 7, pp. 2746–2757, Jul. 2013.

[331] ——, "Maximizing energy-efficiency in multi-relay OFDMA cellular networks," in *Proceedings of the IEEE Global Telecommunications Conference*, Atlanta, GA, USA, Dec. 2013.

[332] K. Cheung, S. Yang, and L. Hanzo, "Spectral and energy spectral efficiency optimization of joint transmit and receive beamforming based multi-relay MIMO-OFDMA cellular networks," *IEEE Transactions on Wireless Communications*, vol. 13, no. 11, pp. 6147–6165, Nov. 2014.

[333] K. T. K. Cheung, S. Yang, and L. Hanzo, "Distributed energy spectral efficiency optimization for partial full interference alignment in multi-user multi-relay multi-cell MIMO systems," *under review for IEEE Transactions on Signal Processing.*

[334] R. Tichatschke, "On the shoulders of giants: A brief excursion into the history of mathematical programming," Notes for a lecture held on the occasion of the Year of Mathematics, University of Trier, Mar. 2008.

[335] D. Bertsekas, *Nonlinear Programming.* Athena Scientific, Belmont, MA, USA, 1999.

[336] S. Boyd and J. Mattingley, "Branch and bound methods," EE364b course notes, Stanford University, Mar. 2007.

[337] W. Dinkelbach, "On nonlinear fractional programming," *Management Science*, vol. 13, pp. 492–498, Mar. 1967.

[338] M. Avriel, W. Diewert, S. Schaible, and I. Zang, *Generalized Concavity.* Plenum Press, New York, NY, USA, 1988.

[339] D. Palomar and M. Chiang, "A tutorial on decomposition methods for network utility maximization," *IEEE Journal on Selected Areas in Communications*, vol. 24, no. 8, pp. 1439–1451, Aug. 2006.

[340] Z.-Q. Luo and W. Yu, "An introduction to convex optimization for communications and signal processing," *IEEE Journal on Selected Areas in Communications*, vol. 24, no. 8, pp. 1426–1438, Aug. 2006.

[341] T. Quek, H. Shin, and M. Win, "Robust wireless relay networks: Slow power allocation with guaranteed QoS," *IEEE Journal of Selected Topics in Signal Processing*, vol. 1, no. 4, pp. 700–713, Dec. 2007.

[342] S.-J. Kim, A. Magnani, A. Mutapcic, S. Boyd, and Z.-Q. Luo, "Robust beamforming via worst-case SINR maximization," *IEEE Transactions on Signal Processing*, vol. 56, no. 4, pp. 1539–1547, Apr. 2008.

[343] T. Quek, M. Win, and M. Chiani, "Robust power allocation algorithms for wireless relay networks," *IEEE Transactions on Communications*, vol. 58, no. 7, pp. 1931–1938, Jul. 2010.

[344] K. Yang, J. Huang, Y. Wu, X. Wang, and M. Chiang, "Distributed robust optimization (DRO), part i: framework and example," *Springer Journal Optimization and Engineering*, vol. 15, no. 1, pp. 35–67, Mar. 2014.

[345] ——, "Distributed robust optimization (DRO) part ii: Wireless power control," *submitted to Springer Journal Optimization and Engineering*, 2010.

[346] D. Hughes-Hartogs, "Ensemble modem structure for imperfect transmission media," US Patents Nos. 4,679,227 (July 1987) 4,731,816 (March 1988) 4,833,706 (May 1989) and 5,054,034 (Oct 1991).

[347] R. Devarajan, S. Jha, U. Phuyal, and V. Bhargava, "Energy-aware resource allocation for cooperative cellular network using multi-objective optimization approach," *IEEE Transactions on Wireless Communications*, vol. 11, no. 5, pp. 1797–1807, May 2012.

[348] H. Yu, R. Xiao, Y. Li, and J. Wang, "Energy-efficient multi-user relay networks," in *Proceedings of the International Conference on Wireless Communications and Signal Processing (WCSP'11)*, Nanjing, China, Nov. 2011.

[349] J. Zhang, L.-L. Yang, and L. Hanzo, "Energy-efficient channel-dependent cooperative relaying for the multiuser SC-FDMA uplink," *IEEE Transactions on Vehicular Technology*, vol. 60, no. 3, pp. 992–1004, Mar. 2011.

[350] ——, "Energy-efficient dynamic resource allocation for opportunistic-relaying-assisted SC-FDMA using turbo-equalizer-aided soft decode-and-forward," *IEEE Transactions on Vehicular Technology*, vol. 62, no. 1, pp. 235–246, Jan. 2013.

[351] L. Hanzo, O. Alamri, M. El-Hajjar, and N. Wu, *Near-Capacity Multi-Functional MIMO Systems: Sphere-Packing, Iterative Detection and Cooperation.* Wiley-IEEE Press, 2009.

[352] O. Arnold, F. Richter, G. Fettweis, and O. Blume, "Power consumption modeling of different base station types in heterogeneous cellular networks," in *Proceedings of the Future Network and Mobile Summit*, Florence, Italy, Jun. 2010.

[353] W. Yu and R. Lui, "Dual methods for nonconvex spectrum optimization of multicarrier systems," *IEEE Transactions on Communications*, vol. 54, no. 7, pp. 1310–1322, Jul. 2006.

[354] 3GPP, "TR 36.814 V9.0.0: further advancements for E-UTRA, physical layer aspects (release 9)," Mar. 2010.

[355] G. Caire and S. Shamai Shitz, "On the achievable throughput of a multiantenna Gaussian broadcast channel," *IEEE Transactions on Information Theory*, vol. 49, no. 7, pp. 1691–1706, Jul. 2003.

[356] S. Vishwanath, N. Jindal, and A. Goldsmith, "Duality, achievable rates, and sum-rate capacity of Gaussian MIMO broadcast channels," *IEEE Transactions on Information Theory*, vol. 49, no. 10, pp. 2658–2668, Oct. 2003.

[357] M. Costa, "Writing on dirty paper," *IEEE Transactions on Information Theory*, vol. 29, no. 3, pp. 439–441, May 1983.

[358] A. Ahrens, S. X. Ng, V. Khn, and L. Hanzo, "Modulation-mode assignment for SVD-aided and BICM-assisted spatial division multiplexing," *Elsevier Physical Communication*, vol. 1, no. 1, pp. 60–66, Mar. 2008.

[359] N. Ul Hassan and M. Assaad, "Low complexity margin adaptive resource allocation in downlink MIMO-OFDMA system," *IEEE Transactions on Wireless Communications*, vol. 8, no. 7, pp. 3365–3371, Jul. 2009.

[360] K.-K. Wong, R. Murch, and K. Letaief, "A joint-channel diagonalization for multiuser MIMO antenna systems," *IEEE Transactions on Wireless Communications*, vol. 2, no. 4, pp. 773–786, Jul. 2003.

[361] M. Sharif and B. Hassibi, "On the capacity of MIMO broadcast channels with partial side information," *IEEE Transactions on Information Theory*, vol. 51, no. 2, pp. 506–522, Feb. 2005.

[362] Z. Shen, R. Chen, J. Andrews, R. Heath, and B. Evans, "Low complexity user selection algorithms for multiuser MIMO systems with block diagonalization," *IEEE Transactions on Signal Processing*, vol. 54, no. 9, pp. 3658–3663, Sept. 2006.

[363] W. Yu and T. Lan, "Transmitter optimization for the multi-antenna downlink with per-antenna power constraints," *IEEE Transactions on Signal Processing*, vol. 55, no. 6, pp. 2646–2660, Jun. 2007.

[364] E. Lo, P. Chan, V. Lau, R. Cheng, K. Letaief, R. Murch, and W.-H. Mow, "Adaptive resource allocation and capacity comparison of downlink multiuser MIMO-MC-CDMA and MIMO-OFDMA," *IEEE Transactions on Wireless Communications*, vol. 6, no. 3, pp. 1083–1093, Mar. 2007.

[365] G. Brante, I. Stupia, R. Souza, and L. Vandendorpe, "Outage probability and energy efficiency of cooperative MIMO with antenna selection," *IEEE Transactions on Wireless Communications*, vol. 12, no. 11, pp. 5896–5907, Nov. 2013.

[366] A. Zappone, P. Cao, and E. Jorswieck, "Energy efficiency optimization in relay-assisted MIMO systems with perfect and statistical CSI," *IEEE Transactions on Signal Processing*, vol. 62, no. 2, pp. 443–457, Jan. 2014.

[367] A. Yeredor, "Non-orthogonal joint diagonalization in the least-squares sense with application in blind source separation," *IEEE Transactions on Signal Processing*, vol. 50, no. 7, pp. 1545–1553, Jul. 2002.

[368] P. Comon and C. Jutten, *Handbook of Blind Source Separation: Independent Component Analysis and Applications*. Academic Press, 2010.

[369] G. Auer, O. Blume, V. Giannini, I. Godor, M. Imran, Y. Jading, E. Katranaras, M. Olsson, D. Sabella, P. Skillermark, and W. Wajda, "D2.3: Energy efficiency analysis of the reference systems, areas of improvements and target breakdown," *INFSO-ICT-247733 EARTH (Energy Aware Radio and NeTwork TecHnologies), Technical Report*, Nov. 2010. [Online]. Available: https://bscw.ict-earth.eu/pub/bscw.cgi/d71252/EARTH_WP2_D2.3_v2.pdf

[370] H. Holtkamp, G. Auer, S. Bazzi, and H. Haas, "Minimizing base station power consumption," *IEEE Journal on Selected Areas in Communications*, vol. 32, no. 2, pp. 297–306, Feb. 2014.

[371] O. El-Ayach, S. Peters, and R. Heath, "The practical challenges of interference alignment," *IEEE Wireless Communications Magazine*, vol. 20, no. 1, pp. 35–42, Feb. 2013.

[372] C. Suh and D. Tse, "Interference alignment for cellular networks," in *Allerton Conference on Communication, Control, and Computing*, Urbana-Champaign, IL, USA, Sept. 2008, pp. 1037–1044.

[373] H. Gao, T. Lv, D. Fang, S. Yang, and C. Yuen, "Limited feedback-based interference alignment for interfering multi-access channels," *IEEE Communications Letters*, vol. 18, no. 4, pp. 540–543, Apr. 2014.

[374] C. Suh, M. Ho, and D. Tse, "Downlink interference alignment," *IEEE Transactions on Communications*, vol. 59, no. 9, pp. 2616–2626, Sept. 2011.

[375] D. Kim and M. Torlak, "Optimization of interference alignment beamforming vectors," *IEEE Journal on Selected Areas in Communications*, vol. 28, no. 9, pp. 1425–1434, Dec. 2010.

[376] B. Da and R. Zhang, "Exploiting interference alignment in multi-cell cooperative OFDMA resource allocation," in *Proceedings of the IEEE Global Telecommunications Conference*, Houston, TX, USA, Dec. 2011.

[377] K. Gomadam, V. Cadambe, and S. Jafar, "A distributed numerical approach to interference alignment and applications to wireless interference networks," *IEEE Transactions on Information Theory*, vol. 57, no. 6, pp. 3309–3322, Jun. 2011.

[378] M. Rezaee and S. Nader-Esfahani, "Interference alignment for downlink transmission of multiple interfering cells," *IEEE Wireless Communications Letters*, vol. 1, no. 5, pp. 460–463, Oct. 2012.

[379] J. Tang and S. Lambotharan, "Interference alignment techniques for MIMO multi-cell interfering broadcast channels," *IEEE Transactions on Communications*, vol. 61, no. 1, pp. 164–175, Feb. 2013.

[380] H. J. Yang, W.-Y. Shin, B. C. Jung, C. Suh, and A. Paulraj, "Opportunistic downlink interference alignment." [Online]. Available: http://arxiv.org/abs/1312.7198

[381] M. Maddah-Ali, A. Motahari, and A. Khandani, "Communication over X channel: Signalling and multiplexing gain," *Technical Report. UW-ECE-2006-12, University of Waterloo*, Jul. 2006.

[382] ——, "Communication over X channel: Signaling and performance analysis," *Technical Report. UW-ECE-2006-27, University of Waterloo*, Dec. 2006.

[383] ——, "Signaling over MIMO multi-base systems: Combination of multi-access and broadcast schemes," in *Proceedings of the IEEE International Symposium on Information Theory*, Seattle, WA, USA, Jul. 2006, pp. 2104–2108.

[384] ——, "Communication over MIMO X channels: Interference alignment, decomposition, and performance analysis," *IEEE Transactions on Information Theory*, vol. 54, no. 8, pp. 3457–3470, Aug. 2008.

[385] V. Cadambe and S. Jafar, "Interference alignment and degrees of freedom of the k -user interference channel," *IEEE Transactions on Information Theory*, vol. 54, no. 8, pp. 3425–3441, Aug. 2008.

[386] H. Sung, S.-H. Park, K.-J. Lee, and I. Lee, "Linear precoder designs for $K$-user interference channels," *IEEE Transactions on Wireless Communications*, vol. 9, no. 1, pp. 291–301, Jan. 2010.

[387] G. Alexandropoulos and C. Papadias, "A reconfigurable distributed algorithm for $K$-user MIMO interference networks," in *IEEE International Conference on Communications*, Budapest, Hungary, Jun. 2013, pp. 3063–3067.

[388] K. Ronasi, B. Niu, V. W. Wong, S. Gopalakrishnan, and R. Schober, "Throughput-efficient scheduling and interference alignment for MIMO wireless systems," *IEEE Transactions on Wireless Communications*, vol. 13, no. 4, pp. 1779–1789, Apr. 2014.

[389] X. Chen and C. Yuen, "Performance analysis and optimization for interference alignment over MIMO interference channels with limited feedback," *IEEE Transactions on Signal Processing*, vol. 62, no. 7, pp. 1785–1795, Apr. 2014.

[390] L. Yang and W. Zhang, "Opportunistic interference alignment in heterogeneous two-cell uplink network," in *IEEE International Conference on Communications (ICC'13)*, Budapest, Hungary, Jun. 2013, pp. 5448–5452.

[391] R. Blum, "MIMO capacity with interference," *IEEE Journal on Selected Areas in Communications*, vol. 21, no. 5, pp. 793–801, Jun. 2003.

[392] M. Chiang, S. H. Low, A. Calderbank, and J. Doyle, "Layering as optimization decomposition: a mathematical theory of network architectures," *Proceedings of the IEEE*, vol. 95, no. 1, pp. 255–312, Jan. 2007.

[393] S. Zhou, A. Goldsmith, and Z. Niu, "On optimal relay placement and sleep control to improve energy efficiency in cellular networks," in *IEEE International Conference on Communications*, Kyoto, Japan, Jun. 2011.

[394] W. Guo and T. O'Farrell, "Relay deployment in cellular networks: Planning and optimization," *IEEE Journal on Selected Areas in Communications*, vol. 31, no. 8, pp. 1597–1606, Aug. 2013.

# Author Index